Evidence of Panspermia: From Astronomy to Meteorites

Jamie Hamilton Wallis

Thesis submitted in candidature for the degree of Doctor of Philosophy
at Cardiff University

Cardiff School of Mathematics, Cardiff University
2014

To Rebecca and Emily

DECLARATION

This work has not been submitted in substance for any other degree or award at this or any other university or place of learning, nor is being submitted concurrently in candidature for any degree or other award.

Signed …… (candidate) Date ……

STATEMENT 1

This thesis is being submitted in partial fulfillment of the requirements for the degree of PhD.

Signed …… (candidate) Date ……

STATEMENT 2

This thesis is the result of my own independent work/investigation, except where otherwise stated. Other sources are acknowledged by explicit references. The views expressed are my own.

Signed …… (candidate) Date ……

STATEMENT 3

I hereby give consent for my thesis, if accepted, to be available for photocopying and for inter-library loan, and for the title and summary to be made available to outside organisations.

Signed …… (candidate) Date ……

STATEMENT 4: BAR ON ACCESS APPROVED

I hereby give consent for my thesis, if accepted, to be available for photocopying and for inter-library loans **after expiry of a bar on access** approved by the Academic Standards & Quality Committee.

Signed …… (candidate) Date ……

Acknowledgements

I wish to express my grateful thanks to my supervisor, Professor N. C. Wickramasinghe, for his invaluable advice, guidance and supervision throughout the course of these studies.

I am also very grateful also to Max Wallis, Richard Hoover and Alexei Yu. Rozanov, for their many helpful and insightful discussions.

I also wish to thank Tony Oldroyd, Professor Andres Pack, Nori Miyake and Sunali Purba for their invaluable assistance with the various pieces of scientific apparatus required during these studies. A special thanks also to Warwick Analytical for their help with the ICP-OES and GC-MS experiments.

Finally, I would like to thank my family for their support and especially my wife for her unwaivering patience and encouragement throughout my research.

Summary

The theory of cometary panspermia is tested in the wake of two reported falls in Tissint, Morocco on July 18, 2011 and in the central province of Polonnaruwa, Sri Lanka on December 29, 2012. Samples of the Tissint and Polonnaruwa stones were studied using a variety of laboratory procedures and equipment including ICP-OES, GC-MS, SEM, EDAX, CHN, FTIR, Raman Spectroscopy, XRD and Optical Spectroscopy.

Results of Tissint show the presence of several 5-50µm pyrite grains rimmed by a layer of reduced organic carbon with graphitisation levels consistent with other Martian meteorites. A complex precursor carbon inventory is demonstrated with peak temperatures ~ 250 ^{O}C and elemental ratios typical of high volatility bituminous coals.

A theoretical model of the ecology of arsenic on early Mars is then developed and discussed involving microbial reduction of Fe-oxides. This hypothesis is shown to be supported by SEM observations of spherical chains of pits, with morphologies distinct from abiotic alteration features but closely comparable to biologically mediated microstructures created by Fe- and S-oxidising microbes.

The contribution of core-mantle grains to mid-IR emission features is then modelled using extinction and scattering efficiencies for composite spheres based on the Guttler extension of the Mie formulae. Results show that kerogen-pyrite grains closely adhere to observed 9-13µm emission characteristics observed in the Trapezium nebula.

Results of studies on Polonnaruwa show a highly porous Si-K-rich, Al-depleted, amorphous melt enclosing trace (commonly <1µm) anorthoclase, albite, anorthite and quartz. Bound H_2O < 0.03wt% indicates origin from hypervelocity impact. SEM analysis revealed several fossil microorganisms similar to acritarchs, hystrichospheres and diatoms.

Geologic age of the stones is determined by N/C atomic ratio depletion that indicate the presence of embedded fossil remains that date back to at least ~300 Ma. Triple oxygen isotope analysis provide values of $\Delta^{17}O$ = - 0.335 with $\delta^{17}O$ = 8.978 ± 0.050 and $\delta^{18}O$ = 17.816 ± 0.100 that is shown to be consistent with non-terrestrial sources.

Results are seen to substantially support the theory of cometary panspermia.

Extended Summary

In 1981, F. Hoyle and N.C. Wickramasinghe proposed that comets provided an ideal vehicle for the distribution of life throughout the cosmos and thereby advanced the theory of cometary panspermia. To this day it offers a powerful unifying hypothesis for a substantial body of otherwise disparate scientific data that collectively imply a cosmic setting for the origin of life. The theory directly opposes the prevailing 'Primordial Soup' hypothesis that has held sway since the late 1920s in which abiogenesis takes place on a primitive Earth rich in abiotic organics and liquid water.

The prediction that cometary dust, and by implication interstellar dust, would be organic in nature has now been established and is almost universally accepted. However these observations are still interpreted by many scientists as evidence of abiotic pre-biology. Concurrent work on stratospheric sampling of interplanetary dust particles (IDPs) (e.g. Brownlee, 1978; Lal *et al*., 1996; Harris *et al.*, 2002; Narlikar *et al*., 2003; Wainwright *et al.*, 2004; 2008; Rauf *et al*, 2010a; Wallis *et al*. 2002; Miyake, 2009) however shows evidence of undeniably biological structures as well as embedded diatom frustule fragments (Wainwright *et al.*, 2013a; 2013b). Further work on microfossils in meteorites show similar results (Claus and Nagy, 1961, 1963; Pflug, 1984a, 1984b; McKay *et al.*, 1996, 2009; Hoover, 2005, 2009, 2011). These results have been consistently challenged on the grounds of terrestrial contamination or the limitations of morphology as an unequivocal means of life detection (Anders and Fitch, 1962a, 1962b, 1964; Fitch and Andres, 1963a, 1963b; Fitch *et al.*, 1962; Garcia-Ruiz, 1999).

While these criticisms have prevented a convergence of thinking among investigators in favour of the unequivocal detection of life in non-terrestrial artefacts, the matter continues essentially unresolved. The McKay (1996) findings of an ancient Martian biota in ALH84001 faced intractable complications from its ~13,000 year stay in Antarctica.

The objective of this study is to test the theory of cometary panspermia in the light of a unique opportunity that has been provided by two events that have taken place during the past three years. The first of these occurred on July 18, 2011 when several eyewitnesses observed a brilliant yellow fireball over the Oued Drâa Valley East of Tata, Morocco at 2:00 AM. In October 2011 nomads found a 47g pale grey stone encased in a fresh, glistening black, glassy fusion crust in a remote area of the Oued Drâa watershed 48km SSW of the village of Tissint, Morocco (29^{o} 28.917'N,

7°36.674'W). Early analysis of the recovered meteorite revealed it to comprise of a depleted picritic shergottite of Martian origin similar to EETA79001A. The minimal level of terrestrial alteration of Tissint has been confirmed by Aoudjehane *et al,* (2012) via stepped combustion mass spectrometry that show total C abundances of 173 ppm with a $\delta^{13}C = -26.6$ ‰ and 12.7 ppm nitrogen with total $\delta^{15}N = -4.5$ ‰ supporting the view that much of Tissint's organic material is of Martian origin.

The second event occurred during the last week of December 2012 in the skies above the Central Provinces of Sri Lanka. Several eyewitnesses in the North Central District of Polonnaruwa reported seeing a bright yellow fireball that turned green as it travelled across the sky at approximately 18:30 PM on December 29, 2012. The inferred NE to SW trajectory was determined from numerous eyewitness observations. The green fireball was reported to disintegrate with some luminescent fragments falling towards the ground in the village of Aralagonwila (7°46'0" N and 81°10'60" E) about 35 km south of the ancient town of Polonnaruwa. A number of stones were immediately recovered from the ground in the vicinity of Aralagonwila. The events were heavily covered on Sri Lankan TV networks and included interviews with geologists from the University of Peradeniya, Sri Lanka.

The Tissint Martian Meteorite (Olivine-Phyric Shergottite)

Five fragments of the Tissint Martian meteorite were utilised in these studies. Sample verification was by measurement of elemental partitions determined using Inductively Coupled Plasma Optical Emission Spectrometry. These quantities were then compared with analogous values reported by independent teams and found to closely accord with published data. Sampling heterogeneity was investigated using optical and SEM petrographic studies on two 30µm thin sections and one polished thick section prepared at the School of Earth and Ocean Sciences at Cardiff University. This analysis revealed no significant variation in lithic or mineralogic structure or composition. Contamination screening was undertaken using 3keV SEM investigation prior to experimental procedures to ensure that all components were parental to the meteorite and contained no foreign lithic, mineralogic or precipitated components.

SEM and EDAX analysis of freshly cleaved surfaces is shown to reveal the presence of several 5-50µm spherical carbonaceous structures. These are characterized as smooth immiscible spheres with curved boundaries. Low energy (15KeV) electron beam attenuation together with 2-D x-ray elemental mapping is then used to identify elements mobilised during the attenuation process. Analysis of EDAX spectra together with derived oxide compositions are used to show increases in S and Fe with stoichiometric ratios consistent with FeS_2 (pyrite). The detection of sulphide grains

rimmed by a layer of reduced organic carbon, previously reported in carbonaceous chondrites, chondritic IDPs (Rietmeijer and Mackinnon, 1985; 1987) and primitive chondritic meteorites (Tagish Lake) (Nakamura et al., 2002) is discussed. The formation mechanisms of similar structures found in terrestrial environments, including Proterozoic and Ordovician sandstones in Canada (Nardi, 1994) and hydrothermal calcite veins in carboniferous limestones in central Ireland (Lindgren *et al.,* 2011) is also considered.

The question of contamination and origin of the structures is investigated using Raman spectroscopy. Raman spectroscopic signatures are known to reflect a range of factors including metamorphic grade and crystallinity. These are characterised by a 'disordered' graphitic band known as the D-band together with an associated 'ordered' band known as the G-band. Resolution of the spectra show G-band peak parameters Ω_G (cm^{-1}) = 1577 ± 0.3 with associated Γ_G (cm^{-1}) = 130 ± 0.1 and corresponding D-band peak Ω_D (cm^{-1}) = 1349 ± 0.3 and Γ_D (cm^{-1}) = 220 ±0.7. It is shown that the D-band intensity/G-band intensity parameter of R1 = I_D / I_G = 0.915 ± 0.038 indicates a level of graphitisation consistent with comparable Martian meteorites. R1 = I_D/I_G against Γ_D (cm^{-1}) band parameter plots of the carbonaceous coatings are shown to imply a complex precursor carbon inventory comparable to the precursor carbon component of materials of known biotic source (plants, algae, fungi, crustaceans, prokaryotes).

Estimated peak metamorphic temperatures are then determined using the method proposed by Huss *et al*., (2006). These are shown to correlate to first order with chondrites from all classes on a trend determined by a second order polynomial (R^2 = 0.95) PMT (^OC) = 931-5.10 × Γ_D × cm^1 + 0.0091 × Γ_D^2 × cm^2 ~ 250 ^OC suggesting a possible link with the hydrothermal precipitation processes responsible for the formation of similar globules observed in hydrothermal calcite veins. It is further shown that the Ω_G (cm^{-1}), Γ_G (cm^{-1}), Ω_D (cm^{-1}) and Γ_D (cm^{-1}) parameters imply a level of crystallinity and disorder of the carbon consistent with carbonaceous material recovered from a variety of other non-terrestrial sources, ruling out contamination as an explanation for observations. Elemental ratios of Cl, N, O and S to C are shown to be typical of high volatility bituminous coals and distinctly higher than equivalent graphite standards. It is concluded that the carbonaceous component of the structures were of biological origin and represent a previously observed and hypothesised affinity between aqueous organic carbon and pyrite.

The potential for humic substances to influence the redox state and the complexation of arsenic (As) thus shifting As partitioning in favour of the solute phase is then considered. SEM and EDAX are used to identify the presence of enriched arsenic domains in one polished 30µm thin section and one polished thick section of Tissint. Once identified, Raman spectroscopy is then utilised to constrain

the observed mineral phases. Results identify the presence of a relatively rare secondary iron arsenate-sulphate mineral named bukovskýite – $Fe^{3+}{}_2(As^{5+}O_4)(S^{6+}O_4)(OH)\bullet 7(H_2O)$ - found in a shock melt vein of the Tissint Martian meteorite. This is the first observation of this mineral in any meteorite.

It is hypothesised that the mineral formed when high concentrations of aqueous H^+, Fe(III), SO_4 and AsO_4 were maintained for long periods of time in microenvironments created within wet subsurface Martian clays. It is noted that the abiotic formation of bukovskýite on Earth is characterised by the presence of substantial quantities of arsenopyrite that supply the required As for mineral crystallisation. The presence of arsenopyrite was not noted in the samples in any abundance. However, the observation of trace bukovskýite in biological processes, most notably in biologically induced mineralisation Márquez *et al.,* (2006) is considered. The observation of iron arsenate and arsenate-sulphates, together with trace bukovskýite, in ferruginous bacterial accretions in acidic mine waters in France is further considered (Leblanc *et al.*, 1996).

A theoretical model of the ecology of As on early Mars is then developed and discussed. This model involves the microbial oxidation of FeS_2 with concurrent release of sequestrated As. The availability of aqueous AsO_4 is considered to have been complemented by dissolution by-products of the microbial reduction of Fe-oxides influenced by dissolved organic matter.

This hypothesis is shown to be substantially supported by SEM analysis of a 15µm spherical structure comprising of a carbonaceous outer coating with an inner core of FeS_2 (pyrite). SEM is used to examine the interface between the pyrite and organic coating and shown to reveal the presence of spherical pits, and chains of pits, with morphologies distinct from abiotic alteration features. The pits and channels are shown to have a clustered, geometric distribution, typical of microbial activity, and are closely comparable to biologically mediated microstructures created by Fe- and S-oxidising microbes in the laboratory. These microstructures are interpreted as trace fossils resulting from the attachment of bacteria to the pyrite surfaces.

The role of carbonaceous coated pyrite grains is then further investigated in a wider astronomical setting. A computer routine for calculating extinction efficiencies for composite spheres based on the Guttler extension of the Mie formulae is utilised. The optical properties of a variety of degraded kerogenous materials together with comparable parameters for crystalline pyrite are taken from the literature. Spectral observations of the interstellar medium are then compared with the theoretical curve derived in the model. Results show that composite organic carbon/pyrite grains closely adhere to observed interstellar features and may play a critical role in observed extinction features.

The Polonnaruwa Stones

Eight fragments of the Polonnaruwa stones were analysed in these studies. Bulk chemical compositions were determined using Inductively Coupled Plasma Optical Emission Spectrometry. Crystalline phases were assessed using X-ray diffraction techniques carried out on a Philips PW1710 Automated Powder Diffractometer. Amorphous phase transitions were investigated by Infrared spectroscopy using a Perkin-Elmer Spectrum 65 spectrometer equipped with Perkin-Elmer's Universal Attenuated Total Reflectance (ATR) unit. Petrology was investigated by optical and SEM petrographic analysis with in situ mineral chemistry determined by analytical SEM at the School of Earth and Ocean Sciences, Cardiff University.

Results of studies show the Polonnaruwa stones to comprise of a highly porous (~80-90% porosity) Si and K-rich, Al-depleted, amorphous melt enclosing a number of euhedral and subhedral mineral grains (1-10µm, commonly <1µm) with elongate to equant shapes. Minerals included anorthoclase, albite, anorthite and quartz. FTIR analysis of the OH stretching vibration and H-O-H bending vibration modes characteristic of the main IR band at 3660 cm^{-1} are shown to infer a bound H_2O abundance of <0.03wt% and in line with the findings of Beran and Koeberl (1996) it is concluded that the stones originate from hypervelocity impact and are inconsistent with glasses of volcanic terrestrial origin.

SEM analysis is used to show the presence of several fossil microorganisms similar to acritarchs and hystrichospheres, as well as several diatom frustules consistent with benthic and planktonic pennates of epipelic and epipsammic type, covering a wide range of evolutionary history.

Terrestrial contamination is ruled out on the basis of three separate lines of investigation. Firstly, gas chromatography–mass spectrometry is used to show the absence of biologically relevant organic compounds (amino acids) composed of amine (-NH2) and carboxylic acid (-COOH) functional groups that would be expected from the presence of recently living organisms. These include Glycine, Glutamic acid, Alanine, Valine, Proline and Aspartic acid that are ubiquitous to all life on Earth. Secondly, EDAX elemental analysis is used to show permineralization of fossils by comparison of elemental abundances in the body, the attached substrate, and the neighbouring substrate. Finally, visual inspection of the SEM images is used to confirm the presence of multiple examples of biological structures embedded or fused into the sample substrate. Further images show structures biologically anchored to their surroundings, with numerous examples of partially degraded and damaged diatom frustules. The results were interpreted as evidence that the observed biology was indigenous to the Polonnaruwa stones.

The geologic age of the stones is investigated by the N/C atomic ratio depletion rates of the embedded biological structures. These were found to be < 0.0064 as indicated by the 0.5% detection limit of nitrogen by the EDAX apparatus. Thesse ratios are shown to be consistent with the completion of diagenesis and comparable to coals and kerogen in ancient microfossils. In particular, these values are shown to accord well with 300-350 Ma anthracite (atomic N/C = ~0.007) but also shown to fall within the range of Precambrian microfossils (540 Ma to 4.6 By) where N/C atomic ratios are reported in the range of 0.0015-0.03. These results were further supported by thermal CHN elemental analysis that showed N/C atomic ratios consistent with precambrian microfossils. It was concluded that the fossil remains date back at least ~300 Ma.

Examination the interface between the amorphous glass and rougher substrate phases characteristic of biological colonisation are shown to reveal evidence of microbial pitting consistent with diatom and cyanobacteria dissolution of glass. This observation demonstrates occupancy and biological activity within the substrate over an extended period of time. It is concluded that the biological microorganisms represent the late stage colonisation of an existing substrate and are comprised of entirely fossil remains.

The non-terrestrial origin of the stones is determined using triple oxygen isotope analysis conducted in the stable isotope laboratory at the University of Göttingen, Germany. Results of this analysis provide values of $\Delta^{17}O$ = - 0.335 with $\delta^{17}O$ = 8.978 ± 0.050 and $\delta^{18}O$ = 17.816 ± 0.100. These values are discussed and shown to be consistent with non-terrestrial sources (e.g. Meta-C chondrites such as B9704 and Y86789 - Clayton *et al.*, 1999) but fall outside comparable values for terrestrial rocks.

An attempt to reconcile the triple oxygen isotope results with anthropogenic origin is discussed but shown to be inconsistent with observations. The suggestion that the porosity (between 80-90%) of the Polonnaruwa stones makes them too fragile to survive atmospheric re-entry based on current canonical models is also considered. These models show fragile meteorites suffering catastrophic fragmentation at high altitude unless the bolide speed was unusually low or is protected against thermal shock by vigorous ablation. The effects of atmospheric entry are considered on the basis of kinetic energy loss through deceleration and ablation in accordance with the literature (Baldwin, 1971; Bronshten, 1983; Melosh, 1989). Starting with the equations of motion for an incoming bolide (Landau and Lifshitz, 1959) it is shown that survival dependance critically relates to the heat of ablation ζ of the meteor body and the cross sectional area of the incoming bolide.

Applying the physical properties of the Polonnaruwa stones (i.e. high silica glass) it is shown that when vapourised they form both the gaseous dioxide and monoxide in highly endothermic reactions such that the heated solid dioxide softens and forms a liquid layer which vapourises and injects the gaseous dioxide, the monoxide, and the oxygen into the gaseous boundary layer, thickening the layer (Steg and Lew, 1962). It is shown that the effect of the above is to distance the dissociated gaseous hypersonic boundary layer from the bolide surface decreasing the heat flux to the surface. Results of modelling demonstrate that the Polonnaruwa stones would certainly survive atmospheric re-entry. These arguments are seen to be intuitively correct. The Polonnaruwa stones comprise of an amorphous silica matrix with ~90 % porosity. Early thermal protection systems developed for the space shuttle program comprised of a matrix of silica glass of ~ 94% porosity while a 10cm cube of the material could readily be crushed in one hand.

Results of the Tissint meteorite study are interpreted as providing substantial evidence in support of the presence of a past Martian biota. The study is seen to overcome many of the criticisms of previous work (McKay *et al.*, 1996; 2009) that centred on possible terrestrial contamination or the shortcomings of morphological identification. Similarly, the Polonnaruwa study supports the findings of a host of previous investigators on cometary material including Claus and Nagy (1961), Pflug (1984), Zhmur *et al.*, (1997) and the more recent work of Hoover (1997; 2008; 2011). As such it is seen to provide substantial support for the Hoyle-Wickramasinghe theory of cometary panspermia.

Publications arising from this study:

Coulson, S., Wallis, M. K., Miyake, N., Wallis, J., and Wickramasinghe, N. C. (2013) 'Dynamics of the Polonnaruwa meteorite fall', *European Planetary Science Congress 2013*, (8-13 September), London: UK. Available at: http://meetings. copernicus.org/epsc2013, id. EPSC2013-803, 8, pp. 803.

Hoover, R. B., Wallis, J., Wickramarathne, K., Samaranayake, A., Williams, G., Jerman, G., and Wickramasinghe, N. C. (2013) 'Fossilized diatoms in meteorites from recent falls in Sri Lanka', *International Society for Optics and Photonics*: *SPIE Optical Engineering Applications*, pp. 886506-886506.

Miyake, N., Matsui, T., Wallis, J., Wallis, D. H., Samaranayake, A., Wickramarathne, K., and Wickramasinghe, N. C. (2013) 'Discovery of Uranium in Outer Coat of Sri Lankan Red Rain Cells', *Journal of Cosmology*, 22(4).

Wallis, J., Miyake, N., Hoover, R. B., Oldroyd, A., Wallis, D. H., Samaranayake, A. and Wickramasinghe, N. C. (2013) 'The Polonnaruwa meteorite: oxygen isotope, crystalline and biological composition', *arXiv preprint arXiv*, pp. 1303.1845.

Wallis, J., Wickramasinghe, C., Wallis, D., Miyake, N., Wallis, M., Di Gregorio, B. and Al Mufti, S. (2012) 'Discovery of Biological Structures in the Tissint Mars Meteorite', *J. Cosmology*, 18, pp. 8500-8505.

Wallis, J., Wickramasinghe, N. C., Wallis, D. H., Miyake, N., Wallis, M. K., Di Gregorio, B. and Hoover, R. (2012) 'Possible biological structures in the Tissint Mars Meteorite', *International Society for Optics and Photonics: SPIE Optical Engineering+ Applications*, pp. 85210R-85210R.

Wallis, J., Wickramasinghe, N. C., Wallis, D. H., Miyake, N., Wallis, M. K., Hoover, R. B. and Oldroyd, A. (2013) 'Physical, chemical, and mineral properties of the Polonnaruwa stones', *SPIE Optical Engineering+ Applications: International Society for Optics and Photonics*, pp. 886508-886508.

Wallis, J., Wickramasinghe, N. C., Wallis, D. H., Miyake, N., Wallis, M. K. and Hoover, R. B. (2014) 'Carbonaceous Core-Mantle Structures in the Tissint Martian Meteorite', *In Review.*

Wallis, J., Wickramasinghe, N. C., Wallis, D. H., Miyake, N., Wallis, M. K. and Hoover, R. B. (2014) 'Chemical and Structural Composition of Organic Carbonaceous Structures in Tissint: Evidence for a Biogenetic Origin', *In Review.*

Wallis, J., Wickramasinghe, N. C., Wallis, D. H., Miyake, N., Wallis, M. K. and Hoover, R. B. (2014) 'Evidence of Ancient Microbial Activity on Mars', *In Review.*

Wickramasinghe, N. C., Samaranayake, A., Wickramarathne, K., Wallis, D. H., Wallis, M. K., Miyake, N., Coulson, S. J., Hoover, R. B., Gibson, C. H. and Wallis, J. (2013) 'Living Diatoms In The Polonnaruwa Meteorite – Possible Link To Red And Yellow Rain', *Journal of Cosmology*, 21, 40.

Wickramasinghe, N. C., Wallis, J. H., Gibson, C. H., and Schild, R. E. (2010) 'Evolution of primordial planets in relation to the cosmological origin of life', *SPIE Optical Engineering+ Applications: International Society for Optics and Photonics*, pp. 78190D-78190D.

Wickramasinghe, N. C., Wallis, J., Miyake, N., Wallis, D. H., Samaranayake, A., Wickramarathne, K. and Wallis, M. K. (2013) 'Authenticity of the life-bearing Polonnaruwa meteorite', *Journal of Cosmology*, 21(39).

Wickramasinghe, N. C., Wallis, J., Wallis, D. H. and Samaranayake, A. (2013) 'Fossil diatoms in a new carbonaceous meteorite', *arXiv preprint arXiv*, pp. 1303-2398.

Wickramasinghe, N. C., Wallis, J., Wallis, D. H., Schild, R. E. and Gibson, C. H. (2012) 'Life-bearing primordial planets in the solar vicinity', *Astrophysics and Space Science*, 341(2), pp. 295-299.

Wickramasinghe, N. C., Wallis, J., Wallis, D. H., Wallis, M. K., Al-Mufti, S., Wickramasinghe, J. T. and Wickramarathne, K. (2013) 'On the cometary origin of the Polonnaruwa meteorite', *Journal of Cosmology*, 21(38).

Wickramasinghe, N. C., Wallis, J., Wallis, D. H., Wallis, M. K., Miyake, N., Coulson, S. G. and Hoover, R. B. (2013) 'Incidence of low-density meteoroids of the Polonnaruwa type', *arXiv preprint arXiv*, pp. 1303.2597.

Wickramasinghe, N. C., Wallis, M. K., Gibson, C. H., Wallis, J., Al-Mufti, S. and Miyake, N. (2010) 'Bacterial morphologies in carbonaceous meteorites and comet dust', In *Proc. SPIE*, 7819, pp. 781913.

Wickramasinghe, N. C., Wallis, M. K., Miyake, N., Wallis, J. and Wallis, D. H. (2013) 'Microfossils in the Polonnaruwa meteorite-evidence for a cometary ecosystem', In *European Planetary Science Congress 2013*, held 8-13 September in London: UK. Available at: http://meetings.copernicus.org/epsc2013, id. EPSC2013-690, 8, pp. 690.

Wickramasinghe, N. C., Wickramasinghe, J. T., Wallis, J., Hoover, R. B. and Rozanov, A. Y. (2012) 'Comets as parent bodies of CI1 carbonaceous meteorites and possible habitats of ice-microbes', In *SPIE Optical Engineering+ Applications: International Society for Optics and Photonics*, pp. 85210Q-85210Q.

Wickramasinghe, N., Wallis, J. and Wallis, D. (2013) 'Panspermia: Evidence from Astronomy to Meteorites', *Modern Physics Letters A*, 28(14).

Contents

Chapter 1

Evidence for Panspermia

1.1 EARTH-BOUND ABIOGENESIS

After more than a century of scientific research, the greatest biological enigma of all time – the origins of life – remains essentially unresolved. For more than two millennia, and well into the mid-19th century, the old Aristotelian doctrine of spontaneous generation held sway. Based on the precept that the ordinary formation of living organisms could routinely and spontaneously arise from inanimate matter, the theory took more than two hundred years of persistent scientific argument to finally dislodge - Francesco Redi in 1668, Pier Antonio Micheli in 1729, John Needham in 1745, Lazzaro Spallanzani in 1768, Joseph Priestley in 1803 and Charles Cagniard de la Tour and Theodor Schwann in 1837 - (Levine and Evers, 1999). Throughout this period, systematic challenges to the prevailing doctrine met heavy resistance from observers who interpreted such things as fleas appearing from dust, maggots from decaying flesh and even the seasonal appearance of mice from the clay of the Nile as unequivocal empirical evidence in support of the incumbent philosophy.

The matter was eventually settled by Louis Pasteur in 1859. By boiling meat broth in a swan neck flask he demonstrated a causal link between the presence of microbial spores in the air and the apparent generation of life in the culture. The implications of the discovery were encapsulated in the dictum later enunciated by Pasteur – *Omne vivum e vivo* – all life from antecedent life. The acceptance of this empirical fact however, led to the obvious question of origin. If life always derives from antecedent life in a causal chain, the question naturally arises as to when this connection ceased.

Consideration of this problem led swiftly to the transfer of interest from the old doctrine of spontaneous generation to an idea first introduced into Western Philosophy by Aristarchus of Samos (310-230 BC) – that of panspermia (seeds of life everywhere). The idea quickly attracted some influential scientific thinkers of the day. In his 1871 presidential address to the British Association for the Advancement of Science, Lord Kelvin stated "…we must regard it as probable in the highest degree that there are countless seed-bearing meteoric stones moving about through space. If at the

present instant no life existed upon this Earth, one such stone falling upon it might, by what we blindly call natural causes, lead to it becoming covered with vegetation".

These early ideas were later synthesised more coherently in a short paper by Nobel Laureate Svante Arrhenius (1903), and then later in his book entitled 'Worlds in the Making' (1908). Arrhenius demonstrated by experiment the survivability of seeds subjected to temperatures of nearly zero degrees Kelvin, which coupled with calculations on the effects of starlight radiation pressure on spores led him to argue that living particles could be successfully propelled from one star system to another. The idea attracted swift opposition, and in 1924 Becquerel (1924) mounted an attack on Arrhenius' views based on the perceived damage or deactivation of bacteria that would inevitably result from the action of ultraviolet radiation. The attack was widely accepted and has been used as a one-line disproof of the concepts of panspermia many times since.

We know now, of course, that the strident claims of Becquerel were wrong. From the 1940s onwards the emerging science of microbiology began to reveal a world of microorganisms capable of withstanding extremes of temperature and pressure as well as extraordinarily high doses of ultraviolet and ionising radiation. From *hyperthermophiles* that thrive in high-temperature, high-pressure oceanic thermal vents to *Deinococcus radiodurans* that repair radiation damaged DNA through single-stranded annealing and homologous recombination, research consistently revealed that some microorganisms were surprisingly space hardy.

Later work by Dombrowski (1963) demonstrated the viability of a strain of spore forming bacteria (similar to *bacillius circulans*) trapped in Permian age (254-271 Mya) NaCl salt crystals. Hoover and Pikuta (2012) extended this time frame by recovering viable spore forming bacteria from the interior of Sylvite and Halite crystals of age ~ 350 million years. Nonetheless, the effect of Bacquerel's intervention at the time was to divert attention from the theory of panspermia and open the way for the acceptance of a newly reformulated version of the old doctrine of spontaneous generation called the 'primordial soup' theory.

The ideas behind the 'Primordial Soup' theory were formally consolidated in the late 1920s when it was first proposed by Oparin (1953) and Haldane (1929). Here, the primitive Earth atmosphere comprised of a reducing mixture of methane, hydrogen, ammonia and other compounds. The energy to dissociate these molecules was provided by solar ultraviolet and lightening, and the radicals thus formed recombined through a cascade of chemical reactions to produce biochemical monomers such as amino acids, sugars and nucleotide bases from which life subsequently arose.

Within decades of the emergence of the "Primordial Soup" theory the viability of the Oparin-Haldane chemistry was illustrated with the ground-breaking experiments of Miller and Urey (1959). Simple organic compounds were successfully synthesised in an experiment that replicated the presumed conditions of primordial Earth; a gaseous mixture of CH_4, NH_3, H_2 and H_2O was circulated in a flask, subjected to electric discharges and the mixture continuously filtered for high molecular weight compounds. Trace quantities of biologically relevant organics were detected (glycine, alanine, α-aminobutyric acid and others). Similar experiments were repeated by others who altered the source of energy that initiated the mixture into free radicals thus altering the propagation mechanisms and subsequently the products leading to a whole host of relevant molecules such as adenine, ribose and deoxyribose.

The success of the Miller-Urey experiments originally led to the conviction that it was only a matter of time before the next step from biochemical monomers to life could be demonstrated in the laboratory. Despite over half a century of continued effort however, this goal has proven stubbornly elusive, and it is now generally accepted that the path from chemicals to self-replicating biology must progress through a sequence of organisational steps of ever-increasing complexity. By the early 1960s, gaining insight into the likely processes affecting the first of these steps became a high priority for biologists.

Early work by Bernal (1951) had already considered the prebiotic replication of complex organic molecules on mineral surfaces. The catalytic activity of such mineral complexes had been utilised for some time in the petrochemical industry, but by the late 1950s, its potential importance in nature attracted increasing interest. Bernal's attention had been drawn to clay minerals and particularly to the smectite and montmorillonite type of expanding clay minerals that permit intercalation of exchangeable cations and polar molecules as interlayers forming an integral part of the crystal structure. Extensive work then followed that demonstrated the efficiency with which clay mineral surfaces lower the activation energy for reaction between organic molecules and in 1966 Cairns-Smith (1966) proposed the "Clay World" hypothesis involving an inorganic clay system serving as a primitive informational template.

A number of alternative mechanisms for the transition of organic molecules have since been proposed. All of these contain a complex chemical lattice as the first template in the progression to life such as the "RNA-World Hypothesis" (Woese (1967); Gilbert (1986)). Here, nucleotides polymerise into random RNA molecules that lead to autonomously self-replicating macromolecules (ribozymes) without the need for an intermediary enzyme (Orgel, 1968 and Crick, 1968).

Similar mechanisms such as the "PAH-World Hypothesis" suggest that layers of complex poly aromatic hydrocarbons (PAH's) form the lattice structure. This hypothesis is of interest to discussions on mechanism because of the identical distance between layers of PAH's and nucleic acids within RNA (0.34nm) (S.N Platts, 2005). Other contenders of prebiotic development include the "Iron-sulphur World" (Wachterchauser, 1990) and the "PNA (Peptide Nucleic Acid) World" (Bohler et al, 1995). The progression from these intermediate systems to protogene systems possessing prescriptive information for evolution, and finally to DNA-protein-based cellular life however, remain to this day in the realm of speculation or hypothesis.

At about the time the "Clay World" hypothesis was first attracting interest however, a contribution to the enigma of the origins of life was to come from astronomers who had been working for over three decades on the high priority problem of constraining the composition of cosmic dust particles. These particles occupy the immense voids between the stars of the Milky Way, and appear as a dense cosmic fog capable of obscuring the light of distant stars. Of interest to astronomers was that the physical and chemical characteristics of the dust grains in these clouds appeared to be roughly the same irrespective of the direction they were observed. Of further interest was that the total mass of interstellar dust in the galaxy required nearly all the available C, N and O in interstellar space to be condensed in the grains, and was about three times too large for the grains to be *predominantly* composed of the next commonest elements Mg and Si.

1.2 INTERSTELLAR GRAINS

During the early 1960s the prevailing theory on interstellar grains was that they comprised of dirty ice particles that had nucleated and grown in the tenuous clouds of interstellar space. The first reliable signs that this was incorrect came with the proposition that graphite grains were being formed in the atmospheres of carbon stars (Hoyle and Wickramasinghe, 1962). This led scientists to search for a grain model that agreed with available remote sensing data. Initial research centred on the absorption and scattering properties of the dust that resulted in the extinction of light from stars and the subsequent re-emission of the absorbed radiation in the infrared. At the time (and until 1965) reliable data on the extinction of starlight by cosmic grains was constrained to the $1.25 \leq \lambda^{-1} \leq 2.9$ μm wavelength range, and appeared to be comprised of two straight line segments intersecting at $\lambda^{-1} = 2.3$ μm, with the near ultraviolet contribution having about a 30 percent lower gradient than that at the longer wavelength (Nandy 1964).

This observation was consistent with the hypothesis of absorption by graphite or graphite core-ice mantle grains (Nandy and Wickramasinghe, 1965). At about this time, the further discovery of an

extinction feature at λ 2200 Å (Stecher, 1965) that broadly matched predictions for small spherical graphite particles led to the conclusion that cosmic grains were both refractory and carbonaceous and the prevailing paradigm was that the dust largely comprised of either graphite, composite core-mantle grains of graphite and water-ice (or predominantly water ice).

During the years that followed, a number of observations were made that somewhat disrupted this thinking. Despite considerable effort, a significant absorption feature near 3.1μm for crystalline ice of in excess of 30,000 cm^{-1} (Bertie *et al*., 1969) was in wild disagreement with observational data and in many cases suggested a mass fraction contribution of water ice grains of no more than about 1 part in 700.

Furthermore, the advent of observations in the infrared led to the discovery of a 10 μm spectral feature in the Trapezium Nebula that was more consistent (though only approximately) with the spectral characteristics of silicates. Initial enquiries focused on a graphite-silicate grain mixture (Hoyle and Wickramasinghe, 1969) though the amount of silicate required to produce observed spectral features contradicted, by orders of magnitude, cosmic ray abundance data.

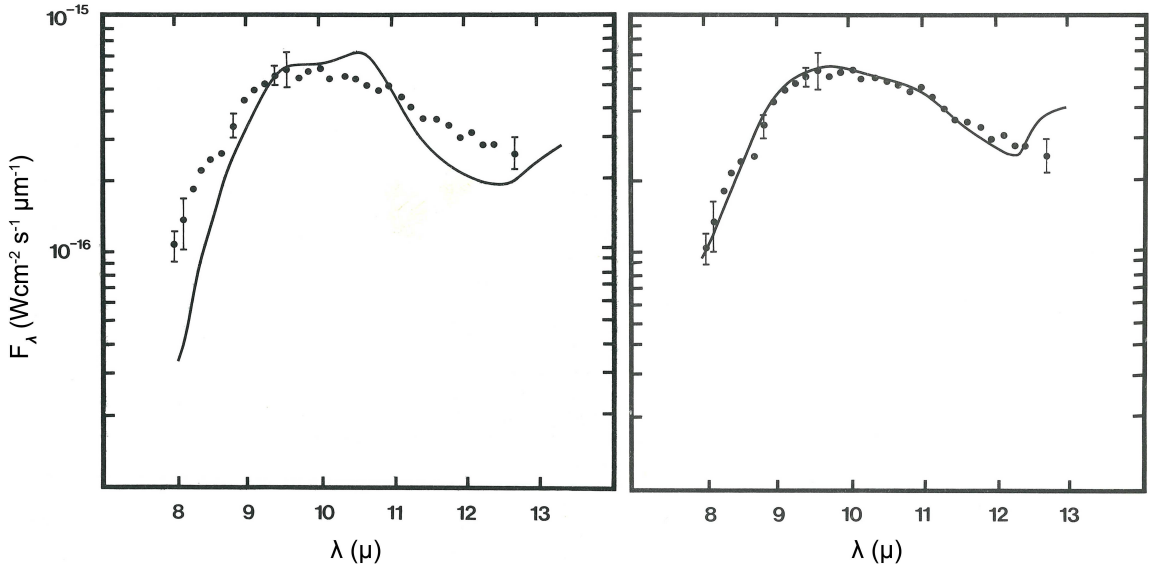

Figure 1.1 Shows the observed flux from the Trapezium Nebula (Forrest *et al.,* 1975a, b) compared to (left panel) the behaviour of a silicate sample comprising of moon rock heated to 175^{o}K and (right panel) the behaviour of biological grains at a temperature of 175^{o}K. Normalisation of the curve is to F = 6 x 10^{-16}W cm^{-2} s^{-1} at λ = 9.5 μm (Hoyle *et al.,* 1982).

Over time, details of the interstellar extinction curve improved in accuracy while the 10 μm spectral feature, observed in a number of astronomical sources, defied explanation by silicate materials alone.

This situation did not improve with time. Astronomical data was gathered for a wide range of wavelengths, from 30 μm in the infrared, through the near infrared and visible spectrum, and on into the ultraviolet. As new data steadily accumulated, grain composition models that fitted one aspect of the data were readily shown to be in contradiction of other aspects. It soon became apparent that the problem of constraining the composition of cosmic dust was proving to be remarkably intractable. However, in 1974 another class of materials comprising of the four commonest elements of carbon, nitrogen, oxygen and hydrogen were recognised as a potential alternative – namely organic materials (Wickramasinghe, 1974).

Initial investigations into the possible role of polymeric type organics were immediately encouraging. Previous comparisons of the observed flux of the Trapezium Nebula with silicate grains were greatly improved with comparative predictions for a polyformaldehyde grain model (Wickramasinghe, 1974), and still further improved by using the properties of polysaccharides (Hoyle and Wickramasinghe, 1977).

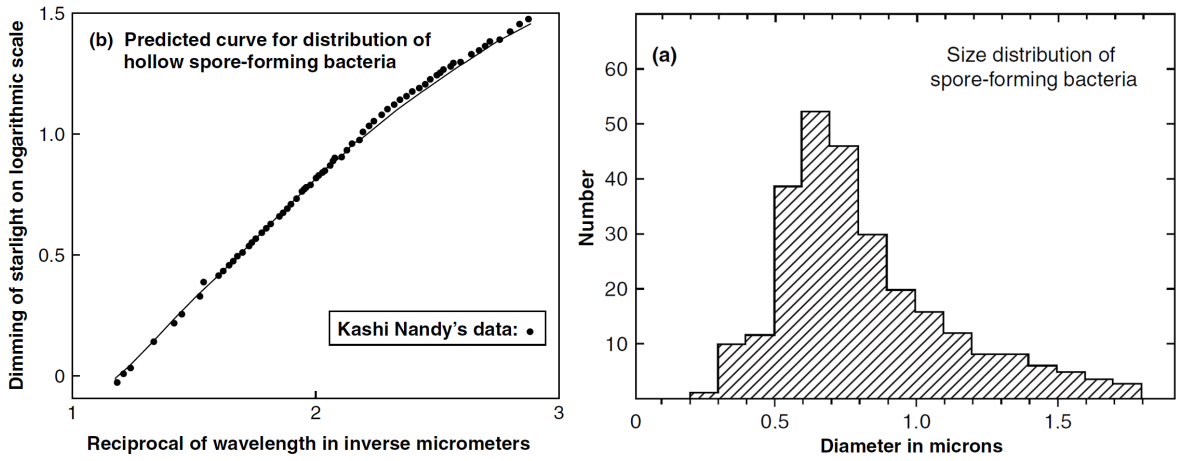

Figure 1.2 (Left panel) shows the visual extinction of starlight normalized to $\triangle m$ = 0.409 at λ^{-1} = 1.62 μm^{-1} and $\triangle m$ = 0.726 at λ^{-1} = 1.94 μm^{-1} (Nandy, 1964) together with the calculated extinction curve utilising classical Mie theory for hollow bacterial grains comprised of organic material with refractive index n = 1.4 with 60% vacuum cavity caused by the removal of free water. The size distribution of terrestrial spore-forming bacteria as given in the histogram in the right panel is used for grain distribution sizes.

It further transpired that a large class of aromatic molecules, (e.g. quinoline and quinozoline) also exhibited a broad absorption feature centred at λ2200 Å that for the previous decade had been attributed to graphite. Furthermore, the spectra of several infrared sources associated with molecular clouds indicated the presence of a possible absorption feature near 3.4 μm. These included the BN Nebular (Gillett and Forrest, 1973), CRL 2591 (Merrill and Soifer, 1974), NGC 2264IR and CRL 490 (Merrill, Russell and Soifer, 1976), OH 01-477 (Wickramasinghe and Allen, 1980) and the galactic centre source IRS 7 (Soifer, Russell and Merrill, 1976; Wickramasinghe and Allen, 1980; Allen and Wickramasinghe, 1981).

The spectrum of GC-IRS7 was of particular interest because this source revealed a highly detailed absorption profile extending over the wavelength region $2.9 \leq \lambda \leq 3.8$ μm that was indicative of combined CH, OH and NH stretching modes. Previous suggestions concerning the nature of the material included carbonaceous compounds (Knacke, 1977), a polysaccharide model (Hoyle and Wickramasinghe, 1977) as well as various chemical functional groups bound at reactive sites on carbon grains (Duley and Williams, 1981).

In 1982 Hoyle and Wickramasinghe extended their observations of the Trapezium Nebular to include an analysis of the GC-IRS7 spectrum. By comparing a laboratory acquired spectra of the desiccated bacterium *E. Coli* they used a simple modeling procedure to demonstrate an exceedingly close point-by-point match to astronomical data over the entire GC-IRS7 $2.0 \leq \lambda \leq 4.0$ μm waveband (figure 1.3) (Hoyle *et al*, 1982). This led them to conclude that a large fraction of interstellar dust was spectroscopically indistinguishable from freeze-dried bacterial material (in combination with their degradation products).

At about the same time, two scientists with NASA Goddard Space Flight Centre had been attempting to synthesise organic residues with dominant infrared signatures near the 3.4 μm and 9.9 μm absorption wavelengths in accordance with those observed in GC-IRS7 and OH 01-477 (Moore and Donn, 1982). Here a gaseous mixture of H_2O+NH_3+CH_4 was deposited onto a low temperature (20K) aluminium mirror to form a film ≤ 5 μm thick and the ice irradiated with 1 MeV protons. The total amount of energy absorbed was estimated to be equivalent to that absorbed by the outer layers of a comet in the Oort cloud in $\sim 2 \times 10^9$ yr. The infrared spectrum of the residue for $2.5 \leq \lambda \leq 15$ μm was then measured.

Moore and Dunn reported close adherence to the observed interstellar absorption feature in the 3.4 μm region. By way of a *note added in proof* they further maintained that the spectrum of the laboratory-synthesised residue matched closely that of *E. Coli* and that since these were the input

parameters utilised in the Hoyle *et al.*, (1982) theoretical model, it followed that their abiotically generated residue would similarly match, and as such was a much more plausible candidate for the 3.4 μm absorption feature than dried microorganisms.

This observation however, did not stand up to objective scrutiny. By photographically enlarging Moore and Dunn's key figure to a scale sufficient to obtain transmittance values to one and a half decimal accuracy, Hoyle and Wickramasinghe (1984) compared the spectra for laboratory measured *E.Coli* with that of the laboratory-synthesised residue. Substantial variance between the spectra was apparent, calling into doubt the validity of Moore and Dunn's statement. Subsequent claims by Kroto (1983), suggesting that an acyclic sesquiterpene alcohol named Farnesol exhibited spectra similar to *E. Coli* were similarly examined and shown to be inaccurate (Hoyle and Wickramasinghe, 1984).

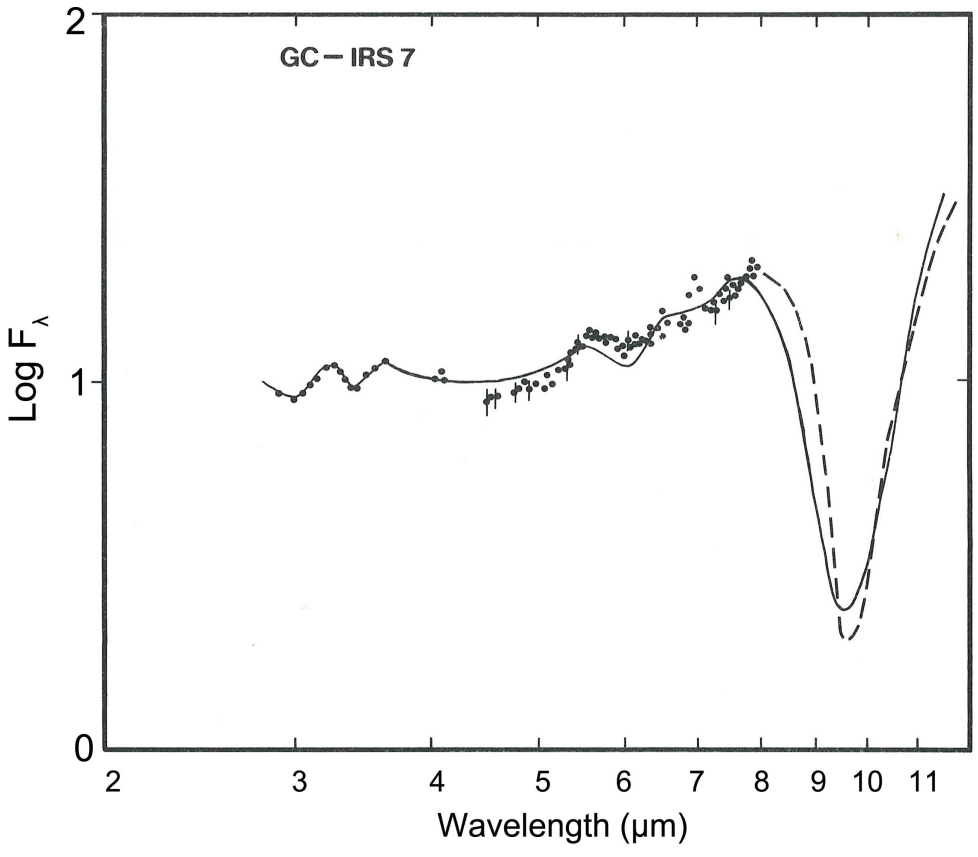

Figure 1.3 The observed flux from GC IRS7 shown as dots from Allen and Wickramasinghe (1981) for the spectral range $2.9 \leq \lambda \leq 3.8$ μm and from Willner *et al.*, (1979) for the $3.9 \leq \lambda \leq 13$ μm range. The solid line is the calculated flux of dried diatomaceous organisms (Hoyle *et al.*, 1982).

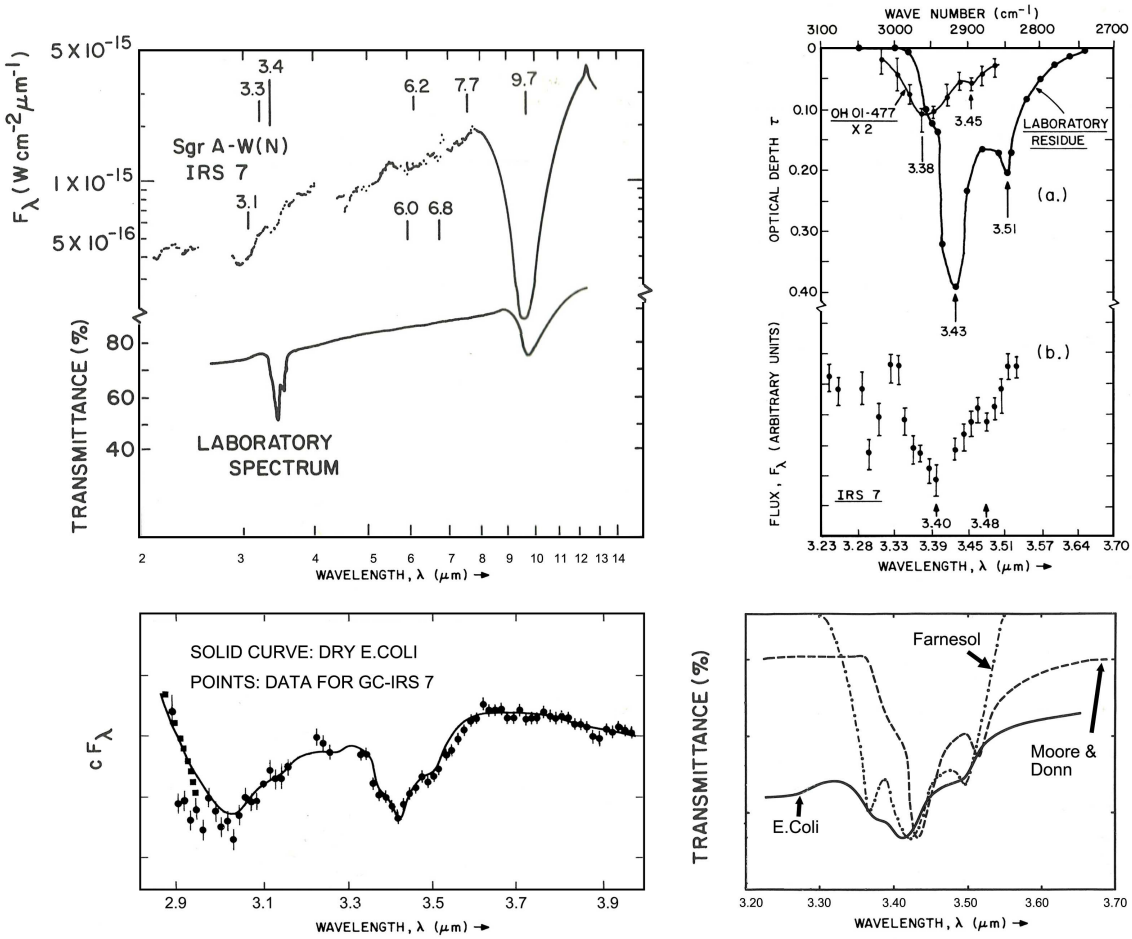

Figure 1.4 (Upper left) shows infrared spectrum of the laboratory residue of Moore and Donn, (1982) compared to the spectrum of IRS 7 for $2 \leq \lambda \leq 15$ μm. (Upper right) shows similar comparison for OH 01-477 for wavelength region $3.23 \leq \lambda \leq 3.70$ μm (Moore and Donn, 1982). Bottom left panel shows comparison of observed reflective flux from GC IRS7 compared to predictions for bacterial model (Hoyle *et al.,* 1982). Bottom right panel shows a comparison between the transmittances measured for E.coli (Solid curve) Moore and Donn sample B (dashed curve) and Farnesol (dot-dash curve) normalised to correspond at minima of 3.4 μm (Hoyle and Wickramasinghe, 1984).

After many decades of enquiries into the composition of interstellar dust, attention inevitably returned to the possibility that life had a cosmic origin. Such considerations had previously been entertained on purely probabilistic grounds, where early calculations suggested astronomically small *a priori* Earth-bound probabilities for randomly obtaining the required set of enzymes for even the simplest living cell. These alone suggested that Earth as life's place of origin could be safely ruled out and was more clearly rooted in the spatially and temporally vaster expanse of the universe. These early arguments have persisted and have now been more comprehensively augmented by Abel and Trevors (2006) and Abel (2009) who suggest that within the framework of Big-Bang type cosmologies, naturalistic protogene formation faces almost insuperable difficulties.

1.3 COMETARY PANSPERMIA

Until the early 1980s, previous attempts to develop the fundamentally philosophical concept of panspermia into an entirely coherent scientific hypothesis had been largely unsuccessful. Arrhenius had argued that electromagnetic effects lifted bacterial cells from the gravitational potential wells of their planets and dispersed them through space by the radiation pressure of stars. For sub-micron sized particles, he demonstrated that the radiation pressure could be substantial, and that particles could attain speeds of ~100 km/s, thereby traversing the distances between interstellar gas clouds in ~100,000 years. A number of difficulties arose with this model however, not least the requirement for expelled grains to overcome the radiation pressure of encountered stars, and in the end even Arrhenius had to admit that the available mechanisms for defeating this problem alone would render the transfer of living material by interstellar panspermia at best a rare event.

However, while the potential for bacteria to survive the harsh conditions of space had been repeatedly demonstrated, the immense power of bacterial replication also began to bear on viability arguments. Given appropriate conditions, a single bacterium with a doubling time of two to three hours would generate a population of $\sim 2^{40}$ offspring in four days occupying a total volume of a few cubic centimetres. Four days later, that volume would increase to the size of a small swimming pool and just four days after that to the size of the Mediterranean Sea. Given an appropriate supply of nutrients, it would take just sixteen days for a single bacterium to grow to a mass comparable to that of a molecular cloud like the Orion Nebula (Hoyle and Wickramasinghe, 1999). Nonetheless, it was recognised that bacteria continually exposed to ultraviolet and ionising radiation in the open regions of interstellar space would inevitably be subject to degradation and eventual destruction culminating in the release of free organic molecules and polymers. The hypothesis that interstellar space was populated with a significant fraction of viable bacterial cells was accompanied by an inevitable component of decay within the model itself.

The link between the formation of comets from interstellar dust, the suitability of their physical composition as potential incubators of microbial life, and their dynamical behaviour as subsequent distributors of that life remains at the heart of the theory of cometary panspermia. The sheer numbers of comets more than compensates for their apparent inconsequentiality when considered in isolation. The present-day Oort cloud contains some 100 billion individual comets and their total mass is comparable to the combined masses of the outer planets Uranus and Neptune ($\sim 10^{29}$g). With about 10^{11} dwarf stars in the galaxy, the total mass of cometary matter is somewhere in the order of $\sim 10^{40}$g, close to the mass of all interstellar grains.

The theory of cometary panspermia proposes that interstellar matter contains a minute quantity of viable biological material distributed by a previous generation of comets. As new star systems form, comets condense, first in the cooler outer regions, resulting in the assimilation of a small quantity of these viable microorganisms. Radiogenic heating maintains a warm liquid interior within the comet for the large part of a million years, providing adequate time for the surviving fraction of interstellar microbes to replicate and fill a substantial volume fraction of the comet. As a stellar or planetary system develops, collisions between cometary bodies result in the expulsion of a fraction of regenerated bacteria back into interstellar space, maintaining a density distribution of fresh biological particles. A fraction of comets would also be deflected into the inner regions of the system and would release quantities of bacteria thus carrying microorganisms to the inner planets. As new stars and star systems form, the whole cycle continues, thus producing and distributing an on-going supply of biologically viable entities.

The theory of cometary panspermia predicts a causal chain that falls within the scope of modern scientific observations, and as such, should be relatively easy to establish or disprove. Firstly, if comets do indeed serve as incubators of biology, then it follows that a significant component of their total mass fraction would comprise of organics, and that some element of this organic component would be expelled into the surrounding space. This implies that *cometary grains are organic* in nature. Secondly, the large-scale distribution of such a component into the interstellar medium would imply that a proportion of interstellar dust particles are either biological, or comprise of the degradation products of biology resulting from long periods of radiation exposure and the inevitable break-up of high molecular weight organic molecules. This would mean that a component of *interstellar dust particles are organic in nature.* Thirdly, the continuing input of cosmic material to Earth implies that *panspermia is an ongoing process,* continually adding biological and organic material to the Earth's ecosystem. Fourthly, the presence of large-scale reservoirs of organic material in interstellar dust, from which planetary systems are subsequently formed, implies the widespread distribution of biology within our own neighbouring solar system bodies, the presence of which would be included in meteoritic material accumulated on the surface.

1.4 THE ORGANIC NATURE OF COMETARY GRAINS

At the time the theory of cometary panspermia was first proposed, cometary grains were believed to largely comprise of silicates and water-ice. This was in sharp contrast to the implications directly arising from the theory itself. The first confirmation of a cometary dust composition similar to organics came with the detection of a 3.4 μm emission feature in the dust from comet Halley (Wickramasinghe and Allen, 1986). This was later confirmed by independent observations (Danks

et al., 1986; Knack *et al*., 1986; Bass *et al*., 1986; Tokunaga *et al*., 1987) though quantitative comparisons of the entire data set was difficult due to differences in telescope aperture size and spectral quality (Wickramasinghe *et al.*, 1987).

These observations however, did demonstrate concurrence in the detection of a broad emission feature over the wavelength interval $3.28 \leq \lambda \leq 3.6$ μm. Features in the $3.28 \leq \lambda \leq 3.39\mu$m waveband region were normally associated with the C-H aromatic bond while features in the $2.4 \leq \lambda \leq 3.6$ μm waveband were known to be characteristic of organic solids with further specific absorptions and emissions at 3.36 μm normally attributed to the aliphatic bonds (C-H) in saturated hydrocarbons.

Predictions for a biological model involving *E.Coli* heated to 320K for the wavelength $2.8 \leq \lambda \leq 4$ μm showed close adherence with the observed data, but whilst there was no dispute as to the general conclusion that these must originate from the superposition of functional groups involving CH, it was argued that the fit, in itself, was not a unique indicator of the presence of bacteria. It was hoped however, that the matter would be settled by the direct analysis of comet dust that was carried out on board the Giotto spacecraft. Here, dust particles from comet Halley impacted an on-board mass spectrometer at speeds of ~30 km/s (Kissel and Krueger, 1987).

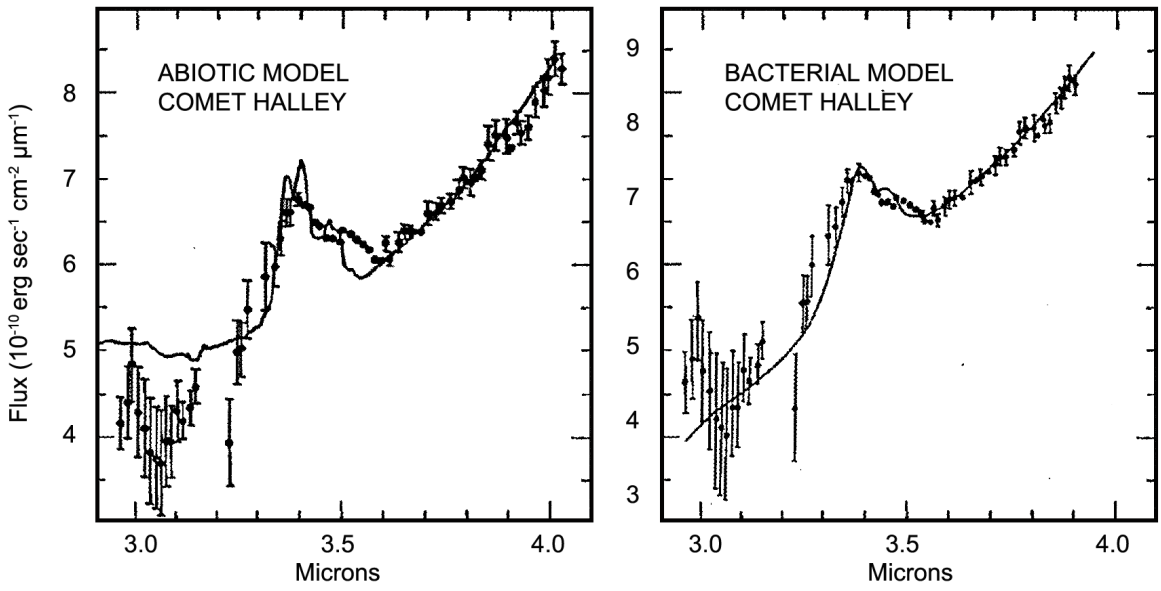

Figure 1.5 Observational data for dust from Comet Halley (Wickramasinghe and Allen, 1986) compared to predictions for (left panel) abiotic and (right panel) biological model involving *E.Coli* heated to 320K. (Wickramasinghe, 2002).

Analysis of the masses of break-up products showed a large fraction of the grains to be organic "CHON" particles with compositions that included long-chain hydrocarbons and nitrogenated polyaromatic molecules.

Though these molecular structures were fully consistent with the break-up of bacterial cells, this was initially rejected because the break-up material did not show evidence of the biologically important element phosphorus. However, it was quickly argued that the molecular ion-mass spectra of Kissel and Krueger (1987) did indicate plausible combinations of P with other elements. The break-up of phosphorus groups (as in DNA) could lead to possible mass peaks corresponding to PO_3^+ (79), PO_2^+ (63) or PO^+ (47) rather than P^+ (31). The further claim that mass peaks corresponding to two other biologically significant elements Na and K were too low for biology was also challenged. Although cultures of freeze-dried vegetative bacteria may be ~100 times richer in Na and K, it was argued not to be the case for nutrient starved bacteria nor for spores (Hoyle and Wickramasinghe, 1993).

Since the exploration of comet Halley, new infrared spectra of cometary dust has consistently shown close adherence with predictions for an organic-biological grain model. Furthermore, growing evidence that the composition of cometary dust is very similar to that of interstellar dust has also been mounting.

Spectral features near 19, 24, 28 and 34 μm observed by the ISO (Infrared Space Observatory) have been attributed to hydrated silicates in a number of protoplanetary disks as well as in comet Hale-Bopp (Matsuoka et al., 2011; Crovisier et al., 1997). In both cases, it has been shown that the contribution of hydrated silicates (established from the principal infrared bands) can only make up a few percent of the mass of the dust, the remainder being largely organic (Wickramasinghe, 1967). This is consistent with the observed infrared flux curve of comet Hale-Bopp, obtained by Crovisier et al., (1997) when the comet was at a heliocentric distance of 2.9 AU.

The dashed curve in Figure 1.5 shows predictions for a mixed culture of microorganisms containing about 20% by mass in the form of diatoms. The much higher mass absorption coefficient within the absorption bands of olivine dust contributes 10% by mass in this model. Similarly, the *Stardust* mission to comet Wild 2 launched in 1999 captured dust from the tail of the comet in blocks of aerogel.

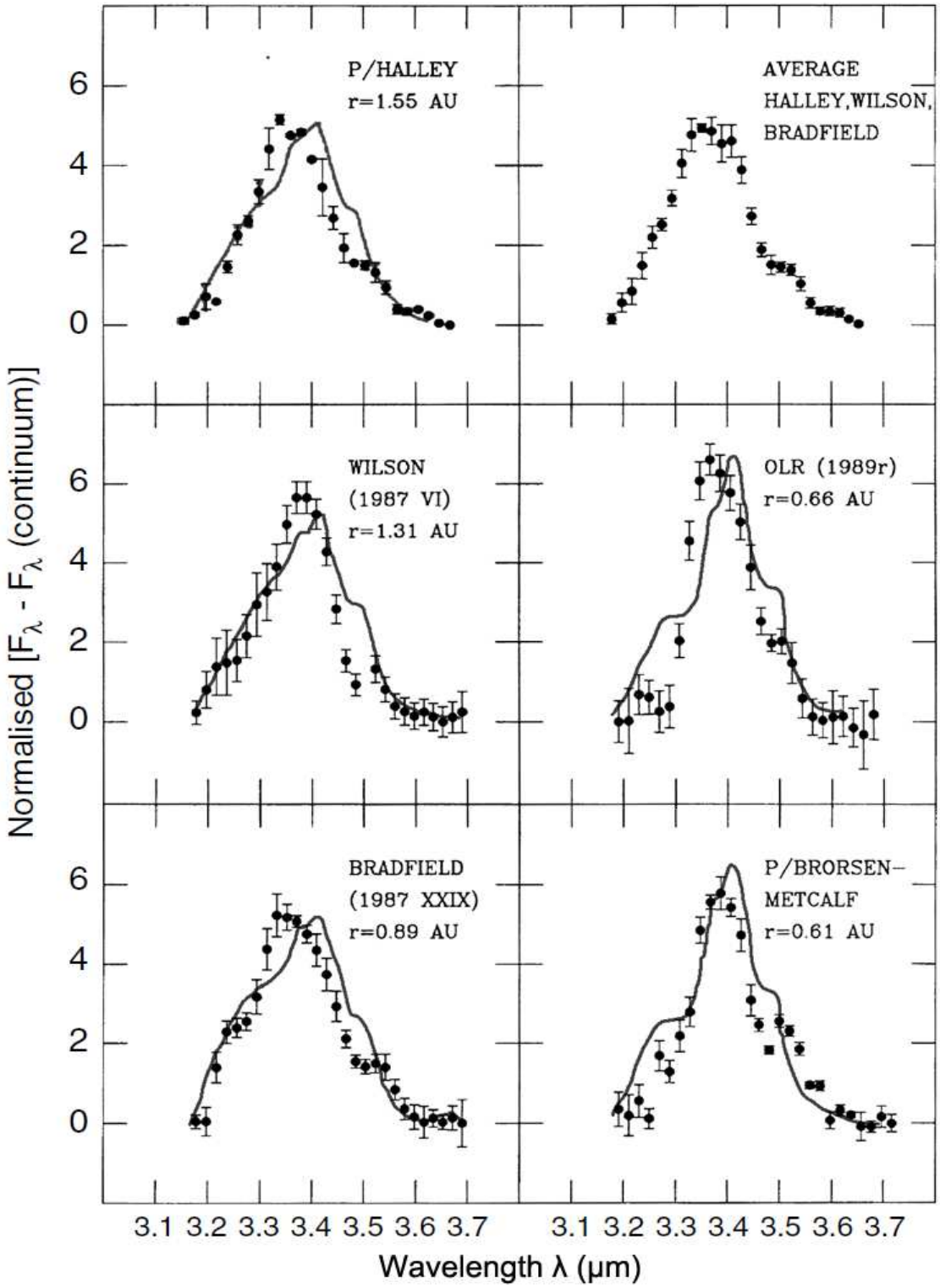

Figure 1.6 Spectral profile of the emission feature in comets P/Halley, Willson 1987 VII, Bradfield 1987 XXIX, Okazaki-Levy-Rudenko 1989 and Borsen-Metcalf (Brooke *et al.*, 1991) for the wavelength interval $3.1 \leq \lambda \leq 3.7$ μm. In each case the continuum was subtracted and the points normalised. Solid curves represent proposed models involving bacterial grains (Festou *et al.*, 1993).

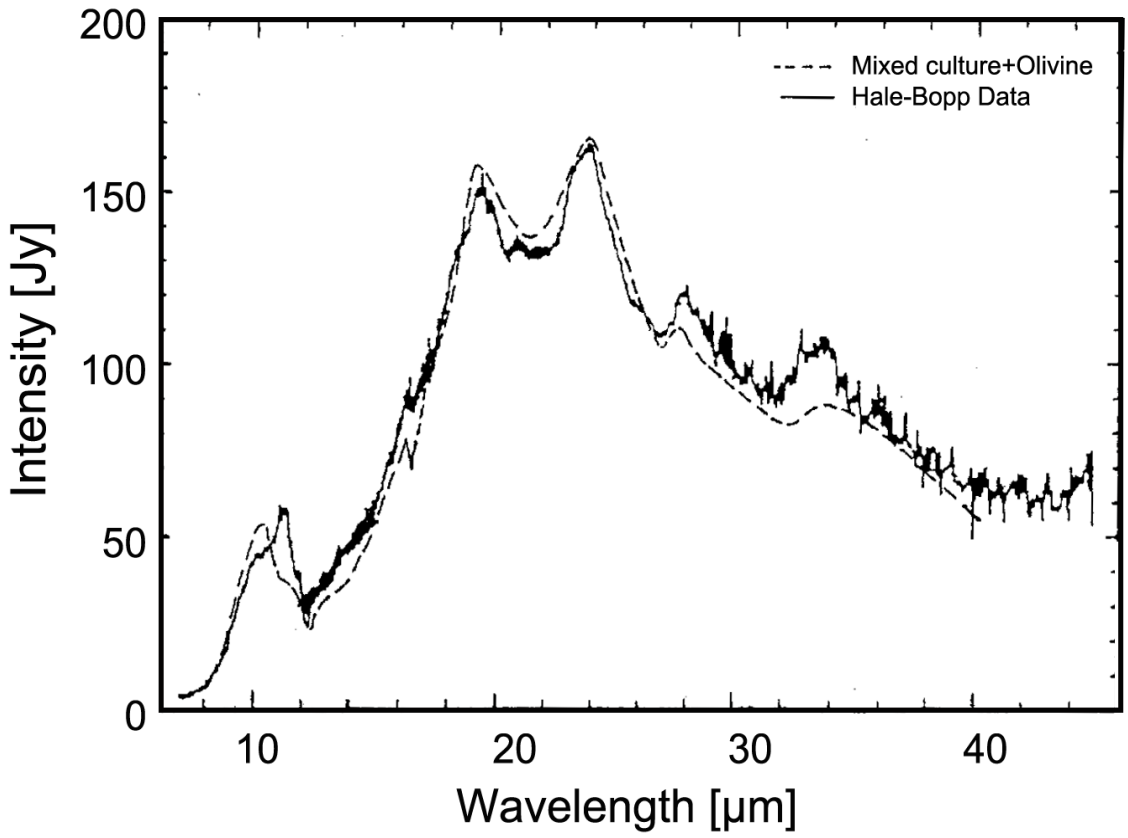

Figure 1.7 Shows **t**he infrared radiation from Comet Hale-Bopp at a heliocentric distance of 2.9 AU as observed by Crovisier et al. (1997) (solid line) together with (dashed curve) normalized spectrum calculated for a mixture of a bioculture, containing about 20% by mass in the form of diatoms, and olivine dust. The olivine is assumed to have a temperature of 175 K and the bioculture a temperature of 200 K corresponding to a mass fraction of about 10% olivine (Hoyle and Wickramasinghe, 1999).

Unfortunately, the mission and experiments were planned in the decade that preceded the launch at a time when cometary microorganisms were entirely dismissed as a reasonable possibility. Consequently, the procedures utilised for particle collection would not have allowed the survival of intact cells with particles impacting the aerogel at an initial speed of ~6km/s and excavating a track along which break-up debris was deposited.

Subsequent analysis showed that along the tracks a wide range of organic molecules including the amino acid glycine was discovered. The presence of heteroaromatic molecules rich in N and O is a plausible indicator of degraded biomaterial, biology being particularly rich in such structures. Further evidence of fragments with atomic mass units greater than 2000, consistent with the presence of pyrrole, furan sub-structures and quinines were also found. The subsequent *Deep Impact* mission to comet Temple 1 involving a high speed impact that crashed and ruptured the

comet's surface similarly found evidence of water and a range of organics as well as, for the first time, clay particles.

1.5 THE ORGANIC NATURE OF COSMIC GRAINS

From the 1990s onwards a range of high resolution infrared spectra were obtained from a variety of astronomical sources, and interest again returned to the broad emission feature over the wavelength $3.28 \leq \lambda \leq 3.6$ μm.

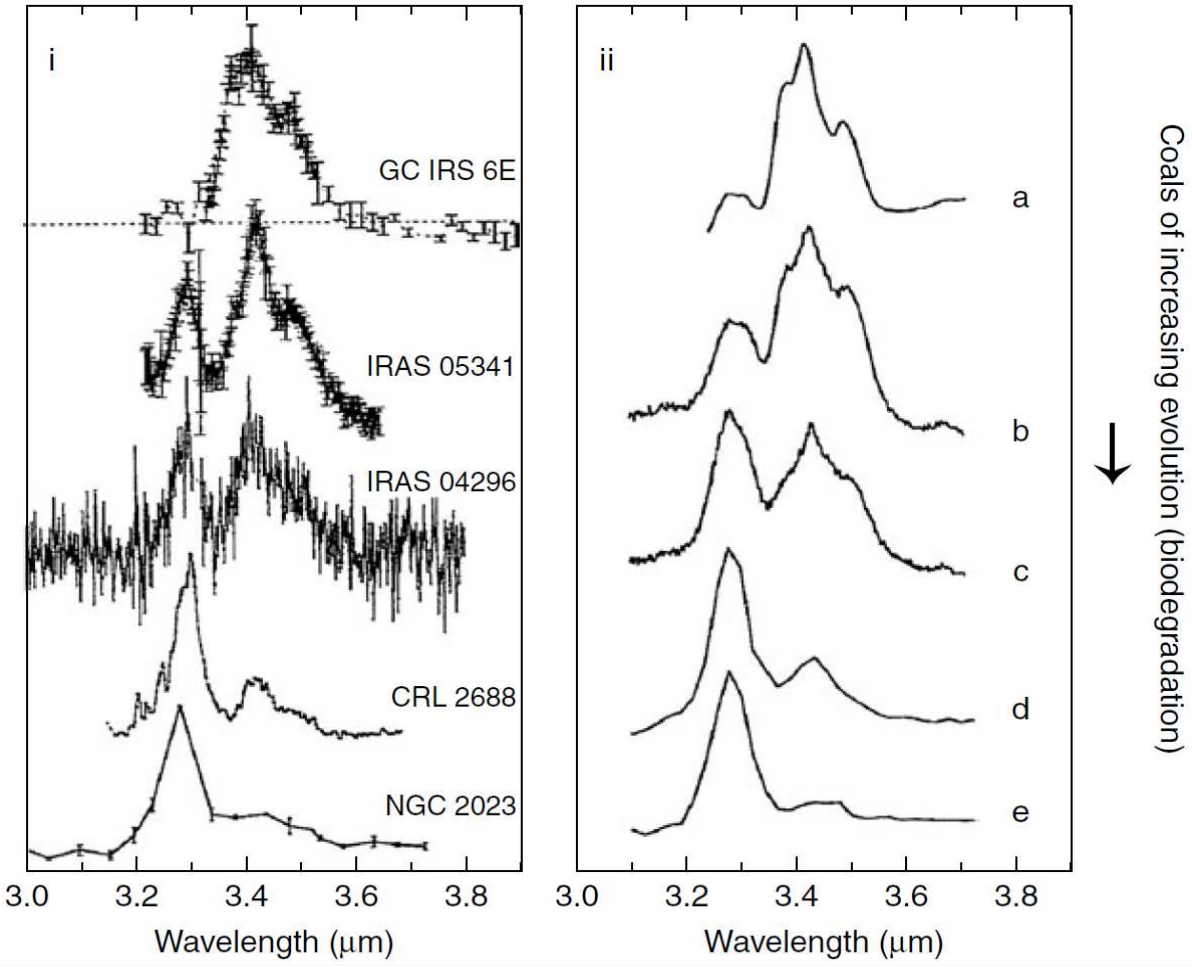

Figure 1.8 (Left Panel) Normalised absorption profiles for the five galactic infrared sources GC IRS 6E, IRAS 05341, IRAS 04296, CRL 2688 and NGC 2023 for the wavelength interval $3.0 \leq \lambda \leq 3.8$ μm. (Right Panel) Spectra of coals of varying degrees of degradation (a) being the closest to desiccated bacteria. The various spectra for coal are close fits to the observed absorption profiles for the several galactic infrared sources.

Several spectroscopic observations taken from GC IRS 6E, IRAS 05341, IRAS 04296, CRL 2688 and NGC 2023 showed coincidence with similar spectroscopic observations made of comets P/Halley, Wilson, OLR, Bradfield and P/Brorsen-Metcalf (see Figure 1.6).

However, unlike the spectroscopic observations of the several comets examined that demonstrated some degree of concurrence in the absorption feature, those of distant infrared sources exhibited a degree of variation. These features were quickly identified as being indicative of the degradation of biology, with coals of increasing biodegradation providing excellent fits to all sources. Figure 1.8 shows infrared sources over the $3.0 \leq \lambda \leq 3.8$ μm wavelength region together with corresponding spectra for increasingly degraded coals.

By the late 1990s attention turned to the extended red emission (ERE) of interstellar dust that showed up as a broad fluorescence emission band over the range λ5000Å – λ7500Å. Of particular interest was that EREs were observed in dark nebulae (Mattila, 1979), planetary nebulae (Furton and Witt, 1992), HII regions (Sivan and Perrin, 1993), and in extragalactic systems (Perrin, Darbon and Sivan, 1995; Darbon, Perrin and Sivan, 1998) as well as in high latitude cirrus clouds (Szomouru and Guhathakurta, 1998).

Here, an optical spectroscopic survey was found to include a broad peak at λ6000Å consistent with PAH type organic grains. Competing models based on emission by compact PAH systems were generally unsatisfactory. Hexa-peri-benzocoronene - one of a class of compact polyaromatic hydrocarbons was discussed extensively in the astronomical literature but it displayed an inconsistent match in terms of the width and central wavelength of its fluorescent emission. Hoyle and Wickramasinghe (1996) and Wickramasinghe *et al*. (2002) argued that it was unlikely that these would be forming in the very low density - high radiation intensity conditions, and suggested instead that the feature may represent infalling primordial planets, breaking up and releasing organic compounds. This phenomenon was a self-consistent explanation on the basis of fluorescence of biological chromophores (pigments), e.g. chloroplasts and phytochrome. Figure 1.10 shows the normalised excess flux over scattering continua from Furton and Witt (1992) and Perrin *et al.,* (1995) together with the fluorescence spectrum of hexa-peri-benzocoronene and relative fluorescence intensity of spinach chloroplasts at a temperature of 77K.

During the same period it was also observed that infrared emissions of the Antennae galaxies some 63 million light years away were found to match the laboratory spectrum of anthracite (Guillois *et al.*, 1999), this being a product of biological (bacterial) degradation. Later, Caltaldo, Keheyan and

Heyman (2002) demonstrated that aromatic distillates of petroleum, another biological product, exhibited correspondences with the astronomical diffuse infrared bands (DIBs) as well as the λ2175 Å ultraviolet extinction feature. By the turn of the millennia, the λ2175Å band feature had also been identified in the lens galaxy of the gravitational lens SBS0909+532 which has a redshift of $z = 0.86$ – some 7 to 9 billion light years away (Motta *et al.*, 2002).

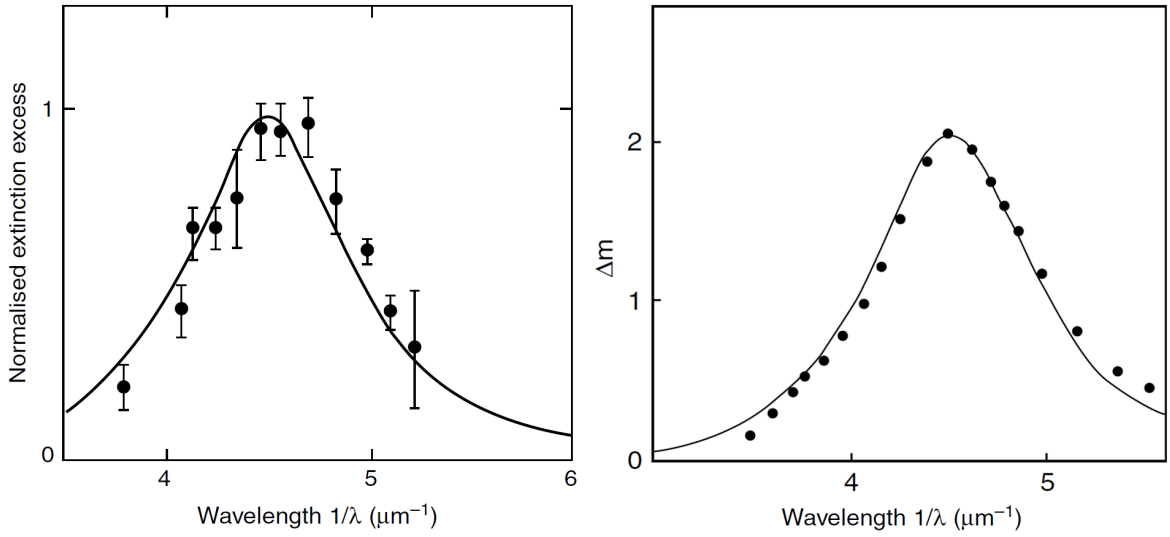

Figure 1.9 (Left Panel) Observations for the galaxy SBS0909 + 532 (Motta *et al.*, 2002). Dots represent total extinction from which an underlying bacterial scattering component has been subtracted. Solid line is the normalised absorption coefficient of an ensemble of 115 biological aromatic molecules (Wickramasinghe 2010). Right Panel - same, but for our galaxy.

UIBs	PPNe	Algae	Grasses	Bituminous coal	Anthracite coal
3.3	3.3	3.3	-	3.3	3.3
-	3.4	3.4	3.4	3.4	3.4
6.2	6.2	6.0	6.1	6.2	6.2
-	6.9	6.9	6.9	6.9	6.9
-	7.2	7.2	7.2	7.2	7.2
7.7	7.7	-	7.6	-	-
-	8.0	8.0	8.0	-	-
8.6	8.6	8.6	-	-	-
11.3	11.3	11.3	11.1	11.5	11.3
-	12.2	12.1	12.05	12.3	12.5
-	13.3	-	-	-	13.4

Table 1.1. Distribution of central wavelengths (micron) of absorption bands in astronomical sources (UIB and PPNe) and in laboratory samples derived from biolmaterial (Rauf and Wickramasinghe, 2010)

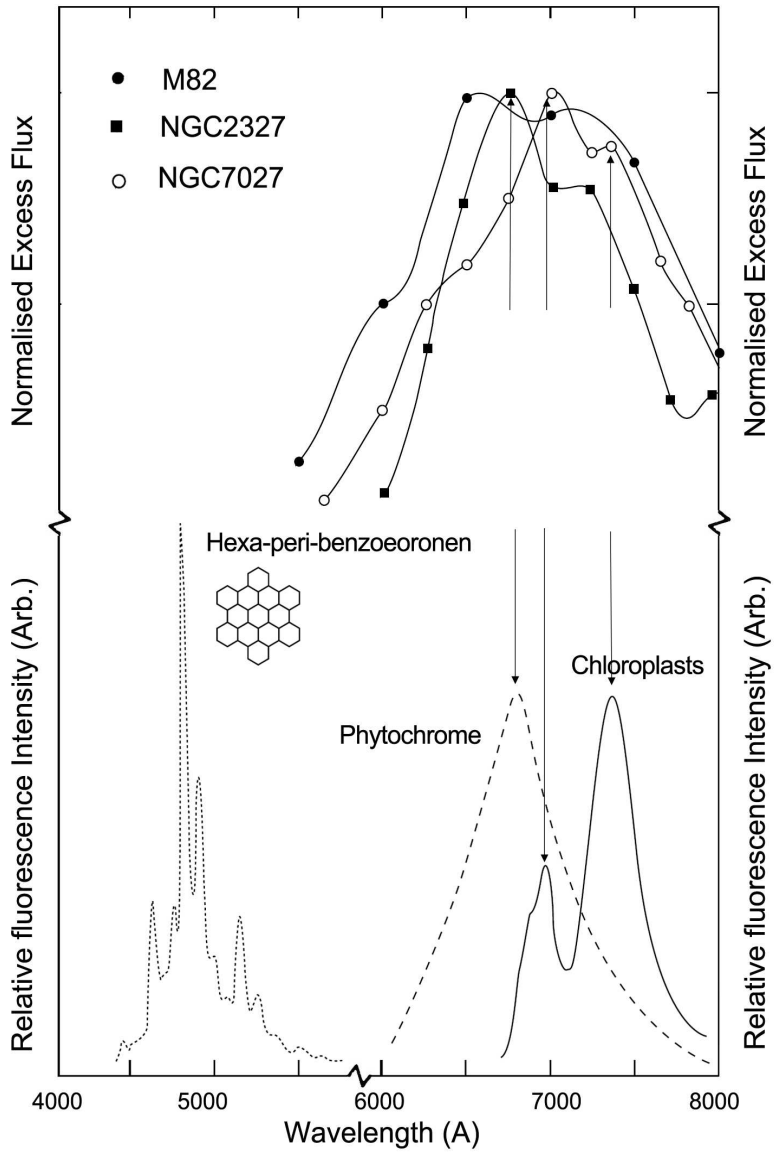

Figure 1.10 (Upper points) show normalised excess flux over scattering continua (Furton and Witt, 1992; Perrin *et al.*, 1995) (Lower) the fluorescence spectrum of hexa-peri-benzocoronene (right) shows the relative fluorescence intensity of spinach chloroplasts at a temperature of 77K (solid line) while the dashed curve shows the relative fluorescence intensity of phytochrome.

Comparison of the data points and the theoretical curve for biological aromatics showed a realistic explanation of an absorption feature in a galaxy located at a redshift of z = 0.83. This was an epoch when the universe was nearly half its present radius. Figure 1.9 shows the λ=2175Å absorption feature associated with SBS0909+532 (Motta *et al.*, 2002) together with the normalised absorption coefficient of an ensemble of 115 biological aromatic molecules.

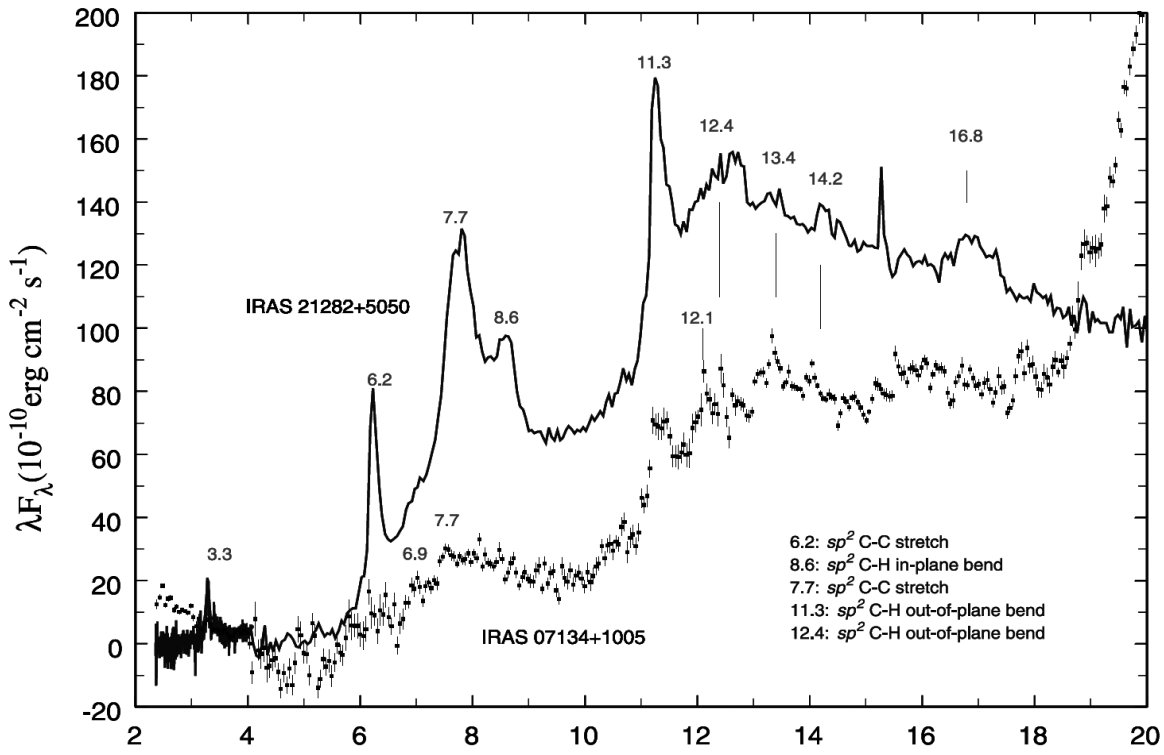

Figure 1.10a ISO SWS01 spectra of the young PN IRAS 21282+5050 and the PPN IRAS 07134+1005, showing various aromatic C–H and C–C stretching and bending modes at 3.3, 6.2, 7.7, 8.6, and 11.3 µm. Figure from Kwok (2009).

By the turn of the millennia, further infrared emission studies of ISO SWS01 spectra of the young Planetary Nebula IRAS 21282+5050 and the Protoplanetary Nebula IRAS 07134+1005 (Kwok, 2009) show the distribution of unidentified infrared bands (UIBs) between 3.3 µm and 22 µm comparable to major IR absorption bands in laboratory models of organic terrestrial origin (Rauf and Wickramasinghe, 2010a).

Though these nebular are specific in source, most recent studies of UIBs for a large number of galactic and extragalactic sources obtained using the Spitzer Space Telescope (Smith *et al.*, 2007) show a 3.3 µm to 22 µm range distribution that is almost identical in wavelengths from differing emission sources and that is broadly independent of ambient conditions.

Whilst inorganically formed PAHs remain the favoured model for the UIBs, no truly satisfactory agreement with available astronomical data has thus far been shown for abiotic PAHs (Hoyle and Wickramasinghe, 1991). This is a particularly serious problem since it is the starlight energy

absorbed in the ultraviolet band that is re-emitted as UIBs in the infrared, meaning that the set of UIB emitters and the 2175 Å absorbers need by necessity to be one and the same.

1.6 ONGOING PANSPERMIA

The continuing input of cometary material to Earth was first investigated in the 1970s by D.E. Brownlee and his colleagues (Brownlee, 1978). Here, high velocity IDPs were recovered from the stratosphere using U2 aircraft flown at high altitude that passed large quantities of lower stratospheric aerosols over adhesive mediums. IDPs that were generally in the form of highly porous, fluffy aggregates of siliceous dust were then diligently separated from terrestrial contaminants.

Analysis of the IDPs revealed evidence of a range of heavy organic molecules of complexity and diversity approaching those recently reported in the Murchison meteorite (Clemett *et al*.,1993). Furthermore, a number of micron-sized carbonaceous structures were also identified within the recovered particles with morphologies strikingly similar to known microorganisms. Figure 1.11 shows a micron-sized carbonaceous structure recovered from one of Brownlee's particles compared to an iron-oxidizing microorganism found in the Gunflint cherts of Northern Minnesota.

Nonetheless, it was generally acknowledged that the methods utilised in this study suffered from the obvious problem of terrestrial contamination as well as breakage of fragile particles striking the collecting medium at ~200 m s^{-1}. However, recovery of high velocity IDPs from the stratosphere persisted as a viable field of enquiry because the Earths tenuous air at ~100 km gradually slows down particles of size < 100 μm while still smaller ones (< 20 μm) are only moderately heated given favourable density and entry zenith angle (Coulsen and Wickramasinghe, 2003). Consequently, such particles would lose volatiles but retain more complex organics taking weeks to months to descend below the stratosphere.

The early experiments of Brownlee were repeated during the 1990s onwards, this time using sterilized cryogenically cooled pumps lofted into the stratosphere on balloons. Early flights reached heights of ~30 km while subsequent flights attained heights of 40-45 km (Lal *et al.,* 1996). Particulate matter was extracted by passing the compressed stratospheric air through sterilised micropore filters. In January 2001 pristine cometary dust was aseptically collected using cryoprobes at heights of 41km (Harris *et al.,* 2002; Narlikar *et al.,* 2003; Wainwright *et al.,* 2004). Analysis of the recovered material showed a range of pristine carbonaceous cometary dust particles bearing morphologies similar to bacterial fossils. In particular, morphological similarities to cocoidal and

Figure 1.11. An organic particle in a Brownlee clump (left panel) compared to a terrestrial bacterial fossil found in the Gunflint cherts of Northern Minnesota (Hoyle *et al.,* 1985)

rod-shaped bacteria were noted by several investigators (Harris *et al,* 2002; Wainwright *et al*, 2008; Rauf *et al*, 2010a). In a few instances evidence of fimbrae and biofilm appeared to corroborate a biological interpretation, and in all cases EDAX analyses showed high C abundances (Wallis, *et al.,* 2006; Wainwright *et al*., 2008).

A number of examples of acritarchs were also identified within the IDP collection (Wallis *et al.* 2002; Miyake, 2009). Acritarchs are organic-walled microfossils found in terrestrial sedimentary rocks and represent the remains of archaea, bacteria or eukaryotes. They possess diverse shapes and forms and have been identified in pre-Cambrian sediments dating from 3.2 Bya as well as being present in sediments of more recent times. Figure 1.12 shows a selection of SEM images exhibiting diverse structures and coatings including a putative microbial fossil, two spherical IDPs resembling the Orgueil acritarchs (Wallis *et al.,* 2002) and a possible acritarch showing a toroidal shell similar to that found in Tagish Lake (Rauf *et al.,* 2010b).

Further investigations pointed to the possible presence of viable microorganisms in the samples. Figure 1.13 shows a confocal microscope image of a clump of cocci from the 2001 collection flourescing under the application of a carbocyanine dye that detects DNA molecules (Harris *et al,* 2002) indicating the presence of viable but not culturable microorganism. The height of 41 km from which the collections were made is arguably too high for lofting a 10μm sized clump of bacteria from the surface leading to the conclusion that the structures encountered clearly represented infalling cometary dust.

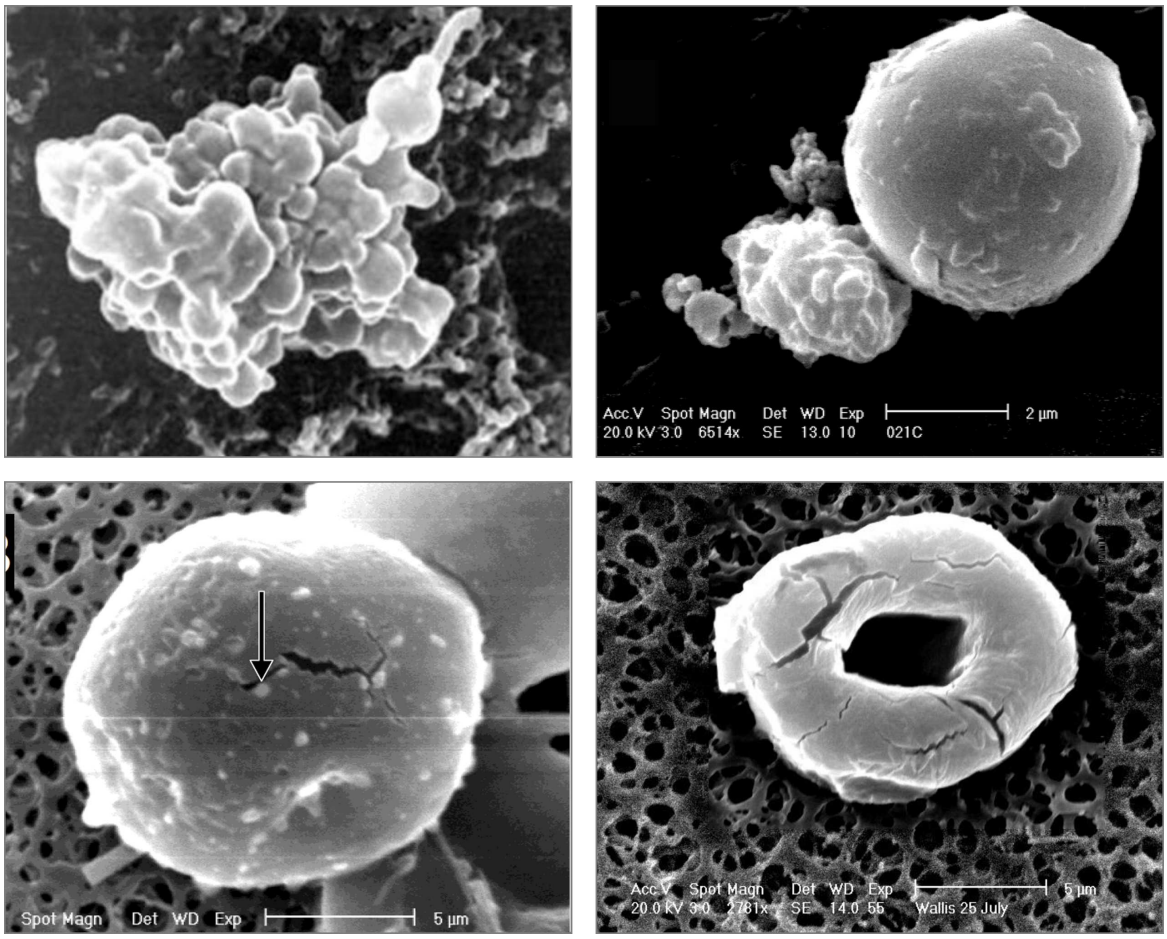

Figure 1.12. (Upper left) Putative microbial fossil in stratospheric aerosols (Harris *et al.,* 2002). (Upper right and lower left) Spherical IDPs resembling the Orgueil acritarchs (Wallis *et al.,* 2002) on 0.45 μm micropore cellulose acetate filter with gold coating. Image by Philips XL-20 scanning electron microscope. (Bottom right) Possible acritarch showing toroidal shell similar to that found in Tagish Lake (Rauf *et al.,* 2010)

These experiments were again repeated in 2013 when a balloon borne stratospheric sampling device was launched from Chester, NW England on 11 July 2013 (Wainwright *et al.,* 2013a). The sampling drawer was opened for 17 minutes during the ascent between 22,026m to 27,008m after which it returned to Earth undamaged and intact by parachute. Previous control flights confirmed that the particles recovered had been aseptically collected, many of which were shown to have an undeniably biological origin when examined under a scanning electron microscope. Further large particles, including one of size ~300 μm included seemingly biological filaments embedded in the mineral surface. Of further interest was the recovery of an inorganic particle-mass of approximately 60 μm width.

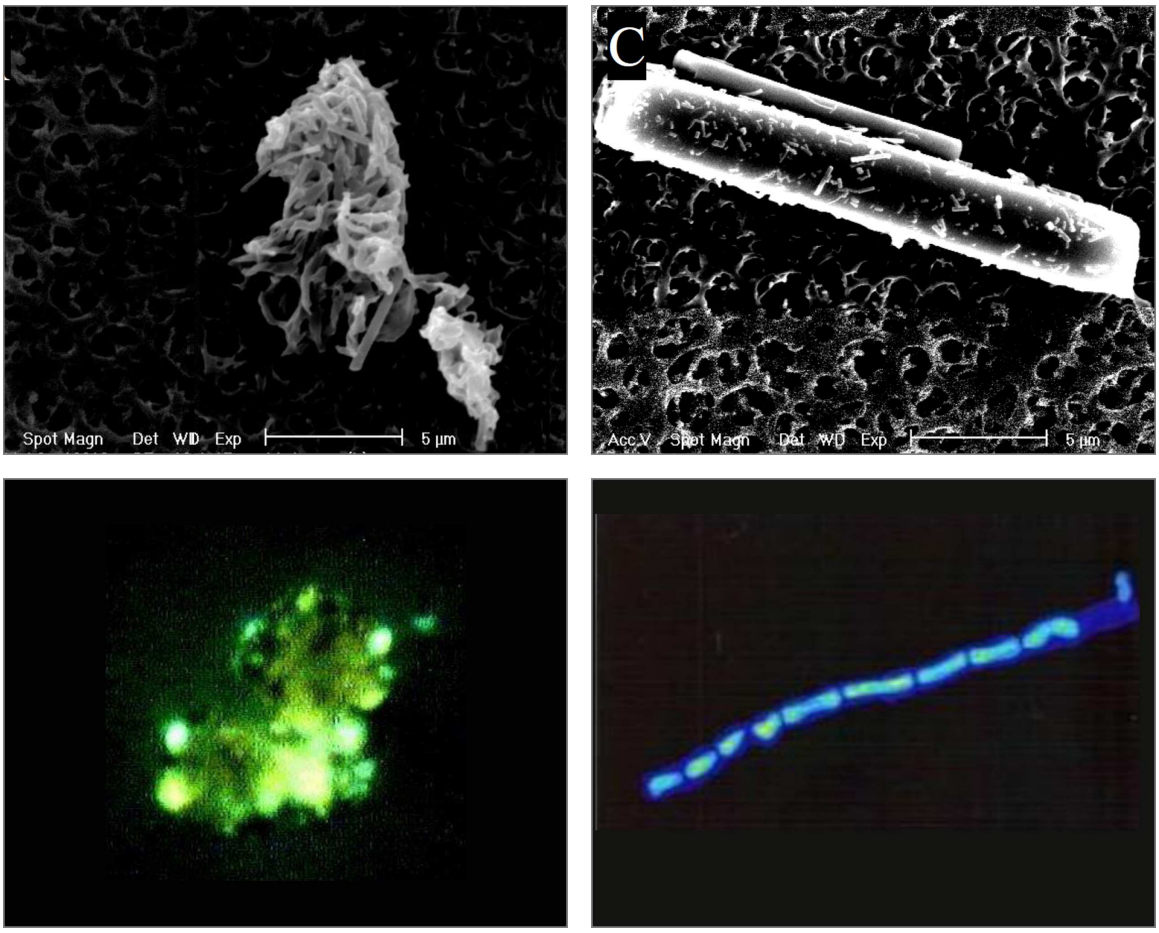

Figure 1.13. (Upper left) shows a clump of individual siliceous fibres while (upper right) shows a large (3 μm diameter by 20 μm long) fibre with a smaller fibre attached. (Bottom left) shows a clump of putative cells fluorescing under confocal microscopy after application with carbocyanine dye. (Bottom right) shows 0.7 μm microfiber membrane stained with nucleic acid dye showing fluorescence.

Examination of this particle revealed the presence of an embedded diatom frustule fragment, with characteristic regularly spaced non-rounded holes i.e. fibulae. This fragment differed from a previously recovered frustule in that it was not a freely existing particle and Wainwright *et al.*, (2013b) concluded that the particles must have originated in an aquatic environment.

The widely accepted view (Rosen, 1969) is that particles of size greater than 5 μm cannot be transported from the surface of the Earth, through the tropopause, and into the stratosphere other than by an exceptionally violent volcanic eruption. In particular, the isothermal temperature between about 15 and 25km is an almost insuperable barrier to upward transport mechanisms while the rapidly rising temperature at higher levels makes the stratosphere almost impervious to particles from lower regions (Bigg, 1984).

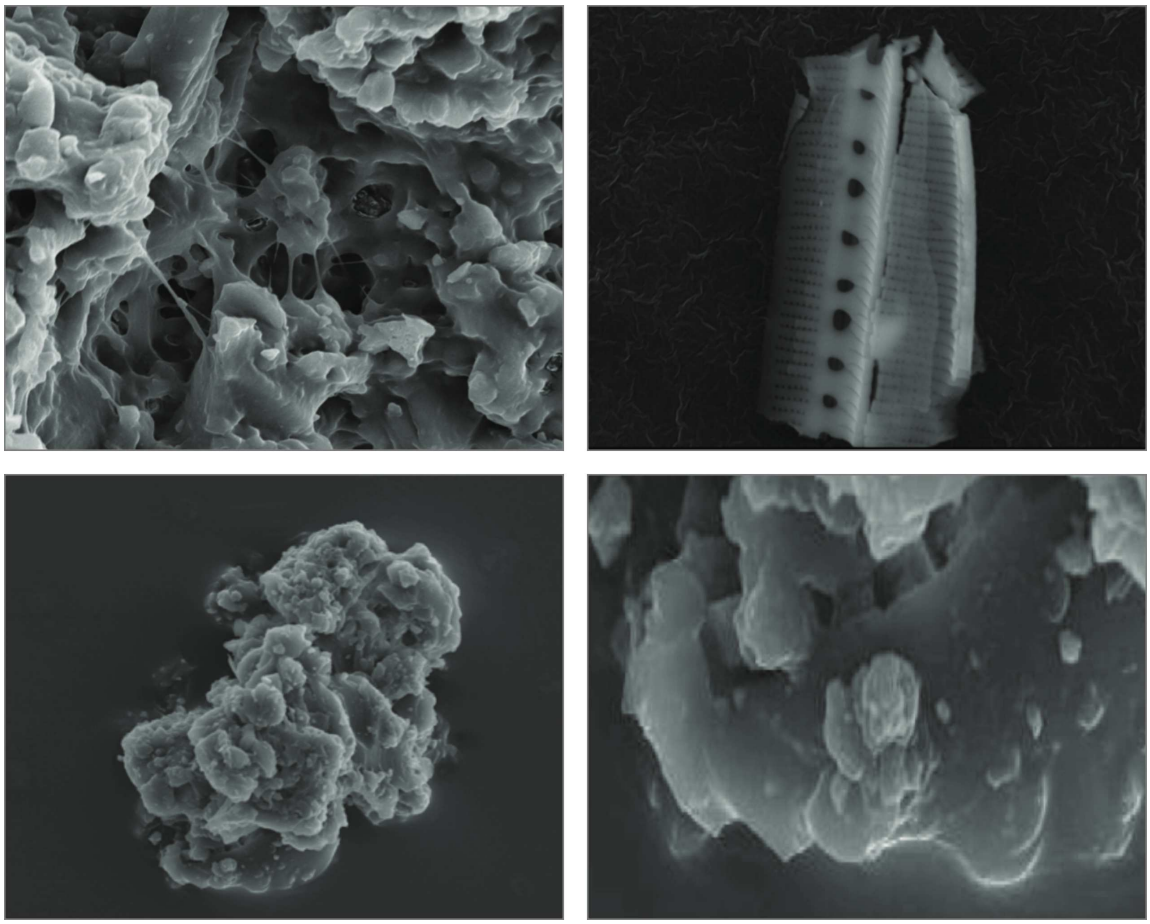

Figure 1.14. (upper left) shows a large particle mass isolated from the stratosphere showing microbial filaments, some of which show branching, (upper right) a diatom frustule (possibly a Nitzschia species) captured on a stub from a height of 25km in the stratosphere, (bottom left) an inorganic rich particle mass (approximately 60 micron across) and (bottom right) detail from the bottom left corner of particle mass; note regularly spaced diatom fibulae. Photos and captions from Wainwright *et al.,* (2013a, b and c)

Nonetheless, Wainwright *et al.,* (2013) paid particular attention to other possible mechanisms for both Earth lofting and infalling from commercial aircraft or orbiting space stations but eventually concluded that the particles recovered in their experiments most likely arose from the infalling of cometary dust particles from space.

1.7 COSMOLOGY AND COMETARY PANSPERMIA

While the theory of cometary panspermia provides a vehicle for the distribution of the seeds of life, it also somewhat disrupts the commonly accepted Λ-cold-dark-matter cosmological theory (ΛCDMHC) based on the Jeans (1902) linear theory of acoustic gravitational instability. In this

model, stars are produced by gas, and planets in turn are produced from stars. A natural corollary of the principals of panspermia follows from the derivation of life from antecedent life in a causal chain, leading to the question of how life naturally arose within the framework of cometary panspermia, and how the large-scale transmission of microbial information between planets then took place. Early attempts to explain this centred on the probabilistic advantage gained by transporting the originating processes, whatever they may be, to a cosmic environment, and cometary panspermia was thus framed within accepted Oparin-Haldine chemistry. Nonetheless, the large-scale transmission of microbial information between planets within the prevailing cosmological model was somewhat hampered by the availability of feasible mechanisms, since the collision time between planets of different stars of a galaxy is roughly a billion times the age of the present universe.

The currently accepted Λ-cold-dark-matter cosmological theory arises from the principles of fluid mechanics where, in the early days, strong simplifications were necessary that have continued to this day. In particular, it was assumed that the fluids in the early universe were frictionless, irrotational, linear and ideal. In effect, the Jeans (1902) linear theory of acoustic gravitational instability reduced the problem of gravitational instability of a nearly uniform ideal gas to one of gravitational acoustics. This was done by linear pertubation stability analysis (neglecting turbulence) of the Euler fluid momentum equations (neglecting viscous forces), and assuming the density ρ only as a function of pressure (the barotropic assumption).

To reconcile the equations with the linearised collisionless Boltzmann's equations and the resulting Poisson's equation for the gravitational potential, it was necessary to assume the density was zero. The critical wavelength for stability is the Jeans length scale L_J given by $L_J = V_S / [\rho G]^{1/2}$, where V_S is the speed of sound, ρ is the density, G is Newton's gravitational constant and $[\rho G]^{1/2}$ is the gravitational free fall time. If we consider the sudden arrival of a perturbation mass M(0) with scale $L << L_J$ within the structure of a motionless fluid of constant density ρ at time t=0, the mass M(t) will increase as $M(t) = M(0) \exp [2\pi\rho G t^2]$ unless viscous, turbulent, diffusion or other forces arise to prevent the exponential growth (Gibson 2000). For t>0, mass moves towards or away from the origin depending on the sign of the differential. For positive values, a sudden increase in density occurs near the origin and mass builds up. Hydrostatic equilibrium is established as local pressure increases to balance gravity. Density and temperature increases and hydrodynamic effects become relevant. For negative values, a void appears at the origin as density decreases and propagates radially outwards as a rarefication wave, limited by the speed of sound, and mass moves radially away due to gravity.

It follows from Newton's law of gravity the radial velocity $v_r \approx -GM(0)t/r^2$ so the mass flow is given by $d/dt\ M(t) \approx -\rho 4\pi r^2 v_r \approx 4\pi\rho GM(t)t$. The diffusion velocity is D/L for diffusivity D at distance L and the gravitational velocity is $L(\rho G)^{1/2}$. The Schwarz length scale is when the two velocities are equal and is given by $L_{SD} = [\ D^2 / \rho G\ ]^{1/4}$. The viscous Schwarz scale is the length scale at which viscous forces per unit volume ($\rho\nu\gamma L^2$) match gravitational forces ($\rho^2 G L^4$) and is given by $L_{SV} = [\ \gamma\nu / \rho G\ ]^{1/2}$, where γ is the rate of strain and ν is the kinematic viscosity of the fluid. The turbulent forces ($\rho\varepsilon^{2/3}L^{8/3}$) match the gravitational forces at the turbulent Schwarz scale, that is, $L_{ST} = \varepsilon^{1/2} [\ \rho G\ ]^{3/4}$ where ε is the viscous dissipation rate of turbulent kinetic energy.

Only the Jeans 1902 criterion that gravitational structure formation cannot occur for scales less than the Jeans length scale L_J is used in the standard cosmological model. Variations of density are assumed unstable at length scales larger than L_J but stable for smaller scales. Because the speed of sound in the plasma epoch after the big bang is nearly the speed of light, the Jeans scale for the plasma is always larger than the scale of causal connection (L_H=ct), where c is the speed of light and t is the time since the big bang, so no gravitational structures can form in the plasma. Because of this it was necessary to introduce cold dark matter (CDM) and to assume it was collisionless, like neutrinos, with a very large diffusivity D so that its L_{SD} scale during the plasma epoch exceeded the scale of causal connection.

In 1996, prompted by emerging observations that suggested that major modification of the Λ-cold-dark-matter cosmological theory was required, Gibson (1996) reworked the original theory to include the effects of viscosity, diffusivity and stratified turbulent transport mechanisms, and proposed the Hydro-gravitational-dynamics (HGD) cosmological model (Gibson, 2005, 2004, 2000, 1996, Gibson and Schild 2007a, 2007b, 2002, and Schild and Gibson 2008). In this cosmology, primordial planets formed at z = 1100 , $t = 10^{13}$ s in protoglobularstarcluster clumps are the source of all stars and the dark matter of galaxies. The concept of "dark energy" arising from the commonly accepted Λ-cold-dark-matter (ΛCDM) cosmological theory is no longer compatible.

Almost immediately after Gibson's HGD predictions in 1996, the presence of these trillion-plant-clump PGCs were independently identified by Schild (1996) as the dark matter of galaxies from the intrinsic twinkling frequency and brightness variations between galaxy-microlensed quasar-images adjusted for their time delays. From Schild's data it can be inferred that "rogue planets" are indeed so abundant that they could account for a large fraction of the much debated "dark baryonic matter" – the missing mass of the galaxy (Gibson 1996; Gibson and Schild, 2009). Estimates of the total number of planets in the galaxy, in particular the population of unbound, "free-floating" planets, have been upwardly revised over the past decade (Sumi *et al*, 2011; Cassan *et al*, 2012). Cassan *et*

al (2012) estimate ~ 10^{11} exoplanets in the galaxy and Sumi *et al* (2011) have argued for a similar number of unbound planets.

A fraction of the planets condensing from globular cluster-mass clumps coalesce into massive stars that end as supernovae producing heavy elements (C,N,O) at a very early stage. The bulk of the primordial planets envisaged in the Gibson-Schild theory constitute a universal total of 10^{80} planetary bodies with interiors that remain warm and liquid for millions of years. It is within this set of "connected" primordial planets that it has been argued that life originated in the early Universe (Gibson, Schild and Wickramasinghe, 2010).

After the lapse of a further few million years, the Universe cools below the freezing point of H_2 permitting extensive mantles of solid hydrogen to form (Wickramasinghe *et al.,* 2010). Such frozen planets, containing an accumulating complement of heavy elements and life, are the building blocks of galaxies and stars that form at later cosmological epochs (Gibson, 1996). In summary, it can be seen that the results of this independent work suggest a plausible, internally self-consistent vehicle for the theory of cometary panspermia and the origins of life within the accepted Oparin-Haldine chemical theory for abiogenesis.

1.8 MICROFOSSILS IN METEORITES

The first investigations into organic microstructures in carbonaceous chondrites arose in the early 1960s. Claus and Nagy (1961) had been working on biogenic hydrocarbons in the Orgueil CI1 chondrite and suspected that organic compounds indigenous to the meteorite were more consistent with those reported in ancient rocks rather than recent terrestrial sediments. This led them to microscopically examine grains of the Orgueil and Ivuna CI1 chondrites that had been crumbled in water and glycerol and placed on glass slides. A number of organic microstructures were found with morphologies resembling known terrestrial species. At least one further structure was identified that was morphologically dissimilar to any known terrestrial microorganism (Claus and Nagy, 1961, 1963). Independent studies carried out at various laboratories soon confirmed, or partially confirmed, the findings (Reimer, 1961; Staplin, 1962; Palik, 1962, 1963 and Cholnoky, 1962). In particular, a sample of Orgueil taken from the meteorite collection at the British Museum was examined by Ross (1962) who described what he thought to be indigenous microstructures of biological origin. Further studies of the Mokoia carbonaceous meteorite (Biggs and Kitto, 1962) found what were thought to be indigenous, stainable microstructures while Timofeev (1962) found fossilised microorganisms in the Mighei carbonaceous chondrite.

The conclusions reached by Nagy *et al.*, 1962 attracted bitter controversy and criticism, primarily from their chief protagonists, E. Anders and F. Fitch who had consistently argued that biogenic hydrocarbons (and the microstructures) were the result of contamination by terrestrial organics and pollen (Anders and Fitch, 1962a, 1962b, 1964; Fitch and Andres, 1963a, 1963b; Fitch *et al.*, 1962). While this theory was later dismissed conclusively by two leading microfossil and pollen experts (Rossignol-Strick and Barghoom, 1971) the 'contamination by pollen' argument eventually defeated the findings and it is now widely believed that the microorganisms detected arose from terrestrial contaminants.

We know now, of course, that the strident claims of Fitch and Anders were wrong. The indigenous nature of complex organic compounds in CI1 chondrites was eventually settled by Martins *et al.*, (2008) when measured Carbon isotope ratios for xanthine and related chemicals, including the RNA component uracil, established that they were not of terrestrial origin. Subsequent work on the Murchison meteorite by Schmitt-Kopplin *et al.*, (2010) identified about 70 amino acids in the meteorite sample, while a potential 50,000 or more unique molecular compositions, and possibility millions of distinct organic compounds, are also thought to be present (Matson, 2010).

Nonetheless, the effect of the controversy was to seriously undermine future investigations into microstructures in meteorites. Nearly 40 years later, the 1999 ESA Exobiology Science Team Study report revealed the extent of residual prejudice towards this type of scientific research. This was most succinctly reflected in the concluding statements on the issue: 'It should not be considered unscientific to indulge in detailed characterization of the organic matter in carbonaceous chondrites from the point of view of Exobiology (Nagy *et al*, 1961) but as already stated this is almost a taboo area'.

Nearly two decades later the problem of microbial fossils in carbonaceous meteorites was re-examined by Hans D. Pflug with special attention being paid to avoid the criticisms of earlier work (Pflug, 1984a, 1984b). Here, a thin section (< 1mm) of the Murchison meteorite was placed on a membrane filter of 0.01 μm pore diameter and exposed to HF and HCL vapour. In this way *in situ* demineralisation was achieved, the mineral component being removed though the pores of the filter, leaving carbonaceous structures indigenous to the meteorite in-tact. Particular attention was paid to the preparation of the thin sections to avoid risk of contamination. Examination of the membrane filters after demineralisation revealed a wealth of morphologies with distinctive biological characteristics. Figure 1.15 - panels (a) to (e) - show a range of examples identified in the study together with comparable known terrestrial microorganisms such as rod-shaped bacterial type structures.

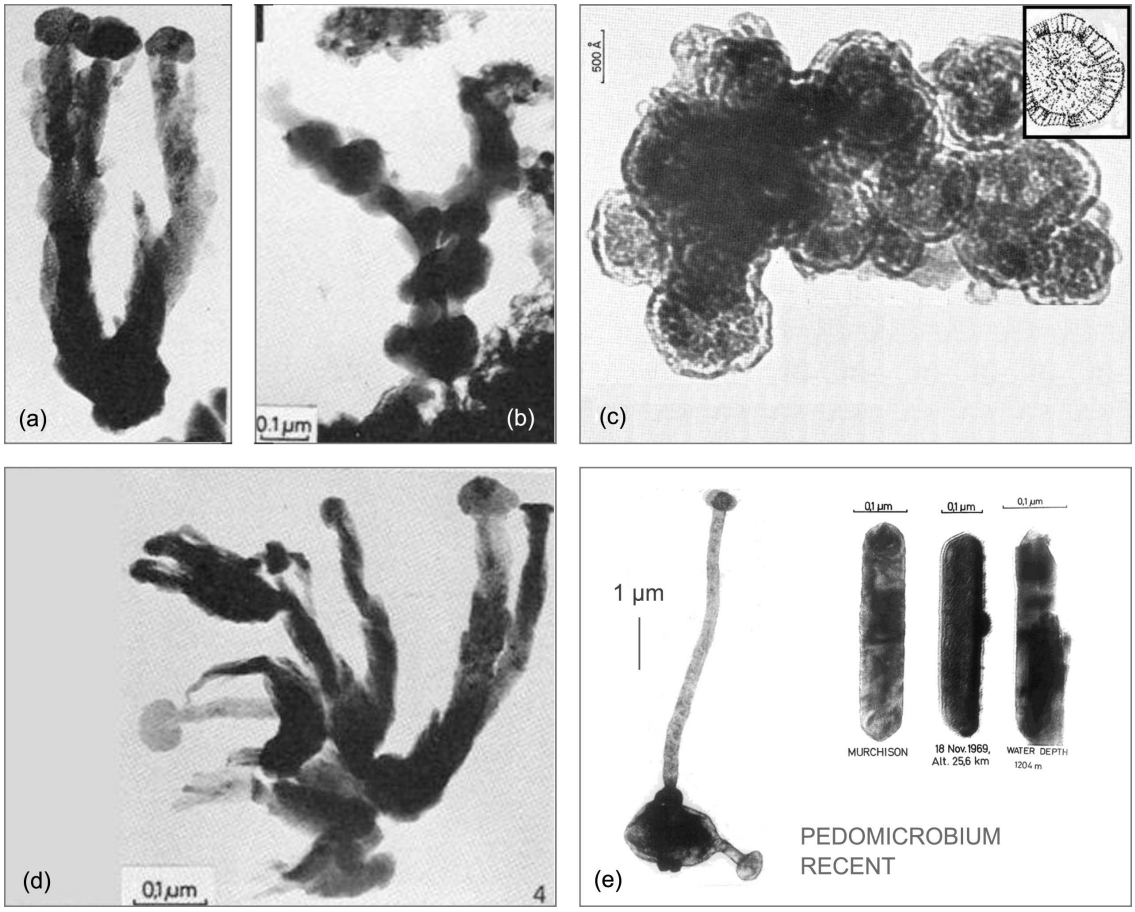

Figure 1.15 show a range of microstructures recovered from the Murchison, Orgueil and Allende carbonaceous chondrites by Pflug (1984a,b). Panel (a), (b) and (d) show characteristically biological structures in the Murchison meterorite with (e - left image) showing a similar structure corresponding to a modern iron-oxidising microorganism – *pedomicrobium*, and (e –right image) showing a rod-shaped structure recovered from the Murchison meteorite compared to similar bacterial microorganisms found in ocean sediments and the atmosphere. (c) An electron micrograph of a structure resembling a clump of viruses found in the Murchison meteorite. The inset shows a modern influenza virus displaying remarkable similarities in structure and form to the putative clump of fossil viruses.

similar to microorganisms found in ocean sediments and in the atmosphere together with structures remarkably similar to a well-known bacterium *pedomicrobium*. In consideration of the potential issue of terrestrial contamination, Pflug observed that the structures were found closely connected to the meteorite minerals and were either included in crystals or embedded in the hydrosilicate matrix having been impregnated or encrusted within it. He also observed that many specimens of the same morphology occurred in the rock, and were so abundant as to represent a substantial proportion of the meteorite organic matter, an observation that was entirely inconsistent with local contamination.

A little over a decade after Pflug's initial findings were published the subject of microfossils in meteorites again emerged but this time in the form of a press conference by NASA announcing the possible detection of bacteria-like fossils in the Allen Hills Martian meteorite ALH 84001 (McKay *et al.,* 1996). The structures, revealed under scanning electron microscope, were between 20-100 nanometres in diameter, similar in size to theoretical nanobacteria, but were smaller than any known cellular life at the time of their discovery. McKay and his team argued that micrographs of the structures indicated that they were both intergrown and embedded in the indigenous material in a manner that was inconsistent with the idea of terrestrial contamination.

In support of this early work McKay *et al.* (2009) have more recently reported studies of potential biofossils (carbon-associated 'biomorphs') in additional Martian meteorites Nakhla and Yamato-593. These results however continue to be challenged, in particular by the conclusions of other studies that demonstrate a number of abiotic crystallisation processes that produce microstructures with morphologies strongly resembling living microorganisms (Garcia-Ruiz, 1999). This has led to the commonly held belief that morphology alone cannot be used unambiguously as a tool for primitive life detection.

This paradigm was challenged however by the work of Hoover (2005). Here, Environmental (ESEM) and Field (FESEM) Electron Microscopy investigations on CI1 carbonaceous meteorites yielded a range of images of large complex filaments embedded in freshly fractured internal surfaces of the stones.

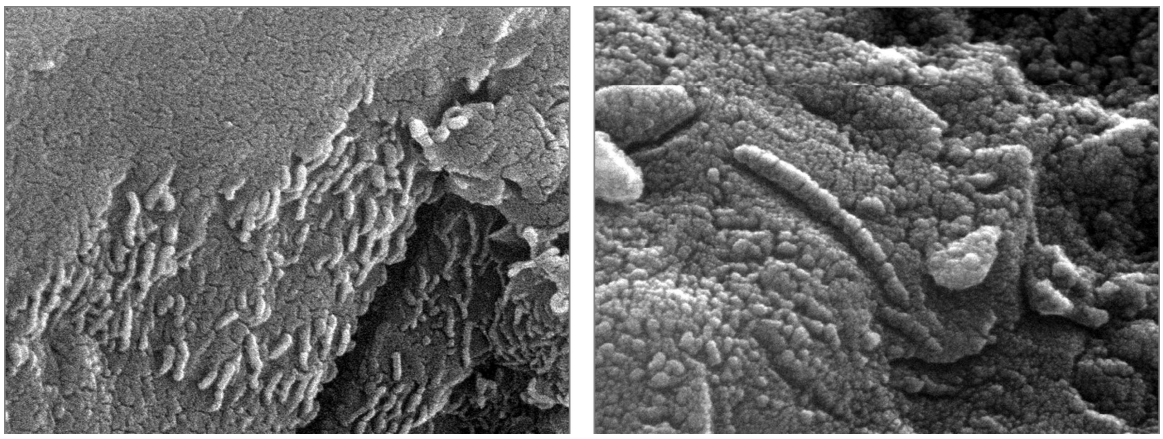

Figure 1.16 Shows an electron microscope image revealing chain structures in a meteorite fragment of ALH84001 with morphological features consistent with living organisms (McKay *et al.,* 1996).

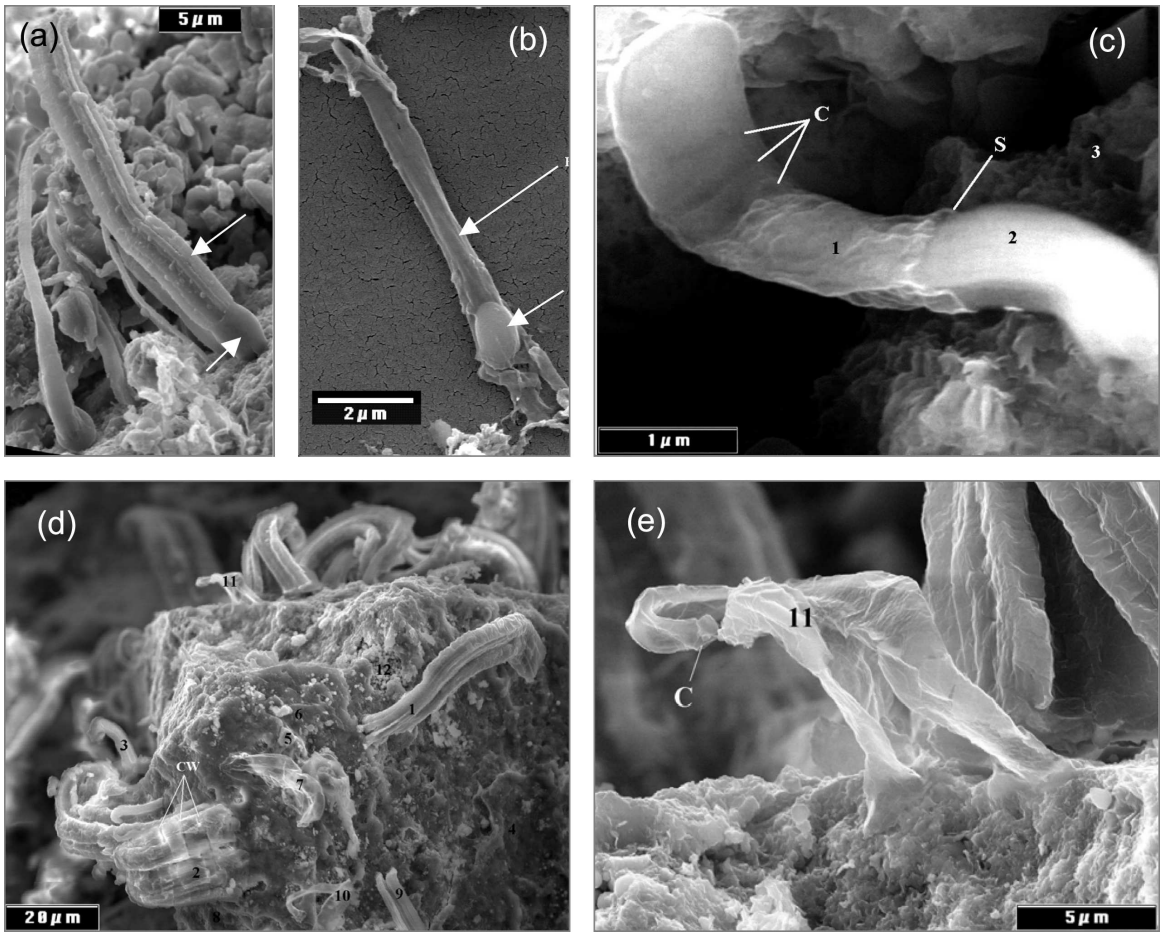

Figure 1.17. FESEM images showing a variety of filaments present in carbonaceous chondrites. **(a)** micro structure in the Orgueil meteorite showing tapered filaments (diameter ~ 1 to 2.5 μm) with apparent heterocysts interpreted as morphotypes of the cyanobacterium *Calothrix* **(b)** living filament of *Calothrix* sp. with a diameter ~ 0.8 μm and a basal heterocyst from the White River, Washington. **(c)** micro structure in the Ivuna CI1 meteorite filament (0.8 μm diameter) with dark lines marked 'C', EDS data of the filament sheath at spot 1 shows biogenic elements N and P (<0.5%). It is enriched in C (13.1%) as compared with nearby meteorite matrix (C 7.2%) at spot 3; **(d)** low magnification (1000X) image from the Orgueil CI1 meteorite showing dense population with several different types of embedded filaments and electron transparent sheaths and **(e)** high magnification (6000x) image of sheath in (d) (Hoover, 2005; 2009; 2011).

Hoover concluded that observed filaments exhibited recognizable features, such as size, location and arrangement of internal cells within sheaths that were diagnostic of known genera and species of filamentous trichomic cyanobacteria and other trichomic prokaryotes.

Furthermore, studies of living and fossil cyanobacteria exhibited morphologies (uniseriate and multiseriate, branched or unbranched, isodiametric or tapered, polarized or unpolarized filaments

with trichomes encased within thin or thick external sheaths) similar to the filaments found in the meteorites. Closer inspection revealed the presence of specialized cells and structures that are used by cyanobacteria for a range of biological processes including reproduction (baeocytes, akinetes and hormogonia), nitrogen fixation (basal, intercalary or apical heterocysts), attachment (pili or fimbriae) or indicative of oscillatoria type locomotion (escaped or coiling hormogonia and flattened and coiled empty sheaths).

Figure 1.17 shows a selection of FESEM images (Hoover, 2005) of a variety of filaments present in the Orgueil and Ivuna CI1 carbonaceous chondrites. Microstructures of tapered filaments (diameter ~ 1 to 2.5 μm) with apparent heterocysts (interpreted as morphotypes of the cyanobacterium *Calothrix*) are shown with comparative images of living filaments of *Calothrix*.

The initial report by Hoover (2009; 2011) met with bitter controversy that soon extended to the Editor of the Journal who had passed the paper for publication. Amidst the furore of NASA press conferences, accusations, resignations and counter-accusations, the observation that Hoover's work did not rely on morphology alone, but included an analysis of elemental abundances associated with the microstructures examined, was somewhat lost. The general consensus of opinion among scientists now is that the broad claim that microorganisms have been found in meteorites has not been conclusively resolved on a proof-positive basis for either side.

1.9 CONCLUSION

The value of a scientific theory ultimately lies in its ability to make testable predictions. Proof or falsification of those predictions is at the heart of the process by which science ultimately converges on an objective truth. The theory of cometary panspermia made several explicit predictions during the early 1980s. In the years that have followed, substantial evidence from astronomy, biology, geology and meteoritics has amassed in support of those predictions.

The organic nature of cometary grains and interstellar dust in now almost universally accepted, though the prevailing paradigm still asserts (without proof) that this implies the operation of prebiotic chemical evolution on a cosmic scale. Evidence of ongoing panspermia has also grown over the years and is now in sharp focus as numerous stratospheric experiments are both planned and underway. Again, the detection of biochemically relevant material in IDPs and micrometeorites hitting the upper stratosphere is interpreted as evidence of residual prebiotic chemical components, while undeniably biological structures are interpreted as evidence of surface lofting.

The nature of the organic component in meteorites has similarly advanced in support of panspermia. The indigenous nature of these components, particularly in the carbonaceous chondrites, has been unambiguously established by carbon isotope analysis of extracted xanthine and uracil (Martins *et al.,* 2008) as well as the subsequent unambiguous identification of about 70 amino acids in Murchison itself (Schmitt-Kopplin *et al.,* 2010). Furthermore, Matson (2010) suggests a potential 50,000 or more unique molecular compositions, and possibly millions of distinct organic compounds, may also be present in Murchison.

The presence of microfossils in non-terrestrial materials remains controversial. The identification of biological morphologies relies on an element of interpretation, and the difficulties arising from this are also reflected in the opposing views on ancient terrestrial biota (Pflug, 1967; Altermann, 2001; Walsh 1992; Brasier *et al.,* 2006; Buik, 2001; Sugitani, 2007; Javaux, Marshall and Bekker, 2010). However, more recently, the use of refined analytical procedures have again supported the presence of biological material in some remarkably ancient artefacts going back to ~4bya.

Nonetheless, the theory of cometary panspermia continues, after 35 years of rigorous debate, to provide a powerful unifying theory for a collection of otherwise unconnected and disparate scientific data from a range of disciplines.

Chapter 2

Carbonaceous Core-Mantle Structures in the Tissint Martian Meteorite

2.1 INTRODUCTION

The detection of polyaromatic hydrocarbons (PAH) in the Martian meteorite ALH84001 sparked the debate as to the presence of a possible Martian biota (McKay *et al.,* 1996). These PAHs were found on fractured surfaces containing carbonate disks and were claimed to be similar to those formed during the thermal decomposition of bacterial matter. Together with the discovery of bacteria-like morphologies, this led to the early conclusion supporting the presence of ancient Martian life in ALH84001. Despite nearly two decades of subsequent work however, this early hypothesis has neither been validated nor disproved.

The problem of contamination of ALH84001 by terrestrial carbon during its ~13,000 years in Antarctica remains an intractable complication. Jull (1998) found that most of the organic carbon in ALH84001 was terrestrial, with live ^{14}C, while the small remaining inventory may indeed have originated from Martian organics, but may also have come from occluded carbonate grains. Bada *et al.,* (1998) found that the amino acids in ALH84001 are clearly terrestrial. During the many studies that have followed, McKay's original hypothesis has been relegated to one of a number of competing explanations ranging from high-temperature shock (Scott, 1999) to cold abiotic groundwater (McSween and Harvey, 1998).

The problem of contamination by terrestrial organic material makes the search for indigenous bio-signatures in meteorites inherently problematic. Definitive conclusions of origin frequently result in lengthy and unresolved scientific debate. Tissint (Morocco) represents a rare opportunity to study a fresh Martian basaltic rock that has been subjected to minimal terrestrial contamination. It is the fifth observed fall of its kind, the others including *Chassigny* in Marne, France in 1815 (Dunite, ~4 kg), *Shergotty* in Bihar, India in 1865 (Basalt ~5 kg), *Nakhla* in Alexandria, Egypt in 1911 (Clinopyroxenite, ~10 kg) and *Zagami* in Katsina, Nigeria in 1962 (Basalt ~18 kg). These samples however, while collected within relatively short periods of time, have certainly been exposed to terrestrial organic contaminants during storage.

The minimal level of terrestrial alteration of Tissint has been confirmed by Aoudjehane *et al,* (2012) via stepped combustion mass spectrometry that show total C abundances of 173 ppm with a $\delta^{13}C$ =

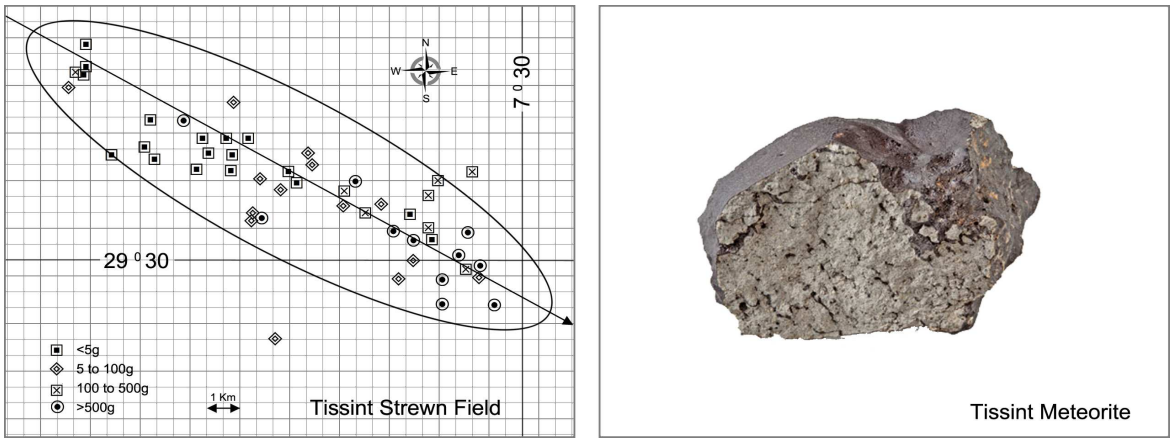

Figure 2.1. (Left Panel) The size-distribution of fragments in the strewnfield with corresponding locations (Ibhi *et al.*, 2013). (Right panel) a fragment of the Tissint meteorite (BM.2012,M1) of mass ~1.1kg exhibiting a black fusion crust with glossy olivines. Photograph: Natural History Museum, London.

–26.6 ‰ and 12.7 ppm nitrogen with total $\delta^{15}N$ = – 4.5 ‰ supporting the view that much of Tissint's organic material is of Martian origin. In this study the results of Scanning Electron Microscopic analysis of five samples of the Tissint Martian Meteorite are reported. Results show the presence of pyrite grains rimmed by thin layers of poorly graphitised carbon characterised as immiscible globules with curved boundaries within the substrate.

Sulphide grains rimmed by a layer of reduced organic carbon have previously been detected in a variety of astronomical sources including carbonaceous chondrites, chondritic IDPs (Rietmeijer and Mackinnon, 1985; 1987) and primitive chondritic meteorites (Tagish Lake) (Nakamura *et al.*, 2002). Similar structures have been found in the geological record in Proterozoic and Ordovician sandstones from Canada (Nardi, 1994) and in hydrothermal calcite veins from Carboniferous limestones in central Ireland (Lindgren *et al.*, 2011). The affinity between FeS_2 (pyrite) and organic matter has been examined extensively in the literature in view of its potential as a mechanism for bringing organic molecules close enough to interact using the surface of pyrite as a substrate (Tessis *et al.*, 1999; Cody *et al*., 2000; Pontes-Buarques *et al*., 2001; Cohn *et al*., 2001; Hatton and Rickard, 2008).

2.2 FALL HISTORY

Several eyewitnesses observed a brilliant yellow fireball over the Oued Drâa Valley East of Tata, Morocco at 2:00 AM on July 18, 2011. Two sonic booms were heard across the valley as the bolide turned green and split into two parts. In October 2011 nomads found a 47 g pale grey stone encased

in a fresh, glistening black, glassy fusion crust in a remote area of the Oued Drâa watershed 48 km SSW of the village of Tissint, Morocco (29^{o} 28.917'N, 7^{o}36.674'W). Much larger stones (up to 987 g) were later found near the El Ga'idat plateau and smaller stones were collected from the El Aglâb mountains. The inferred NW to SE trajectory was determined from eyewitness observations and accords well with the distribution of stones as recovered from the strewn field that extends at least 15 km from the west-north-west to east-south-east covering an area of approximately 60 km^{2}. In total, a mass of approximately 17kg has been recovered to date, with the largest fragments measuring between 0.1 to 2 kg, clustered to the south-east of the strewn field. The vast majority of the fragments comprised of many thousands of smaller splinters. The larger of the specimens are now preserved at the Natural History Museums in London (UK) and Wien (Austria).

2.3 EXPERIMENTAL SAMPLES AND ANALYTICAL METHODS

Five fragments of the Tissint meteorite were used in this study of mass 0.960g, 0.963g, 1.030g, 1.270g and 0.966g. In order to preserve the integrity of the samples, preparation of the SEM stubs was carried out under laboratory conditions with adherence to protocols necessary to minimize the risk of contamination from local sources. A Circulaire VLF650E laminar flow clean air unit was used during all preparations with the samples remaining in their original containers until they were placed inside the cabinet. All aluminium stubs and cutting tools were placed inside the cabinet, sterilized using ethanol and left to dry under flow for several hours.

Several control samples were similarly prepared from the olivine rich Dolerite thought to contain similar mineralogy to Tissint. In addition, samples of the Murchison and Dhofar meteorites were also prepared in the same sitting and using the same procedures and protocols outlined above. In order to utilize as much of the sample as possible, unused fragments were collected inside a sterilized clear plastic container. Advantage of the adhesive nature of the carbon tape was then taken by using it to collect as many pieces as possible onto a single stub. This allowed the examination of several dozen small fragments on a single stub. In order to exclude contamination from coating, the samples were first inspected uncoated. Features of interest that could be shown to exist prior to a coating event were recorded and mapped so that some samples could then be coated with gold in order to take advantage of higher resolution imaging possible under high vacuum.

Between sessions the samples were stored inside the same container used for transporting the subs and left under laminar flow. Whenever it was not possible to maintain power to the cabinet the samples were stored inside a hard wall clean laboratory located in a facility nearby. Whilst no direct

contact was possible with any artefacts inside this facility the benches were nevertheless sterilized using 3M's HFE solution.

One polished 30µm thin section (section A - 15 x 10 mm), one unpolished 30µm thin section (section B -16 x 19 mm) and one polished thick section (16 x 21 x 3mm) were also prepared at the School of Earth and Ocean Sciences at Cardiff University.

Optical microscopy was conducted using an RM-1POL polarising light microscope with 360º rotating analyser. Image capture was via a 9M pixel digital trinocular camera unit processed by View7 PC software for output to hard drive. Scanning Electron Microscopy (SEM) was conducted using the FEI (Phillips) XL30 FEG ESEM (Environmental Scanning Electron Microscope) FEG (Field Emission Gun) at the School of Earth and Ocean Sciences at Cardiff University. The unit incorporates a secondary electron detector (SE), a back scatter electron detector (BSE) and a gaseous secondary electron detector (GSE). It also has an Oxford Instruments INCA ENERGY (EDX) x-ray analysis system. Image recording is via a SONY video graphics printer or digital by processing image frames in a 16 bit framestore computer for output to hard drive.

Whole rock chemical analysis of aliquots of a ground, homogenised powder of the sample fragments were carried out using a Perkin Elmer Dual-View Optima 5300 Inductively Coupled Plasma Optical Emission Spectrometer. Calibration was based on the analysis of reference rock powders USGS DTS-1 (dunite), USGS BCR-2 (basalt) and ANRT BR (basalt). 50 mg aliquots of the samples and standards were dissolved in an Anton Paar Multiwave 3000 microwave digestion unit in high-pressure, high temperature PTFE ('teflon') vessels (210°C, 8 bar). Samples were first dissolved in mixtures of concentrated high-purity acids HF, HNO_3 and HCL. The procedure utilised does not allow the content of Boron to be determined, because the element is added when the mixture is neutralised by the addition of Boric Acid.

High resolution Raman spectra were analysed for a selection of carbonaceous domains identified during SEM studies. These were acquired using a Renishaw inVia microRaman system at the School of Chemistry, Cardiff University, UK. The unit was fitted with a research grade Leica analytical microscope (10x, 20x, 40x and 100x objectives) and a 514.5 nm Ar laser line. Data processing was via the Wire2 software application for data output to hard drive. Spectroscopy was performed on both polished and unpolished 30µm sections as well as freshly cleaved surfaces at room temperature with spectra collected through the 100x objective. Spectra were analysed to ensure commonality between the various carbonaceous components being studied

Table 2.1 – Experimental Samples

Sample	Mass (mg)	Source [a]	Description [b]
Experimental Samples			
T960/001	420	T960	~ 1.5 mm interior fragment for inclusion on sections A, B and C
T960/002	388	T960	~ 2 mm interior fragment for SEM studies at SES-CU
T960/003	121	T960	powder from aliquot A[c] used for ICP-OES
T963/001	326	T963	~ 1.2 mm interior fragment for inclusion on sections A, B and C
T963/002	515	T963	~ 1.8 mm interior fragment for SEM studies at SES-CU
T963/003	98	T963	powder from aliquot B[d] used for FTIR
T103/001	281	T103	~ 1.0 mm interior fragment for inclusion on sections A, B and C
T103/002	467	T103	~ 2 mm interior fragment for SEM studies at SES-CU
T103/003	252	T103	powder from aliquot C[e] used for ICP-OES
T127/001	412	T127	~ 1.5 mm interior fragment for inclusion on sections A, B and C
T127/002	732	T127	~ 3 mm interior fragment for SEM studies at SES-CU
T966/001	-	T966	~ 4 mm interior fragment for SEM studies at NASA- MSFC
Control and Comparative Samples			
D288/001		-	Olivine-rich Dolerite

[a] Source Code: Internal fragments of Tissint Meteorite weighing. T960 (0.960g); T963 (0.963g); T103 (1.030g); T127 (1.270g) and T966 (0.966g). Samples supplied by Michael Farmer, Tucson, AZ, USA
[b] Description Code: SES-CU – School of Earth and Ocean Science, Cardiff University; NASA- MSFC - Marshall Space Flight Centre, NASA
[c] Aliquot A – Two interior fragments and dust weighing a combined 121mg taken from sample T960.
[d] Aliquot B – One fragment and dust from interior weighing a combined 98mg taken from sample T963.
[e] Aliquot C – Dust weighing a combined 252mg taken from sample T103.

2.4 CONTAMINATION SCREENING

The ubiquitous nature of organics on Earth poses a serious problem to the study of biomarkers in meteorites. Previous work on the nature and origin of organic carbon detected in non-terrestrial sources has routinely been compromised by the suggestion of terrestrial contamination (Claus and Nagy, 1961; Nagy *et al*., 1962; Pflug, 1984; McKay, 1996; Hoover, 2005). This problem is further exacerbated by the possibility of contamination arising during storage. Studies on a chip of the Murchison meteorite kept in a sealed sterile container for 12 years between SEM imaging sessions revealed the presence of invasive and extensive fungal contamination (Steele *et al.*, 1999). One suggested solution to this problem involves the application of a rapid screening mechanism to ensure that all experimental samples are free from contamination prior to the onset of experimental analysis (Steele *et al.*, 1999).

All five fragments of the Tissint meteorite utilised in this study were first screened for evidence of the presence of terrestrial contaminants. This was undertaken by examining the textural, mineralogical and chemical characteristics of the stones to ensure that all components were parental to the meteorite matrix and contained no foreign lithic, mineralogic or precipitated components.

Results of optical, scanning electron microscopy (SEM) and Inductively Coupled Plasma Optical Emission Spectrometry were then compared with published data (Irving *et al.*, 2012; Aoudjehane *et al*, 2012; Steele, *et al*., 2012). Further SEM surface screening was undertaken at 3KeV for micron sized terrestrial microorganisms prior to investigation at 20 KeV. A complete list of samples utilised in the study is detailed in Table 2.1.

2.4.1 Overall Petrology

Figure 2.2 (a) shows an optical light micrograph of section A (polished 30µm thin section) in plane polarised light (offset nicols). The interior of the sample can be seen to comprise of a fine-grained (pale grey) matrix of pyroxene, with enclosed sub-mm to mm-sized pale yellow olivine macrocrysts and amorphous plagioclase (maskelynite) grains. Numerous micron sized fractures were observed, some breaching both olivine macrocrysts and neighbouring pyroxene phases (figure 2.2 b). Inclusions of maskelynite were characterised by smooth pockets that were absent of cleavage, intragranular cracks or shock-induced fractures while adjacent phases exhibited evidence of pervasive shock (figure 2.2 (c)). Evidence of grain fracture and subsequent release into the liquid maskelynite was also found. Figure 2.2 (c) shows one fragment of pyroxene situated in the centre of a maskelynite pocket that had clearly fractured from the periphery and been set afloat as shown in figure 2.2 (d).

Offshoots of maskelynite commonly filled neighbouring shock induced fractures in adjacent phases of pyroxene and olivine. These offshoots generally occurred as long, smooth, thin and irregular branches that were occasionally interconnected. Many offshoots also exhibited expansion cracks radiating from the parental grains. This indicates that they were formed by injection of the dense plagioclase melt after formation of the shock-induced fractures and not through a pre-shock process of igneous crystallization. Results of shock experiments on a grabbo similar to the Shergotty meteorite (Engelhardt *et al.,* 1970) suggest that melting and vesiculation of plagioclase occurs at a shock pressure of about 60 to 80 GPa.

Olivine inclusions occurred as macrocrysts of up to 1.2mm in size and microphenocrysts < 0.5mm in size, though our samples were relatively small (0.960g, 0.963g, 1.030g, 1.270g and 0.966g) and are probably not representative of the bulk specimen. Only one large macrocryst of size ~1.2mm was sampled in the 1.27g fragment. Olivine macrocrysts were zoned from the core and exhibited thin ferroan rims against the bulk matrix together with small chromite inclusions. Evidence of patchy zoning was apparent in pyroxenes containing orthopyroxene cores, pigeonite and subcalcic augite.

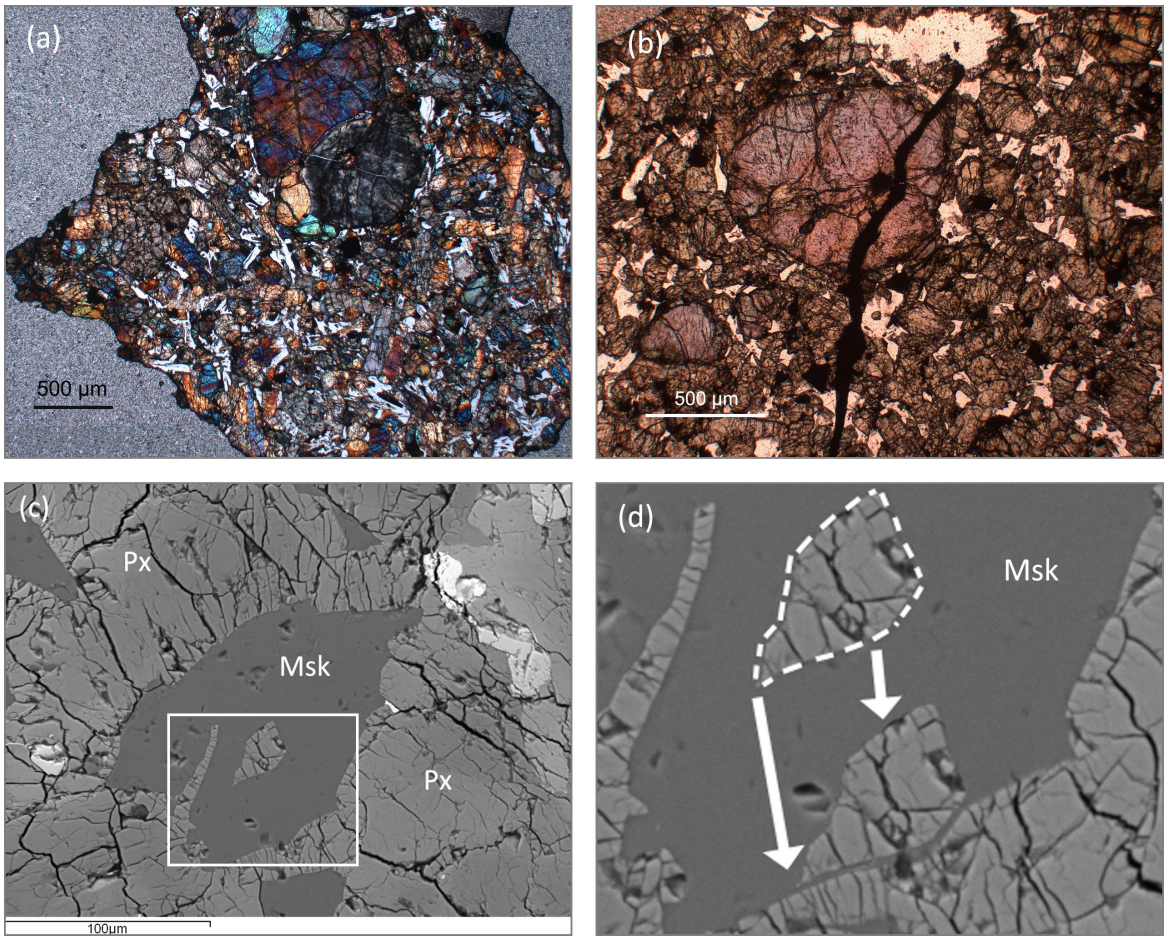

Figure 2.2. Micrographs of section A (polished 30µm thin section) in (a) plane polarised light with crossed nicols (offsets), (b) plane polarised light, (c) and (d) backscatter SEM image (Px – pyroxene; Msk – Maskelynite). Note the way the pyroxene 'island' fits the contours of the phase interfaces.

All observations closely matched reported studies on the Tissint meteorite (Irving *et al.*, 2012; Aoudjehane *et al*, 2012; Steele, *et al*., 2012) and no foreign lithic or mineralogic components could be detected.

2.4.2 Mineral Chemistry

Mineral chemistry was determined by measurement of elemental abundances using the Analytical Scanning Electron Microscope (A-SEM) at the School of Earth and Ocean Sciences at Cardiff University. The A-SEM comprises of an LEO (Cambridge) S360 Electron Microscope, an Oxford Instruments INCA ENERGY X-Ray analyser and an Oxford Instruments INCA WAVE X-Ray analyser. Calibration was via standards which included SiO_2 for O-K, Al_2O_3 for Al-K, MgO for Mg-

K, SiO_2 for Si-K, GaP for P-K, Orthoclase for K-K, AgCl for Cl-K and Wollastonite for Ca-K. For the other elements (Na, P, Ti, and Mn) K factors were estimated using standard calibration curves.

Both the larger olivine macrocrysts and smaller olivine microphenocrysts showed similar composition with no difference between large and small crystals. Most exhibited thin ferroan rims at interfaces with adjacent phases, while some ferroan zones also appeared along fractures within the interior of olivine crystals. Figure 2.3 (a) shows a backscatter SEM image of section C showing zoned olivine crystals with adjacent phases of maskelynite while figure 2.3 (b) shows a single olivine crystal with ferroan outer rim against the groundmass and tiny chromite inclusions.

Results of the spot analysis of twelve samples of olivine (core and rim), pyroxene and maskelynite show close correlation with those reported in the literature. Table 2.2 shows average oxide representations for EDAX measurements taken from the rim and core of twelve sampled olivine crystals together with data for sample pigeonite, augite and maskelynite. Similar compositions reported by Aoudjehane, *et al.* (2012) are also presented for comparison.

2.4.3 Low kV SEM Screening

The use of low kV SEM imaging in detecting the presence of contaminating organisms has been examined previously by Steele *et al.,* (1999). Figure 2.3 (e) shows a SEM micrograph of ALH84001 taken at 3 KeV compared to (f) the same image taken at 15 KeV where the organisms detected have reduced to the level of indistinct marks on the surface appearing as interesting mineral phases. All samples utilised in this study were first scanned at 3 KeV after mounting on aluminium stubs. No microorganisms were detected on any of the samples analysed. To avoid the possibility of subsequent contamination only globules detected in the session including contamination screening were utilised in this study.

2.5 BULK CHEMISTRY

Whole rock major and trace element compositions of the Tissint meteorite were determined by ICP-OES and are presented in Table 2.3. Comparative data from Aoudjehane, *et al.,* (2012) together with data for Dhofar 019 (Taylor, 2002) and typical compositional data for basaltic shergottites, ol-bearing shergottites and lherzolitic shergottites are also included. Data for the basaltic shergottites included Shergotty, Zagami, Los Angeles, Queen Alexandra Range 94201, Elephant Moraine (EET) A79001B (Meyer, 1998; Warren *et al*., 2000).

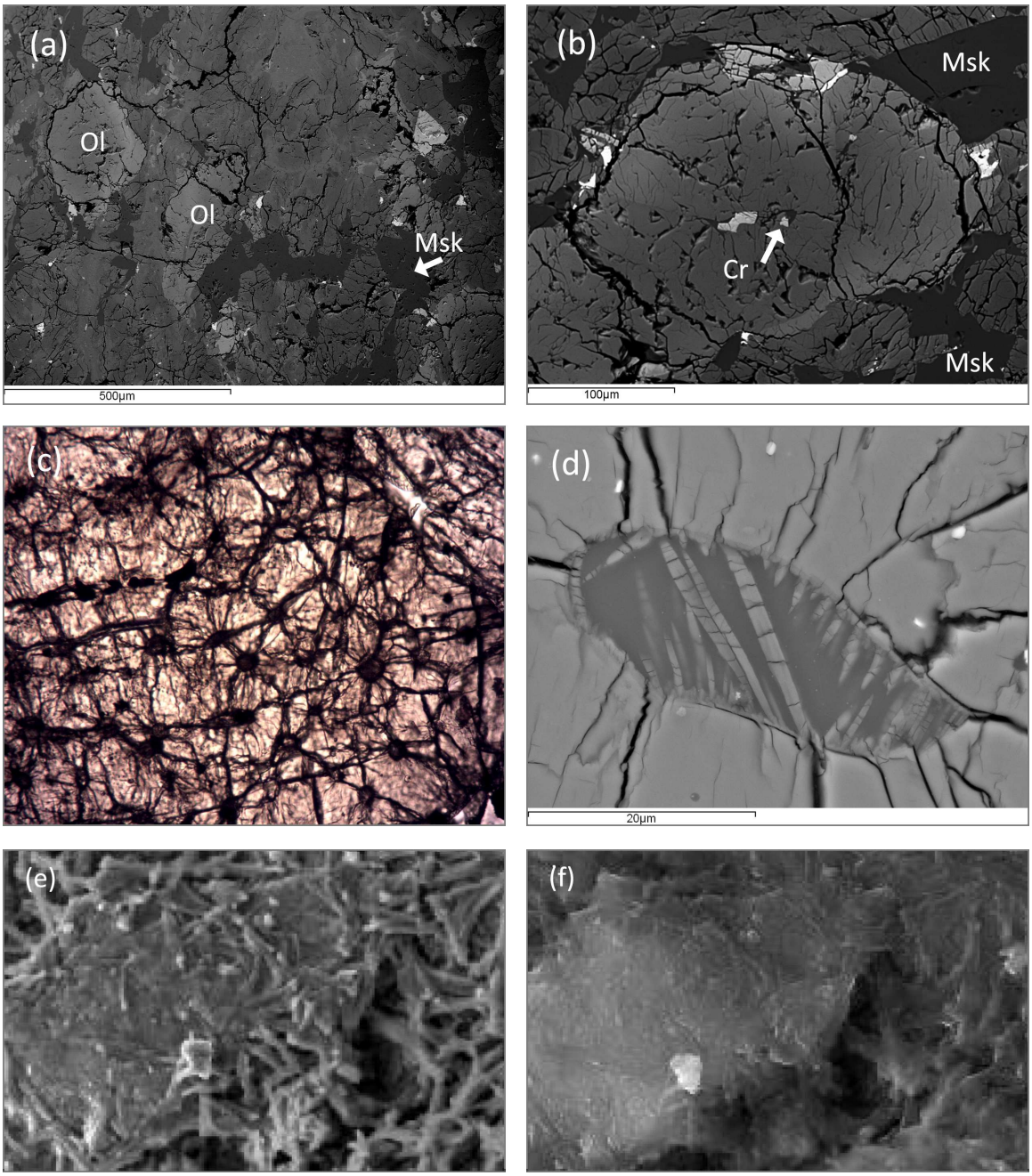

Figure 2.3. (a) Backscatter SEM micrograph of polished 30µm thin section (section A) showing olivine microphenocrysts with ferroan rims at interfaces with adjacent phases, (b) single olivine crystal with tiny chromite inclusions (c) optical micrograph in plane polarised light showing an array of crystals with amorphous melt inclusions and radiating fractures (d) backscatter SEM micrograph of core from (c), (e and f) SEM backscatter micrograph of bacterial contamination of ALH84001 shown with (e) 3KeV and (f) 15 KeV (micrographs from Steel *et al*, 1999).

Table 2.2
Representative compositions of Olivine, Pyroxenes and shocked isotropic plagioclase (Maskelynite) grains in Tissint together with comparative compositions of maskelynite taken from the literature

	Olivine: S1, S2–Rim: S3, S4-Core				Pyroxene: S5, S6–Pigeonite, S7, S8-Augite				Maskelynite: S9, S10 – Study, S11, S12 - Lit			
	S1	S2	S3	S4	S5	S6	S7	S8	S9	S10	S11	S12
SiO_2	34.55	35.42	38.37	39.21	54.00	49.54	50.47	48.99	51.14	55.88	51.83	56.78
Al_2O_3	0.03	0.03	0.03	0.05	0.56	0.79	0.81	0.92	30.07	27.12	30.39	26.42
Na_2O	0.05	0.02	0.01	0.01	0.06	0.06	0.08	0.19	3.72	4.99	3.42	5.13
MgO	17.37	22.97	37.82	40.22	21.37	15.49	16.11	14.41	0.07	0.08	0.13	0.05
K_2O	0.00	0.00	0.00	0.00	0.01	0.00	0.00	0.03	0.05	0.48	0.04	0.50
CaO	0.34	0.34	0.24	0.23	3.49	4.96	11.77	12.97	13.21	9.90	13.66	9.90
FeO	47.32	41.78	23.99	21.02	19.37	27.11	19.61	20.23	0.65	0.65	0.65	0.68
TiO_2	0.05	0.00	0.00	0.00	0.07	0.64	0.19	1.09	0.03	0.07	0.04	0.08
MnO	0.79	0.82	0.49	0.33	0.49	0.66	0.38	0.69	0.03	0.03	0.04	0.02
NiO	0.00	0.01	0.22	0.18	0.00	0.00	0.00	0.00	0.00	0.00	0.00	0.00
Cr_2O_3	0.04	0.04	0.22	0.21	0.47	0.19	0.49	0.17	0.01	0.01	0.01	0.00
Total	100.54	101.43	101.39	101.46	99.89	99.44	99.11	99.69	98.98	99.21	100.21	99.56
	Cations = 4				Cations = 6				Cations = 8			
Si	1.018	1.004	1.130	1.002	2.008	1.941	1.876	1.904	2.346	2.531	2.378	2.562
Al	0.001	0.001	0.001	0.002	0.025	0.037	0.036	0.042	1.639	1.459	1.656	1.416
Na	0.003	0.001	0.001	0.000	0.004	0.005	0.006	0.004	0.331	0.438	0.304	0.449
Mg	0.763	0.970	1.661	1.532	1.184	0.905	0.893	0.835	0.005	0.005	0.009	0.003
K	0.000	0.000	0.000	0.000	0.000	0.000	0.000	0.000	0.003	0.028	0.002	0.029
Ca	0.011	0.01	0.008	0.006	0.139	0.208	0.469	0.540	0.649	0.480	0.671	0.479
Fe	1.166	0.990	0.591	0.449	0.602	0.888	0.610	0.658	0.025	0.025	0.025	0.026
Ti	0.001	0.000	0.000	0.000	0.002	0.019	0.005	0.032	0.001	0.002	0.001	0.001
Mn	0.002	0.020	0.012	0.007	0.015	0.022	0.012	0.023	0.001	0.001	0.002	0.001
Tot	2.982	2.996	3.404	2.998	3.980	4.024	3.907	4.050	5.000	4.970	5.049	4.966

S1, S2 taken from rim of olivine crystal, S3, S4 taken from core. S5, S6 taken from sample pigeonite, S7, S8 from Augite inclusion. S9, S10 taken from sample maskelynite compared to S11, S12 of maskelynite taken from Aoudjehane, *et al.* (2012).

Data for Ol-bearing shergottites included Dar al Gani (DaG) 476, DaG 489, and EETA79001A (Meyer, 1998; Zipfel *et al*. 2000; Folco et al., 2000) and for the lherzolitic shergottites, Lewis Cliff 88516, Allan Hills A77005 and Yamato-793605 (Meyer, 1998).

Whole rock chemical compositions for the samples included in this study show close correlation to corresponding data from Aoudjehane, *et al.,* (2012). Of particular note was the consistency of the Ti, Fe, Mg, Ca and P abundances indicating that the main mineral components were present in previously reported abundances. While some degree of compositional variation was expected, particularly in view of the small size of the experimental samples and the consequential variations in the presence of the larger olivine macrocrysts, no evidence of the presence of foreign lithic,

Table 2.3
Chemical composition of Tissint in comparison with other shergottites.

	Tissint[a]	Tissint[b]	Dhofar 019[c]	Basaltic shergottites[d]	Ol-bearing shergottites[e]	Lherzolitic shergottites[f]
SiO_2	45.89		45.52	48.0–51.4	45.8–50.6	43.1–45.4
TiO_2	0.67	0.63	0.594	0.73–1.98	0.35–0.70	0.35–0.44
Al_2O_3	6.24	4.86	6.72	5.70–13.4	4.19–5.85	2.32–3.45
Cr_2O_3	-	0.41	0.574	0.01–0.20	0.63–0.83	0.84–1.03
FeO	21.01	21.15	17.93	17.0–21.4	16.1–18.5	19.7–20.9
MnO	0.52	0.52	0.461	0.41–0.52	0.39–0.49	0.44–0.51
MgO	17.51	17.06	14.61	3.53–9.28	14.6–19.4	23.7–27.7
CaO	6.16	6.53	9.27	10.0–11.5	7.42–7.83	3.35–4.25
Na_2O	1.35	0.72	0.677	1.20–2.17	0.51–0.80	0.35–0.59
K_2O	0.00	0.02	0.053	0.04–0.03	0.03–0.04	0.02–0.03
P_2O_5	0.46	0.48	0.401	0.48–1.50	0.32–0.49	-
SO_3	-	-	1.15	-	-	-
Total	**99.80**	**-**	**99.77**	**-**	**-**	**-**
Li	3	2.18	2.86	2.2–5.6	2.6–4.5	1.3–1.6
Sc	35	-	31.2	43–59	28–37	21–25
V	205	194	175.1	103–380	171–230	132–202
Cr	3000	3042	3417	96–1389	4290–5700	5672–6900
Co	40	58.1	44.5	24–51	43–51	63–72
Ni	225	269	65.3	20–83	128–300	250–370
Cu	6	13.8	9.54	11–139	7–80	5–80
Zn	63	63.0	62	54–130	49–85	47–90
Ga	36	12.05	10.21	14–30	8–14	6–9
Rb	-	0.376	0.49	0.1–14	0.9–6.9	0.17
Sr	32	34.78	363	35–80	40–87	8–30
Y	9	14.91	6.78	10–28	8	5.7–6.2
Zr	24	23.14	17.4	41–97	8–90	10–19
Nb	2	0.28	0.3	0.7–22	0.13	0.5–0.6
Ba	2	3.54	19.4	25–80	<48	2.3–6
La	<1	0.315	0.24	0.4–5.3	0.1–0.5	0.2–0.3
Ce	-	1.16	1.45	1.6–13	0.4–1.7	0.9–1.1
Pr	-	0.237	0.11	0.7–0.9	-	0.13
Nd	-	1.63	0.69	2.4–11	0.6–1.2	0.8–1.1
Sm	-	1.07	0.48	1.2–3.4	0.4–0.8	0.3–0.4
Eu	2	0.503	0.2	0.5–1.2	0.2–0.4	0.1–0.2
Gd	13	1.85	0.99	1.6–4.3	1	0.4–1.1
Tb	2	0.364	0.2	0.4–0.9	0.2–0.3	0.1–0.2
Dy	3	2.38	1.3	1.7–6.1	1.4–2.2	0.6–1.3
Ho	<1	0.504	0.27	0.6–1.3	0.3–0.5	0.2–0.3
Er	<1	1.48	0.81	-	0.9	0.3–0.7
Tm	<1	0.204	0.12	0.2–0.4	0.1–0.2	0.08–0.12
Yb	2	1.30	0.81	1.4–3.5	0.8–1.2	0.4–0.5
Lu	3	0.190	0.12	0.2–0.5	0.1–0.2	0.06–0.08
Hf	<2	1.01	0.48	1.9–3.4	0.4–1.0	0.4–0.6

[a] Chemical composition of Tissint as determined by ICP-OES (This Study)
[b] Chemical composition of Tissint (Aoudjehane, *et al.*, 2012).
[c] Dhofar 019 (Taylor, 2002).
[d] Range data from Meyer (1998) and Warren *et al*., (2000) for Shergotty, Zagami, Los Angeles, Queen Alexandra Range 94201, Elephant Moraine (EET) A79001B
[e] Range data from Meyer (1998); Zipfel *et al*. (2000) and Folco et al. (2000) for Dar al Gani (DaG) 476, DaG 489, and EETA79001A
[f] Range data from Meyer (1998) for Lewis Cliff 88516, Allan Hills A77005 and Yamato-793605

mineralogic or precipitated components were found. Variations in some trace element abundances, (e.g. Gd) were interpreted as arising from sampling heterogeneity.

2.6 SEM RESULTS

Several 5-50µm globules and plates were observed in the SEM images. Some of these were embedded in the rough substrate of loosely aggregated pyroxene grains, while others were unbound and appeared to have been dislodged during the fracturing process. The presence of a pool of macromolecular carbon (MMC) within both carbonate globules and the host pyroxene have been previously reported in the martian meteorite ALH84001 (McKay, 1996: Stephan, *et al*, 2003).

Steele *et al.,* (2006) conducted Raman microprobe imaging and spectral data acquisition of a cross section of one globule in ALH84001 and found a complex structure comprising of a core of carbonate, hematite and magnetite followed by a magnesite rich carbonate shell bounded by an outer rim of hematite, magnetite and magnesite. These shells were found to contain layers of macromolecular carbon at both the centre and periphery of the globule that was determined to be organic carbon indigenous to ALH84001.

Initial observations of the globules located in the SEM images suggested the presence of either a hollow core or a more complex heterogeneous composition. In particular, structures were readly damaged due to expansion by heating of the electron beam at the point of capture while other structures displayed evidence of expansion when subjected to high vacuum. Figure 2.4 (a) below shows a ~25 µm carbonaceous disk-shaped structure embedded in the pyropxene substrate while figure 2.4 (b) shows structural deformation at the centre of the disk following EDAX capture. Similarly, figure 2.4 (c) shows a 10µm carbonaceous egg-shaped globule shown here unbound in the rough substrate of loosely aggregated grains.

The ‘egg cracking’ visible under higher magnification (d) occured as a result of expansion of the gold coated globule when the SEM chamber was subjected to high vaccum. Expansion features were commonly localised (see figure 2.5a) indicating some level of compositional heterogeneity or the possible presence of an offset void or other inclusion. Common voids were found in the pyroxene substrate and were characterised by cavities in the loosely bound unabraded angular rock. More geometrically spherical voids were common in the denser amorphous phases. Figure 2.5 (b) shows a typical cavity in the pyroxene groundmass while figure 2.5 (d) shows a number of spherical voids surrounding a larger sub-rounded cavity. It appears probable that globules were dislodged from such cavities during fracturing.

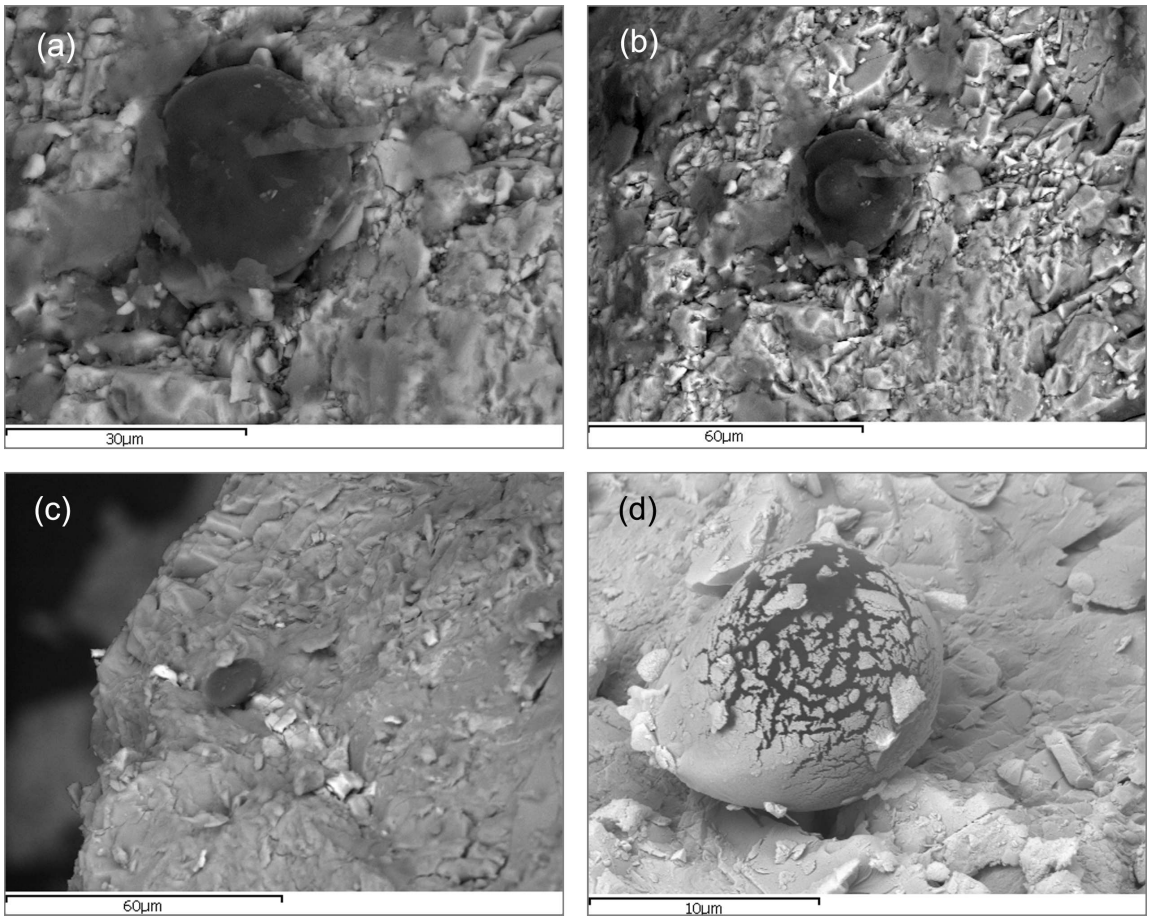

Figure 2.4. (a) 25 µm carbonaceous disk-shaped structure embedded in the pyropxene substrate (b) same structure but showing structural deformation at the centre of the disk following EDAX capture (c) an unbound 10µm carbonaceous egg-shaped globule (d) same structure as (c) but after gold coating and exposure to high vacuum in the SEM chamber.

High magnification examination of one globule tentatively suggested the presence of an enclosed mineral core. Figure 2.5(c) shows an unbound 8µm carbonaceous globule on a pyroxene groundmass base. Local variations in the curved boundary are visible at points marked by arrows A and B. A further feature (marked by arrow C) indicates a concave distortion matching the apparent shape of the enclosed grain. Further features marked by arrow D indicate the presence of small (~200nm) voids within the enclosed grain.

To further elucidate the composition of the enclosed mineral core a low energey (15KeV) electron beam was used to attenuate the surface of one carbonaceous globule at 4 points on its surface and at one point on the surface of a neighbouring globule. A 2-D x-ray elemental map was then acquired in order to identify the presence of elements mobilised during the process.

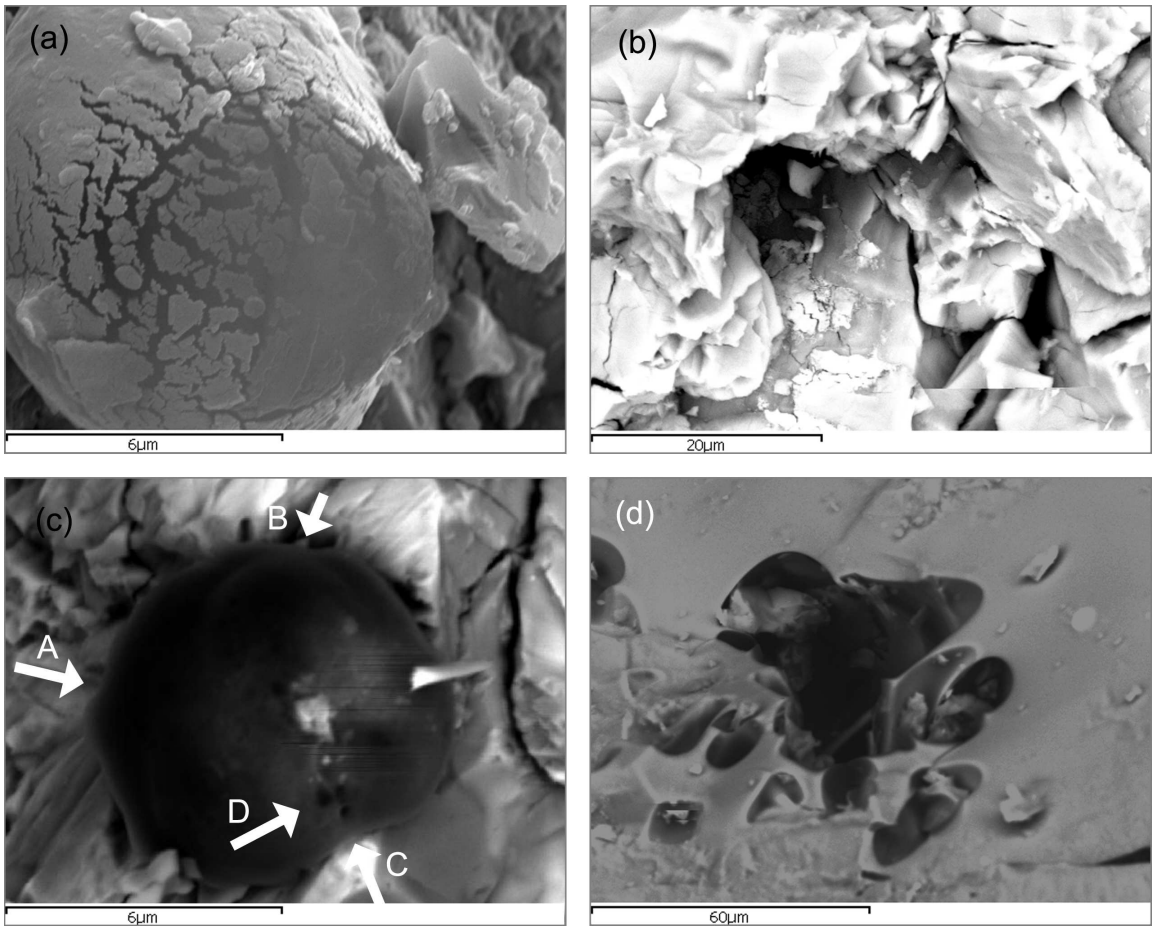

Figure 2.5 (a) Shows localised structural deformation of a 10µm globule after gold coating and exposure to high vacuum in the SEM chamber, (b) shows a typical cavity in the loosely bound unabraded angular rock substrate while (d) shows more geometrically spherical voids common in the denser amorphous phases, (c) an unbound 8µm carbonaceous globule on pyroxene groundmass. Note the indentiations in the curved boundary marked by arrows A and B as well as a concave distortion at C matching the apparent shape of the enclosed grain togetehr with small (~200nm) voids in the surface of the enclosed grain.

Figure 2.6 (a) shows the two globules selected while (b) shows a high magnification image of the same globules with arrows marking the points of attenuation of the carbonaceous mantle by 15KeV electron beam. Inserts (ii) to (xii) show results of the 2-D elemental x-ray map corresponding to C, O, Mg, Si, S, Ca, Ti, Al, Cr, Mn and Fe respectively. Insert (d) shows a 2-D elemental map for Carbon (red) overlaid by Sulphur (yellow). It can readily be seen from the position of arrows showing surface weakening in (c) and the corresponding detection of S in the vicinity of the weakened points in (d) that sulphur was released during the attenuation process. Images were taken at NASA Marshall Space Flight Centre using a Hitachi S-3700N Field Emission Scanning Electron Microscope fitted with Secondary Electron (SE) detector and Back Scatter Electron (BSE) detector.

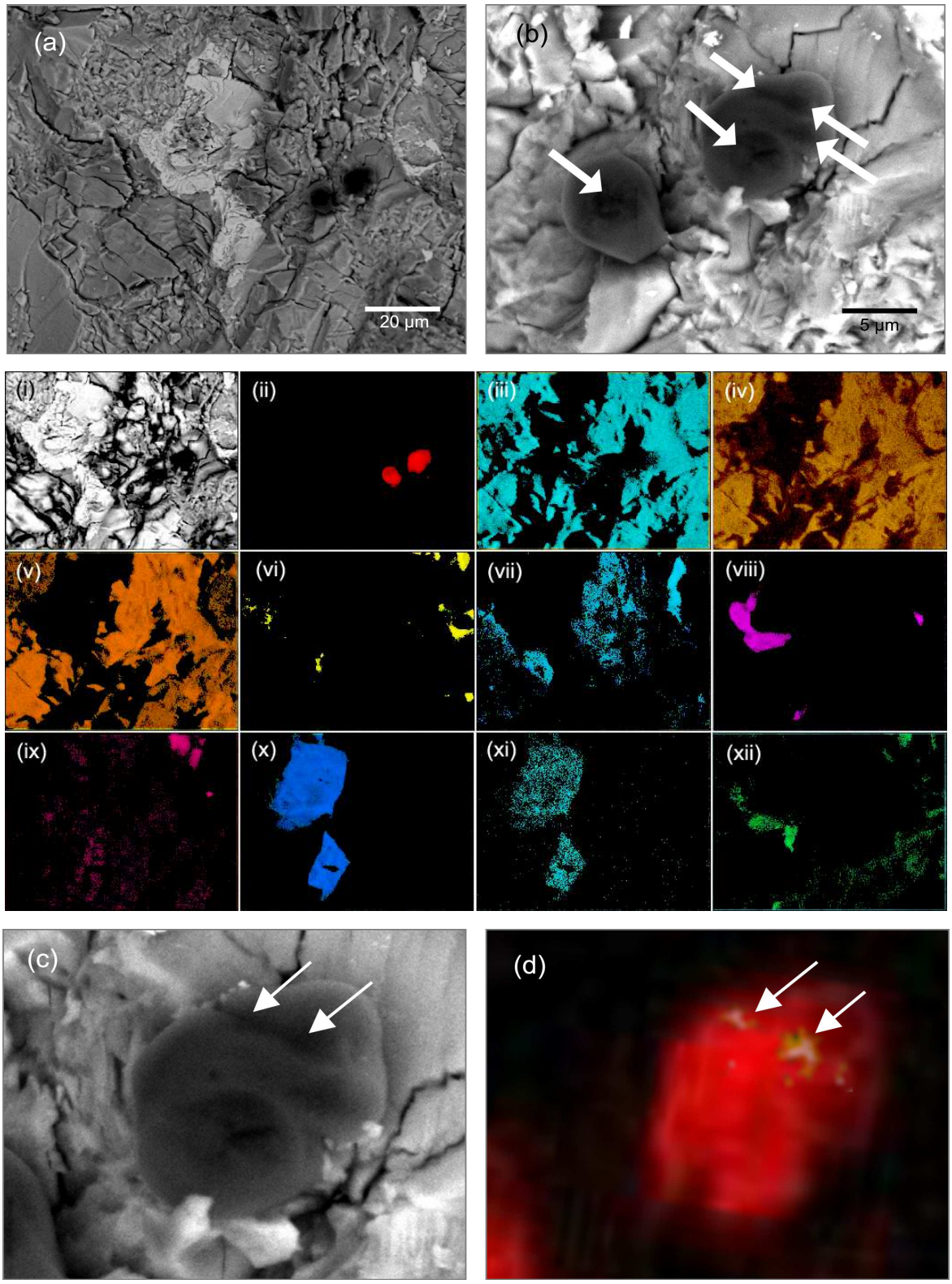

Figure 2.6 (a) SEM micrograph of two carbonaceous globules selected for surface attenuation by 15KeV electron beam together with (b) high magnification micrograph of the globules (i) SEM contextual image of the same with arrows marking the points of attenuation of the carbonaceous mantle. Inserts (ii) to (xii) show 2-D elemental x-ray map corresponding to C, O, Mg, Si, S, Ca, Ti, Al, Cr, Mn, Fe respectively. (Lower) (c) high magnification image of the upper globule shown in (i) above after attenuation (d) shows 2-D elemental map for Carbon (red) overlaid by Sulphur (yellow). Note in particular the arrows showing surface weakening in (a) and the corresponding detection of S in the vicinity of the weakened points in (b).

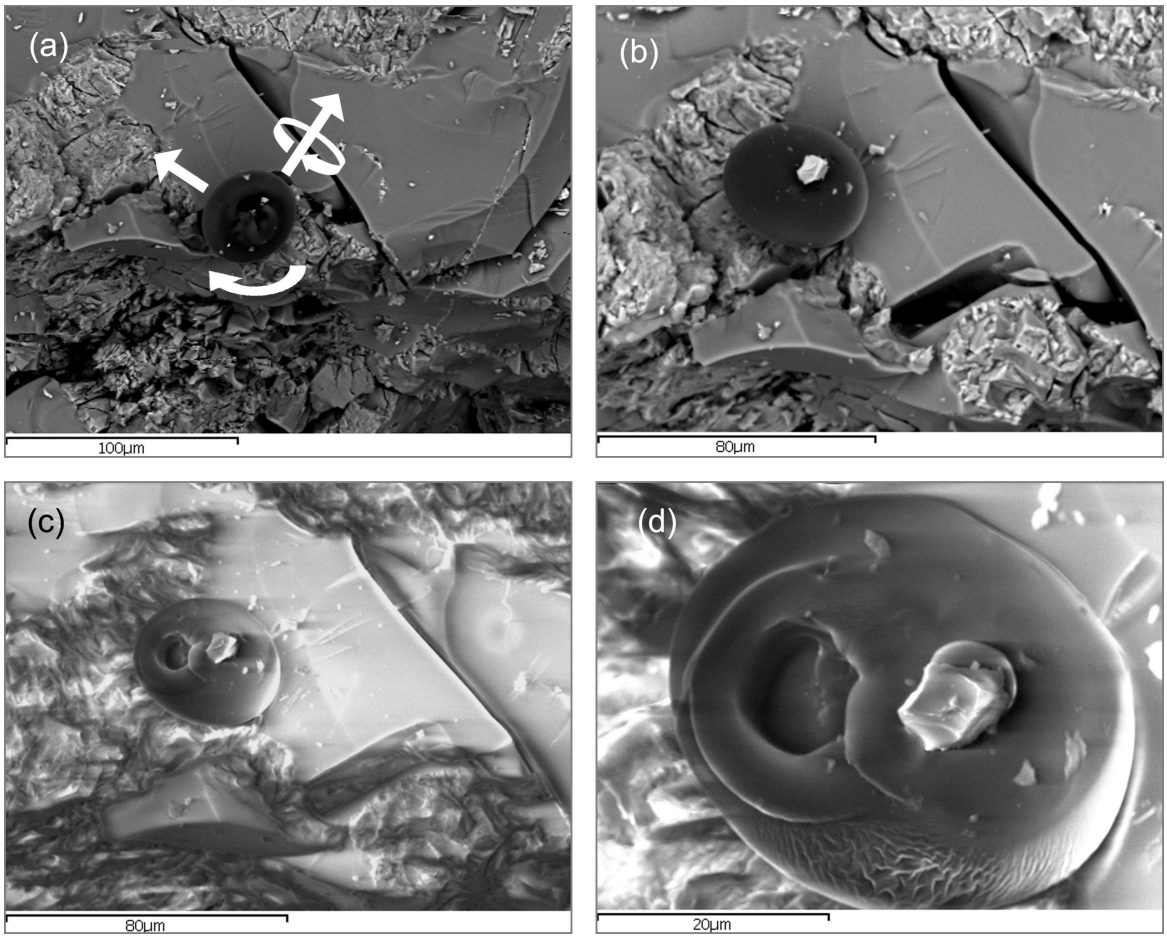

Figure 2.7 (a) Back scatter SEM micrograph of 40µm unbound carbonaceous globule and its free movement within the SEM chamber to a new resting position in (b). (c) GSE micrograph of the same globule following acquisition of elemental data by 20KeV electron beam and (d) same globule after repeated exposure to beam showing general degradation of the globule including flattening in shape and apparent damage to the carbonaceous coating away from the point of beam capture.

Figure 2.7 (a) shows a backscatter SEM micrograph of a selected globule using the FEI (Phillips) XL30 FEG ESEM at the School of Earth and Ocean Sciences at Cardiff University. The unbound nature of this globule is demonstrated by its movement within the SEM chamber from the position shown in (a) to a new resting position in (b).

Figure 2.7 (c) shows a GSE micrograph of the same globule following acquisition of elemental data and consequential damage by the 20KeV electron beam. It was noted that repeated use of the electron beam failed to penetrate the carbonaceous mantle to a greater depth indicating that the carbonaceous mantle was ~2 µm thick at this point. However, further degradation of the globule was noted including a general flattening in shape and apparent damage to the carbonaceous coating

away from the point of beam capture. Results of the EDS elemental analysis are provided in Figure 2.8 above for both the carbonaceous globule and an area of substrate ~50 µm to the right.

In order to confirm the nature of the S-bearing mineral core, EDAX measurements were taken of the larger 40 µm globule. Figure 2.8 shows EDS elemental spectra for the globule identified in figure 2.7. The carbonaceous nature of the globule is evident from the spectra when compared to a similar spectra taken from a region of the host matrix approximately 50 µm to the right of the globule. The presence of S was only evident in the second spectra acquired from the same damaged area as the first and appears to reflect sampling from the core inclusion. Comparative representative oxide compositions indicate an increased presence of Fe and S in succesive spectra acquired from globules indicating atomic ratios of 2:1 in favour of S. Consequently, EDS analysis indicates that the globules comprise of a carbonaceous outer coating with a inner core of FeS_2 (pyrite).

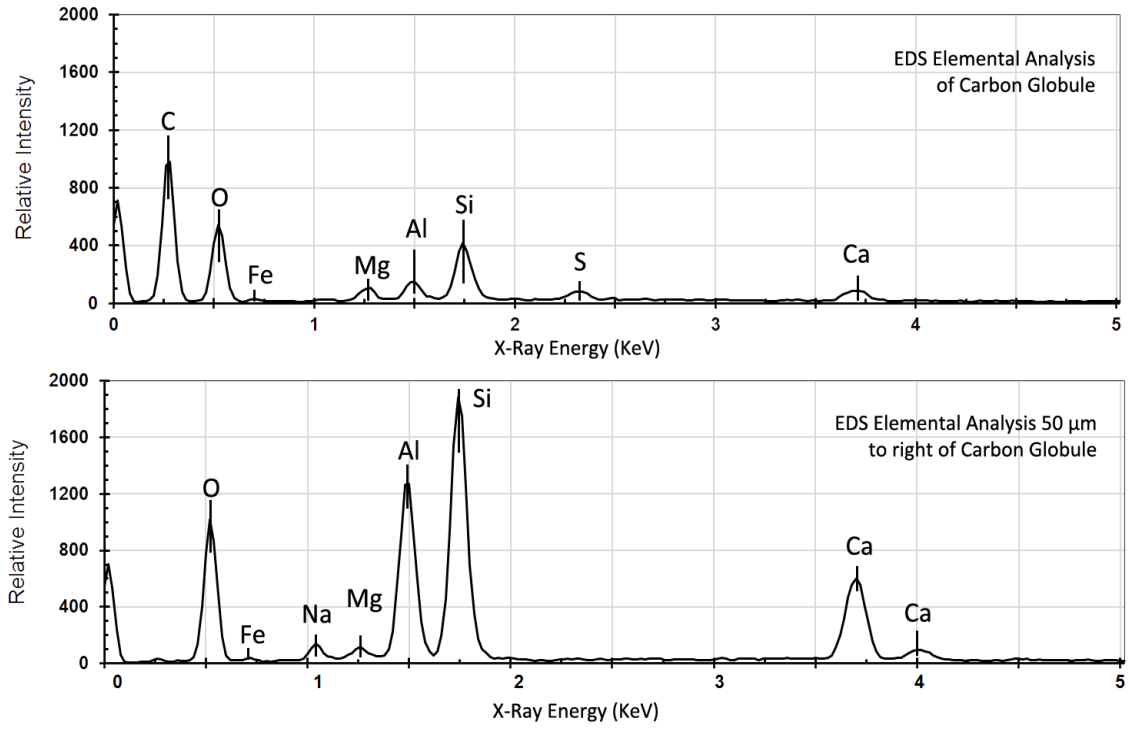

Figure 2.8 EDS elemental spectra for the globule identified in figure 2.7 (upper) compared to similar spectra taken from a region of the host matrix approximately 50 µm to the right of the globule. The carbonaceous nature of the globule is evident from the comparative spectra. Note also the presence of S in the spectra which is the second spectra acquired from the same damaged area.

To verify the incidence of the above observation, a further 11 globules were identified and successive EDS spectra acquired with corresponding representative oxide compositions then compared for four successive acquisition procedures. In each case the presence of S and increased Fe was detected with stoichiometric ratios consistent with the presence of pyrite inclusions.

2.7 AFFINITY BETWEEN PYRITE AND ORGANIC MATTER

The relationship between pyrite and organic matter is of interest to both the surface mediated chemoautrophic origin-of-life hypothesis (Wachtershauser, 1990a, 1990b, 1991, 1992, 1993) as well as non-surface related (i.e. geological) formation processes responsible for the widespread occurrence of organic matter in hydrothermal ore and sulphide deposits (Landais, 1997). Both pyrite and organic carbon are ubiquitous on Earth. Pyrite is found in submarine hydrothermal vents (Hannington *et al.*, 1995) hot spring environments (Day and Allen, 1925) and anoxic groundwater systems (Larsen and Postma, 1997). Furthermore, the affinity between pyrite and migrated organic matter has been observed in the geological record in hydrothermal calcite veins from carboniferous limestones in central Ireland (Lingren *et al.*, 2011). Here, the formation of pyrite and organic matter structures takes place beneath the surface, with the organic matter characterised as coatings around pyrite crystals as well as immiscible globules with curved boundaries in the calcite substrate.

Figure 2.9 (a) shows a back scatter SEM micrograph of the 40µm unbound carbonaceous structure located in Tissint and previously described in Figures 2.7 (a) and (b). For comparison, Figure 2.9 (b) shows a similar carbonaceous structure located in the carboniferous limestones in central Ireland (Lingren *et al.*, 2011). Similarly, Figure 2.9 (c) shows a backscatter SEM micrograph of a pyrite crystal coated with organic matter in the Tissint meteorite. The pyrite crystal appears white, the organic matter is black and the substrate grey. The inserts show ED X-ray maps for sulphur (green) and carbon (red). Raman Spectroscopy was utilised in the comparison of the spectral signatures of the carbonaceous material sampled in the globules with that of the thin sections to ensure that characteristic factors reflecting metamorphic grade and crystallinity matched. This ensured that carbon introduced during the preparation of the thin sections was not sampled and compared with organic material present in the mantle of the carbonaceous structures.

For comparison, a similar image is shown for a pyrite crystal coated with organic matter in the hydrothermal calcite veins of Mullaghwornia quarry in central Ireland (Lingren *et al.*, 2011). These authors found evidence of pyrite acting as an attractive substrate for the collection of organic matter in twenty-four of twenty-six observed pyrite crystals occurring in six blocks and thin sections from two different branches of the vein deposits.

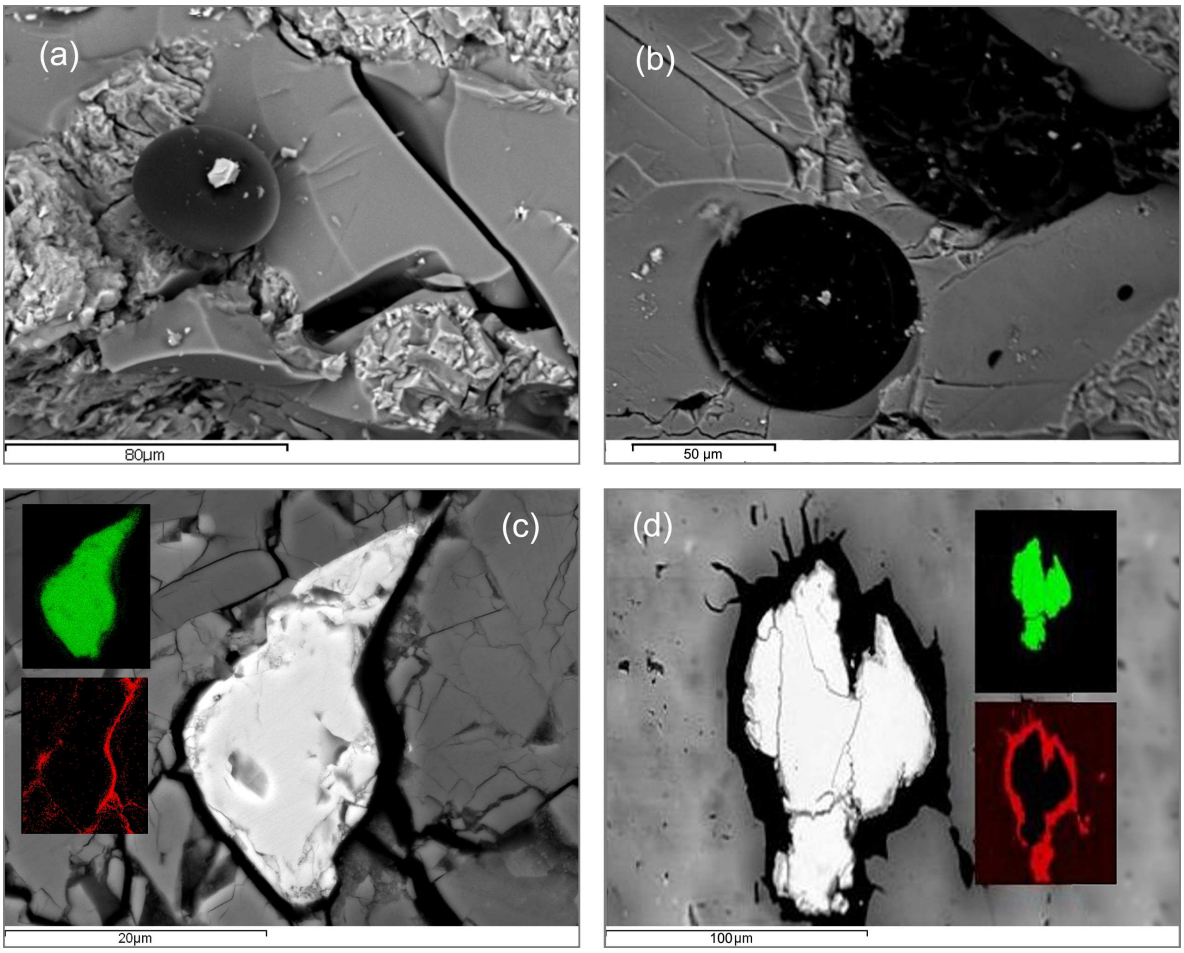

Figure 2.9. (a) shows a back scatter SEM micrograph of a 40µm unbound carbonaceous globule located in Tissint compared to (b) a similar carbonaceous globule located in the carboniferous limestones in central Ireland. Similarly, (c) shows a backscatter SEM micrograph of a pyrite crystal coated with organic matter in the Tissint meteorite. The pyrite crystal appears white, the organic matter is black and the substrate grey. The inserts show ED X-ray maps for sulphur (green) and carbon (red). For comparison an identical image is shown for a pyrite crystal coated with organic matter in the hydrothermal calcite veins of Mullaghwornia Quarry in central Ireland. Images (b) and (d) adapted from Lingren *et al.*, (2011).

The relationship between pyrite and organic material is not always straightforward. Parnell, Carey and Bottell (1994) found numerous examples of the direct precipitation and growth of authigenic minerals including pyrite in bitumen. Alternatively, Leventhal *et al.*, (1987) found a probable connection between the abrasion of pyrite from surrounding rock by migrating organics in the Claude deposit of Cluff Lake, Canada. Furthermore, the formation of pyrite can arise both abiogenically (pyrite framboids arising from fast crystal growth) and biogenically (pyrite framboids arising from microbial activity or sulphate reducing bacteria). Consequently, it is not possible to

deduce from the morphology of the structures alone if the mechanisms responsible for their formation involved purely abiotic or part-biotic processes.

In their study, Lingren *et al.,* (2011) suggest that the immiscibility and morphology of the globules found in the Mullaghwornia deposits indicates that the organic precipitating fluid may have coexisted with the calcite precipitating fluid. Alternatively they suggest that the organic matter may have been deposited at a later stage as a secondary infilling of dissolution cavities in the calcite substrate. The identification of organic material within pyrite crystal fractures certainly appears to support this latter conjecture. However, the presence of pyrite cores surrounded by organic mantles exhibiting observable geometric coincidence with the crystal core appears to rule this out in the case of Tissint. In particular, whilst abundant cavities were noted in the pyroxene substrate of Tissint, together with more geometrically uniform cavities in the denser more amorphous phases, the likelihood of near spherical pyrite crystals forming within near spherical dissolution cavities renders this an unlikely circumstance.

The nature of the precipitated precursor organic material however, remains of key interest to the question of origin. A highly complex precursor organic may represent evidence of the detritus of biology while the accumulation of low molecular weight organic compounds may provide support for the suggestion that the formation of pyrite could be the first energy source for life (Wachtershauser, 1988). Here, interactions dictated by either electrostatic forces alone, or alternatively a combination of electrostatic forces and chemical bonding may be responsible for interactions between the sorbate and pyrite surface. Bebie and Schoonen (2000) investigated the interaction of various types of organic molecules with pyrite as a function of pH under anoxic conditions by electrophoresis and batch sorption experiments. Results indicate that the interaction of organic aqueous species with pyrite surfaces under anoxic conditions cannot be satisfactorily described using general surface charge arguments alone.

Metal sulphide surfaces contain at least two types of surface functional groups (thiol surface group and iron surface group) thus enabling the binding of chemically different species. Electron transfer between co-absorbers can thus generate chemical products that would be difficult to form on a single surface site. Furthermore, electron transfer between co-absorbers is facilitated by the semiconductor nature of pyrite since electron exchange can occur by the injection and withdrawing of electrons from the semiconductor (Xu *et al.,* 1996; Schoonen *et al.,* 1998; Xu *et al.,* 1995). This effectively means that co-absorbates only require orbital overlap with surface atoms and not with each other further facilitating the formation of chemical species unlikely to otherwise form in solution.

2.8 CONCLUDING REMARKS

The viability of several of the initiating chemical reactions proposed in the iron-sulphur world hypothesis have been satisfactorily demonstrated in the laboratory. Nonetheless, *in-situ* evidence of the more complex chemical transformations required to explain the immiscible nature of the carbonaceous coatings observed in Tissint have not been reported. The 2μm depth of the carbonaceous membrane bound to the pyrite core is more easily explained by the membrane comprising of high molecular weight complex organics as oppose to low molecular weight organic monomers. At this stage it appears more likely that pyrite crystals, rounded or sub-rounded by abrasion in a precipitating fluid, acted as an attractive substrate for the collection of complex organic matter in a hydrothermal environment. Further studies on the nature of the organic component in Tissint may help to eventually resolve this issue.

Chapter 3

Chemical and Structural Composition of Organic Carbonaceous Structures in Tissint: Evidence for a Biogenetic Origin

3.1 INTRODUCTION

Sulphide grains rimmed by a layer of reduced organic carbon have previously been detected in carbonaceous chondrites, chondritic IDPs (Rietmeijer and Mackinnon, 1985; 1987) and primitive chondritic meteorites (Tagish Lake) (Nakamura *et al*., 2002). Similar structures have been found in terrestrial environments including Proterozoic and Ordovician sandstones in Canada (Nardi, 1994) and hydrothermal calcite veins in Carboniferous limestones in central Ireland (Lindgren *et al.*, 2011). The detection of pyrite grains coated with thin carbonaceous mantles in the Tissint Martian meteorite poses the important question of nature and origin. A highly complex precursor organic mantle may represent evidence of the precipitation of the detritus of biology while the accumulation of low molecular weight organic compounds may alternatively provide *in-situ* evidence of several of the chemical processes predicted by the iron-sulphur world hypothesis.

Raman spectroscopy can be a useful tool in the correlation of the spectral signatures of carbonaceous materials. These signatures reflect a range of factors including metamorphic grade and crystallinity and are characterised by a 'disordered' graphitic band known as the D-band (at ~1350 cm^{-1}) together with an associated 'ordered' band known as the G-band at (~1580 cm^{-1}). The D-band may also reflect the presence of hetero atoms (H, N, O) resulting in in-plane defects (Beny-Bassez and Rouzaud, 1985). G-band spectral properties are insensitive to laser excitation wavelength and power, but there is some indication that corresponding D-band characteristics may be sensitive to slight variations in these parameters (Wang *et al*., 1990, Schopf *et al*., 2005). The general characteristics of the D and G-bands, such as width, relative intensity and peak position can vary depending on the degree of thermal alteration, the complexity of the precursor carbonaceous material and the level of crystallinity of the carbon (Pasteris and Wopenka, 2003; Busemann *et al*., 2007; Marshall *et al*., 2010). These features have recently been relied upon in a number of fossil studies as sensitive indicators of metamorphic history (Allwood *et al.*, 2006; Bernard *et al.*, 2007; Marshall *et al.*, 2010).

The residue of biogenic material (i.e. once living organisms) however, comprises primarily of several different benzene ring-containing, C-O-H-dominated molecules and is commonly referred to as kerogen. While Raman spectroscopy typically shows generic spectral features associated with discontinuous arrays of condensed benzene rings, it does not show evidence of functional groups such as CH, CH_2, CH_3, CO and CN. This means that the same kind of Raman spectral signature is generated by kerogen as by other poorly ordered carbonaceous materials that may be produced by a variety of abiotic processes. Consequently, whilst Raman spectroscopy can provide important insight into the nature of precursor carbonaceous material, the level of crystallinity of the carbon, or the degree of thermal alteration, it cannot definitively identify a sample as 'kerogen', but only as 'disordered carbonaceous material' (Pasteris and Wopenka, 2003).

3.2 RAMAN SPECTROSCOPY

Raman spectroscopy detects the inelastic scattering, or Raman scattering, of monochromatic light interacting with the vibrational modes of molecular bonds or crystal lattices. The interaction with molecular vibrations results in the energy of incident photons being shifted up or down which in turn gives rise to information about the vibrational modes of the system. This information includes the electronic configuration of graphitic sp^2 versus diamond sp^3 hybridisation and thus detects the structural order of carbonaceous material.

Several approaches have been utilised to theoretically model the lattice dynamics of the experimentally derived Raman spectra of graphite (Nenamich and Solin, 1979; Lespade *et al.*, 1982) giving rise to some important points on the interpretation of the Raman signatures of naturally occurring carbonaceous material. Firstly, only two in-plane modes among the 12 zone-centre optical lattice modes in well crystallised graphite are Raman active. In practice, one of these is so low in frequency (42 cm^{-1}) that it cannot be resolved from Rayleigh scattering meaning that only the E_{2g} mode at 1582 ± 1 cm^{-1} is observed in the first order Raman spectra of well crystallised graphite. Secondly, while the theoretical wave-vector selection rules remain valid for crystals of infinite in-plane crystallite size, they break down as crystallite size decreases below a minimum value. This allows associated light scattering processes to occur from phonons outside the zone centre of the phonon dispersion curve. Essentially the graphitic structure becomes disordered in the Raman spectroscopic sense and can be observed in both first and second-order Raman spectra. This accounts for the additional disorder-induced D-band at ~1350 cm^{-1} observed in the Raman spectra of carbonaceous material in microcrystalline form.

3.3 ANALYTICAL METHODS

In order to further understand the origin, nature and metamorphic history of the carbonaceous globules identified during previous SEM studies, high resolution Raman imaging spectroscopy was undertaken on a selection of globules that were located in both bound and unbound states within the pyroxene groundmass of the Tissint meteorite. Raman signatures would also assist in the identification of terrestrial contaminants since modern graphite would be unlikely to exhibit spectral features corresponding to indigenous macromolecular carbon already identified in numerous Martian meteorites such as ALH84001, DaG 476, Dhofar 019, Nakhla, Zagami, NWA 1110 and Tissint (Steele *et al.,* 2012). Such identifications have confirmed the nature of indigenous reduced macromolecular carbon, though the provenance of this carbon component is still debated. Hypothesis on origin include input from meteoritic chondrites (Becker *et al.,* 1999), thermal decomposition of carbonate minerals (Steele *et al*., 2007; Treiman, 2003; Zolotov and Shock, 2000), aqueous precipitation (Steele *et al*., 2007), terrestrial contamination (Jull *et al*., 1998; Stephan *et al*., 2003) and the remnants of ancient biota (McKay *et al.*, 1996).

High resolution Raman spectra were analysed for a selection of nine sample carbonaceous structures identified in SEM studies. These were acquired using a Renishaw inVia microRaman system at the School of Chemistry, Cardiff University, UK. Laser focusing of the sample was performed using a research grade Leica analytical microscope fitted with a 100x objective and a 514.5 nm Argon laser line. Data processing was via the Wire2 software application for data output to hard drive. Spectroscopy was performed on unpolished freshly cleaved surfaces at room temperature with spectra collected in 20 increments with a measuring time of 3s each. Control spectra were further acquired using the microRaman system at the Department of Geographical and Earth Sciences, University of Glasgow.

Average G-band and D-band values with standard deviation for G-band peak position and full width half height of the G-band (Γ_G) were recorded. Similarly, D-band peak position, full width half height of the D band (Γ_D) and D-band intensity/G-band intensity (R1) were also determined. Results were compared to corresponding values determined in a previous study of macromolecular carbon in ten Martian meteorites (ALH84001, DaG 476, Dhofar 019, Nakhla, Zagami, NWA 1110, NWA 2986, SAU 130, NWA 998, NWA 1950 and NWA 2737) (Steele *et al.,* 2012).

Results were further compared to organic material extracted from a variety of related extra-terrestrial sources. These included organic matter extracted from meteorites originating from asteroids (Alexander *et al.,* 2007), primitive IDPs (interplanetary dust particles) (‘chondritic

porous') collected by NASA aircraft (Bradley, 2003) and comet Wild 2 dust returned with NASA's Stardust mission (Brownlee *et al*., 2006). Results of Raman spectroscopic analysis, together with a compilation of associated spectral parameters are from Busemann, Alexander & Nittler (2007).

3.4 RESULTS

Results of Raman spectroscopy show a high level of consistency in spectral features in both D and G-band parameters in the carbonaceous globules identified in the samples. In particular, both G-band peak position and Γ_G parameters exhibited only small variation across all samples. Figure 2.9 shows the results of a typical Raman pattern acquired from the 10µm carbonaceous egg-shaped globule shown resting on the loosely aggregated pyroxene groundmass (see Figure 4, Wallis *et al.*, 2014). The spectra showed G-band peak parameters Ω_G (cm^{-1}) = 1577 ± 0.3 with associated Γ_G (cm^{-1}) = 130 ± 0.1 and corresponding D-band peak Ω_D (cm^{-1}) = 1349 ± 0.3 and Γ_D (cm^{-1}) = 220 ±0.7. The D-band intensity/G-band intensity parameter of R1 = I_D /I_G = 0.915 ± 0.038 indicates a level of graphitisation consistent with comparable Martian meteorites.

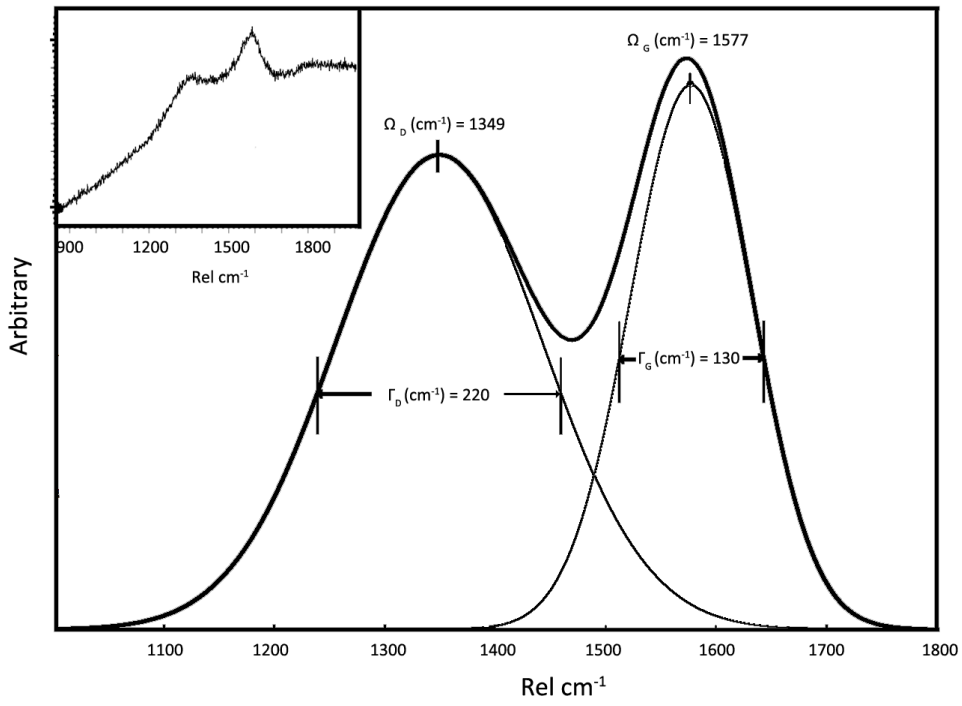

Figure 3.1 Shows a typical Raman spectra for the carbonaceous material sampled in the globules observed in Tissint. The spectra shows a G-band peak parameter Ω_G (cm^{-1}) = 1577 with associated Γ_G (cm^{-1}) = 130 ± 0.1 and corresponding D-band peak Ω_D (cm^{-1}) = 1349 ± 0.3 and Γ_D (cm^{-1}) = 220 ± 0.7. The D-band intensity/G-band intensity parameter of R1 = I_D /I_G = 0.915 ± 0.038. Insert shows raw Raman signal prior to removal of background noise.

3.5 PEAK TEMPERATURES

Raman spectroscopy has previously been used to determine peak temperatures responsible for the thermal metamorphism of insoluble organic matter extracted from the Tieschitz chondrite (Christophe Michael-Levy and Lautie, 1981). Here the relative peak intensity (D-band intensity/G-band intensity) R1 = 1.05 ± 0.04 was used to establish a peak temperature of 300-350 ^{O}C. Busemann, Alexander and Nittler (2007) found a slightly higher R1 ratio of 1.150 ± 0.075 indicating a peak temperature of ~370^{O}C due to either sample heterogeneity or higher peak temperatures being experienced by the bulk insoluble organic matter.

However, there is strong evidence that peak metamorphic temperatures correlate directly with the Raman peak width (Γ_D) and can thus be used directly to infer peak temperatures in meteorites (Busemann, Alexander and Nittler (2007). Busemann, Alexander and Nittler (2007) analysed the Raman properties of insoluble organic matter extracted from 51 unequilibrated chondrites (comprising of 8 CR, 9 CM, 1 CI, 9 CO, 9 CV, 1 CB, 1 E, 10 ordinary and 3 ungrouped chondrites). Results showed systematic trends that correlated to meteorite classification and sub-classification as well as the chemical composition of the insoluble organic matter. In particular, estimated peak metamorphic temperatures as determined by Huss *et al*., (2006) correlated to first order with chondrites from all classes on a trend determined by a second order polynomial (R^2 = 0.95). This yielded the expression for the peak metamorphic temperature (PMT):

$$PMT\ (^{O}C) = 931\text{-}5.10 \times \Gamma_D \times cm^1 + 0.0091 \times \Gamma_D{}^2 \times cm^2 \qquad \text{(eq. 3.1)}$$

Figure 3.2 shows the peak metamorphic temperatures as provided by Huss *et al*., (2006) against, full width half height of the D-band (Γ_D). Correlation is shown using the second order polynomial provided in eq. 3.1. Also shown is the Γ_D (cm^{-1}) = 220 value determined for the carbonaceous material sampled in the globules observed in Tissint from which it can be inferred that the organic material was subjected to a peak temperature of ~250 ^{O}C.

Whilst the above observation suggests that the Raman characteristics of insoluble organic matter are primarily determined by peak temperature, it is noted that there is some evidence to suggest that quite severe heating for short periods does not alter the organic matter to the same extent as prolonged thermal metamorphism (Bussemann, Alexander and Nittler, 2007, 2011). This observation may be important since the complexity of the precursor carbonaceous inventories of meteorites can only be determined in situations where thermal overprinting has not erased diagnostic spectral characteristics.

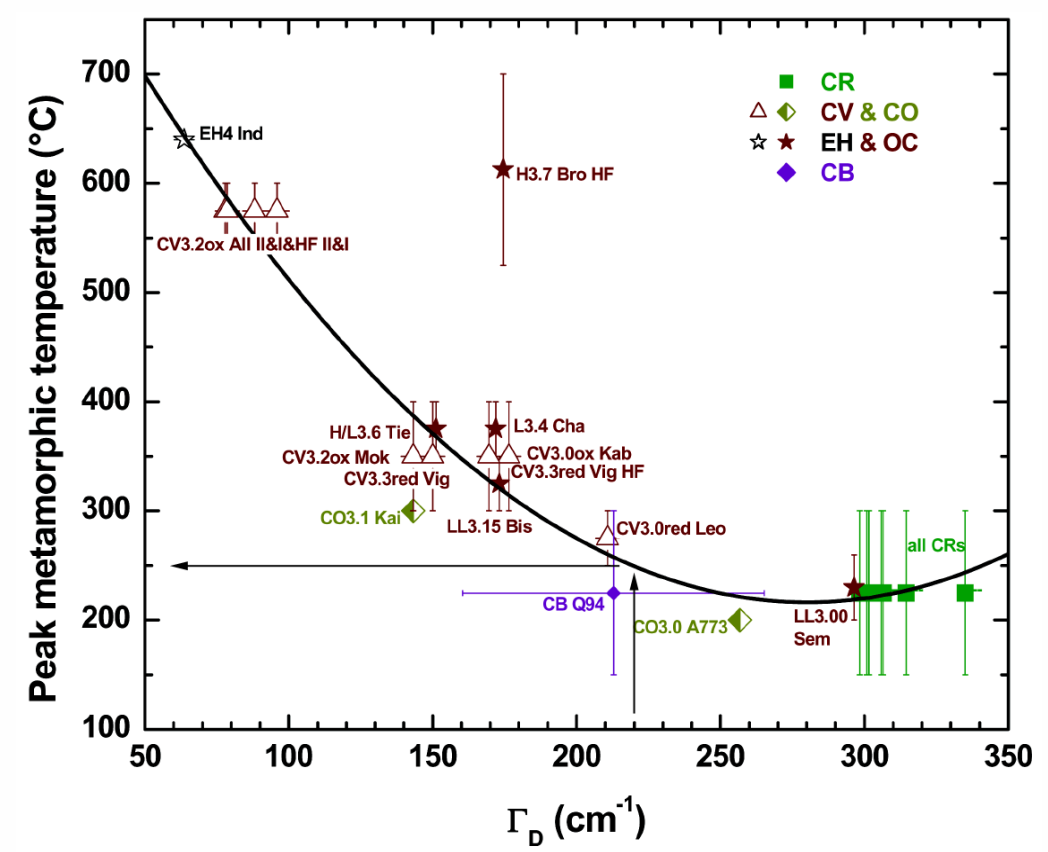

Figure 3.2 Shows peak metamorphic temperatures as provided by Huss *et al.*, (2006) against Raman D-band (Γ_D) parameter. Correlation is shown using the second order polynomial PMT (^{O}C) = 931-5.10 × Γ_D × cm^{1} + 0.0091 × Γ_D^2 × cm^{2}. Also shown is the Γ_D (cm^{-1}) = 220 value determined for the carbonaceous material sampled in the globules observed in Tissint from which it can be inferred that the organic material was subjected to a peak temperature of ~250 ^{O}C. Figure adapted from Busemann, Alexander and Nittler, (2007).

3.6 PRECURSOR CARBONACEOUS INVENTORIES

Bower *et al.*, (2013) used micro Raman spectroscopy to study microfossils from a range of sedimentary rocks of various ages together with CM2 and CV3 carbonaceous chondrites to investigate the nature and provenance of the carbonaceous material.

Here, samples included fossils extracted from the Rhyne chert (Scotland) of age 400 Ma and the Gunflint chert (Ontario Canada, ~1.9Ga) with peak metamorphic temperature exposures <150^{O}C. In these samples the origin of carbonaceous material was of known biotic source (plants, algae,

fungi, crustaceans, prokaryotes). Lower to mid greenschist peak metamorphic temperatures were represented by fossil samples from the Apex Chert (Western Australia, ~3.5 Ga) and the Tumbiana Formation (Australia, ~2.7 Ga). Meteorite samples representing similar peak metamorphic temperatures included the Murchison CM2 carbonaceous chondrite (~4.6 Ga, with low temperature aqueous alteration) and the Allende CV3 carbonaceous chondrite (~4.6 Ga, with aqueous alteration T>1000 ^{O}C followed by rapid cooling).

Bower *et al*., (2013) found that while it was impractical to use D and G-band intensity ratios (R1) alone to elucidate the origins of the carbonaceous materials across all samples, when Γ_D (cm^{-1}) values were plotted against R1 ratios the sample sets clustered into different groups correlating to the complexity of the precursor carbonaceous material.

Figure 3.3 shows a comparison of R1 = I_D /I_G against Γ_D (cm^{-1}) band parameters for a range of reduced carbonaceous material extracted from both terrestrial and non-terrestrial sources.

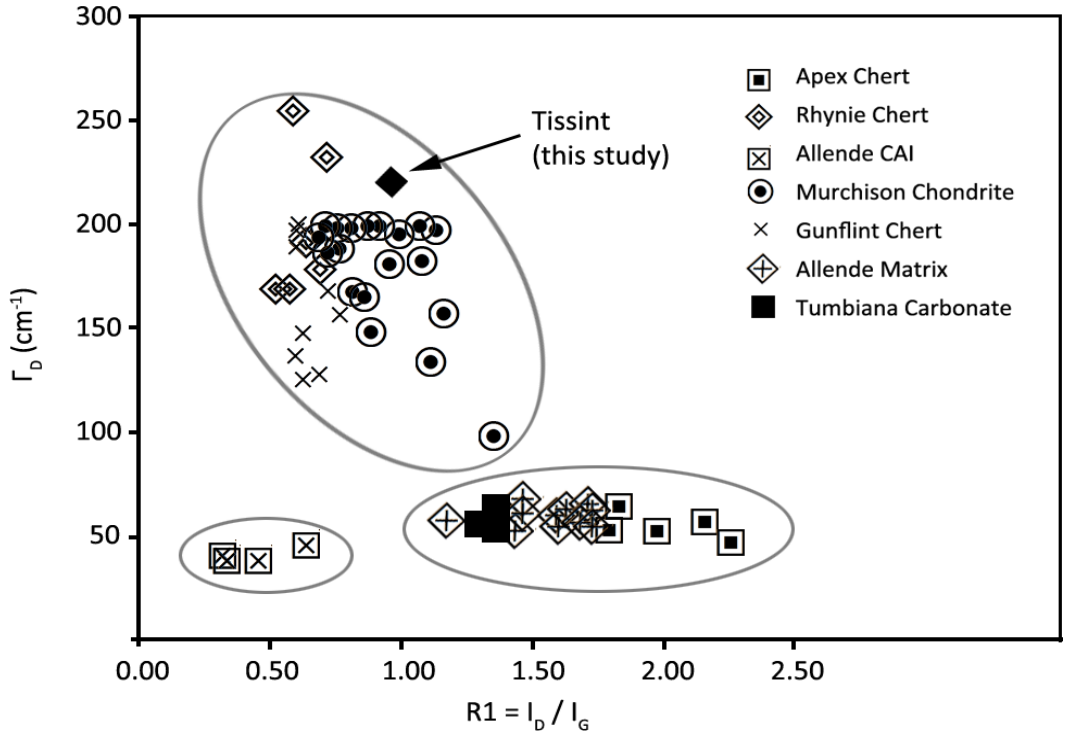

Figure 3.3 Comparison of R1 = I_D / I_G against Γ_D (cm^{-1}) for fossils extracted from a variety of comparative sources. Samples with complex precursor carbonaceous inventories can be seen to cluster - Rhyne chert, Gunflint chert and Murchison CM2 carbonaceous chondrite, ~27 ^{O}C > T < ~150 ^{O}C. Similar clustering can be seen in fossils analysed in the Apex Chert and the Tumbiana Formation ~300 ^{O}C > T < ~1000 ^{O}C. Purely graphitic carbon in the Allende CAI , T > 1000^{O}C is also shown. Data and figure adapted from Bower *et al.*, (2013).

Here, samples with complex precursor carbonaceous inventories can be seen to cluster when compared to sources with less compositionally complex or hydrothermally overprinted material (Bower *et al.*, 2013). It is noted that clustering of R1 = I_D/I_G against Γ_D (cm^{-1}) band parameters that is evident in the results appears to be irrespective of terrestrial or non-terrestrial origin.

The position of $[I_D/ I_G] / \Gamma_D$ (cm^{-1}) plot of carbonaceous material taken from the mantle of the globules identified in SEM studies of Tissint indicate a compositionally complex precursor component associated with metamorphic temperatures up to ~250 ^{O}C and associated D-band disorder parameters Γ_D (cm^{-1}) consistent with both terrestrial and non-terrestrial sources of age between ~400 Ma and ~4.6 Ga.

3.7 ORIGIN OF CARBONACEOUS COMPONENT

The detection of macromolecular carbon (MMC) phases in martian meteorites has previously been reported by Steele *et al*., (2012). Here, Confocal Raman Imaging Spectroscopic (CRIS) studies of MMC phases associated with small oxide grains were found completely encased within silicate hosts. Prior to the acquisition of MMC Raman signatures, isolation of the MMC component was first established by a combination of transmitted and reflected light microscopy (Steele *et al.*, 2012).

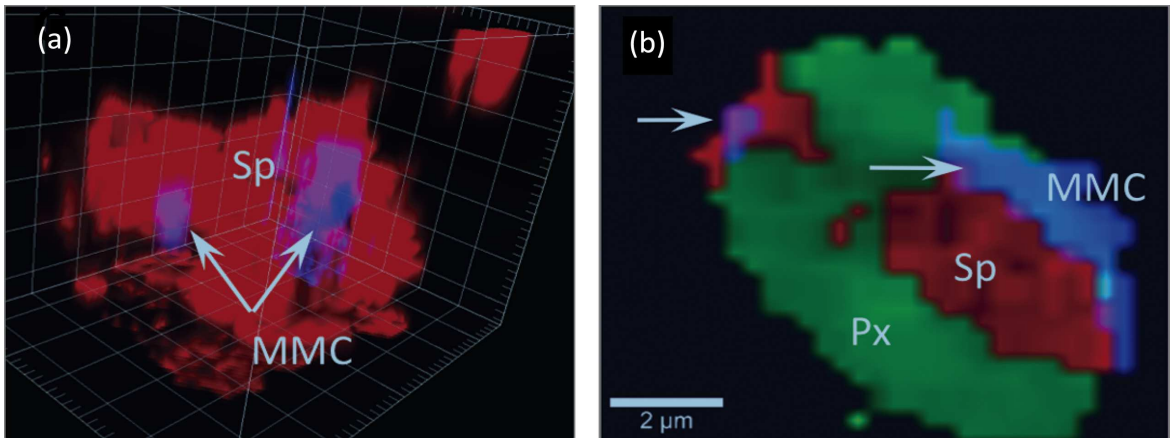

Figure 3.4 (a) Confocal Raman Imaging Spectroscopic 3-D depth profile through a melt inclusion 5 to 20 µm into the sample surface in DaG 476. The red colour indicates the presence of a spinal-group oxide while blue denotes the presence of a reduced carbon component. The grid is in 2 µm increments. Figure 2.12 (b) shows a 2-D Raman map of common macromolecular carbon with an associated oxide phase (Figure from Steele, *et al*., 2012).

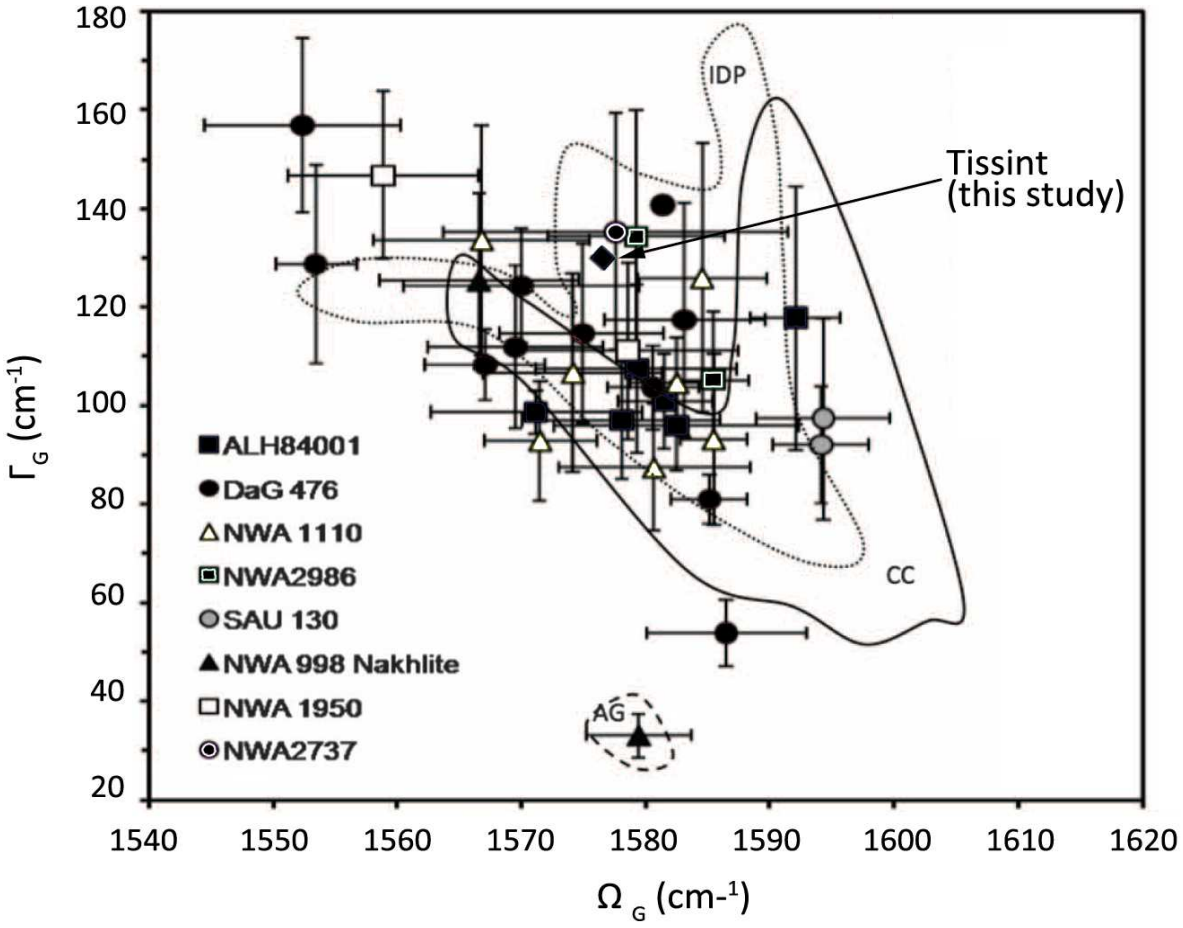

Figure 3.5 Ω_G (cm^{-1}) and Γ_G (cm^{-1}) parameters for macromolecular carbon phases positively detected in eight of eleven Martian meteorites analysed (Steele *et al.*, 2012) comprising of ALH84001, DaG 476, NWA 1110, NWA 2986, SAU 130, NWA 998, NWA 1950 and NWA 2737. Parameters for organic material derived from the mantle of carbonaceous globules identified in this study are represented by a solid black arrow. The black line represents the variation in these parameters as observed in carbonaceous chondrites dotted black line represents variations in similar parameters of interplanetary MMC dust particles (IDP). A standard graphite spectrum is marked AG and represents ordered crystalline carbon. Figure adapted from Steele *et al.*, (2012).

Figure 3.4 (a) shows a CRIS 3-D depth profile through a melt inclusion 5 to 20 µm into the sample surface in DaG 476. The red indicates spinel-group oxide with blue denoting MMC. The grid is in 2 µm increments. Figure 3.4 (b) shows a 2-D Raman map of common MMC with an asscoiated oxide phase. The presence of MMC phases conpletely encased within silicate hosts effectively rules out terrestrial origin and confirms the indiginous nature of the carbon analysed.

MMC phases completely encased within silicate hosts were positively detected in eight of the eleven Martian meteorites analysed including ALH84001, DaG 476, NWA 1110, NWA 2986, SAU

130, NWA 998, NWA 1950 and NWA 2737 (Steele *et al.,* 2012). Ω_G (cm^{-1}) and Γ_G (cm^{-1}) parameters are plotted in Figure 3.5. Parameters for organic material derived from the mantle of carbonaceous globules identified in this study are represented by a solid black arrow. CRIS results indicate that G-band parameters for the carbonaceous mantle component of globules identified in this study of Tissint are entirely consistent with those of indigenous macromolecular carbon located in a range of Martian meteorites. These meteorites crystallised over a ~4.2 billion year period ranging from ALH84001 (4.43 Ga) to NWA 1110 (0.19 Ga).

To further elucidate the nature of the carbonaceous component, a comparison of Ω_D (cm^{-1}) and Γ_D (cm^{-1}) parameters was undertaken by contrasting values derived in this study with similar parameters taken from a variety of extra-terrestrial organic matter (Bussemann, Alexander and Nittler, 2011). Here, insoluble organic matter was extracted from meteorites derived from asteroids, IDPs and JFC Wild 2 dust. The insoluble organic matter was separated from the main chondritic silicates of the meteorite samples by demineralisation and soluble removal (Cody *et a*l., 2002). The remaining material represents ~75% insoluble mass fraction of the meteorite's carbon component, the remaining fraction being soluble in water or organic solvents (Gilmour, 2003).

Of the IDPs examined, a subset were collected during Earth's passage through comet Grigg-Skjellerup's dust stream (GSC) and are thought to contain fresh dust from a known cometary source (Messenger, 2002). By contrast organics in Wild 2 dust were collected in quite harsh conditions having been decelerated from a velocity of 6.1 km/s within a few mm to cm of aerogel and are likely to have suffered flash heating, evaporation, ablation and complete or partial melting. Peak temperatures of T>1000 K may have been experienced for short periods ~1µs (Coulsen, 2009).

Ω_D (cm^{-1}) and Γ_D (cm^{-1}) parameters for the various classes of meteorites are shown in figure 3.6. Classification was based on chemical, isotopic and mineralogical compositions (Weisberg, *et al.,* 2006) and reflects thermal and aqueous alteration. Figure 3.6 also shows Ω_D (cm^{-1}) and Γ_D (cm^{-1}) parameters for GSC-IDPs (Comet Grigg-Skjellerup's IDPs), normal IDPs and Stardust (organics in Wild 2 stardust). Parameters for organic material derived from the mantle of carbonaceous globules identified in this study are represented by a solid black arrow.

Data points in figure 3.6 indicate that the sampled organic material in Tissint shows similar Raman parameters to the less thermally altered more primitive ordinary chondrites (CR, CI, CM) as opposed to the CO, CV and OC chondrites, thought to have experienced greater levels of thermal metamorphism. Bussemann, Alexander and Nittler (2011) similarly observed that comet Wild 2

organic matter, despite severe heating during capture, did not alter the organic matter to the same extent as the prolonged thermal metamorphism of the CV, CO and OC organic component.

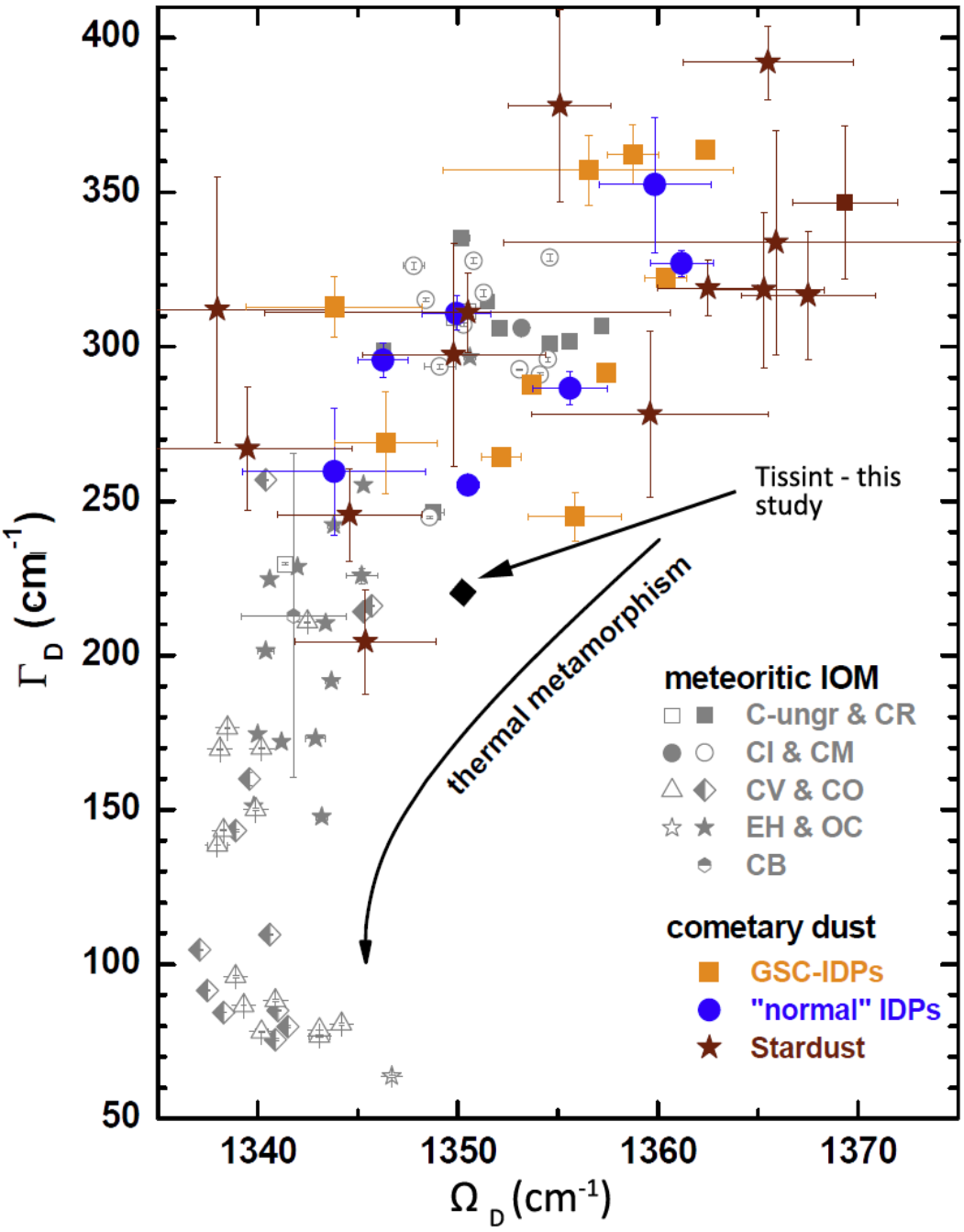

Figure 3.6 Ω_D (cm^{-1}) and Γ_D (cm^{-1}) parameters for the various classes of meteorites based on chemical, isotopic and mineralogical compositions (Weisberg, *et al.*, 2006) together with similar parameters for GSC-IDPs (Comet Grigg-Skjellerup's IDPs), normal IDPs and Stardust (organics in Wild 2 stardust). Parameters for organic material derived from the mantle of carbonaceous globules identified in this study are represented by a solid black arrow. Figure adapted from Bussemann, Alexander and Nittler (2011).

3.8 C, N, O, S AND Cl ABUNDANCES AND RATIOS

To further elucidate the nature of the carbonaceous component of the structures identified in Tisisnt, C, N, O, S and Cl elemental abundances were determined using EDAX analysis undertaken on a selection of globules that were present in both bound and unbound states within the pyroxene groundmass. For continuity, studies were independently conducted at the School of Earth and Ocean Sciences, Cardiff University, and also at the NASA Marshall Space Flight Centre, Huntsville, USA. Results of EDAX analysis indicate average elemental abundances of carbon (~78%), nitrogen (~0.3%), oxygen (~9%), sulphur (~ 1.3%) and chlorine (~0.28%) that are typical of high volatility bituminous coals that exhibit corresponding elemental abundances in the range, carbon (77.7-83.2), nitrogen (0.3-3.0%), oxygen (8.8-13.5%), sulphur (0.62-4.83%) and chlorine (0.03-0.12%) (Gehlhausen and Camahan, 1991; Malhotra, 2012). Corresponding Cl, N, O and S to C elemental ratios are distinctly higher than equivalent graphite standards with the carbonaceous material being particularly Cl- rich. This indicates that the carbonaceous component of the observed structures in Tissint is consistent with biology (kerogen) and not with an igneous process.

3.9 SUMMARY AND DISCUSSION

In spite of the limitations of Raman spectroscopy in unambiguously differentiating biogenic carbon from abiogenic carbon, G and D-band spectral characteristics of the carbonaceous coating of several 5-50 µm globules located in the Tissint Martian meteorite imply a complex precursor carbon inventory. This inventory is comparable to the carbon component of precursor materials of known biotic source (plants, algae, fungi, crustaceans, prokaryotes) that have been subjected to low grade thermal alteration ~27 ^{O}C > T < ~150 ^{O}C. Similarly, the carbonaceous coating of the globules in Tissint is comparable to G and D-band spectral characteristics of the complex carbon component of the Murchison CM2 carbonaceous chondrite. The indigenous nature of organic compounds in carbonaceous chondrites has been unambiguously established by carbon isotope analysis of extracted xanthine and uracil (Martins *et al.,* 2008) as well as the subsequent unambiguous identification of about 70 amino acids in Murchison itself (Schmitt-Kopplin *et al.,* 2010). Matson (2010) suggest that a potential 50,000 or more unique molecular compositions, and possibly millions of distinct organic compounds, may also be present in Murchison.

Correlation between peak metamorphic temperatures and Raman D-band (Γ_D) parameters has led to the suggestion that the second order polynomial PMT (^{O}C) = 931-5.10 × Γ_D × cm^{1} + 0.0091 × Γ_D^2 × cm^{2} can be used as a simple thermometer for determining peak temperatures (Busemann, Alexander and Nittler, 2007). The Γ_D (cm^{-1}) = 220 value determined for the carbonaceous material sampled in

the globules observed in Tissint infer that the organic material was subjected to a peak temperature of ~250 ^{O}C. It is noted that similar structures to those observed in Tissint were found in hydrothermal calcite veins in Carboniferous limestones in central Ireland. Here, the temperature condition of the calcite precipitation fluid was deduced through fluid inclusion microthermometry on nine aqueous fluid inclusions. The homogenization to liquid in all inclusions measured in the range 200 to 275^{O}C (Lindgren *et al.,* 2011), suggesting a possible link with the hydrothermal precipitation process responsible for the formation of the globules. This is somewhat supported by the observation that mineral assemblages enclosed within maskelynite phases of Tissint show the presence of clays and sulphates, favouring a hydrothermal origin for the formation of organic carbon and nitrogen species (Steele *et al.,* 2013).

Ω_G (cm^{-1}), Γ_G (cm^{-1}), Ω_D (cm^{-1}) and Γ_D (cm^{-1}) parameters further imply a level of crystallinity and disorder of the carbon component of the globules consistent with carbonaceous material recovered from a variety of non-terrestrial sources but most significantly from other Martian meteorites. G-band characteristics are nearly coincident with carbonaceous material recovered from the Martian meteorites NWA 2737 and NWA 2986. This clearly demonstrates that the observed globules were indigenous to the Tissint meteorite and were not the product of terrestrial contamination.

Furthermore Steele *et al.,* (2012) studied macromolecular organic material similar in its characteristics to that found in other Martian meteorites that occurred in maskelynite phases of Tissint. Raman spectroscopic mineral maps revealed a series of small 1-3 µm spherical globules enclosed with the maskelynite that were associated with irregular features at the maskelynite pyroxene interface. Raman mapping subsequently confirmed the presence of pyrite and macromolecular carbon phases in 18 maskelynite inclusions in Tissint (Steele *et al.,* 2012). The proximity of macromolecular carbon with pyrite (and magnetite rich assemblages) together with Raman characteristics that match the observed characteristics of the globules found in this study further rule out contamination as possible source for the structures. While these authors interpret these observations as evidence of abiotic formation by igneous processes, this is contrary to the detection of organic carbon filling fractures in olivine and pyroxene in several regions. Furthermore, the accumulation of organic carbon around pyrite crystals, the immiscible nature and morphology of the spherical structures observed, and the elemental composition of the carbonaceous mantles, all strongly point to the precipitation of biologically degraded material in a hydrothermal environment.

Chapter 4

Evidence of Ancient Microbial Activity on Mars

4.1 INTRODUCTION

Speculation about the source and nature of the organic carbon component in Martian meteorites continues. Competing theories include terrestrial contamination (Jull *et al.,* 1998: Stephan *et al*., 2003), abiotic geophysical processes (Treiman, 2003; Zolotov and Shock, 2000; Steele *et al*., 2007) and the detritus of past life (McKay *et al.,* 1996). The new Tissint Martian meteorite offers a rare opportunity to examine the carbon component of a fresh, relatively uncontaminated, Martian basalt. Stepped combustion mass spectrometry has confirmed that much of Tissint's organic material is of Martian origin with total carbon abundances of 173 ppm ($\delta^{13}C$ = –26.6 ‰) and 12.7 ppm nitrogen ($\delta^{15}N$ = –4.5 ‰) (Aoudjehane *et al.,* 2012).

An abiotic (igneous) origin for the reduced organic component in Tissint was initially proposed by Steel *et al*., (2012). This was based on observations of macromolecular carbon inclusions within feldspathic glass phases in a number of Martian meteorites. Subsequent investigations led the authors to revise this interpretation and current thinking now favours fluid precipitation (Steele *et al*., 2013). An independent study by Lin *et al.,* (2013) found two petrographic settings for organic carbon in Tissint, characterised by a) the complete filling of fractures in olivine and pyroxene and b) an entrained component in shock-melt veins. Raman spectral analysis indicated a kerogen-like material with elemental ratios of H, N, O, S, P, F and Cl to C comparable to the coal reference and distinctly higher than graphite standards. C isotope analysis revealed the organic carbon component was characterised by light C isotopes ($\delta^{13}C$ = –13.0 to -33 ‰) which accorded well with the earlier isotope data from Aoudjehane *et al.,* (2012). The clear petrographic settings for the organic carbon together with the C isotope results led the authors to conclude that a) the organic carbon component was deposited from organic-rich fluids and was not magmatic in origin, b) was unlikely to have originated from chondritic debris and c) was more likely of biogenetic origin (Lin *et al.,* 2013).

Our earlier studies of the Tissint Martian meteorite are consistent with the latest findings of Lin *et al.,* (2013) and Steele *et al.,* (2013). We identified the presence of a number of 5-50µm carbonaceous globules both embedded in the rough pyroxene substrate but also in an unbound state, having been dislodged during the experimental fracturing process (Wallis *et al*., 2012). SEM and

EDS elemental spectra for 11 selected globules confirmed that they comprise of a carbonaceous outer coating with an inner core of FeS_2 (pyrite) and are characterised as immiscible globules with curved boundaries. Raman spectral characteristics imply a level of crystallinity and disorder of the carbon component consistent with previous reports of organic carbon in Tissint (Steele *et al.*, 2012). D-band spectral characteristics further imply a complex precursor carbon component comparable to the precursor component of materials of known biotic source (plants, algae, fungi, crustaceans, prokaryotes). Correlation between peak metamorphic temperatures and Raman D-band (Γ_D) parameters further indicate that the carbonaceous component was subjected to a peak temperature of ~250 ^{O}C suggesting a possible link with the hydrothermal precipitation processes responsible for the formation of remarkably similar structures observed in hydrothermal calcite veins in central Ireland (Lindgren *et al.*,2011). This link was confirmed by the petrographic setting of the organic carbon component that showed examples of organic carbon completely occupying the cracks and cleavage around pyrite crystals, suggesting that pyrite had acted as an attractive substrate for the collection of organic material in a hydrothermal setting.

In this study we report the results of SEM, optical microscopy and Raman spectroscopy on the Tissint Martian meteorite. Our results show the presence of a relatively rare secondary iron arsenate-sulphate mineral found in a shock melt vein of the meteorite. The presence of this mineral is interpreted as arising from microbial activity, a position substantially supported by SEM images of a pyrite grain showing morphological alteration features distinct from abiotic alteration features, and closely comparable to biologically mediated microstructures created by Fe- and S-oxidising microbes in the laboratory. These results confirm the observations and interpretations of Steel *et al.*, (2013) and Lin *et al.*, (2013) insofar as Tissint's organic carbon component arose from fluid precipitation. More significantly, they support the conclusions of Lin *et al.*, (2013) that the precipitated organic carbon component had a biogentic origin. Direct evidence of the activity of Fe- and S-oxidising microbes on pyrite surfaces strongly supports the findings of McKay *et al.*, (1996).

4.2 EXPERIMENTAL METHODS

To further examine the viability of the hypothesis being considered, scanning electron microscopy was utilised to first identify the presence of enriched arsenic domains in one polished 30µm thin section (section A) and one polished thick section (Section C) of Tissint that were prepared at the School of Earth and Ocean Sciences, Cardiff University. Details of these sections are provided in section 2.3. Once identified, Raman spectroscopy was then utilised to constrain the observed mineral species.

Further SEM studies were undertaken for the purpose of identifying the presence of bacterial etch pits in the surface of pyrite grains present in the meteorite. SEM studies were conducted using the FEI (Phillips) XL30 FEG ESEM (Environmental Scanning Electron Microscope) FEG (Field Emission Gun) at the School of Earth and Ocean Sciences at Cardiff University. The unit incorporates a secondary electron detector (SE), a back scatter electron detector (BSE) and a gaseous secondary electron detector (GSE). It also has an Oxford Instruments INCA ENERGY (EDX) x-ray analysis system. Image recording is via a SONY video graphics printer or digital by processing image frames in a 16 bit framestore computer for output to hard drive. Optical microscopy was conducted using an RM-1POL polarising light microscope with 360º rotating analyser. Image capture was via a 9M pixel digital trinocular camera unit processed by View7 PC software for output to hard drive.

Independent studies using a separately sourced sample were undertaken using a Hitachi S-3700N Field Emission Scanning Electron Microscope at the NASA Marshall Space Flight Centre. High resolution Raman spectra were acquired using a Renishaw inVia microRaman system at the School of Chemistry, Cardiff University, UK. Laser focusing of the sample was performed using a research grade Leica analytical microscope fitted with a 100x objective and a 514.5 nm Argon laser line. Data processing was via the Wire2 software application for data output to hard drive.

4.3 RESULTS

An arsenic enriched domain was observed in EDAX elemental maps in the vicinity of a ~10 µm wide glass shock vein. Black glass melt pockets and veins are characteristic of Tissint. Figure 4.1 (a) shows an optical light montage in cross polarised transmitted light of a typical glass shock vein cutting through the pyroxene groundmass and passing through an olivine crystal. The white grains are maskelynite while the glass shock veins show up as black. Figure 4.1 (b) shows a similar image of the shock vein containing the arsenic signature with the site of interest highlighted. Also shown beneath it is a typical olivine crystal with a melt inclusion and radiating cracks. Figure 4.1 (c) shows an enlarged image of the vein now seen to enclose a mineral inclusion that is again shown in higher magnification in figure 4.1 (d).

Raman spectroscopy provided an unambiguous identification of the glass melt inclusion as comprising of an iron arsenate sulphate mineral (bukovskýite). Figure 4.1 (e) shows Raman spectra of the grain compared with similar spectra (Rruff ID: R050630) for the iron arsenate sulfate mineral, bukovskýite – $Fe^{3+}{}_2(As^{5+}O_4)(S^{6+}O_4)(OH)\bullet 7(H_2O)$ – sourced from Kutna Hora, Bohemia, Czechoslovakia by the University of Arizona Mineral Museum. Comparison of the spectra provides

an unambiguous identification with distinct bands in the 1000-1200 cm^{-1} range - assigned to the ν_3 $(SO_4)^{2-}$ antisymmetric stretch (δ-Fe-OH bend) - with corresponding coincident bands in the 900-1000 cm^{-1} range (assigned to ν_3 $(AsO_4)^{3-}$ antisymmetric stretch or vibration of water molecules and the ν_1 $(SO_4)^{2-}$ symmetric stretch) (Loun *et al.*, 2011).

Further strong bands assigned to the ν_3 and ν_1 $(AsO_4)^{3-}$ antisymmetric and symmetric stretch at 800-900 cm^{-1} together with lower wavelength bands at ~400 cm^{-1} assigned to the ν_2 $(SO_4)^{2-}$ bend, the ν_4 $(AsO_4)^{3-}$ bend or the Fe-OH and Fe-O stretch were similarly present. One prominent feature at ~ 1040 cm^{-1} that is assigned to the ν_3 $(SO_4)^{2-}$ antisymmetric stretch (δ-Fe-OH bend) (Loun *et al.*, 2011) was evident in the observed spectra but was only observed in weakened form.

The presence of a secondary iron arsenate-sulphate in the Tissint Martian meteorite suggests an As mobilisation and sequestration process operating in the surface or near surface layers of Mars. The ecology of arsenic on early Mars could provide evidence of previous microbial activity or in the alternative constrain our understanding of early Martian surface conditions.

4.4 BUKOVSKÝITE

Bukovskýite is a relatively rare secondary iron arsenate-sulphate first analysed by Antonin Bukovský (Bukovský, 1915) and later by Slavik (1925) and Ulrich (1930). Its structure consists of octahedral-tetrahedral Fe-arsenate chains with sulphate tetrahedral bonded to the chains and free H_2O molecules via a complicated network of hydrogen bonds (Majzlan *et al.*, 2012). It occurs in substantial quantities as the main secondary mineral in medieval dumps near the municipality of Kutná Hora, in the Czech Republic. While it has also been described at several other localities, Kutná Hora is the only site where the mineral occurs in substantial quantities. Novák *et al.*, (1967) conducted the first modern description of bukovskýite using X-ray diffraction, chemical analysis, TEM, and IR spectroscopy. At the time it was proposed that bukovskýite was the arsenate analogue of destinezite ($Fe_2(PO_4)(SO_4)(OH)\cdot 6H_2O$), but this has since been refuted by Johan (1986) and it is now considered an alteration product of arsenopyrite.

The oxidation of arsenopyrite has been the subject of several laboratory studies (e.g. Buckley and Walker, 1988; Richardson and Vaughan, 1989; Nesbit *et al.*, 1995; Nesbit and Muir, 1998). Further studies have concentrated on the precipitation mechanisms and stability of scorodite ($FeAsO_4\cdot H_2O$) - the most common arsenopyrite oxidation product (e.g. Dove and Rimstidt, 1985; Nordstrom and Parks, 1987; Krause and Ettel, 1988). Haffert *et al.*, (2010) reported the presence of bukovskýite at the Golden Port mine in New Zealand, where it occurs with scorodite and As-rich hydrous ferric

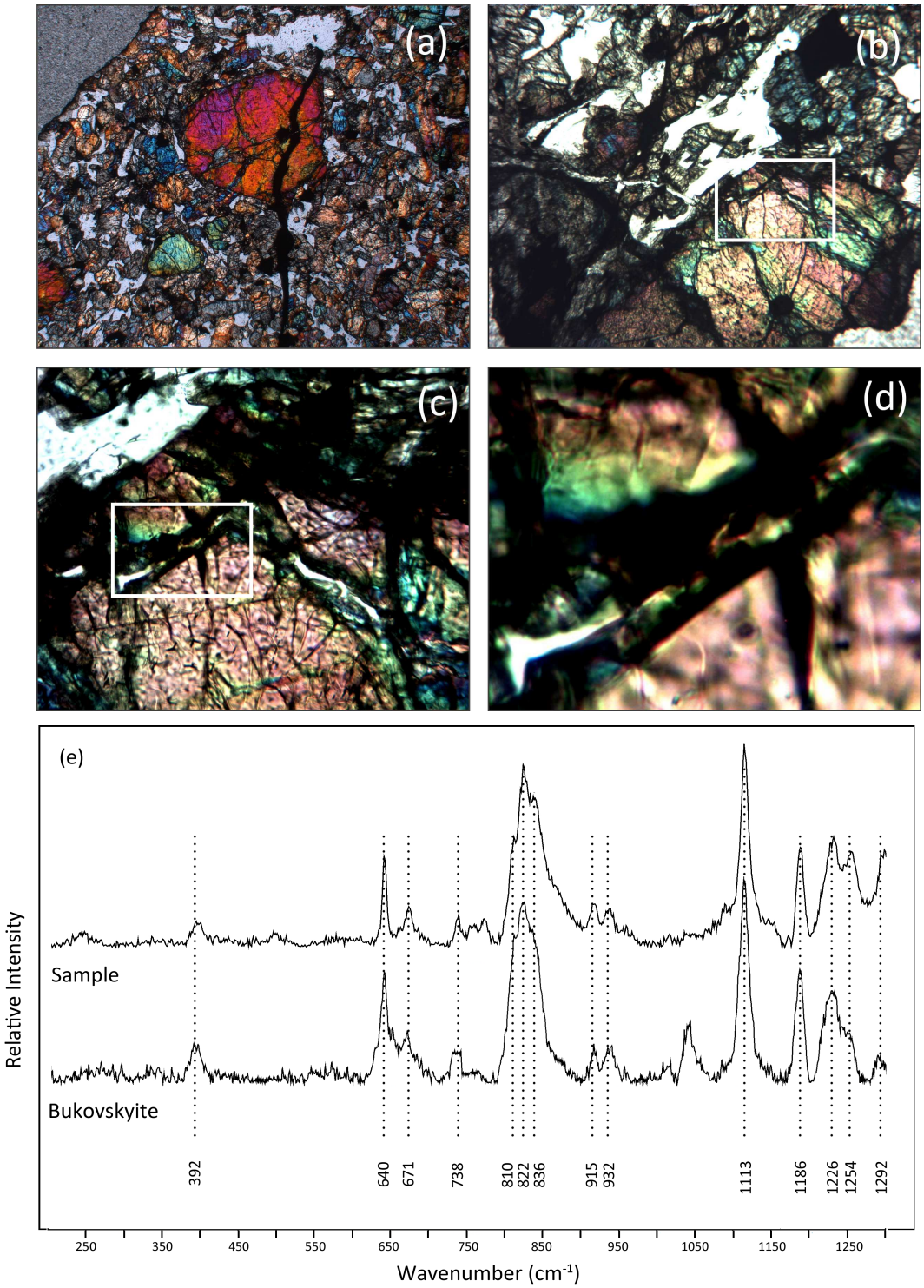

Figure 4.1 (upper) shows optical light images of a 30µm thin section of Tissint in cross polarised transmitted light. Black glass shock veins and pockets show up as black with maskelynite phases in white. (a) typical glass shock vein cutting through the pyroxene groundmass and olivine crystal (b) shock vein containing the arsenic signature with the site of interest highlighted, note also the presence of a typical olivine crystal with a melt inclusion and radiating cracks (c) enlarged image of the vein showing enclose mineral inclusion and (d) same, in higher magnification. Field of view (a) 2.5mm (b) 1mm (c) 250 µm (d) 100 µm. **(Lower)** shows Raman spectra of mineral grain compared with similar spectra (Rruff ID: R050630) for the iron arsenate sulfate mineral, bukovskýite – $Fe^{3+}{}_2(As^{5+}O_4)(S^{6+}O_4)(OH)\bullet 7(H_2O)$ – taken from Kutna Hora, Bohemia, Czechoslovakia. Sample courtesy of the University of Arizona Mineral Museum.

oxides on the interior of waste dumps. These authors concluded that bukovskýite and zýkaite arose in the Golden Port mine as products of weathering resulting in elevated concentrations of sulphates that remained wet most of the time.

In contrast, Majzlan *et al.,* (2012) found that the Fe:As:S (2:1:1) ratio of bukovskýite precipitating gels varied widely and were depleted in S relative to the ideal 2:1:1 stoichiometry. They concluded that bukovskýite cannot originate by simple weathering and decomposition of pyrite or arsenopyrite and that some additional control over the chemical composition and final crystallisation mechanisms must exist (Majzlan *et al.,* 2012).

There are a number of examples of the formation of trace bukovskýite occurring that involve biological processes, most notably biologically induced mineralisation. Márquez *et al.,* (2006) studied a two-step oxidation pre-treatment process involving a combination of bacterial and pressure oxidation of ores mined in the São Bento deposits in Brazil. They observed the presence of minor and trace amounts of zykaite ($Fe_4(AsO_4)_3(SO_4)(OH)\cdot 15\ H_2O$) and bukovskýite as secondary products of the bacterial oxidation of gold ores. At the type locality of the Kaňk deposit in the northern part of Kutná Hora, two types of associations and dumps are distinguishable (Majzlan *et al.,* 2012).

The first type are composed of large rock fragments with open space between them and are associated with scorodite, kaňkite and zýkaite with non-arsenate secondary minerals including gypsum and jarosite. In the second type the rock fragments are completely filled by earthy to clayey material together with anthropogenic material including charcoal, timbers and burnt clay. These areas are associated with abundant bukovskýite and rare parascorodite ($FeAsO_4\cdot H_2O$). This observation has led to the suggestion that clay minerals create sealed microenvironments where high concentrations of aqueous H^+, Fe(III), SO_4 and AsO_4 are maintained for long periods of time (Majzlan *et al.,* 2012).

While the precise processes responsible for the formation of bukovskýite remain unknown, it is not possible to unambiguously associate the formation of this mineral with biological activity. Nonetheless, the initial mobilisation of arsenic from As enriched Fe oxides, the subsequent sequestration of As by precipitating sulphides under anoxic conditions followed by the oxidation to sulphide of sulphate species and the formation of relatively rare As secondary phases are all processes commonly associated with bacterial activity.

4.5 A MICROBIAL MODEL FOR BUKOVSKÝITE ON MARS

The working hypothesis considered here is that $Fe^{3+}{}_2(As^{5+}O_4)(S^{6+}O_4)(OH)\bullet 7(H_2O)$ (bukovskýite) formed when high concentrations of aqueous H^+, Fe(III), SO_4^{2-} and AsO_4^{3-} were maintained for long periods of time in microenvironments created in wet surface and subsurface Martian clays. These ingredients arose as dissolution products of the microbial reduction of Fe-oxides and subsequent microbial oxidation of FeS_2 with concurrent release of sequestrated As to solute phase.

Arsenic (As) is a ubiquitous element known to have a high affinity for newly precipitating Fe oxides where it is both incorporated and subsequently stabilised within the mineral structure during aging and transformation (Jessen *et al.*, 2005; Roberts *et al.*, 2004). The sorption of As on Fe oxides occurs in both ionic outer, and specific inner, surface complexes (Sun and Doner, 1998; Waychunas *et al.*, 1993) resulting in solid phase As enrichment in Fe oxide precipitating sediments.

The potential for humic substances to influence the redox state and the complexation of As, thus shifting As partitioning in favour of the solute phase is commonly seen on Earth. In the sediments of South Asia, hot spots of As enriched aquifers are commonly observed in the vicinity of organic rich buried peat layers. These peat layers comprise of a complex mixture of polyfunctional organic molecules derived from the decomposition of plants, animals and microorganisms (Wang and Mulligan, 2006). While the precise composition of these mixtures varies, they all share common moieties such as polar carboxyl, hydroxyl, amino, sulfhydryl and phenol groups (Aiken *et al.*, 1985). Increasing concentrations of these common moieties were found to increase the chemical reduction of Fe(III) complexes and oxidise H_2S, supporting the assumption that they are indeed the redox active moieties involved in the redox reactions (Bauer, 2008).

In our model, accumulated sedimentary organic material would react with Fe oxides resulting in the mobilisation of arsenic. Under anoxic conditions, sequestration of As may arise from As precipitation in sulphide compounds, the formation of thioarsenic aqueous species or As adsorption (and possibly co-precipitation) onto Fe(II) sulphides (Henke, 2009) forming, for example, FeS_2/As complexes.

Figure 4.3 provides a notional representation of pyrite surface sites and different kinds of interactions namely a) outer-sphere complexation of a non-specific nature and b) inner-sphere complexation of a metal. In this case the figure shows specific interaction with a sulphur surface site.

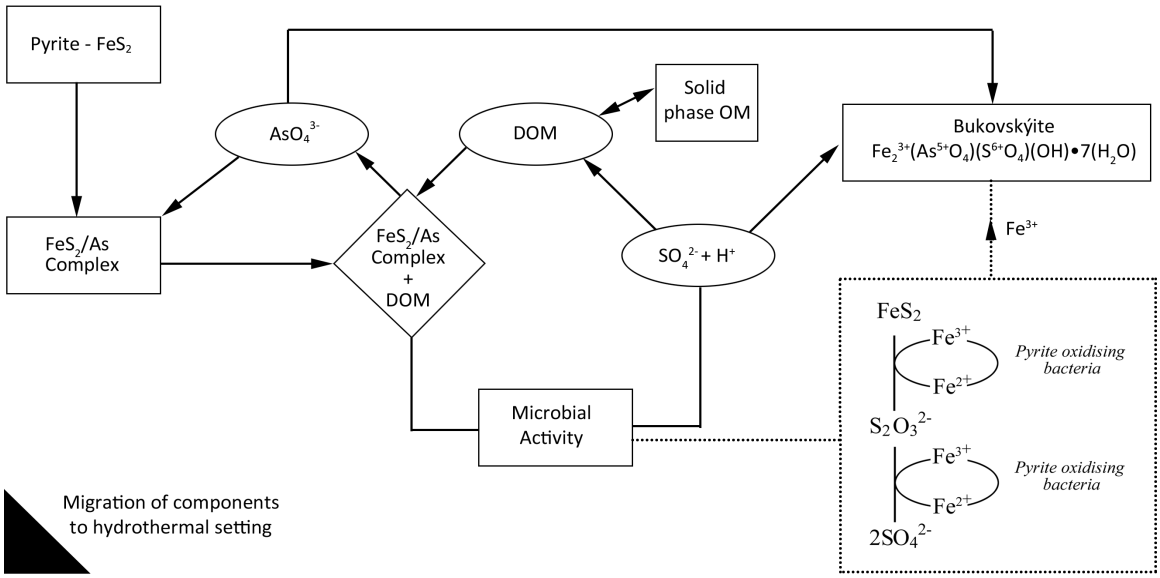

Figure 4.2 Schematic representation of the proposed chemical processes that result in the formation of bukovskyite in closed micro-environments. The mechanism proceeds via anoxic microbial pyrite oxidation and culminates in the accumulation of bukovskyite forming ingredients and conditions. Components of the model would then migrate from sedimentary layers to a hydrothermal environment where organic matter would precipitate on pyrite grains.

The availability of aqueous AsO_4 would be complemented by dissolution by-products of pyrite oxidising bacteria giving rise to a ready supply of H^+, Fe(III) and SO_4^{2-} species as indicated by the following chemical reactions:

$$FeS_2 + 6\ Fe^{3+} + 3\ H_2O \rightarrow S_2O_3^{2-} + 7\ Fe^{2+} + 6\ H^+ \qquad \text{eq. 1}$$

$$S_2O_3^{2-} + 8\ Fe^{3+} + 5\ H_2O \rightarrow 2\ SO_4^{2-} + 8\ Fe^{2+} + 10\ H^+ \qquad \text{eq. 2}$$

The iron (II) ions are oxidised by the bacteria:

$$Fe^{2+} \xrightarrow{\text{bacteria}} Fe^{3+} + e^-$$

High concentrations of these species together with AsO_4 would then be maintained for long periods of time in micro-environments supported in fine Martian clays. Figure 4.2 shows a schematic representation of the proposed chemical processes resulting in the formation of bukovskyite.

Components of the model would then migrate from sedimentary layers to a hydrothermal environment where organic matter would precipitate on pyrite grains.

Leblanc *et al.*, (1996) reported the accumulation of iron-arsenate and arsenate-sulphate precipitates in the acidic stream (pH 2.2-4) of the Carnoulès Pb-(Zn) mine in Garde, France. Here, rod-shaped and sheathed bacterial forms were responsible for ferruginous bacterial accretions, morphologically similar to stromatolites. Stromatolites represent the most ancient records of life on Earth by fossil remains which date from more than 3.5 billion years ago.

Also found within the accretions were living *Thiobacillus*-type bacteria. *Thiobacillus ferrooxidans* oxidise Fe(II) for energy for growth. Bennett and Tributsch, (1978) reported a strong correspondence between the attachment of *Thiobacillus ferrooxidans* to pyrite surfaces and the presence of residual etch pits during bacterial leaching experiments.

The presence of some bacteria in the etch pits confirmed a causal link between the pits in the pyrite surface and the bacteria. Since the *T. ferrooxidans* microbes require oxygen as their terminal electron acceptor, it appears unlikely they would have been present on early Mars. However, purple and green sulphur bacteria (i.e. both Fe- and S-oxidisers) are anaerobic and potentially well suited to Martian conditions.

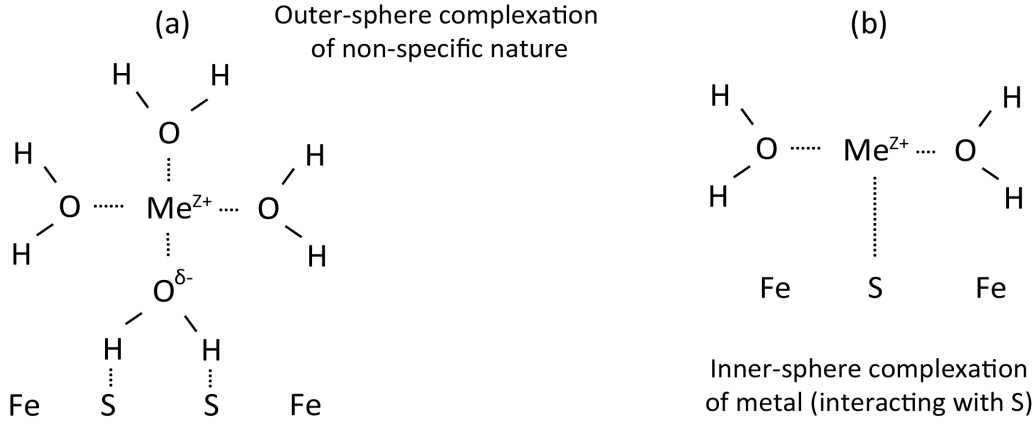

Figure 4. 3 a notional representation of pyrite surface sites and different kinds of interactions (a) Outer-sphere complexation of a non-specific nature; (b) inner-sphere complexation of a metal, specifically interacting with a sulphur surface site

4.6 BACTERIAL ETCH PITS ON PYRITE

Oremland (2003) speculated on the role of dissimilatory arsenate-reducing prokaryotes in a hypothetical microbial 'biome' supported by arsenic cycling in the subsurface layers of Mars. Here, As(III) would be recycled to As(V), possibly by aqueous nitrates permeating through the Martian surface. The activity of anaerobes that use As(V) as their respiratory oxidant is well documented (Switzer et al., 1998; Huber et al., 2000; Glhring and Banfield, 2001) and include several extremophiles adapted to high temperature, pH, and/or salinity. Furthermore, some arsenate-reducing bacterium (e.g. strain OREX-4) can use either arsenate or sulphate as the electron acceptor (Newman *et al.,* 1997) enabling them to operate as both sulphate-reducing and arsenate-reducing bacterium. The OREX-4 bacterium is typically ~2.5 μm in length ~0.4μm in diameter.

Evidence of the previous activity of bacteria was detected in the form of spherical etch pits and chains of pits on the surface of pyrite grains coated with carbonaceous material that were previously identified in the pyroxene substrate of Tissint. These etch pits occurred in clusters, and were comparable to biologically mediated microstructures created by Fe and S-oxidising microbes in the laboratory.

A correspondence between the attachment of some bacteria to pyrite surfaces and the presence of residual etch pits has been reported in bacterial leaching experiments using Thiobacillus ferrooxidans by Bennett and Tributsch, (1978). These authors reported the presence of rounded etch pits, typically between 1-2 μm in diameter, often occurring as pairs or chains with individual pits linearly aligned, or as significant clustered accumulations. In particular, the presence of residual bacteria in some of the pits was observed, establishing a causal between the two. Similarly, Edwards *et al.,* (1998, 1999) reported pitting in experiments using natural populations of microbes from acid mine drainage sites, while Etzel *et al*. (2007) showed that the shape of etch pits created by thermophilic Archaea was strongly related to crystallographic orientation.

Significantly, Wacey *et al.,* (2010) reported on pyrite grains with laminated carbonaceous coatings of early Archean age from the basal quartz arenite member of the 3.43–3.35 Ga Strelley Pool Formation (SPF) in Western Australia. Here, pyrite surfaces at the interface with the carbonaceous coatings exhibited spherical pits, chains of pits and channels that were widespread and had a clustered distribution typical of microbial colonisation. This author interpreted this as trace fossils formed by the attachment of bacteria to the pyrite surfaces.

Figure 4.3(a) shows an SEM image displaying the presence of etch pits on the surface of a pyrite grain coated with carbonaceous material in the Tissint Martian meteorite. This image was previously reported in Wallis *et al* (2013) and was taken using a Hitachi S-3700N Field Emission Scanning Electron Microscope at the Marshall Space Flight Centre by RBH. It is shown here with the contrast improved for the purpose of highlighting surface features present at the interface of the pyrite and carbonaceous mantle. Figure 4.3(b) shows the area marked with arrow (i) in the upper image. Here, a cluster of equally spaced spherical etch pits, arranged in linear order, become visible. Figure 4.3(d) shows an overlay diagram of their position and spacing. Figure 4.3(e) shows a similar set of four rounded pits equally spaced in a straight line as indicated by the four white arrows. For comparison, figure 4.3 (c) shows a cluster of spherical etch pits in the surface of pyrite taken from the Strelley Pool Formation (SPF) in Western Australia (Wacey *et al.,* 2010). These pits can be seen to be equally sized and spaced and linearly aligned.

The significance of the etch pit shape and geometric distribution cannot be overstated since pitting and channelling of pyrite surfaces can result from the non-biological oxidation of pyrite. For example, pits of approximately 200nm deep × 10μm wide have been observed in pyrite under aqueous, O_2 saturated, acidic conditions (Asta *et al*., 2008). Though these significantly differ from those observed in microbial experiments, they do demonstrate that abiotic process can also affect surface features. Similarly, the random distribution of pits of size 30-250nm have been observed during HCl and H_2SO_4 reaction with pyrite (Edwards *et al.,* 1999) and in the radiolytic oxidation of pyrite (Lefticariu *et al.,* 2010). Furthermore, abiotic oxidation by H_2O_2 has also been shown to cause pitting (Lefticariu et al. 2006) though here the pits were larger (~10μm diameter) but did not cluster or form chains of pits. Consequently, the presence of pits alone on pyrite surfaces is not diagnostic of a biological reaction (Wacey *et al.,* 2010). However, the pits in the pyrite of Tissint are rounded and clustered, form chains with equal pit spacing, have dimensions within the range typical of microbes and are distinct from the abiotic features discussed above.

4.7 DISCUSSION

The mobilisation and sequestration cycle of arsenic (As) is neither purely chemical nor purely microbial. However, the process is greatly enhanced by the activity of microorganisms that increase reductive Fe oxide dissolution with concurrent release of As to solute phase. The subsequent sequestration of As under anoxic conditions can then take place via precipitation in sulphide compounds. The presence of relatively rare secondary iron arsenate-sulphates does however tentatively suggest microbial activity. Iron arsenate and arsenate-sulphates, together with the

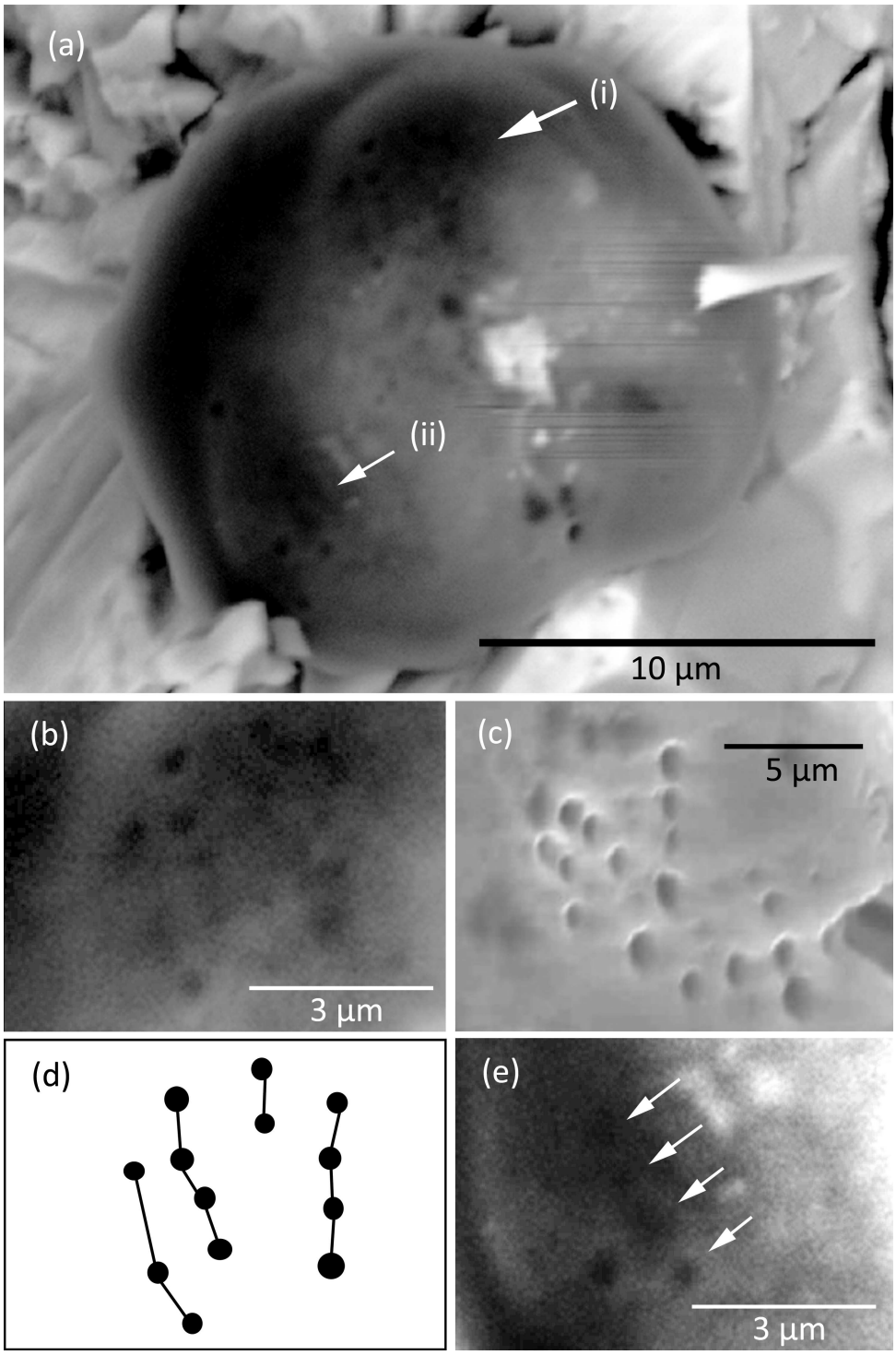

Figure 4.3 (a) shows an SEM image of a pyrite grain coated with carbonaceous material located in the substrate of Tissint (Wallis *et al.*, 2012). The area marked with arrow (i) is shown in higher resolution (b) where a cluster of equally spaced spherical etch pits, arranged in linear order, become visible. (d) shows an overlay diagram of their position and spacing, while (e) shows a similar set of four rounded pits equally spaced in a straight line as indicated by the four white arrows. For comparison, figure 3 (c) shows a cluster of spherical etch pits in the surface of pyrite taken from the Strelley Pool Formation (SPF) in Western Australia (Wacey *et al.*, 2010). These pits can be seen to be equally sized and spaced and linearly aligned.

alteration product, bukovskýite, have all been reported in ferruginous bacterial accretions in acidic mine waters in France. (Leblanc *et al.*, 1996).

Reliance on microfossil morphologies as conclusive indicators of relic life has a controversial history. Even in terrestrial settings the unambiguous identification of ancient biology has not always been easy to establish. Pflug, (1967) reported the presence of 'globular-type A microfossils' in acid macerated shales of the Fig Tree Group, but this has since been questioned by Altermann (2000). Walsh (1992) found ~90 µm Archaean carbonaceous spheroidal microstructures in the carbonate cherts of the Kromberg Formation, though Brazier *et al.*, (2006) have since reinterpreted these as self-organised abiotic structures. Buik (2001) also examined these structures and found that hollow kerogenous filaments associated with them may indeed be biological. Sugitani (2007) interpreted similar-sized morphological structures in the black chert beds of the Gorge Creek Group as 'probable microfossils'.

Significantly however, Javaux, Marshall and Bekker (2010) examined organic-walled microfossils in Mesoarchaean shales and siltstones in the Earth's oldest (3.2 billion years) siliclastic alluvial to tidal estuarine deposits. They found unambiguous evidence in the wall unltrastructure of flattened hollow organic-walled vesicles with visible lumen between the compressed walls and concluded they must be of biological origin. Of significance, these investigators also reported the presence of pyrite and arsenopyrite grains in the walls of the microstructures observed during SEM energy dispersive X-ray analysis. Spheroidal carbonaceous microstructures with sulphide cores have also been observed in Proterozoic and Ordovician sandstones in Canada (Nardi, 1994) and hydrothermal calcite veins in Carboniferous limestones in central Ireland. Here the origin of the organic matter cannot be confirmed but is thought to have derived from the surrounding sedimentary terrain, where the hot hydrothermal fluids generated the migration of organics (Lindgren *et al*., 2011).

Nonetheless, the presence of spherical pits, and chains of pits, with a morphology and geometric distribution that is distinct from abiotic alteration features, and is closely comparable to biologically mediated microstructures created by Fe- and S-oxidising microbes in the laboratory requires further attention. At present, these features are interpreted as trace fossils resulting from the attachment of bacteria to the pyrite surfaces.

Chapter 5

A Model of Pyrite-Core, Kerogen-Mantle Interstellar Grains

5.1 SUMMARY

In the sections that follow, observed infrared emissions in the 8-13 µm range of the Trapezium region of the Orion Nebular are compared with theoretical emission curves of carbonaceous coated pyrite grains calculated using published light scattering algorithms. Transmittance spectra for kerogen rich residues are taken from the literature and used to derive, for the first time, scattering and absorption constants for a new low-temperature conversion by-product of biological waste generated anaerobically at 380-450 ºC under normal pressure. This rapidly carbonised bio-material is considered a close analogue to biologically degraded material likely to be generated in astronomical environments if high order biology was exposed to conditions in space. Results of calculations show a superior fit for the new biochar with further improvements arising from the inclusion of a pyrite core. In each case the contribution to total emission from particles of scattering size was found to be negligible.

5.2 INTRODUCTION

In the previous sections we reported the detection of FeS_2-core, carbonaceous-mantle grains in the Tissint Martian meteorite. Iron-sulphide minerals are ubiquitous in non-terrestrial environments where they are thought to represent the main sulphur bearing species (Zolensky and Thomas 1995; Dai and Bradley 2001). Fe-sulphide grains have also been detected in circumstellar discs (Keller *et al.,* 2002) while carbon coated Fe-sulphide grains have been observed in interplanetary dust particles (Rietmeijer and Mackinnon, 1985; 1987) and primitive carbonaceous chondrites (Nakamura *et al.,* 2002). Nakashima (1992) and Nakashima and Shiota, (2001) explain the formation process of small (~20nm) core-mantle structures by the catalytic transformation of poorly graphitised carbon on mineral surfaces. A variety of coated grains have also been considered as a component of interstellar dust, particularly in relation to interstellar condensates.

The observed core-mantle structures in Tissint however are larger and bear a striking resemblance to similar sized structures observed in terrestrial Proterozoic and Ordovician sandstones in Canada and hydrothermal calcite veins in limestones in central Ireland (Nardi, 1994; Lindgren *et al.,* 2011). Here, the role of liquid H_2O in the organic carbon precipitation process is strongly inferred by the chemistry of pyrite surface interactions. Bebie and Schoonen (2000) demonstrated that the observed interactions between the negatively charged surface of pyrite and sampled organic aqueous species

occurred regardless of the formal charge of the aqueous species itself. This indicates that the interaction between FeS_2 and organic species under anoxic conditions is not dictated by electrostatic forces but by interactions with thiol or Fe surface sites that require the presence of liquid H_2O. The presence of liquid water in comets has been discussed extensively in the literature and remains a core feature of the theory of cometary panspermia. However, while core-mantle structures have been considered previously in regard to interstellar condensates, they have not been considered as the products of cometary biology. In this model, pyrite-core, kerogenous-mantle type structures would arise within comets from interactions between pyrite surfaces and residual aqueous organic components. These structures would then be ejected into interstellar space and their presence may contribute to spectroscopic features reported in a variety of astronomical observations.

The unambiguous identification of such structures from observed astronomical spectra is of course not possible. A wide range of substances can exhibit principal absorption features at very similar wavelengths. For example, in organic material calculations the C-H, O-H and N-H stretching frequencies are observed across the entire 2.6 to 3.7μm range and even within a single stretching mode (e.g. CH) there is a wide range of features (3.3 to 3.5μm) depending on the particular type or configuration of the material.

For grains that are small compared to the wavelength being observed (i.e. $2\pi a/\lambda \ll 1$) the extinction will be due to absorption only (Hoyle and Wickramasinghe, 1991) and it is safe to assume that the extinction optical depths in astronomical sources would be proportional to optical depth values derived from laboratory studies. Thus, for a small particle emitting infrared radiation we can assume that the flux is given by $F(\lambda) = const. B_\lambda(\mathrm{T})\, \tau(\lambda)$ where $B_\lambda(\mathrm{T})$ is the Plank function at the temperature T of the grain and $\tau(\lambda)$ is the laboratory measured optical depth.

For solid grains with size comparable to $\lambda/2\pi$ the situation is more complex and we need to know the refractive index and absorption coefficient as functions of wavelength, and then calculate extinction and absorption efficiencies using the Guttler extension of Mie theory. For particles emitting infrared radiation the flux is then given by $F(\lambda) = const. B_\lambda(\mathrm{T})\, Q_{abs}(\lambda)$ where $B_\lambda(\mathrm{T})$ is the Plank function at the temperature T of the grain and $Q_{abs}(\lambda)$ is the derived absorption efficiency.

5.3 THE 8-13μm FEATURES OF THE TRAPEZIUM NEBULA

The first positive detection of an infrared spectral feature was made in 1969 (Woolf and Ney, 1969; Knacke *et al*., 1969; Ney and Allen, 1969; Stein and Gillett, 1969) when a strong infrared excess above the thermal continuum was reported in several oxygen-rich Mira-type stars (Figure 5.1).

Similar features in the 8-13µm region have since been reported in a variety of astronomical objects including planetary nebulae, compact HII regions, OH/IR sources, the galactic centre, comets and the Trapezium nebular (Russell *et al.,* 1975; Woolf, 1973; Cohen, 1980; Capps *et al.,* 1978; Aitken et al., 1979). The infrared spectra of sources near the galactic centre are significant since they sample a 10 kpc pathlength to the galactic centre and exhibit a consistent 9.7 µm extinction of ~2.5 mag relative to the neighbouring continuum. This consistency provides a strong confirmation that the extinction arises from grains in the 10 kpc line of sight rather than from local sources. Figure 5.2 shows the energy spectra of four luminous infrared sources located in the vicinity of the Galactic centre radio arc (Okuda *et al.,* 1990). Observations were made on Mauna Kea at the University of Hawaii 2.2m telescope, the NASA 3m Infrared telescope facility and the United Kingdom 3.8m infrared telescope. The sources can be seen to exhibit large polarisations in the near-infrared and deep absorptions at ~10µm.

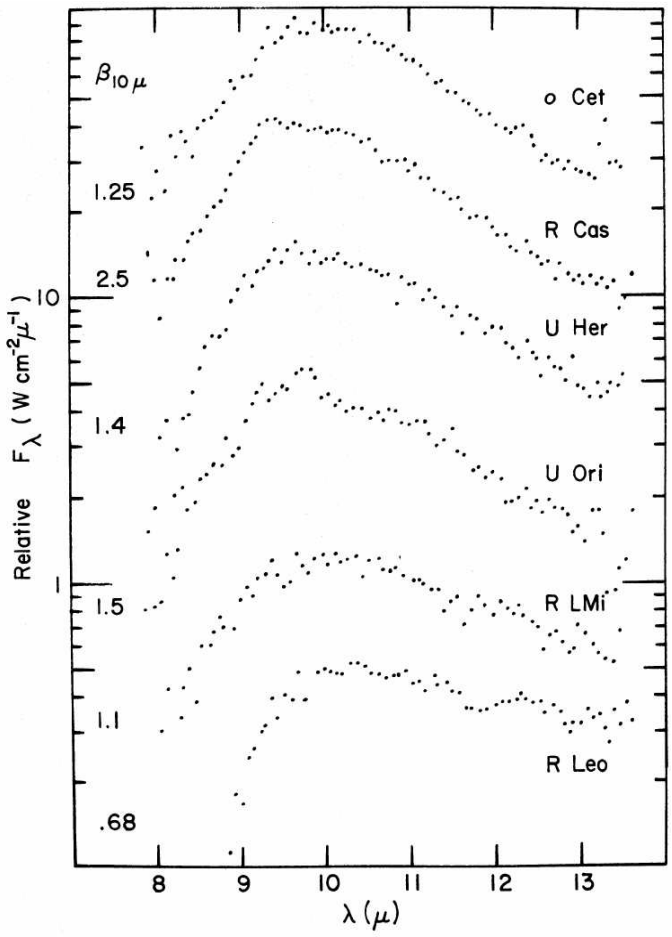

Figure 5.1 Spectal energy distribution of excess emission from several M-type Mira stars. The relative flux represents the actual flux arbitrarily normalised for convenient display. Figure from Forrest *et al.,* 1975

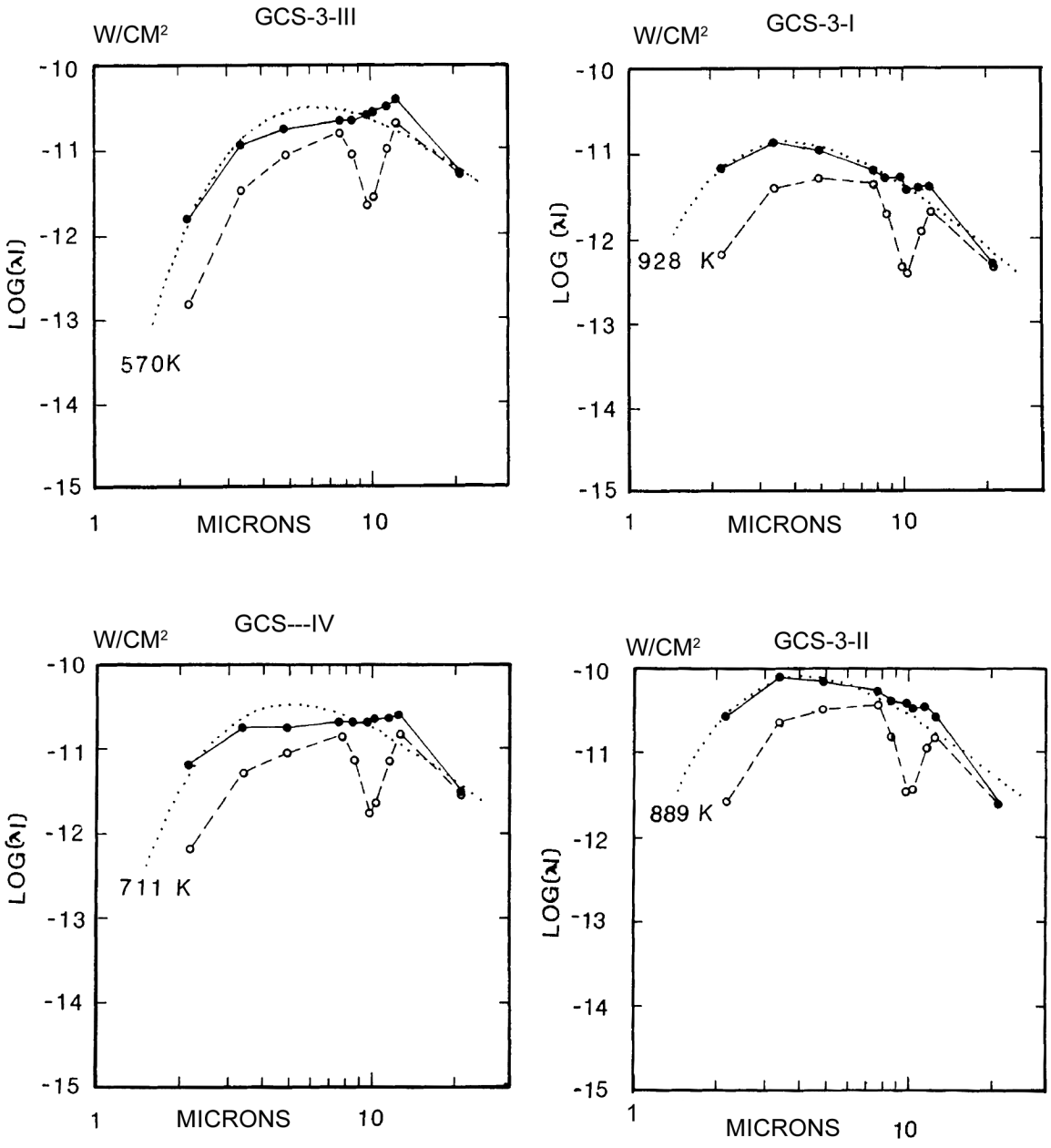

Figure 5.2 shows energy spectra for GCS-3-I, GCS-3-II, GCS-3-III and GCS-3-IV from Okuda *et al.*, (1990). The open circles show the observed intensity and the closed circles show the intrinsic source spectra. The dotted line shows the best fit black body spectra.

It can be seen from figure 5.2 that the intrinsic source spectra does not exhibit a 10µm absorption feature and can be roughly approximated by spectra of simple black bodies enabling source temperatures to be deduced that range from 600K to 1000K. There is little indication of photospheric radiation from the source even at the shortest wavelengths confirming that the observed absorption features arise from the effects of grains lying in the line of sight rather than from local sources.

5.4 MIE AND GUTTLER EFFICIENCY CALCULATIONS

The scattering of light by small homogeneous particles with sizes comparable to the wavelength of light is essentially one in classical electromagnetic theory and involves solution of Maxwell's equation with suitable boundary conditions. Independent solutions were derived by Mie (1908) and Debye (1909) for an incident plane polarised electromagnetic wave on a sphere of radius *a* and complex refractive index *m*. Following the notation of van de Hulst (1957) we define $\pi a^2 Q_{ext}$ and $\pi a^2 Q_{sca}$ to be the cross sections for *extinction* and *scattering*. The objective of the solution developed is the calculation of Q_{ext} and Q_{sca} as a function of

$$x = 2\pi a/\lambda \qquad \text{eq 5.1}$$

and

$$m = n - ik = \sqrt{\varepsilon - 2i\sigma\lambda/c}\,, \qquad \text{eq 5.2}$$

where λ is the wavelength of the incident radiation, n is the index of refraction, k the absorptive index, ε the dialectric constant and σ the optical conductivity of the grain material. The solution provided by Mie (1908) gives

$$Q_{sca} = \frac{2}{x^2}\sum_{n=1}^{\infty}(2n+1)\{|a_n|^2 + |b_n|^2\} \qquad eq\ 5.3$$

$$Q_{ext} = \frac{2}{x^2}\sum_{n=1}^{\infty}(2n+1)\mathrm{Re}\,(a_n + b_n) \qquad eq\ 5.4$$

$$Q_{bk} = \frac{4}{x^2}\sum_{n=1}^{\infty}\left|\left(n+\frac{1}{2}\right)(-1)^n(a_n - b_n)\right|^2 \qquad eq\ 5.5$$

$$Q_{abs} = Q_{ext} - Q_{sca} \qquad \text{eq 5.6}$$

where,

$$a_n = \frac{x\psi_n'(y)\psi_n(x) - y\psi_n'(x)\psi_n(y)}{x\psi_n'(y)\xi_n(x) - y\xi_n'(x)\psi_n(y)} \qquad eq\ 5.7$$

$$b_n = \frac{x\psi_n'(x)\psi_n(y) - y\psi_n'(y)\psi_n(x)}{x\psi_n(y)\xi_n'(x) - y\xi_n(x)\psi_n'(y)} \qquad eq\ 5.8$$

and, ξ_n, ψ_n and $\xi_n(z)$ are the Riccati-Bessel functions with the following identities,

$$\psi_n(z) = \left[\frac{\pi z}{2}\right]^{\frac{1}{2}} \mathrm{J}_{n+\frac{1}{2}}(z) \qquad eq.\ 5.9$$

$$\chi_n(z) = (-1)^n \left[\frac{\pi z}{2}\right]^{\frac{1}{2}} \mathrm{J}_{-n-\frac{1}{2}}(z) \qquad eq.5.10$$

$$\xi_n(z) = \psi_n(z) + i\chi_n(z) \qquad eq.5.11$$

Computation of a_n and b_n then follows from defining $A_n(y) = \psi_n'(y)/\psi_n(y)$ and using the recurrence relations for the Bessel functions (Hoyle and Wickramasinghe, 1991) to give

$$a_n = \frac{[A_n(y)/m + n/x]\mathrm{Re}\{\xi_n(x)\} - \mathrm{Re}\{\xi_{n-1}(x)\}}{[A_n(y)/m + n/x]\,\xi_n(x) - \xi_{n-1}(x)} \qquad eq.5.12$$

$$b_n = \frac{[mA_n(y) + n/x]\mathrm{Re}\{\xi_n(x)\} - \mathrm{Re}\{\xi_{n-1}(x)\}}{[mA_n(y) + n/x]\,\xi_n(x) - \xi_{n-1}(x)} \qquad eq.5.13$$

and generating the functions $\xi_0(x)$ and $\xi_{-1}(x)$ using the recurrence relations

$$\xi_0(x) = \sin x + i\cos x \qquad eq.5.14$$

$$\xi_{-1}(x) = \cos x - i\sin x \qquad eq.5.15$$

$$\xi_n(x) = \frac{2n-1}{x}\xi_{n-1}(x) - \xi_{n-2}(x) \qquad eq.5.16$$

from which $A_n(y)$ follows,

$$A_n(y) = \frac{\psi'(y)}{\psi(y)}, \qquad eq.5.17$$

leading to (Hoyle and Wickramasinghe, 1991),

$$A_n(y) = -\frac{n}{y} + \left[\frac{n}{y} - A_{n-1}(y)\right]^{-1} \qquad eq.5.17$$

$$A_0(y) = \cos y / \sin y \qquad eq.5.17$$

For collections of individual homogeneous particles heated by ambient stellar radiation, infrared emission can then easily be modelled in the optically thin case. The flux F_λ emitted by grains of radii a and absorption efficiency Q_{abs} is given by

$$F_\lambda = Q_{abs}(\lambda)\pi a^2 B_\lambda(T) \qquad eq.5.18$$

where $B_\lambda(T)$ is the Planck function at temperature T. For composite particles comprising of inner cores and outer mantle coatings, a complete scattering solution is provided by Guttler (1952). For composite spheres of inner radius r_1 and refractive index m_1 with outer coating radius r_2 and refractive index m_2 the Guttler formula gives:

$$Q_{ext} = \frac{2}{x^2}\sum_{l=1}^{\infty}(2l+1)\mathrm{Re}\,(a_l + b_l) \qquad eq.\,5.19$$

$$Q_{sca} = \frac{2}{x^2}\sum_{l=1}^{\infty}(2l+1)\,\{|a_l|^2 + |b_{nl}|^2\} \qquad eq.\,5.20$$

where $x = 2\pi r_2/\lambda$ and

$$a_l = \frac{[\psi\psi]'_{l,r_1}[\chi\psi]'_{l,r_2} - [\chi\psi]'_{l,r_1}[\psi\psi]'_{l,r_2}}{[\psi\psi]'_{l,r_1}[\chi\zeta]'_{l,r_2} - [\chi\psi]'_{l,r_1}[\psi\zeta]'_{l,r_2}} \qquad eq.\,5.21$$

$$b_l = \frac{[\psi\psi]''_{l,r_1}[\chi\psi]''_{l,r_2} - [\chi\psi]''_{l,r_1}[\psi\psi]''_{l,r_2}}{[\psi\psi]''_{l,r_1}[\chi\zeta]''_{l,r_2} - [\chi\psi]''_{l,r_1}[\psi\zeta]''_{l,r_2}} \qquad eq.\,5.22$$

Here

$$\begin{aligned}
[\chi\psi]'_{l,r_2} &= \chi'_l(k_2r_2).k_3\psi_l(k_3r_2) - k_2\chi_l(k_2r_2).\psi'_l(k_3r_2)\\
[\chi\zeta]'_{l,r_2} &= \chi'_l(k_2r_2).k_3\zeta_l(k_3r_2) - k_2\chi_l(k_2r_2).\zeta'_l(k_3r_2)\\
[\psi\psi]'_{l,r_2} &= \psi'_l(k_2r_2).k_3\psi_l(k_3r_2) - k_2\psi_l(k_2r_2).\psi'_l(k_3r_2)\\
[\psi\zeta]'_{l,r_2} &= \psi'_l(k_2r_2).k_3\zeta_l(k_3r_2) - k_2\psi_l(k_2r_2).\zeta'_l(k_3r_2)\\
[\chi\psi]''_{l,r_2} &= k_2\chi'_l(k_2r_2).\psi_l(k_3r_2) - \chi_l(k_2r_2).k_3\psi'_l(k_3r_2)\\
[\chi\zeta]''_{l,r_2} &= \chi'_l(k_2r_2).k_3\zeta_l(k_3r_2) - k_2\chi_l(k_2r_2).\zeta'_l(k_3r_2)\\
[\psi\psi]''_{l,r_2} &= \psi'_l(k_2r_2).k_3\psi_l(k_3r_2) - k_2\psi_l(k_2r_2).\psi'_l(k_3r_2)\\
[\psi\zeta]''_{l,r_2} &= \psi'_l(k_2r_2).k_2\zeta_l(k_3r_2) - k_2\psi_l(k_2r_2).\zeta'_l(k_3r_2)\\
[\chi\psi]'_{l,r_1} &= \chi_l(k_2r_1).k_1\psi_l(k_1r_1) - k_2\chi_l(k_2r_1).\psi'_l\,(k_1r_1)\\
[\psi\psi]'_{l,r_1} &= \psi'_l(k_2r_1).k_1\psi_l(k_1r_1) - k_2\psi_l(k_2r_1).\psi'_l(k_1r_1)\\
[\chi\psi]''_{l,r_1} &= k_2\chi'_l(k_2r_1).\psi_l(k_1r_1) - \chi_l(k_2r_1).k_1\psi'_l(k_1r_1)\\
[\psi\psi]''_{l,r_1} &= k_2\psi'_l(k_2r_1).\psi_l(k_1r_1) - \psi_l(k_2r_1).k_1\psi'_l(k_1r_1)
\end{aligned} \qquad eqs.\,5.23$$

where

$$k_1 = m_1\frac{2\pi}{\lambda}\,,\;\; k_2 = m_2\frac{2\pi}{\lambda}\,, k_3 = \frac{2\pi}{\lambda} \qquad eq.\,5.24$$

and, ξ_n, ψ_n and $\xi_n(z)$ are the Riccati-Bessel functions with the following identities, defined in equation 5.9 to 5.11 and computed using the following recurrence relations,

$$\begin{aligned}
\psi_n(z) &= \frac{2n-1}{z}\psi_{n-1}(z) - \psi_{n-2}(z)\\
\psi'_n(z) &= \frac{-n}{z}\psi_n(z) + \psi_{n-1}(z)
\end{aligned} \qquad eqs.\,5.25$$

$$\chi_n(z) = \frac{2n-1}{z}\chi_{n-1}(z) - \chi_{n-2}(z)$$

$$\chi_n'(z) = \frac{n+1}{z}\psi_n(z) - \psi_{n+1}(z)$$

together with,

$$\psi_0(z) = \left(\frac{\pi z}{2}\right)^{1/2} J_{1/2}(z)$$

$$\chi_0(z) = \left(\frac{\pi z}{2}\right)^{1/2} J_{-1/2}(z)$$

$$\psi_0'(z) = \frac{\pi}{4}\left(\frac{\pi z}{2}\right)^{-1/2} J_{1/2}(z) + \left(\frac{\pi z}{2}\right)^{1/2} J_{1/2}'(z) \qquad eqs.5.26$$

$$\chi_0'(z) = \frac{\pi}{4}\left(\frac{\pi z}{2}\right)^{-1/2} J_{-1/2}(z) + \left(\frac{\pi z}{2}\right)^{1/2} J_{-1/2}'(z)$$

$$J_{1/2}(z) = \left(\frac{\pi z}{2}\right)^{-1/2} \sin z$$

$$J_{-1/2}(z) = \left(\frac{\pi z}{2}\right)^{-1/2} \cos z$$

The above enable calculation of equations 5.19 and 5.20 from which Q_{abs} can be calculated from equation 5.6.

5.5 DATA SOURCES

Transmittance spectra for three kerogen-rich sedimentary rocks (coals), one biochar, one oil shale residue and pyrite were taken from the literature. Each spectrum was electronically digitised and calibrated to give a normalised τ(λ) curve such that τ = 1 at λ = 9.5μm. Data sets were then re-converted to transmittance spectra to provide normalised curves for the six selected materials.

Figures 5.3 and 5.4 show normalised transmittance spectra for the selected materials. The first spectra (figure 5.3, upper panel) relates to a low-temperature conversion by-product of biological waste generated by a thermo-catalytic conversion process. The process takes place anaerobically at 380-450°C under normal pressure (Hossain *et al*., 2011). It has been proposed that carbonised products generated in this way should be called “biochars” and are commonly used as soil supplements (McLaughlin et al., 2009). This spectra represents the product of rapidly carbonised bio-material and was considered a close analogue to biologically degraded material likely to be generated in astronomical environments when high order biology is exposed to higher temperatures in space. The raw transmittance spectrum was taken from Qayyum *et al.*, (2012).

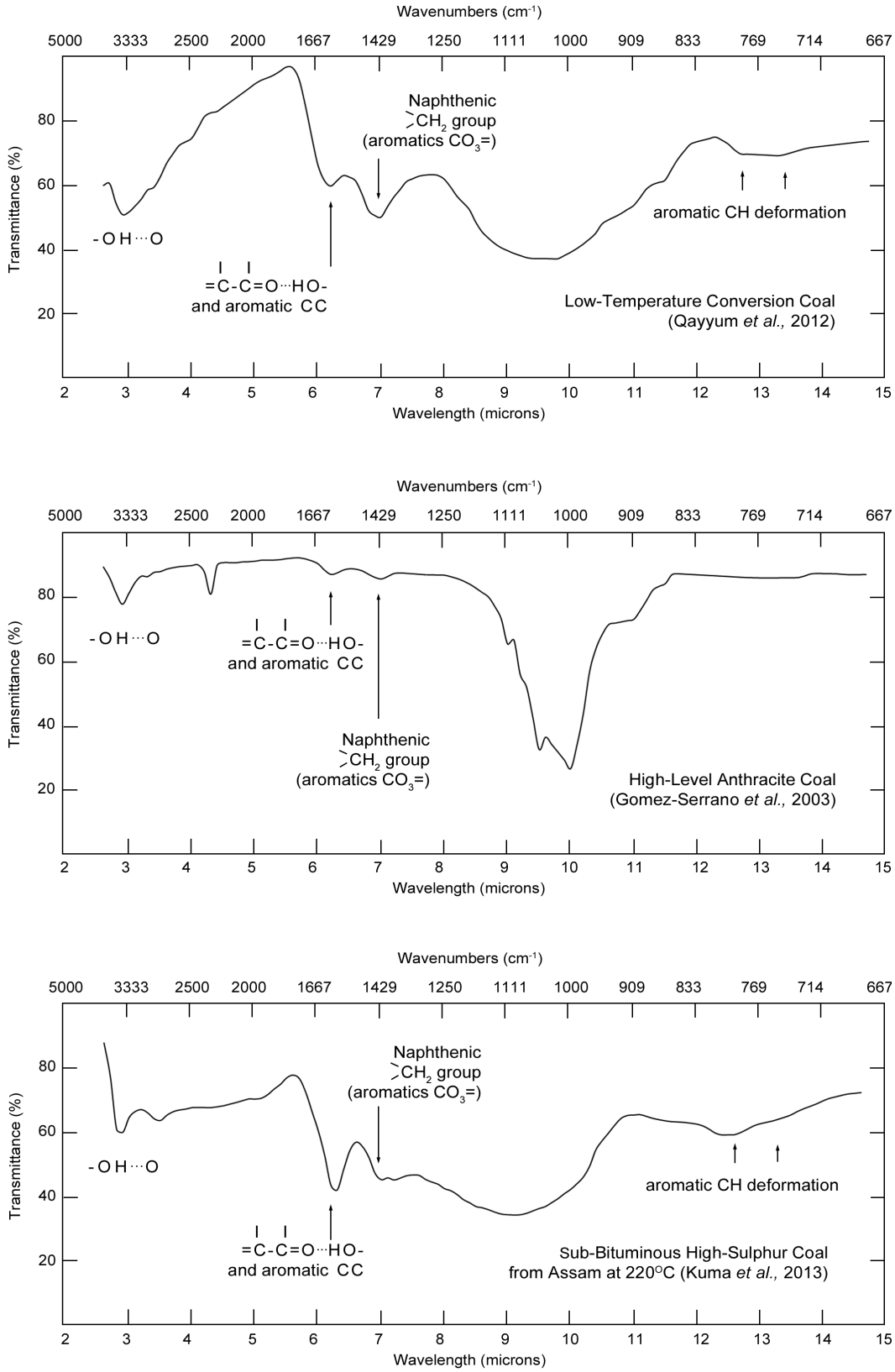

Figure 5.3 Transmittance spectra for (upper) low temp. conversion coal (biochar), (middle) high-level anthracite coal and (lower) sub-bituminous high-sulphur content coal ($220^{O}C$) - source transmittance spectra from Qayyum *et al.*, (2012), Gomez-Serrano *et al.*, 2003 and Kuma *et al.*, (2013) respectively.

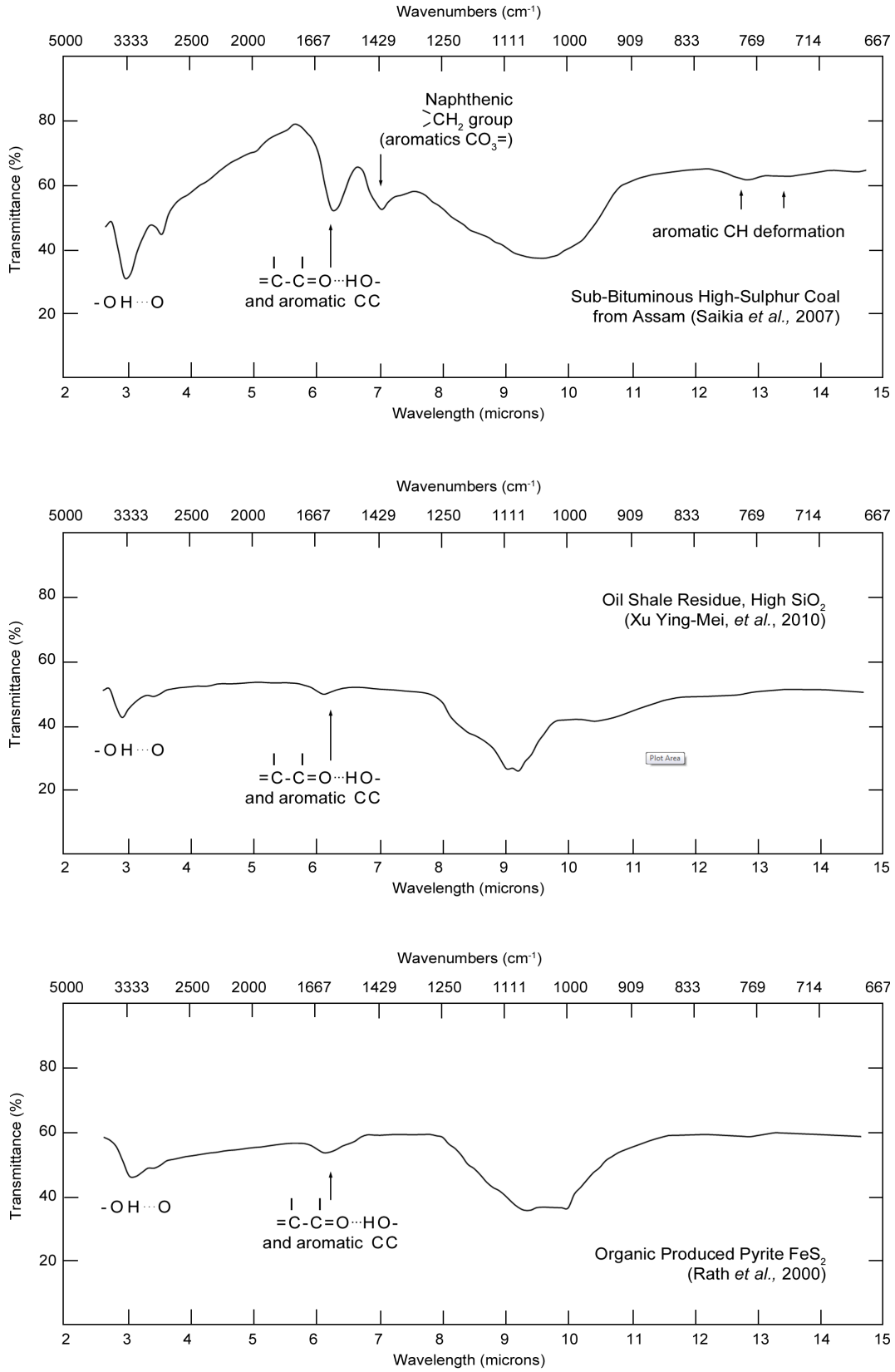

Figure 5.4 Transmittance spectra for (upper) sub-bituminous high-sulphur content coal, (middle) high-SiO_2 Oil shale residue and (lower) FeS_2 Pyrite. Source transmittance spectra from Saikia *et al.*, (2007), Xu Ying-Mei *et al.*, 2010 and Rath *et al.*, (2000) respectively.

The next three materials considered are kerogen-rich sedimentary rocks (coals) of varying degree and are shown by the transmittance spectra in the centre and lower panels of figure 5.3 and the upper panel of figure 5.4. The first is a high-carbon, highly-metamorphosed anthracite coal with data taken from Gómez-Serrano (2003). The second is a sub-bituminous high sulphur content coal from Ledo in the Assam State in the North Eastern region of India. This coal was observed in the temperature range 190-220^{O}C as part of a series of Temperature Programmed Reduction (TPR) studies on the determination of sulphur functional groups present in Ledo coals (Kumar and Srivastava, 2013). The third coal considered was of the same origin and type as above but with transmittance spectra taken from unheated samples (Saikia *et al.*, 2007).

The final two materials considered were the non-organic mass fraction components of a likely mantle-core structure, these being the pyrite core and a probable amorphous silica residual component. SiO_2 is the main component of oil shale residue accounting for more than 50% by mass with a further component of ~20% Al_2O_3 and ~10% Fe_2O_3. The residue sample used here originated from Huadian in China and was processed (i.e. from hydrophilic to hydrophobic-lipophilic state) using vinyl trimethoxysilane from the Peking chemical factory. Transmittance spectra were taken from Xu Ying-Mei *et al.*, (2010). The final sample considered was pyrite obtained from Alminrock Indscer Fabsiks, Bangalore in India. Here the interaction between pyrite and dextrin was investigated through adsorption, flotation and electrokinetic experiments, with modified and residual products studied using FTIR spectroscopy. Resulting transmittance spectra were taken from Rath *et al.*, (2000).

Each of the spectra considered exhibited strong absorption features in the 9-10.5µm region due predominantly to the presence of clay minerals. The specific identification of the infrared bands in this region remains very difficult due to their complicated and non-constant composition but also because band positions can vary significantly due to isomorphous replacements. Furthermore, the poly-component nature of the mineral fraction of kerogen-rich sedimentary rocks means that no single particular mineral is dominant, and the complexities of the overlapping bands often precludes a unambiguous interpretation.

The remaining bands displayed in the coal spectra can be assigned to stretching or bending vibrations in water, carbonates, aluminosilicates, and quartz. The band at 3µm observed in all the spectra can be attributed to the –OH$^{\cdots}$O regime. Normalised $\tau(\lambda)$ curves for the low temperature conversion coal (biochar), the sub-bituminous coal and pyrite are shown in figure 5.5 with coincident absorption features at ~3 µm, ~6.25 µm, ~7 µm and ~13 µm due to aromatic C-C and CO_3 functional groups highlighted with arrows.

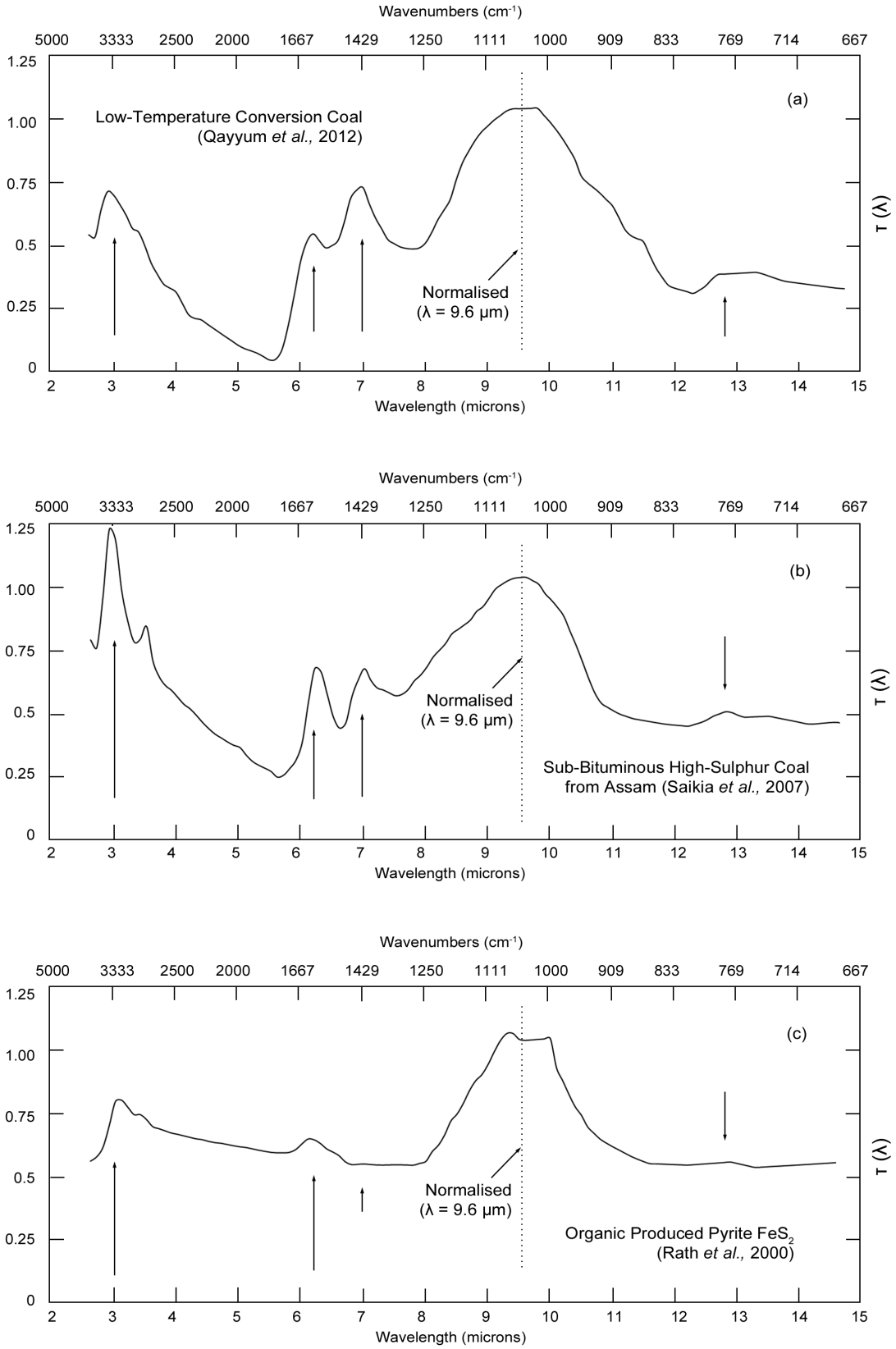

Figure 5.5 Shows normalised optical depth τ(λ) curves (τ = 1 at λ = 9.5μm) for (upper) low temp. conversion coal (biochar), (middle) sub-bituminous high-sulphur content coal and (lower) FeS_2 Pyrite - source transmittance spectra from Qayyum *et al.*, (2012), Saikia *et al.*, (2007), and Rath *et al.*, (2000).

5.6 DERIVATION OF OPTICAL CONSTANTS

In order to proceed with the calculations it is necessary to derive the refractive index m of an absorbing media as a wavelength-dependent complex function $m(\lambda) = n(\lambda) - ik(\lambda)$ where $n(\lambda)$ describes refraction and scattering of light passing through the medium, and $k(\lambda)$ describes the absorption. The optical constants $n(\lambda)$and $k(\lambda)$ are not mutually independent, but fundamentally connected by the Kramers-Kronig relations that are given as,

$$n(\lambda_0) = 1 + \frac{2}{\pi} P \int_0^{\infty} \frac{\lambda k(\lambda)}{\lambda^2 - \lambda_0^2} d\lambda \qquad 5.27$$

$$k(\lambda_0) = 1 + \frac{2\lambda_0}{\pi} P \int_0^{\infty} \frac{n(\lambda)}{\lambda^2 - \lambda_0^2} d\lambda \qquad 5.28$$

where P indicates the Cauchy principal value and λ_0 is a specified wavelength. These relations allow direct calculation of the refractive index from absorption spectra. However, in practical terms absorption parameters are not known for the entire wavelength interval (0, ∞) and it is necessary to extrapolate laboratory data hypothetically, thus introducing an element of uncertainty. This matter is not aided by the convergence rate of the K-K integrals. Wallis (1998) determined that for an unknown resonance feature at wavelength λ_Σ the error introduced in the K-K calculation at a given wavelength λ_0 is given by,

$$E(\lambda_0) = \frac{2}{\pi} \left[\frac{\lambda_\Sigma}{\lambda_\Sigma^2 - \lambda_0^2} \right] \qquad eq.\,5.29$$

To assist with this problem, Arhenkiel (1971) introduced a more rapidly converging modified KK relation integral that is given by,

$$n(\lambda_0) = n(\lambda_1) + \frac{2(\lambda_1^2 - \lambda_0^2)}{\pi} P \int_0^{\infty} \frac{\lambda k(\lambda)}{(\lambda^2 - \lambda_0^2)(\lambda^2 - \lambda_1^2)} d\lambda \qquad 5.30$$

which introduces an error (Wallis, 1998) at a given wavelength λ_0 for an unknown feature at λ_Σ of,

$$E(\lambda_0) = \frac{2}{\pi} \left[\frac{(\lambda_1^2 - \lambda_0^2)\lambda_\Sigma}{(\lambda_\Sigma^2 - \lambda_0^2)(\lambda_\Sigma^2 - \lambda_1^2)} \right] \qquad eq.\,5.31$$

As a first estimate the refractive index for the absorption spectra of the six materials considered were computed using equation 5.27 for wavelength λ = 4.2μm The returned refractive index was

then utilised as the given wavelength and computed from equation 5.30 at wavelength λ = 15μm to take advantage of the more rapidly converging Arhenkiel (1971) modified KK relation. This process was repeated until convergence to 4 decimals was observed. The two computed refractive index parameters (i.e. at λ = 4.2μm and λ = 15μm) were then used in the n[th] order modified Kramers Kronig relation of Wallis and Wickramsinghe (1999) that is given by,

$$n(\lambda_0) = \sum_{i=1}^{n} (-1)^{n+1} \prod_{\substack{j=1 \\ j \neq i}}^{n} \frac{(\lambda_j^2 - \lambda_0^2)}{(\lambda_i^2 - \lambda_j^2)} n(\lambda_i) + \frac{2}{\pi} P \int_0^{\infty} (-1)^{n+1} \frac{\prod_{i=1}^{n} (\lambda_i^2 - \lambda_0^2)}{\prod_{i=0}^{n} (\lambda^2 - \lambda_i^2)} \lambda k(\lambda) d\lambda \quad eq. 5.32$$

with an error (relative to the K-K integral) introduced via a resonance feature at wavelength λ_Σ of

$$E_n(\lambda_0) = \prod_{i=1}^{n} \frac{(\lambda_i^2 - \lambda_0^2)}{(\lambda_\Sigma^2 - \lambda_i^2)} \qquad eq. 5.33$$

This integral has been shown to be rapidly converging and only dependent on values of $k(\lambda)$ for λ close to the spectral region under consideration (Wallis and Wickramasinghe, 1999). A number of numerical procedures are available for calculation of the optical constants $n(\lambda)$ from absorption spectra. Here we use a modified version of the algorithm provided in Wallis (1998) for the numerical determination of equations 5.27, 5.30 and 5.31 using trapezoidal integration for between 2,000 and 34,000 points (depending on the spectral range) though good accuracy was obtained using a coarser mesh size other than in the regions incorporating the discontinuities. Values for $k(\lambda)$ are directly derived from transmittance spectra that give rise to values of the linear absorption coefficient α which is related to $k(\lambda)$ by

$$k(\lambda) = \frac{\propto(\lambda)\lambda}{4\pi} \qquad eq. 5.34$$

The linear absorption coefficient function $\propto(\lambda)$ is proportional to the optical depth τ (λ) and requires knowledge of the path length (i.e. film thickness) for direct computation. This value was calibrated from known values of $k(\lambda)$ for the given materials taken from the literature.

The index of absorption *k* has previously been considered for some low ranking coals using polarised obliquely-incident radiation and the Fresnel equations to generate values of *n* and *k* at fixed wavelengths. Huntjens and van Krevelen (1954) obtained values for *k* ranging from 0.03 to 0.8 at λ = 0.546μm. These values were confirmed by McCartney and Ergun (1959) and Gilbert (1962) though Foster and Hogwarth (1968) reported values of *k* approximately one order of magnitude larger for coals of similar rank. Brewster (1984) used particle extinction techniques and

reported significantly lower values of *k*, generally between 0.01 and 0.1, that was supported by the fact that values of *k* in the visible region for coals of similar carbon content also ranged from 0.03 to 0.1 (van Krevelen, 1961). Later analysis of transmission spectra of a thin coal maceral layer indicated that the *k* value in the wavelength region near 2µm could not be above ~0.005. This value accords reasonably well with the later work of Khare *et al.,* (1991) on kerogen that provides a *k* value of ~0.03 at ~2µm. Kitamura *et al.,* (2007) provided a similar analysis of amorphous silica that gives a value of $k \approx 10^{-2}$ at 2.6 µm while Sato (1984) provide a value of $k = 0.8$ at 2.6 µm for pyrite.

These values were used to calibrate the $k(\lambda)$ curve obtained from the optical depth τ (λ) spectra and equation 5.34. Results of iterative calculations are provided in figures 5.6 and 5.7 for each of the data sets selected in this study.

5.7 PARTICLE POPULATION SIZE DISTRIBUTIONS

The $k(\lambda)$ and $n(\lambda)$ values (for λ = 2.6 to 15 µm) derived in the previous section were used to compute extinction and scattering efficiencies (Q_{ext} (λ) and $Q_{sca}(\lambda)$) via the numerical solution of equations 5.19 and 5.20 from which $Q_{abs}(\lambda)$ was deduced using equation 5.6. The flux F_λ emitted by grains was then calculated using equation 5.18 for a size distribution of particles representing a dust population with mean particle size similar to those of the observed carbonaceous core-mantle structures. This was modelled using a normal type distribution, defined such that the number density of particles of radius in the range (*a, a + da*) is given by,

$$n(a) = exp\left\{-\frac{1}{2}\left[\frac{a-\mu}{\sigma}\right]^2\right\}, \quad a_1 \leq a \leq a_2 \qquad eq.5.35$$

where the parameter µ in this definition is the average particle size (µm) and the parameter σ is its standard deviation. Values of µ = 5, 10, 20, 50 microns were taken as representative of the mean particle size for a population of contributing carbonaceous structures. A value of $a_1 = 0.1$ µm and a standard deviation σ = 1 µm was taken. However, the results discussed below were not found to be sensitive to the precise choice of σ and in general, values of σ across a wide range yielded very similar results. The total flux emitted by a population of particles determined by the distribution function defined above can then be calculated using the expression,

$$F_\lambda = const.\, B_\lambda(T)\, Q_{abs}(\lambda) \sum_{a_i=a_1}^{a_2} exp\left\{-\frac{1}{2}\left[\frac{a_i-\mu}{\sigma}\right]^2\right\} \pi {a_i}^2 \qquad eq.5.36$$

This value was then compared to the total flux calculated directly from the optical depth τ (λ) via the simpler equation F_λ = const. τ (λ) $B_\lambda(T)$.

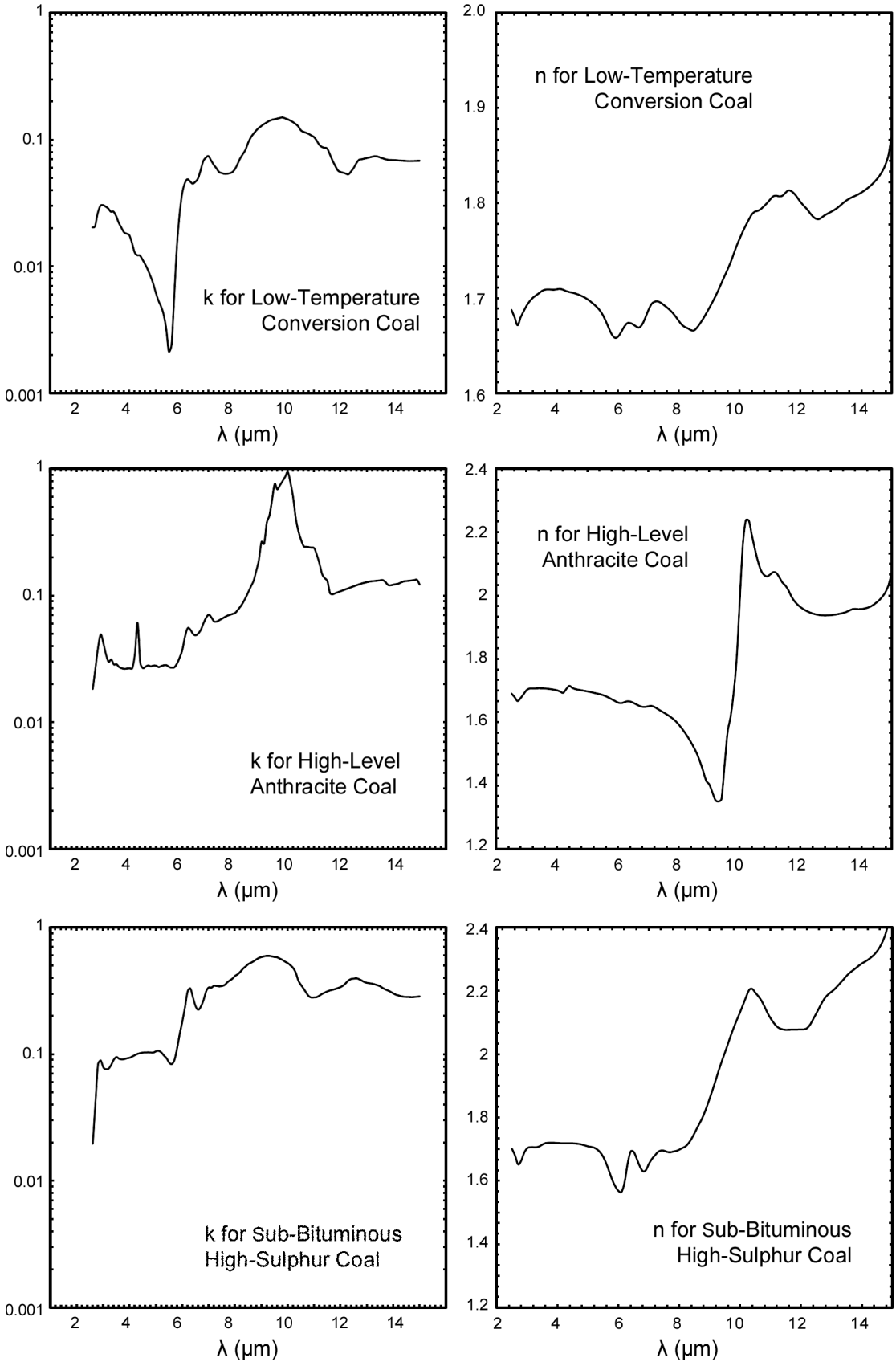

Figure 5.6 Refractive index (n) and imaginary refractive index (k) parameters for (upper) low-temp conversion coal (char), (centre) high-C anthracite, (lower) sub-bituminous high sulphur coal (220^{O}C).

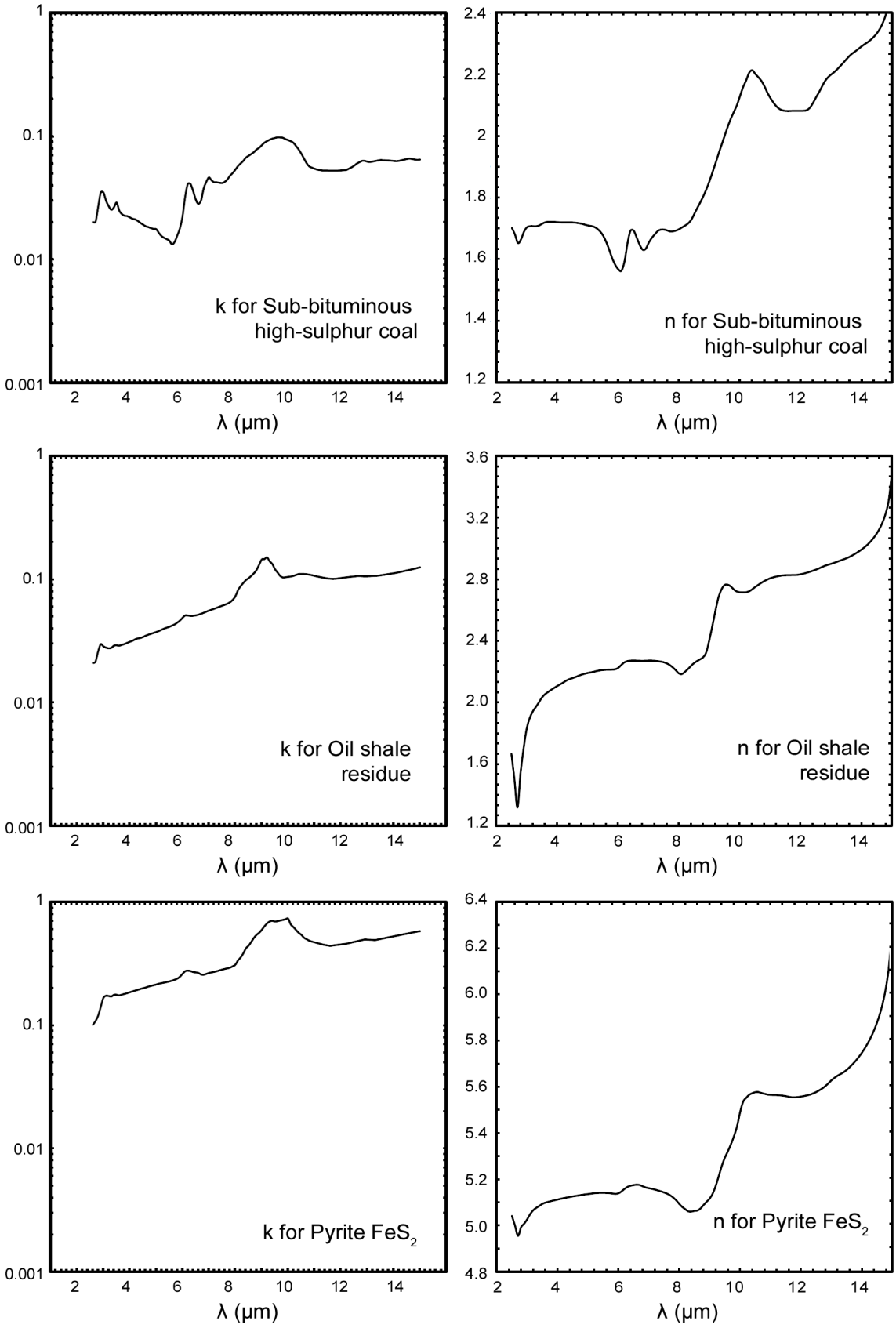

Figure 5.7 Refractive index (n) and imaginary refractive index (k) parameters for (upper) sub-bituminous high sulphur coal, (centre) oil shale residue and (lower) Pyrite FeS_2.

5.8 RESULTS

Results of flux emission curves calculated using equation 5.36 closely accorded with similar curves derived directly from the optical depth calculation. This indicates that the flux emission characteristics of the 8-13 µm wavelength range, for the particle populations under consideration, were generally resistant to variations arising from scattering by the presence of smaller particles in the size distribution range. Larger variations in curve characteristics were observed where population parameters were purposefully biased such that the parameter µ (the average particle size) and the standard deviation σ were chosen to induce a very narrow normal-type distribution with average particle sizes comparable to between 1.5 µm to 2.0 µm. Because this size range was in the lower band of average particle sizes generally representative of the core-mantle carbonaceous structures being considered, overall curve shape was insensitive to the presence of these smaller particles.

Figure 5.8 shows emission curves from 8-13 µm for each of the six sample materials. It can be seen immediately that the curve for the low-temperature conversion coal (biochar) provides a remarkable fit across the wavelength range. This material is the char residual product of biological waste converted by anaerobic heating at 380-450°C. It is considered to be a reasonable representation of the complex organic residue likely to arise if biological material was injected into interstellar space and subsequently heated over a period of time in the absence of oxygen. It can also be seen that while the emission curve for sub-bituminous high-sulphur coal appears to provide a poor fit initially, the fit can be seen to improve in the case where the coal was sampled after heating to 220^{O}C. Here, the curve can be seen to converge with observed values across the 8-10 µm range while concurrently improving via a weakening of the prominent dip in the 10.5-11.5 µm. The curve for FeS_2, while good at shorter wavelengths can be seen to rise too rapidly for wavelengths > 11µm.

Figure 5.9 shows (in the upper left panel) the flux curve for an ensemble of the anthracite and sub-bituminous coals in equal proportions while the upper right panel shows an equivalent flux curve for the coal ensemble mixed with an equal proportion of the low-temperature biochar. The centre left panel provides equivalent results when the proportion of biochar is increased to 70%. In each case discussed mixing was modelled by first normalising the optical depth $\tau(\lambda)$ such that $\tau(\lambda) = 1$ at λ = 9.6 µm for each component material before adding appropriate fractions of the materials together.

The centre right panel and lower panels of figure 5.9 show the effect on the flux curve arising from the addition of pyrite in increasing proportions. In each case $B_\lambda(T)$ is calculated for T = 200K.

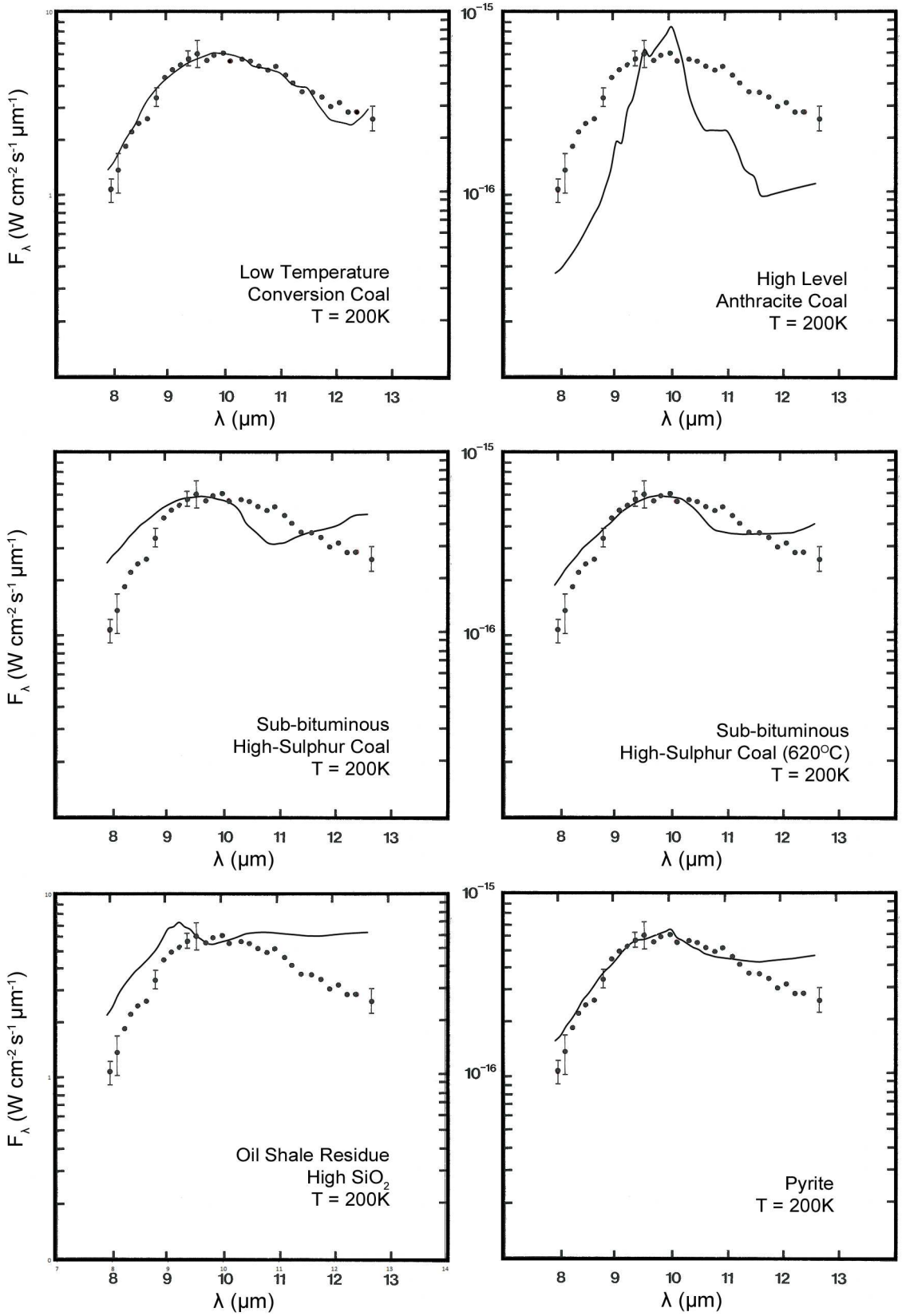

Figure 5.8 Flux curves for each of the six sample materials considered. In each case the Planck function $B_\lambda(T)$ is calculated for T = 200K.

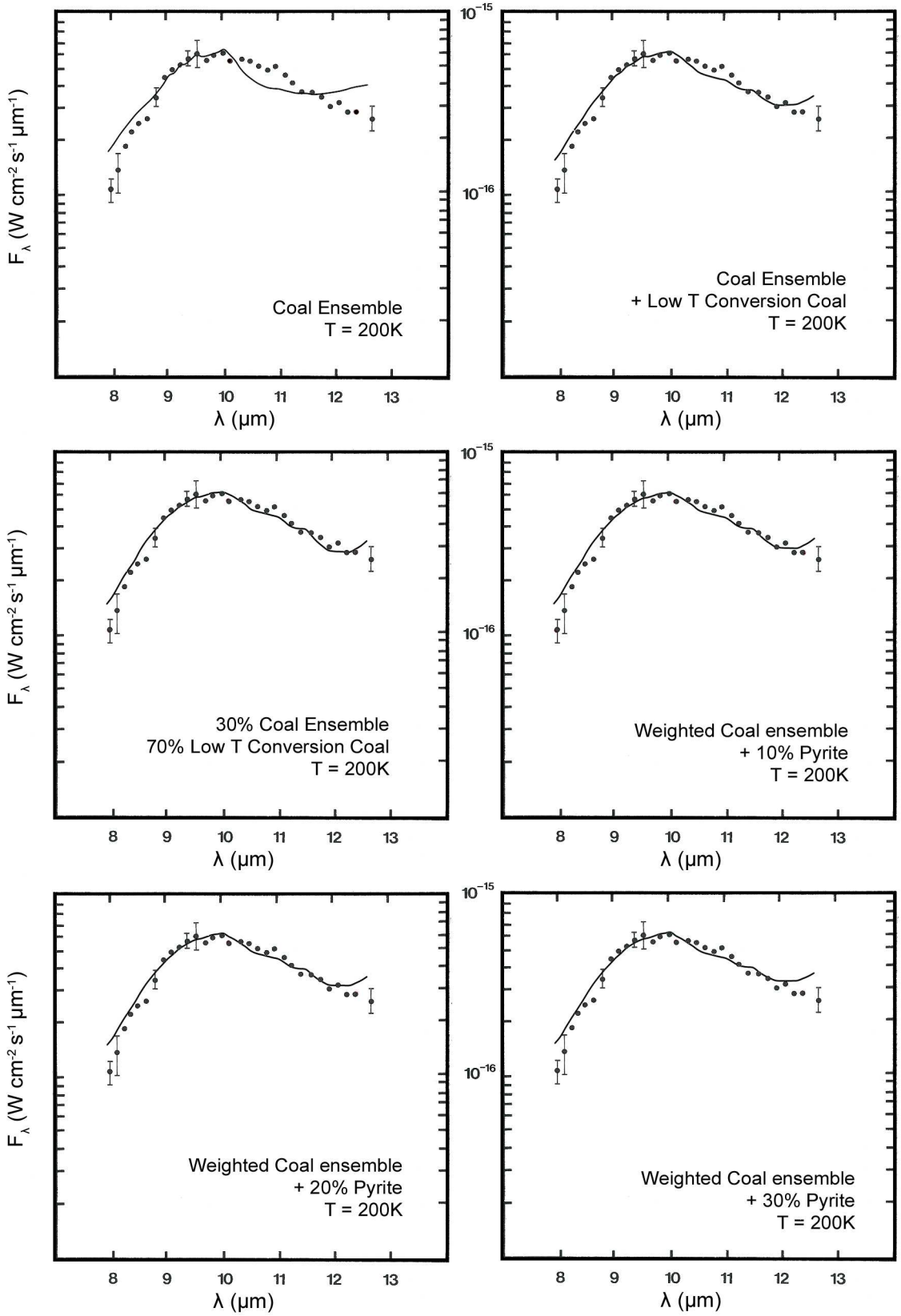

Figure 5.9 Flux curves for an ensemble of coals and low-temperature conversion biochar with 10%, 20% and 30% inclusions of pyrite. In each case the Planck function $B_\lambda(T)$ is calculated for T = 200K.

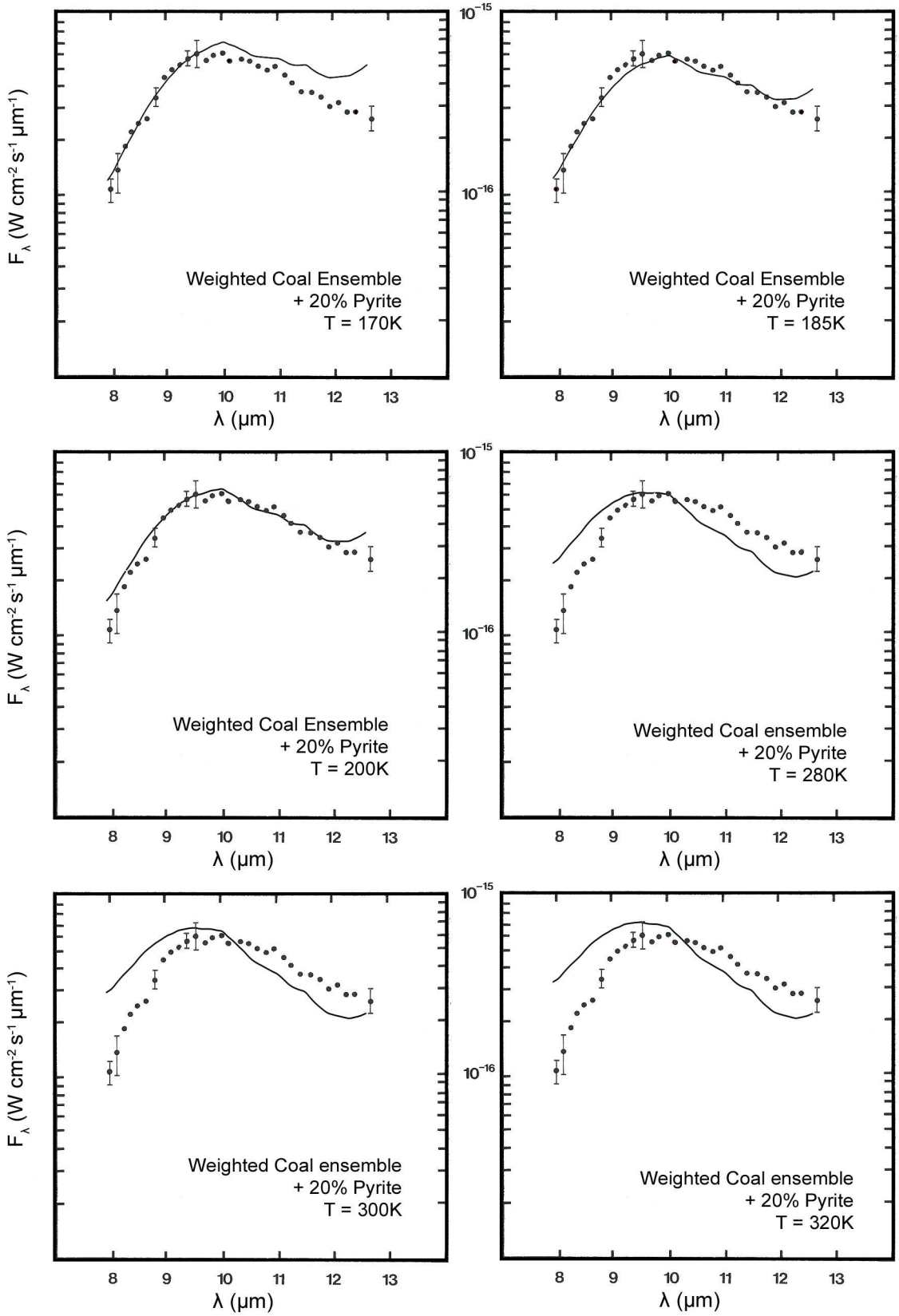

Figure 5.10 Shows the effect on flux emissions for varying T.

Figure 5.10 shows the effect on the computed flux values arising from variations of T .

5.9 CONCLUSION

Results of calculations show that observations of interstellar emissions in the 8-13 μm wavelength range are well matched by core-mantle spherical grains consisting of pyrite cores and kerogenous outer coatings. Anthracite and sub-bituminous coals provide generally poor fits when taken alone but those of the sub-bituminous coals can be seen to improve where the coal has been heated to 220^{O}C. It is possible that this fit could further improve given prolonged exposure to higher temperatures. Further improvements in fit can be seen to arise when pyrite is included. In each case the contribution to total emissions from particles of scattering size was found to be negligible.

Chapter 6

Physical, Chemical and Mineral Properties of the Polonnaruwa Stones

6.1 BACKGROUND

The importance of recovering meteorites after witnessed fireball events cannot be overstated. While sample return missions will always provide the ideal source of non-terrestrial material of known parent body provenance, they remain expensive and uncommon. To date, only the Stardust (Brownlee *et al.,* 2006) and Hayabusa (Yano 2006) missions have returned material from small solar system bodies (81P/Wild 2 and 25143 Itokawa) though several planned sample return missions such as OSIRIS-Rex (Lauretta *et al.,* 2012), Marco Polo (Brucato *et al.,* 2009) and Hayabusa 2 (Yoshikawa *et al.,* 2008) should provide further material within the next 7-15 years. Until sample return missions become routine, the next best source of fresh non-terrestrial material comes in the form of meteorites recovered following observed fireball events, though the problem of predicting which fireballs may produce meteorites persists. This has no doubt contributed to the current situation where only the most energetic fireballs result in significant ground recovery efforts (Werthill and ReVelle, 1981), despite the conclusions of Halliday *et al.,* (1989) that the brightness of the fireball itself is a poor indicator of a meteorite's survival prospects.

This kind of bias may be particularly relevant in relation to meteorites with a cometary progenitor. Conventional thinking asserts that meteor showers do not result in meteorites. This is largely due to the high entry velocities of incoming bolides (~28 km s^{-1}) and the common perception that cometary meteoroids are uniformly comprised of friable, porous material (Ceplecha *et al.,* 1998). Since porosity is inversely proportional to tensile strength, it follows that they are weak and more susceptible to destruction on entry into the atmosphere. However recent work by Brown *et al.,* (2012) questions this paradigm. Here, application of the PE strength criterion (a unidimensional representation of relative strength) was calculated for a defined dataset of instrumentally recorded Taurid fireballs using the Ceplecha (1988) common mass scale conversion. The results clearly demonstrate that Taurid fireballs comprise of a diverse set of strengths capable of producing recoverable meteorites. Past entry-modelling suggests an extreme upper limit of 30 km s^{-1} for entry velocity (Revelle 1979) which is just above the Taurid entry velocity of 29 km s^{-1}, with required fireball end-heights below 35 km and terminal speeds below 10 km s^{-1} (Brown *et al.,* 2012).

The precise mechanisms that determine the persistence of a meteoroid to <35 km and terminal speed to < 10 km s^{-1} are likely to be extremely complex. Larger meteoroids will certainly decelerate more slowly than small ones with consequentially greater dynamic loads at given altitude for the same entry velocity (Halliday *et al.,* 1989). However, recent modelling by Wallis (this study) suggests the survivability of highly porous meteoroids may not be particularly dependent on tensile strength. It is worth noting that the recently recovered Maribo meteorite that fell in Denmark on January 17, 2009 had an entry velocity of 28.5 km s^{-1} and has been linked to the Taurids (Haack *et al.*, 2012). When recovered, the weak 25g fragment appeared in tact but fell into many pieces when touched (Haack *et al.,* 2012). The fragment has now been classified as a CM2 carbonaceous chondrite, a group that exhibits the highest porosities of all meteorites at about 15-20% (Britt and Consolmagno 2003). This adds somewhat to the speculation that relatively high entry velocity, weak and friable material, may survive the extremes of atmospheric entry and fall as recoverable meteorites.

6.2 FALL HISTORY

Against this backdrop a potentially significant fireball event was reported during the last week of December 2012 in the skies above the Central Provinces of Sri Lanka. Several eyewitnesses in the North Central District of Polonnaruwa reported seeing a bright yellow fireball that turned green as it travelled across the sky at approximately 18:30 PM on December 29, 2012. The inferred NE to SW trajectory was determined from numerous eyewitness observations. The green fireball was reported to disintegrate with some luminescent fragments falling towards the ground in the village of Aralagonwila (7°46'0" N and 81°10'60" E) about 35 km south of the ancient town of Polonnaruwa.

A number of stones were immediately recovered from the ground in the vicinity of Aralagonwila. Police records detail reports of low-level burn injuries from immediate contact with the fallen stones and subsequent reports of a strong aroma of tar or asphalt. Local police officials responded immediately by collecting samples and submitting them to the Medical Research Institute of the Ministry of Health in Colombo, Sri Lanka. Further stones were recovered by local farmers in the adjoining fields the following day. These artefacts were all found lying on the surface of undisturbed sandy soil in well cultivated agricultural beds, consistent with the notion that they were fragments from the observed fireball. From now onwards we refer to these stones as the Polonnaruwa stones.

Further stones were recovered about one week later on the western banks of the Ratkinda and Mauru Oja reservoirs, approximately 35 km south-west of Aralagonwila. One witness reported

discovering a small cluster of unusual stones (<5g each) lying on the surface of a sandy area adjacent to his garden path approximately 10 m distance from his home.

On the same day an independent witness recovered three stone fragments from the surface of his rice field a few kilometres south-west in the town of Girandanakotte (7°24'14.4" N and 81°02'17.9" E). These three stones were larger, heavier and less porous and were again transported to the Medical Research Institute at the Ministry of Health in Colombo. From here on we refer to these stones as the Ratkinda stones and Girandanakotte stones respectively. The discovery of larger, denser fragments on the SW flight trajectory of the 29th December 2012 event makes pairing between the fragments most likely. We note parenthetically that at the time of the observed fireball event on December 29, 2012 through to the discovery of the Ratkinda and Girandanakotte stones on the 4th January 2013, the Taurid radiant was positioned above the horizon in the Sri Lankan sky (Figure 6.1).

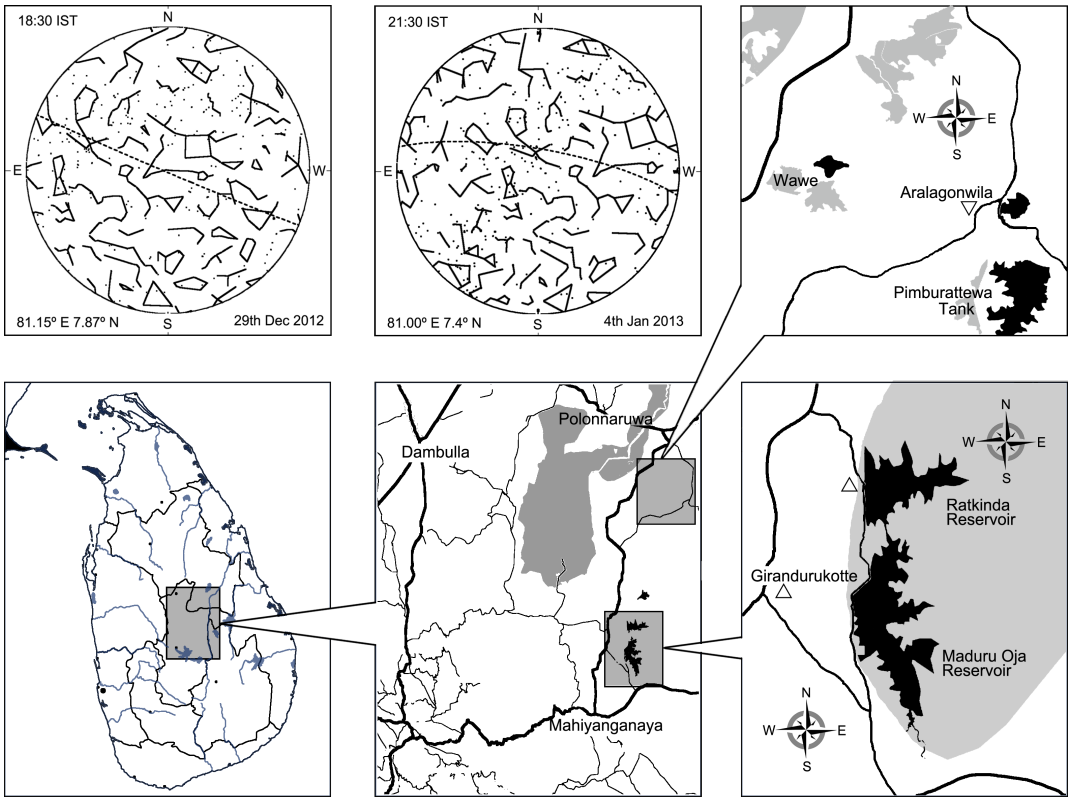

Figure 6.1 Upper panels show the position of the Taurid radiant in the sky above (left) Aralagonwila (7°46'0" N and 81°10'60" E) at 18:30 PM on the 29th December 2012 and (centre) Girandanakotte (7°24'14.4" N and 81°02'17.9" E) at 21:30 PM on the 4th January 2013. Upper right panel shows a map of the find site of the Polonnaruwa stones (▽) near the village of Aralagonwila. Lower right panel shows a map of the find sites of the Ratkinda and Girandanakotte stones (△).

Figure 6.2 (left) Dikiri Banda, eyewitness to the fall with (centre and right) meteorite showing fusion crust and contraction cracks found by Hoover in-situ in Banda's paddy field near Aralaganwila, North Central District, Sri Lanka. Photos*: Richard B. Hoover*

6.3 INITIAL EXAMINATION

Initial examination of the fragments at the Medical Research Institute in Colombo showed the Polonnaruwa stones to be dark grey or black in colour and poorly compacted (density < 1 g cm^{-3}). Optical microscopic examination revealed results that were discordant with mainstream theory on meteorites, and in particular the presence of a range of biological morphologies, some exhibiting apparent motility. A sample was then sent to Cardiff University, where studies of freshly cleaved interior surfaces using the Environmental Scanning Electron Microscope at the University's School of Earth and Ocean Sciences were conducted. These studies confirmed the presence of a range of fossilised diatoms and a separate sample was then sent to the United States, where it was investigated by Richard B. Hoover, using a Hitachi Field Emission Scanning Electron Microscope. Similar examinations by the Department of Geology, University of Peradeniya, Sri Lanka, resulted in swift dismissal of the fragments as possible meteorites. Based on XRD and optical microscope analysis together with the improbability that a meteorite would be recovered from a meteor shower, the fragments were determined to comprise of terrestrial fulgurite, the glassy product of tubes formed when quartzose sand, silica or soil is heated by lightning strikes.

Our observations however, were inconsistent with this assessment. In particular, representative oxide compositions for SiO_2 (73-76 wt%) were low compared to terrstrial fulgurites that showed values of between 90.2 wt% (Holland) to 99.0 wt% (Illinois) (Saikia *et al.*, 2008) while K_2O values (9-14 wt%) were too high compared to typical values for fulgurites of between 0.5-0.75 wt%. Theses high K-values were particularly difficult to reconcile with the fulgurite hypothesis and were more in keeping with K-Si-rich melts found in a variety of non-terrestrial glasses. In the shock veins

of L-chondrites (Goresey *et al.,* 1997) K-enrichment in shocked isotropic plagioclase results from the fractionation between K and Na. The Na is not completely lost from the melt veins but incorporated in liquid phase at high temperate/pressure in majorite-pyrope garnet crystals, (Chen, *et al*., 1996a and 1996b). A major part of the K is lost in vapour phase and subsequently scavenged by maskelynite melt pockets close to the melt veins resulting in K-enrichment.

In this section we report on the the physical, chemical and mineral properties of a number of stone samples recovered following the Polonnaruwa event. These results show that the 29th December 2012 fall represents the first well documented example of a meteorite carrying undeniably non-terrestrial biological morphologies that may provide substantial support for the *Hoyle-Wickramasinghe* Panspermia hypothesis.

6.4 HAND SAMPLES AND CHARACTERISTICS

For the purpose of this study, two stones from the original samples submitted by the Medical Research Institute in Colombo were selected for analysis. These comprised of a 1.591g fragment (designated P159/001) and a 1.661g fragment (designated P166/001) both of which had been collected on the evening of the 29th December 2012 in the village of Aralagonwila. Visual examination of the stones confirmed they were poorly compacted with density less than 1g cm^{-3} i.e. less than all known carbonaceous meteorites. The stones were predominantly black, though dark grey and grey regions could be visually observed along with evidence of a partial fusion crust.

Only a few fragments were recovered from the Ratkinda and Girandanakotte fall sites. In total, three fragments were submitted for analysis from the Ratkinda site comprising of 2.247g, 1.414g and 0.966g particles. All three fragments bore resemblance to the Polonnaruwa stones and exhibited low composite density with a vitreous outer fusion crust. However, these fragments were entirely black in colour, with no visible signs of either light or dark grey regions. From these samples, the 2.247g stone was selected for analysis and was designated as sample M224/001. Two further large stones were examined from three fragments recovered from the Girandanakotte fall site. One much larger, denser stone of 572.162g plus one smaller stone of 44.127g were considered for further study. Neither of these stones bore particular visual resemblance to the Polonnaruwa stones or the stones recovered from the Ratkinda fall site. Consequently, these stones were excluded from this report. In addition to the selected fragments, a sample of sand fulgurite was also analysed for comparative purposes together with a soil sample recovered from the Aralaganwila fall site and a further sample of calcium-rich terrestrial rock selected from the Ratkinda fall site for control purposes. Preliminary oxygen and carbon isotope analysis of the calcium rich control sample produced values of $\delta^{13}C$ = -

9.716 ± 0.02 and $\delta^{18}O$ = -6.488 ± 0.04 which accord well with the values for soil carbonates determined by T.E. Cerling and J. Quade, (1993). All selected fragments were initially portioned and prepared at Cardiff University's School of Earth and Ocean Sciences and subsequently studied using a variety of optical and electron microscopic, chemical and mineralogical techniques to both classify and better understand their origins.

6.5 EXPERIMENTAL SAMPLES AND ANALYTICAL METHODS

A variety of analytical methods were used to examine multiple samples of the Polonnarawa, and Ratkinda stones (Table 4.1). 30µm sections were studied using optical, scanning electron microscopy (SEM) and Raman spectroscopy. These included a 30µm polished section of specimen P166/001-01 prepared at the Paleontological Institute, Moscow in Russia using sequential resin boiling and polishing techniques together with a corresponding 30µm polished section prepared from the same sample at the School of Earth and Ocean Sciences at Cardiff University. One further polished 30µm section from specimen M224/001 was also prepared at Cardiff University.

Optical microscopy was conducted using an RM-1POL polarising light microscope with 360º rotating analyser. Image capture was via a 9M pixel digital trinocular camera unit processed by View7 PC software for output to hard drive. Scanning Electron Microscopy (SEM) was conducted using the FEI (Phillips) XL30 FEG ESEM (Environmental Scanning Electron Microscope) FEG (Field Emission Gun) at the School of Earth and Ocean Sciences at Cardiff University. The unit incorporates a secondary electron detector (SE), a back scatter electron detector (BSE) and a gaseous secondary electron detector (GSE). It also has an Oxford Instruments INCA ENERGY (EDX) x-ray analysis system. Image recording is via a SONY video graphics printer or digital by processing image frames in a 16 bit framestore computer for output to hard drive.

Confocal high resolution Raman spectra were acquired using a Renishaw inVia microRaman system at the School of Chemistry, Cardiff University, UK. The unit was fitted with a research grade Leica analytical microscope (4x, 10x, 20x and 40x objectives) and a 514.5 nm Ar laser line. Data processing was via the Wire2 software application for data output to hard drive. Spectroscopy was performed on both polished and unpolished 30µm thin section samples at room temperature with spectra collected through the 40x objective.

Three further bulk samples were prepared for interior section scanning, two derived from sample P166/001, one from sample M224/001. Sample preparation involved the use of a flame sterilised wide-bore hypodermic needle to fracture the fragments before mounting on aluminium stubs. The

FEI (Phillips) XL30 FEG ESEM was also used for electron petrography (BSE Imaging). Elemental abundances were determined using the Analytical Scanning Electron Microscope (A-SEM) at the School of Earth and Ocean Sciences at Cardiff University. The A-SEM comprises of an LEO (Cambridge) S360 Electron Microscope, an Oxford Instruments INCA ENERGY X-Ray analyser and an Oxford Instruments INCA WAVE X-Ray analyser. Calibration was via standards which included SiO_2 for O-K, Al_2O_3 for Al-K, MgO for Mg-K, SiO_2 for Si-K, GaP for P-K, Orthoclase for K-K, AgCl for Cl-K and Wollastonite for Ca-K. For the other elements (Na, P, Ti, and Mn) K factors were estimated using standard calibration curves.

Five additional samples, derived from two different bulk sample aliquots (A, B) were analysed using Inductively Coupled Plasma Optical Emission Spectrometry (ICP-OES), Fourier Transform Spectroscopy (FTIR), Triple Oxygen Isotope analysis and X-Ray Diffraction (XRD).

Table 6.1 – Experimental Samples

Sample	Mass (mg)	Source [a]	Description [b]
Experimental Samples			
P159/001-01	448	AR	~ 8 mm interior fragment for SEM studies at SES-CU
P159/001-02	177	AR	~ 5 mm interior fragment for SEM studies at NASA- MSFC
P159/001-03	512	AR	Silica-rich powder from aliquot A[c] used for XRD at SES-CU
P159/001-04	998	AR	Si-rich powder from aliquot A[c] used for O_2 Isotope Analysis at UG
P159/001-05	2048	AR	Si-rich powder from aliquot A[c] used for ICP-OES, FTIR and CHN
P166/001-01	-	AR	~ 1.2cm wide, polished thin section prepared for petrography at PI
P166/001-02	-	AR	~ 9 mm wide, polished thin section for petrography at SES-CU
M224/001-01	168	RK	~ 4 mm interior fragment for SEM studies at SES-CU
M224/001-02	509	RK	Si-rich powder from aliquot B[d] used for XRD Analysis at SES-CU
M224/001-03	1978	RK	Si-rich powder from aliquot B[d] used for ICP-OES, FTIR and CHN
M224/001-04	-	RK	~ 9 mm wide, polished thin section for petrography at SES-CU
Control and Comparative Samples			
D159/001-01	3072	RK	Soil Carbonate from Dambulla , Sri Lanka
F159/001-02	1667	-	Fulgurite from the Sarhara Desert
S159/001-05	3074	AR	Soil Sample from Araganwila, Sri Lanka

[a] Source Code: AR – Aralaganwila (7°46'0"N, 81°10'60" E); RK – Ratkinda (7°24'14.4" N, 81°02'17.9" E) ; Samples supplied by Anil Samaranayake and K. Wickramarathne of the Medical Research Institute of the Ministry of Health in Colombo, Sri Lanka.

[b] Description Code: SES-CU – School of Earth and Ocean Science, Cardiff University; NASA- MSFC NASA Marshall Space Flight Centre; PI – Paleontological Institute, Moscow, Russia; UG – Stable Isotope Laboratory, University of Göttingen, Germany.

[c] Aliquot A – Three interior fragments and dust weighing 2.41g taken from sample P159/001.

[d] Aliquot B – Dust from interior weighing a combined 1.91g taken from sample M224/001.

Triple oxygen isotope analysis was conducted at the stable isotope laboratory at the University of Göttingen, Germany. Approximately 2mg of crushed sample was placed inside a Ni sample holder, evacuated overnight and heated to 70°C. An infrared (IR) laser (50W CO_2 laser, λ = 10.6µm) was used to fluorinate the samples in purified F_2 gas under pressures of approximately 20 mbar and sample O_2 was purified through the removal of excess F_2 by reaction with NaCl at 110°C to form NaF. Cl_2 gas was collected at a cold trap at -196°C.

Sample oxygen was then collected at a 5Å molecular sieve at -196°C, expanded into a stainless steel capillary, transported with He carrier gas and re-trapped before release at 92°C through a 5Å molecular sieve GC-column of a Thermo Scientific GasBench II. The GC column was utilised to separate interfering NF_3, from O_2, as required for analysis of ^{17}O (Pack *et al.*, 2008). The resulting purified sample O_2 was then expanded to the dual inlet system of a Thermo MAT 253 gas mass spectrometer. Results are presented in δ- and $\Delta^{17}O$-notation. Data are reported relative to SMOW. Error bars are about ± 0.1 ‰ for $\delta^{17}O$ and $\delta^{18}O$ and about ± 0.01 ‰ or better for $\Delta^{17}O$. The reference gas was analysed relative to SMOW calibrated O_2 by E. Barkan (Hebrew University of Jerusalem). All δ values are permil unless otherwise stated.

X-Ray Diffraction was carried out using a Philips PW1710 Automated Powder Diffractometer using Cu Kα radiation at 35kV and 40mA, between 2 and 70 $^o2\theta$ at a scan speed of 0.04^o 2θ/s. From the scans, phases were identified using PC-Identity software and from the peak areas, semi-quantitative analysis was performed and the percentage of each phase calculated. Each of the four samples provided for analysis were powdered, mixed with a small amount of acetone and pipetted out onto glass slides. Detailed phase analysis was performed using Crystal Impact's 'Phase Identification from Powder Diffraction' software module version 2. Sample preparation and analysis was conducted at the School of Earth and Ocean Sciences at Cardiff University.

Whole rock chemical analysis of aliquots of a ground, homogenised powder of the sample fragments were carried out using a Perkin Elmer Dual-View Optima 5300 Inductively Coupled Plasma Optical Emission Spectrometer. Calibration was based on the analysis of reference rock powders USGS DTS-1 (dunite), USGS BCR-2 (basalt) and ANRT BR (basalt). 50 mg aliquots of the samples and standards were dissolved in an Anton Paar Multiwave 3000 microwave digestion unit in high-pressure, high temperature PTFE ('teflon') vessels (210°C, 8 bar). The procedure was adapted from Mareels (2004). Samples were first dissolved in mixtures of concentrated high-purity acids HF, HNO_3 and HCL. The bulk composition of the stones has been derived from an average or combination of the results of two separate sample runs. The procedure utilised does not allow the

content of Boron to be determined, because the element is added when the mixture is neutralised by the addition of Boric Acid.

InfraRed spectroscopy was conducted using a Perkin-Elmer Spectrum 65 spectrometer equipped with Perkin-Elmer's Universal Attenuated Total Reflectance (ATR) sampling module incorporating a diamond crystal. Samples were prepared by crushing the aliquot contents into a fine powder using a mortar and pestle in order to achieve good contact with the diamond surface. Verification of apparatus calibration was achieved by performing four background scans and four sample scans. Data output was via Perkin-Elmer's Spectrum 10 software module with spectrum analysis performed using the RRUFF analytical software application incorporating the Caltech Raman database and RRUFF Project database of minerals.

CHN analysis was conducted by total combustion using a CE440 Elemental Analyser. Samples were weighed into disposable tin capsules and injected into a high temperature furnace combusted in pure oxygen under static conditions. Resulting combustion products were then passed through specialised reagents to produce CO_2, H_2O and N_2 and N oxides that were then passed over pure copper wire to remove excess oxygen and to reduce oxides of nitrogen to elemental N. Resultant gases were then passed into a mixing chamber to ensure a homogeneous mixture at constant temperature and pressure before passing through a series of high-precision thermal conductivity detectors, where the differential signal between the cells provides C, H and N readings against a helium reference.

6.6 PETROLOGY AND MINEROLOGY

In thin section, the Polonnaruwa and Ratkinda stones exhibit highly porous (Figure 6.3) textures comprising of amorphous silica-rich hosts enclosing trace (commonly <1µm) subangular to subrounded polymineralic grains (Figure 6.3d). The chemical composition of the host matrix varies between samples, but both were rich in SiO_2.

One feature of particular note is that both the host matrix and enclosed melt pockets display a heterogeneous enrichment in potassium and aluminium. This was noted in both P166/001-02 (SiO_2 = 75-80 wt%, K_2O = 9-11 wt%) and sample M224/001-04 (SiO_2 = 70-75 wt%, K_2O = 9-11 wt%). K-rich glasses of similar composition have been reported in a variety of non-terrestrial material ranging from rare iron meteroites (e.g. Mittlefehldt *et al.,* 1998; Ruzicka *et al.,* 2006) to LL chondritic breccias (Bischoff *et al*., 1993; King *et al.,* 2005; Sokol *et al.,* 2007) and Lunar granites collected during the Apollo missions (Papike *et al.,* 1998). The Lunar granites in particular were

characterised by high SiO_2 (60 to 74 wt%) and K_2O (2 to 10.4 wt%), and low Na_2O (0.4 to 1.9 wt%) (Papike *et al*.,1998).

Similar compositional values were reported by Leroux and Cordier (2006) in silica-rich melt pockets occurring as patches between maskelynite laths or between pyroxene and maskelynite in the Martian meteorite NWA 856. The bulk chemical composition of the pockets differed from one another (SiO_2 = 75-80, Al_2O_3 = 11-15, CaO = 0.5-1.5, Na_2O = 2-5, K_2O = 1-5, FeO = 0.2-1, TiO_2 = 0.2-0.8) but along with Lunar granites accord reasonably well with equivalent compositional values observed in P166/001 and M224/001.

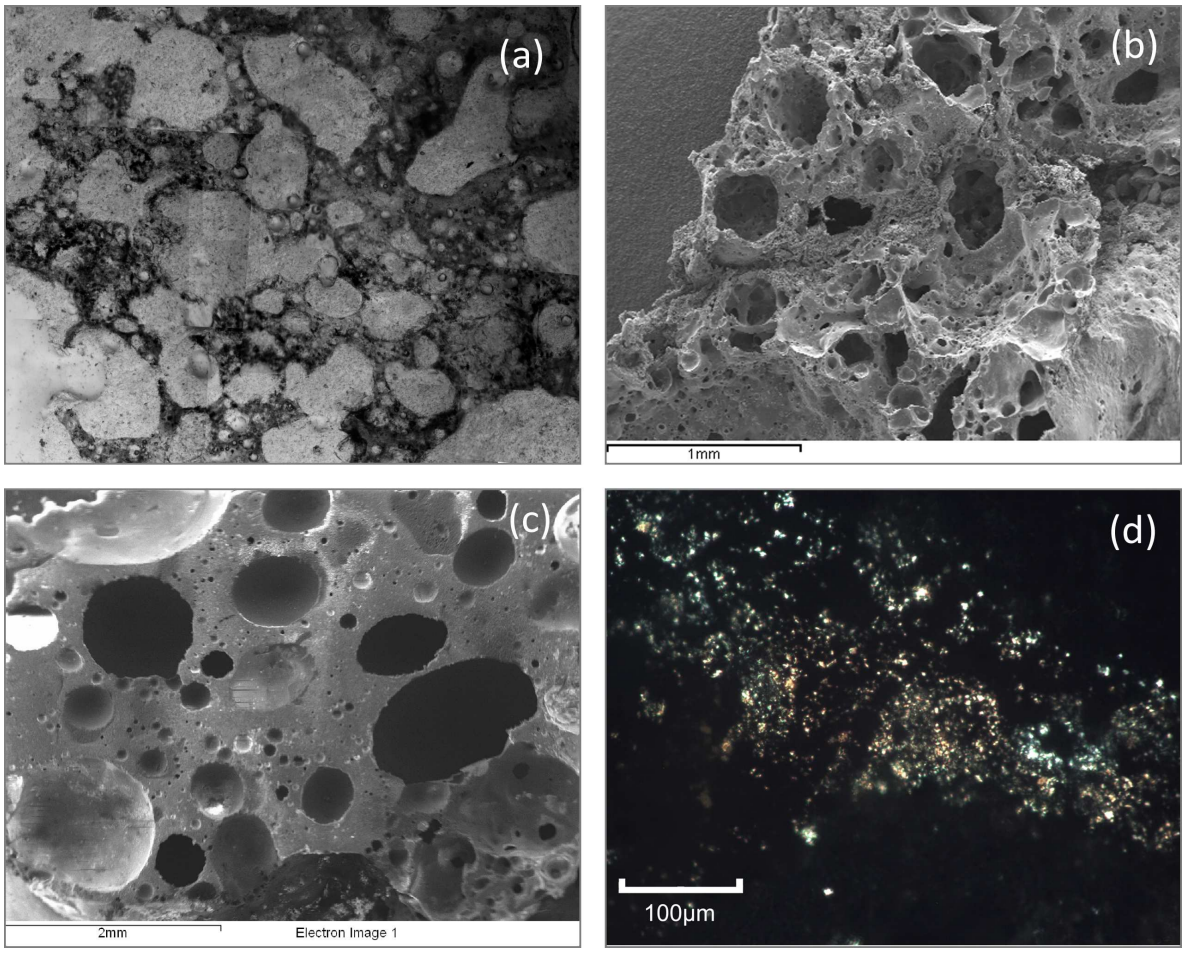

Figure 6.3 shows the highly porous nature of P166/100 and M224/100. (a) Thin section montage of P166/100 in plane polarised light. Voids show up in light grey (resin pores) with K-rich glass in dark grey/black. (b) SEM (GSE) of P166/001 showing extensive voids. (c) SEM (BSE) of M224/001 (flattened) and (d) Thin section montage of P166/100 in plane polarised light (crossed nicols), prepared at the School of Earth and Ocean Sciences at Cardiff University.

Within the matrix, silica-rich melt pockets exhibited poorly-defined interfaces with the adjacent phase and a general absence of cleavage, intergranular cracks or shock induced fractures.

It is noted that in the shock veins of L-chondrites (Goresey *et al*., 1997) K-enrichment in shocked isotropic plagioclase results from the fractionation between K and Na. The Na is not completely lost from the melt veins but incorporated in liquid phase at high temperate/pressure in majorite-pyrope garnet crystals (Chen, *et al.*, 1996a and 1996b). A major part of the K is lost in vapour phase and subsequently scavenged by maskelynite melt pockets close to the melt veins resulting in K-enrichment.

In the Peace River L-chondrite, elemental X-ray maps of shock veins show the presence of K-rich phases in the shock induced fractures of pyroxene and olivine crystals that are in contact with both the veins and the maskelynite. Table 4.2 displays representative SEM-EDAX compositions (wt%) for the Si-K-rich glass host matrix of P166/001 together with comparative compositions (wt%) for NEA003-A (Haloda *et al.*, 2009), NWA 856 (Leroux and Cordier, 2006) and Miles IIE (Ruzicka and Hutson, 2010).

Quartz was detected in P166/100 but was not found in sample M224/001. In P166/100 it is characterised by a number of euhedral and subhedral grains (1-10 µm, commonly <1 µm) with elongate to equant shapes. The presence of quartz in meteorites has been reported in silica rich pockets of order ~100 µm in the Martian meteorite NWA 856 (Leroux and Cordier, 2006). Here, quartz grains of size ~5 µm together with similar sized grains of the high temperature polymorph cristobalite were evident in polarised light observations under an optical microscope.

A possible example of shock was observed in the formation of the high temperature SiO_2 polymorph cristobalite within quartz crystals. Even at relatively small sample areas, Raman spectra displayed consistent evidence of contributions from both quartz and cristobalite. Figure 6.4 shows the Raman spectra of one such example found. Here the spectrum was acquired through a 40x objective with a beam size occupying approximately 25% of the crystal's surface area. Library spectra for quartz and cristobalite are also shown for comparison, but primary and secondary spectral features in the 100 cm^{-1} to 500 cm^{-1} region can be clearly seen to contribute to the observed pattern.

At this stage, it remains uncertain if these inclusions represent evidence of formation by hydrothermal alternation or alternatively, direct evidence for silica enrichment by other processes, though the presence of silica grains in both samples tentatively suggest the former.

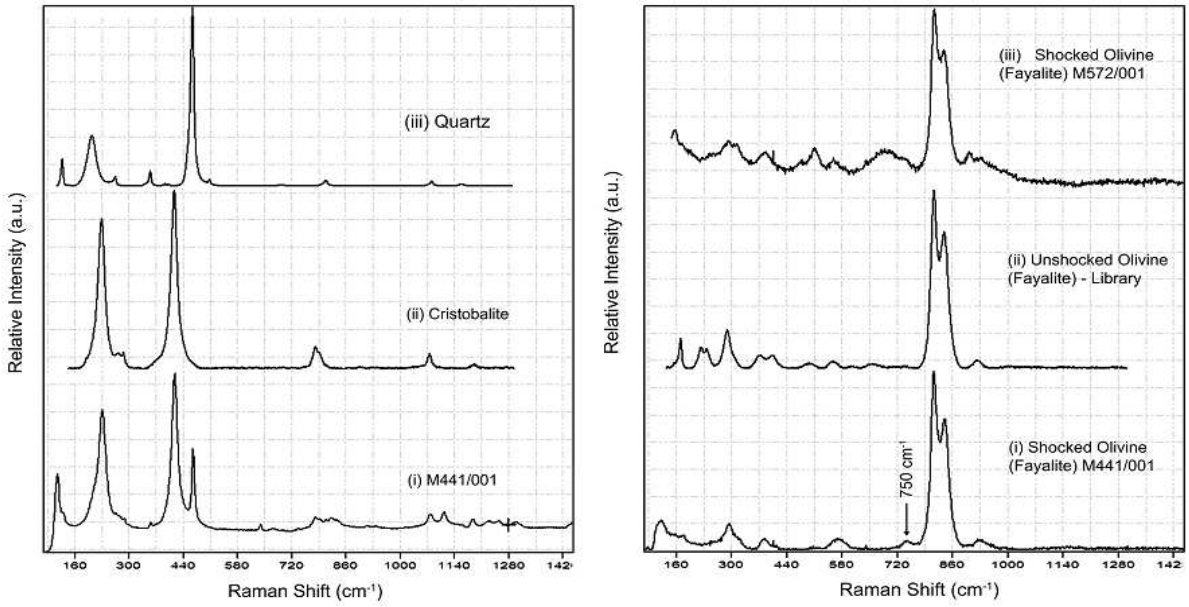

Figure 6.4 (left panel) shows the high resolution Raman spectra (i) of a typical quartz inclusion acquired through a 40x objective with a beam size occupying approximately 25% of the mineral's surface area. Library patterns for pure quartz and cristobalite are shown in spectra (iii) and (ii) respectively. Note the contribution to spectra (i) of both primary and secondary features in the 100 cm^{-1} to 500 cm^{-1} region in spectra (iii) and (ii) that can be seen to contribute to the observed pattern. All spectra were acquired at the School of Chemistry, Cardiff University, UK using the Renishaw inVia microRaman system.

Table 6.2 provides representative oxide compositions for melt inclusions within the amorphous matrix of sample P166/001. For comparison, comparable values for Si-K-rich melt inclusions in Miles IIE (Ruzicka and Hutson, 2010), Northwest Africa 856 (Leroux and Cordier, 2006) and Northeast Africa 003-A (Haloda *et al.*, 2009) are also provided. Equivalent maskelynite compositions for Dar al Gani 476 (Chen, 1999), Dar al Gani 355 (Chen, 1999) and Northwest Africa 856 (Leroux and Cordier, 2006) are provided to illustrate typical maskelynite compositions.

The far-infrared spectral characteristics of amorphous plagioclase provide useful information about the nature of a given sample and its relative position between crystalline and amorphous state. For example, the absorption spectra in the region 580 cm^{-1} to 380 cm^{-1} that is dominated by the Si-O-Si or Si-O-Al absorption band (Cohen and Roy, 1965) and controlled by the ordering between Si and O or Al and O causes an observable shift in the peak present at 380 cm^{-1} in crystalline plagioclase towards 480 cm^{-1} in fully fused maskelynite (Bunch and Cohen, 1967). Figure 6.5 shows the FTIR spectral characteristics of samples of the Polonnaruwa and Ratkinda stones that were analysed with reference to the 380cm^{-1} to 1250 cm^{-1} region. The FTIR spectra reveal a number of absorption bands

Table 6.2
Representative compositions of melt inclusions and comparative shocked isotropic plagioclase (Maskelynite)

	P166/001: Si-K-rich glass inclusions			NEA003-A, NWA 856, Miles: Si-K-rich glass			NWA 856, DAG 355, DAG 476: Maskelynite		
	S1	S2	S3	S4	S5	S6	S7	S8	S9
SiO_2	76.56	74.70	73.16	63.9	75.8	76.10	52.16	66.55	55.2
Al_2O_3	10.37	15.00	12.75	18.1	14.3	12.80	29.45	22.35	29.8
Na_2O	0.72	0.17	nd	1.12	2.2	0.67	3.98	8.14	2.0
MgO	0.26	0.24	0.05	0.02	nd	0.32	0.17	0.08	nd
K_2O	9.11	9.00	9.27	14.8	5.5	8.67	0.08	1.64	0.4
CaO	1.01	0.28	0.06	0.02	0.5	0.45	13.42	1.69	12.2
FeO	4.43	0.00	0.00	0.96	1.1	0.62	0.60	0.42	0.5
TiO_2	0.77	0.00	0.00	0.08	0.8	0.56	nd	nd	nd
MnO	nd	0.00	0.00	<0.01	nd	0.04	nd	nd	nd
Total	103.22	99.40	95.29	99.01	100.2	100.23	99.87	100.87	94.11
Number of cations (oxygens) = 8									
Si	3.268	3.271	3.343	-	3.57	-	2.38	2.90	2.94
Al	0.575	0.780	0.692	-	0.40	-	1.58	1.14	0.93
Na	0.065	0.015	-	-	0.10	-	0.35	0.69	0.10
Mg	0.018	0.016	0.003	-	-	-	0.01	0.00	-
K	0.545	0.502	0.541	-	0.17	-	0.00	0.09	0.01
Ca	0.051	0.013	0.003	-	0.03	-	0.66	0.08	0.70
Fe	0.173	-	-	-	0.05	-	0.04	0.01	0.02
Ti	0.027	-	-	-	0.02	-	-	-	-
Mn	-	-	-	-	-	-	-	-	-
Tot	4.722	4.597	4.582	-	4.34	-	5.02	4.91	5.092

Nd - not detected. S1 – P166/001; S2, S3 – M224/001; S4 – Miles IIE, (Ruzicka and Hutson, 2010); S5 – Northwest Africa 856 (Leroux and Cordier, 2006); S6 – Northeast Africa 003-A (Haloda *et al.,* 2009); S7 – Dar al Gani 476 (Chen, 1999); S8 - Dar al Gani 355 (Chen, 1999); S9 - Northwest Africa 856 (Leroux and Cordier, 2006).

in the 380-480 cm^{-1} region, with clear movement of the 380 cm^{-1} feature to 416 cm^{-1} in sample P166/001-05 and a corresponding shift of the feature to 443 cm^{-1} in sample M224/001-03. The Si-O-Si bending vibration region of quartz (400-700 cm^{-1}) includes a band at 695 cm^{-1} that is unique to the crystalline phase (Parthasarathy *et al.*,2001).

The 695 cm^{-1} band was detected in sample P166/100 showing the presence of crystalline quartz but was not detected in M224/001-03. The absence of the 695 cm^{-1} feature in M224/001-02 suggests that in this sample the silica was entirely in amorphous form.

The absorption band at 695 cm^{-1} is due to vibrations in the octahedral site symmetry while a corresponding band at 780 cm^{-1} is due to vibrations in the tetrahedral site symmetry (Schneider, 1974; Parthasarathy *et al.*, 2001, Saika *et al.*, 2007). The octahedral site symmetry is weaker than the tetrahedral site symmetry resulting in structural damage being observed in the 695 cm^{-1} region first. A band corresponding to the 780 cm^{-1} feature was present in P159/001-05 (776 cm^{-1}) but was not present in M224/001-03 indicating that in this sample shock/thermal deformation was more severe.

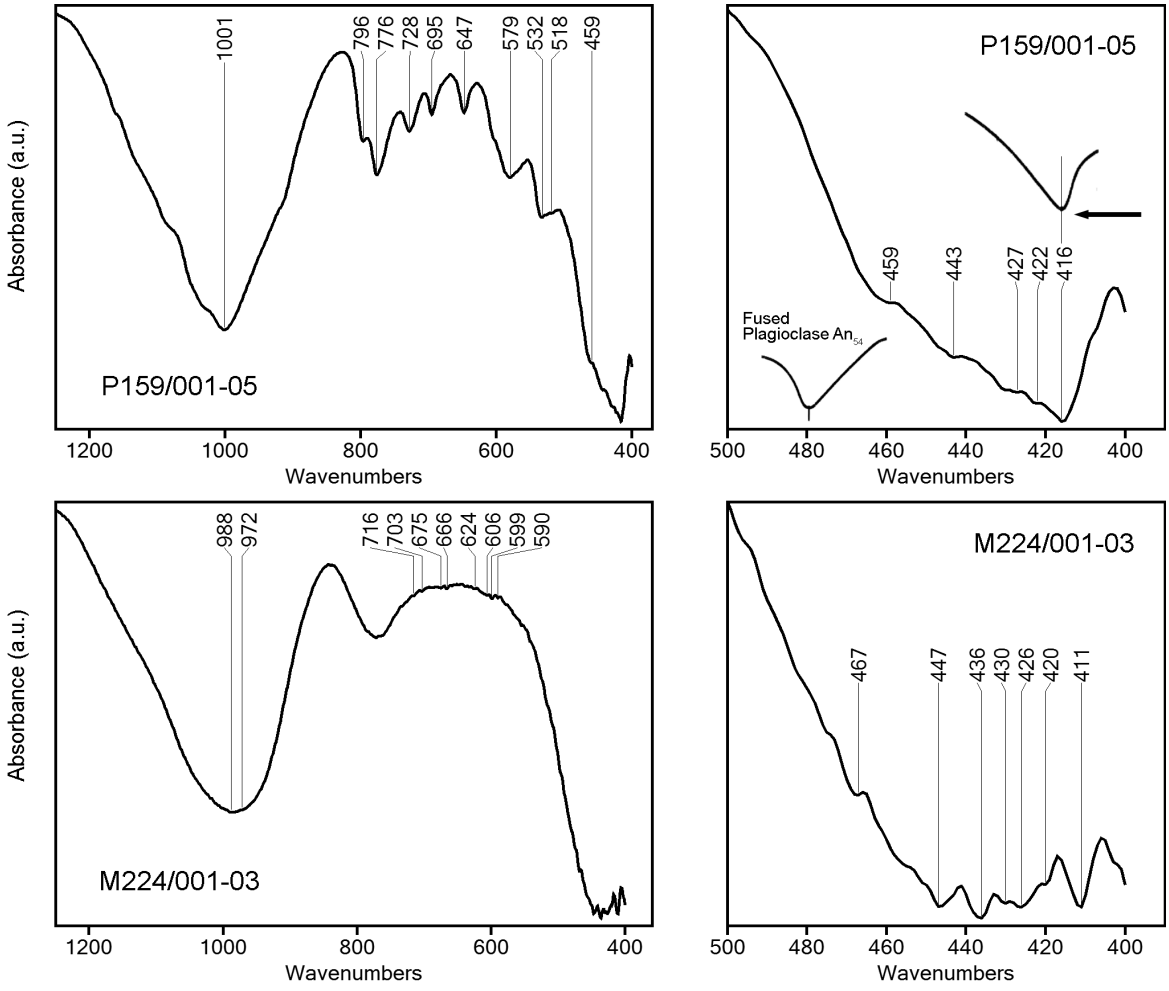

Figure 6.5 Shows FTIR spectra for samples P159/001-05 and M224/001-03. The degradation of spectral features in the 480 cm^{-1} to 580 cm^{-1} region can be seen in M224/001-03. The band at 459 cm^{-1} corresponds to the Si-O asymmetrical band of vibration. Note the absence of a band at 780 cm^{-1} due to vibrations in tetrahedral site symmetry (Schneider, 1974; Parthasarathy *et al.*, 2001, Saika *et al.*, 2007).

6.7 BOUND H_2O

The H_2O content of glass in usually determined by FTIR analysis. Water in silica glass is detected in two main IR bands in the spectrum at 3660 cm^{-1} and 1610 cm^{-1}. These reflect the OH stretching vibration and H-O-H bending vibration modes rather than discrete H_2O molecules (Gilchrist *et al.*, 1969). FTIR analysis of the Polonnaruwa stones failed to detect features at either 3660 cm^{-1} or 1610 cm^{-1}, indicating a very low bound H_2O component. Detection limits for the apparatus and procedure are quoted at ~0.05 wt%. However, these lower detection limits can be affected by the nature of a sample as well as sample preparation technique.

To test this parameter, a sample of North American tektite with < 0.03 wt% H_2O was also examined. This sample showed evidence of bound H_2O by way of a faint feature at 3660 cm^{-1} (see figure 6.6). Consequently, we take the H_2O content of the Polonnaruwa stones to be < 0.03 wt%. It was noted that the closest terrestrial volcanic glass comparable to the Polonnaruwa stones in appearance and chemistry would be the obsidians, but the significant variation in CaO (0.6 wt% in obsidians compared to ~5.3 wt% in Pol), MgO (0.03 wt% in obsidians compared to ~4.5 wt% in Pol) and MnO (<0.1 wt % in obsidians compared to ~1.25 wt% in Pol) would indicate a parent material different to an igneous rock.

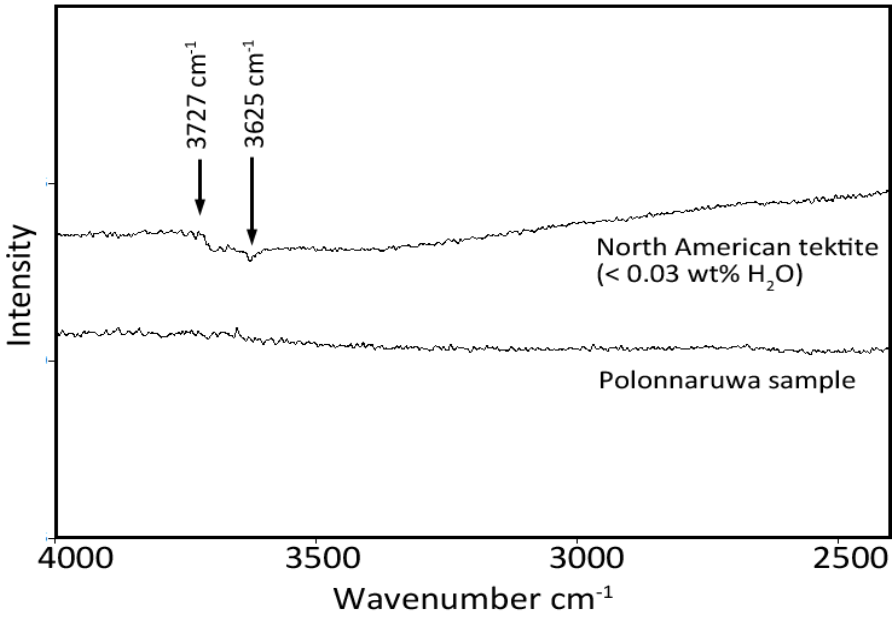

Figure 6.6 Shows FTIR spectra from 2500 to 4000 cm^{-1}. Note the instrument detection of faint feature at ~3660 cm^{-1} reflecting the presence of the OH stretching vibration and H-O-H bending vibration modes in a sample of < 0.03 wt% H_2O.

Furthermore, glasses of volcanic origin in general are much wetter than impactites with the H_2O content of magmatic melts ranging from 6.2 wt% from the 1974 Fuego eruption to ~0.2 wt% in Low-K_2O glass inclusions from the 3 Ka medicine Lake Claifornia eruption (Sisson and Lane, 1993). These values accord well with with volcanic glasses in general (0.6-5.0 wt% H_2O) (Di Muro *et al.,* 2006).

The first precise measurements on the content of bound H_2O in impactites was reported by Gilchrist *et al.,* (1969) using infrared spectroscopy. This study indicated a H_2O content of ~0.01 wt%. A more accurate study was undertaken by Beran and Koeberl (1997) where 51 impact glasses comprising of 26 tektites (from all four known strew fields) and 25 impact glasses (8 Libyian desert glasses, 2 from the Aouelloul crater, 2 from Rio Cuarto crater and 7 from the Zhamanshin crate) were analysed for bound H_2O. Results showed that impactities are extremely dry with structurally bound H_2O abundances ranging from 0.002-0.030 wt% (average 0.014 ± 0.008 wt%) for tektites and 0.008-0.166 wt% for impact glasses.

Beran and Koeberl (1996) concluded that impactities are very dry (< 0.03 wt % H_2O) and much dryer than glasses of volcanic origin and that H_2O contents < 0.05 wt% can be used as very good evidence for origin by impact when considering glasses of unknown origin. In line with the findings of Beran and Koeberl (1996) we conclude that the Polonnaruwa stones originate from hypervelocity impact and are inconsistent with glasses of volcanic terrestrial origin.

6.8 BULK COMPOSITION

6.8.1 Crystalline Phases

The presence of crystalline phases was determined using X-Ray Diffraction techniques carried out on a Philips PW1710 Automated Powder Diffractometer on two different aliquot samples of the Polonnaruwa and Ratkinda stones. Results are displayed in Figures 6.7 and 6.8. The broad hump displayed in P159/001-03 and M224/001-02 at ~18-38^o 2θ corresponds to a bulk composition of amorphous phases comprising of between 75-95% by volume. In the case of M224/001-02 no crystalline phases were identifiable with any degree of confidence.

In the case of P159/001-03 the presence of crystalline quartz was confirmed, with strong features at 20.83^o 2θ, 26.71^o 2θ and 60.06^o 2θ together with numerous lesser features. A strong feature at ~21.8 2θ together with weaker coincident features in the 24.3-35.8^o 2θ range was identified as

(NaK)$AlSi_3O_8$ (anorthoclase) (Harlow, 1982). Further peaks at 13.81° 2θ and in the 21.85-35.72° 2θ range were reported as due to the presence of $NaAlSi_3O_8$ (albite) (Gualtieri, 2000). A further strong peak at 27.82° 2θ together with lesser peaks in the 20.83-35.72° 2θ range was consistent with the presence of $CaAl_2Si_2O_8$ anorthite (Matsui and Kimata, 1997). The presence of both cristobalite and stishovite was tentatively confirmed from the residual peaks of the XRD pattern.

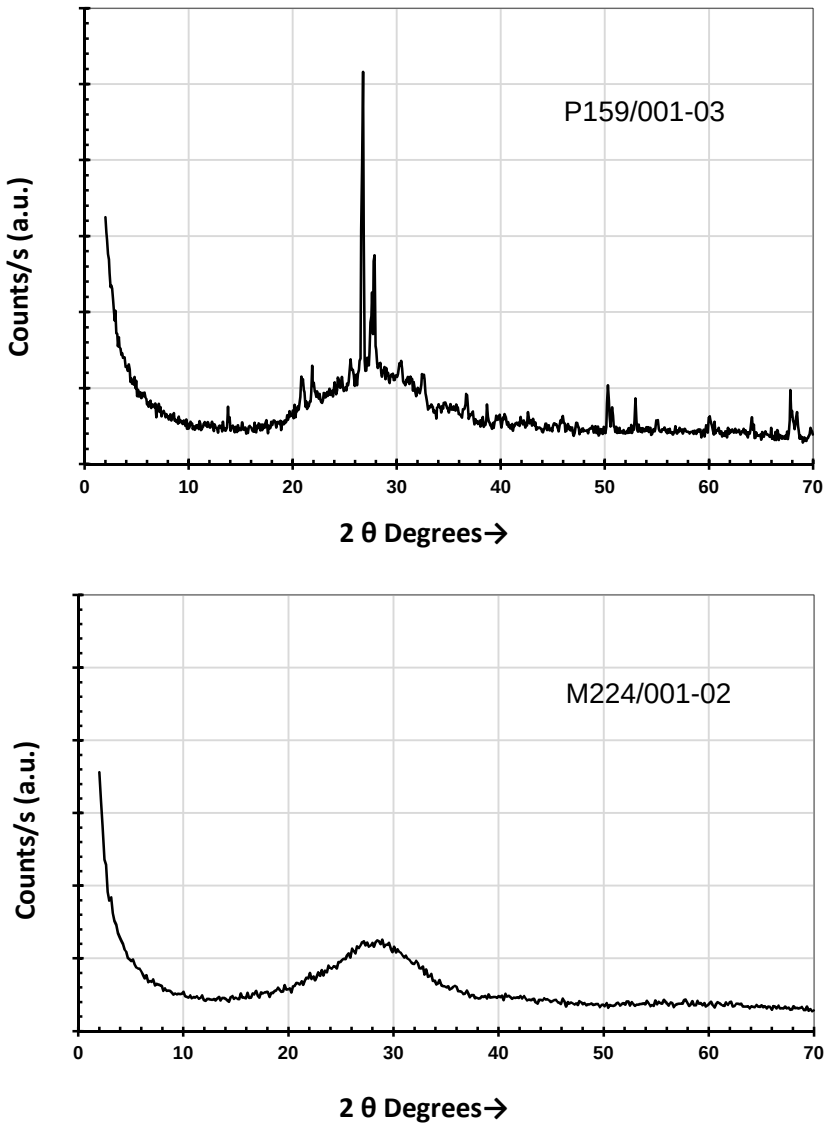

Figure 6.7: X-Ray Diffraction results (counts/s against 2θ degrees). Panels show diffractograms of aliquot samples P159/001-03 (upper) and M224/001-02 (lower), using Cu Kα radiation at 35kV and 40mA, between 2 and 70 °2θ at a scan speed of 0.04° 2θ/s. Analysis software reports the presence of: (i) $Al1._{911}Ca0._{716}Mn0._{196}Na0._{045}O_8Si2._{089}$ - Anorthite (Matsui and Kimata, 1997), (ii) $AlK0._{333}Na0._{667}O_8Si_3$ - Anorthoclase (Harlow, 1982), (iii) SiO_2 - Quartz Lo (Machatschki and Kristallstruktur von Tiefquarz, 1936), (iv) $Al1._{02}Ca0._{02}Na0._{98}O_8Si2._{98}$ - Albite (Gualtieri, 2000), (v) SiO_2 – Cristobalite (Peacor, 1973), (vi) SiO_2 – Stishovite (Yamanaka, Fukuda and Tsuchiya, 2002). The broad humps displayed in samples P159/001-03, M224/001-02 are due to bulk composition of amorphous phases of (between 75-100%).

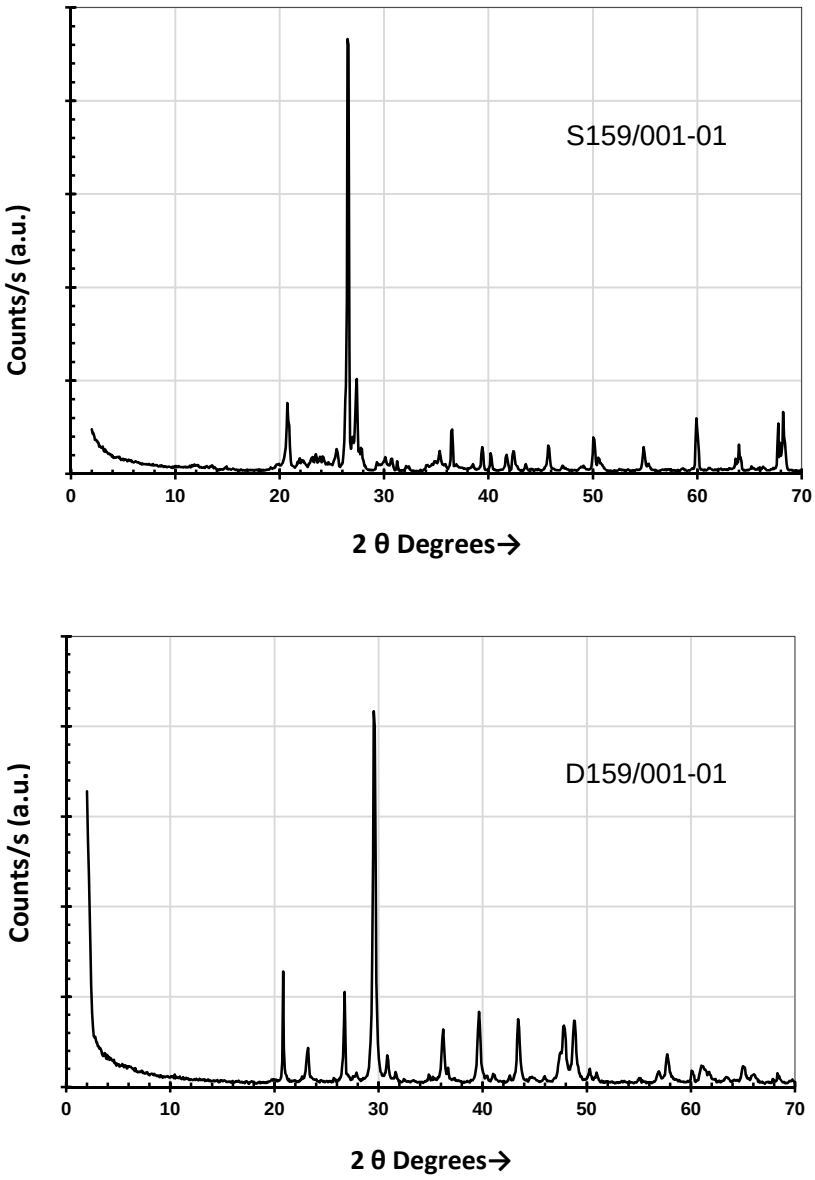

Figure 6.8: X-Ray Diffraction results (counts/s against 2θ degrees). Panels show diffractograms of aliquot samples S159/001-01 (soil sample) (upper) and D159/001-0 (control) (lower) using Cu Kα radiation at 35kV and 40mA, between 2 and 70 $^{o}2\theta$ at a scan speed of 0.04^{o} 2θ/s. Analysis software reports in S159/001-05 (soil) the expected presence of approximately 75% quartz, 17% $KAlSi_3O_8$ (microcline), 4% $(NaK)AlSi_3O_8$, 3% $Al_2Si_2O_5(OH)_4$ (kaolinite) and 1% opal. Results reported for the control sample D159/001-01 were consisted with the available literature on soil carbonates comprising of 81% calcite, 13% quartz, 4% ankerite and 2% anorthite.

S159/001-05 (soil) reported the expected presence of approximately 75% quartz, 17% $KAlSi_3O_8$ (microcline), 4% $(NaK)AlSi_3O_8$, 3% $Al_2Si_2O_5(OH)_4$ (kaolinite) and 1% opal. Results reported for the control sample D159/001-01 were consisted with the available literature on soil carbonates comprising of 81% calcite, 13% quartz, 4% ankerite and 2% anorthite.

In summary (and taken in isolation) XRD data implies that P159/001 comprises of approximately 80-90% amorphous glass with trace (<5%) quartz, anorthoclase, albite and hematite with the lesser but possible inclusion of cristobalite and stishovite. M224/001 comprises almost entirely of amorphous glass.

6.8.2 Bulk Chemistry

Two different samples of the Polonnaruwa and Ratkinda stones were analysed for bulk major element abundances using inductively coupled plasma optical emission spectrometry (ICP-OES). These included portions of aliquot samples A, B, taken from P159/001 and M224/001 respectively. Representative oxide compositions are given in Table 6.3.

Both the major and trace element data for the samples display some degree of spatial variation in composition, primarily in those elements that concentrate in metal. This certainly reflects an inhomogeneous distribution of these phases, and the data above represents the average of multiple ICP-OES sample runs. Nonetheless, the somewhat heterogeneous nature of the samples justifies a wider sampling process in future studies. In general, however, the samples were characterized by high K compositions. In contrast, Fe content was low and comparable to high and low potassium felsic glasses. Samples also displayed a marked depletion in Ti.

Five of the six classes of glass examined were determined to have an impact origin as determined by the presence of metal with meteoritic Fe:Ni ratios (~94:6) within the glass fragments, the volatilisation of alkali elements and that their composition was dissimilar to previously recognized eruptive lunar samples. These included classes of Low-Ti Basaltic, High-Ti Basaltic, High-Al Basaltic, Basaltic Andesite, KREEP and Felspathic Lunar materials. Only one class – the Green Glass Beads – had an obvious eruptive origin (Delano, 1986: Shearer and Papike, 1993).

6.9 OXYGEN ISOTOPE ANALYSIS

Results are presented in δ-notation such that: $\delta^{x}O_{VSMOW}$ /1000 = $[(^{x}O/^{16}O)_{sample} / (^{x}O/^{16}O)_{VSMOW}]$ - 1. We use a slope of 0.5251 for the terrestrial fractionation line and linearized form of the δ-notation so that $\Delta^{17}O = \delta^{17}O - 0.5251\ \delta^{18}O$. Error has been established through observation of the standard deviation in 290 single analyses of terrestrial rocks and minerals, carried out in 30 sessions at this stable isotope laboratory using the same equipment and is reported as +/- 0.06‰ (Gehler *et al*., 2011).

Table 6.3

Average bulk compositions of samples P159/001 and M224/001 together with comparative compositions taken from the literature

	S1 –P159/001, S2 – M224/001		S3 – Fusion Crust MIL 05035, S4 Bulk Rec, S5 – Bulk Rock			S6, S7 – Core and rim of Mafic glass S8, S9 – High K/Low K Felsic Glass			
	S1	S2	S3	S4	S5	S6	S7	S8	S9
SiO_2	60.65	65.46	45.50	47.0	48.4	51.10	49.82	66.41	65.36
Al_2O_3	0.00	0.19	9.61	9.26	8.85	13.38	13.17	17.87	18.96
Na_2O	0.54	0.54	0.32	0.26	0.21	0.20	1.21	0.56	0.61
MgO	4.97	3.98	5.83	7.44	7.79	8.34	7.72	0.21	0.19
K_2O	22.69	22.69	0.05	0.03	0.01	1.41	0.06	5.80	3.95
CaO	4.90	5.18	11.9	11.8	12.1	10.91	10.82	4.99	7.04
FeO	0.35	0.17	22.5	22.0	20.7	13.17	15.52	1.97	1.96
TiO_2	0.00	0.00	1.99	1.44	0.90	0.73	0.72	1.04	1.11
MnO	1.29	1.16	0.36	0.32	0.33	0.47	0.54	0.08	0.05
Cr_2O_3	na	na	0.30	0.33	0.30	0.45	0.43	0.26	0.49
P_2O_5	na	na	0.05	0.05	0.02	0.01	0.07	0.01	0.00
SO_2	na	na	0.05	0.11	na	na	na	na	na
Total	97.45	101.44	98.5	100	99.3	100.17	100.08	99.20	99.72
Mg#	96.23	97.61	31.6	37.8	40.2	28.02	28.74	24.63	39.20

Na - not analysed. S1 –P159/001-05, S2 – M224/001-03, S3 – Fusion Crust (MIL 05035) (Thaisen and Lawrence, 2009), S4 – Bulk rock composition of MIL 05035 (Liu *et al.*, 2009), S5 – Bulk rock composition of MIL 05035 (Joy *et al.*, 2007), S6/S7 – NWA 1664 Core and Rim mafic glass (Barrat *et al.*, 2012) S8/S9 – NWA 1664 High K/low K felsic glass (Barrat *et al.*, 2012).

Results of analysis show $\Delta^{17}O$ = - 0.335 with $\delta^{17}O$ = 8.978 ± 0.050 and $\delta^{18}O$ = 17.816 ± 0.100 . Figure 14 shows a plot of $\delta^{17}O$/ $\delta^{18}O$ values compared to those of known CI chondrites as reported by Clayton and Mayeda (1998). It is noted that $\delta^{18}O$ values are relatively high but are within the range of CI and CI-like chondrites (Meta-C).

The effects of oxygen isotopic exchange during terrestrial atmospheric entry have been examined in part by the STONE experiment. Here, samples of terrestrial rock were secured to the surface of the ablative heat shield of a recoverable Foton-12 spacecraft and flown in low earth orbit for in excess of 14 days before atmospheric re-entry and recovery of the capsule (Brack *et al.*, 2002). The conditions experienced by the capsule during re-entry closely mimicked those under which natural meteorites are subjected to on atmospheric entry and were sufficient to melt basalt and silica glass.

The isotopic composition of tropospheric O_2 is given by Luz *et al*., (1999) as $\Delta^{17}O$ = - 0.34 and is characterised by a mass-independently fractionated component derived from stratospheric photochemical processes involving O_2, O_3, and CO_2. Results of the STONE experiment showed that the silica 'fusion crust' of one (analogue) sample was characterised by a $\Delta^{17}O$ = - 0.208 while the corresponding interior exhibited no offset from a terrestrial silicate or oxide. This provides strong evidence for oxygen isotopic exchange during entry. Furthermore, by taking the carbonaceous interior of the sample holder and tropospheric O_2 as end-members, Brack *et al.*, (2002) demonstrated that the silica 'fusion crust' oxygen isotope data fits on a mixing line (regression coefficient R^2=0.998) with tropospheric O_2.

For the purpose of comparison, samples of the well-preserved silica fusion crust and interior of an LL6 ordinary chondrite (Appley Bridge) were similarly analysed. These also exhibited $\Delta^{17}O$ variations of comparable magnitude though no apparent change in $\delta^{18}O$ values were observed. This has been interpretted by Brack *et al*., (2002) as implying a more complex isotopic exchange process in the case of this chondrite.

The broad similarity between the $\Delta^{17}O$ and $\delta^{18}O$ values of P159/001-04 and tropospheric O_2 leads naturally to the question of whether they represent, in part, evidence of some oxygen isotope exchange during entry in the upper atmosphere.

P159/001-04 comprised of three interior fragments and dust weighing a combined 2.41g taken from the interior of sample P159/001 while the isotope values exhibited in the Brack *et al.*, (2002) study comprised of 'fusion crust'. In recovered meteorite fragments, the fusion crust is normally quite thin in comparison to the 5mm depth from which P159/001-04 was extracted. However, the 'fusion crust' glass in the STONE experiments was noted to approximate that of the pre-flight stones, but were characterised by enrichment in SiO_2 (48.1 to 51.9 wt%), CaO (16.7-17.6% wt%) and K_2O (1.6 to 2.2 wt%) yet depleted in TiO_2 (2.1 to 3.8 wt%) FeO (5.2 to 9.1 wt %) and MgO (3.5 to 4.8 wt%) which broadly accord with the oxide compositions of some of our samples.

One possible explanation for this could be related to heating of the host material by super-heated gas that pervaded the pore spaces. This mechanism was identified in the STONE experiments as a likely cause for the melting of basalt fragments within the substrate below the fusion crust and deep within the regolith sample. However, such an exchange mechanism would require a total exchange of oxygen with the incoming bolid and this is not regarded as a plausible possibility.

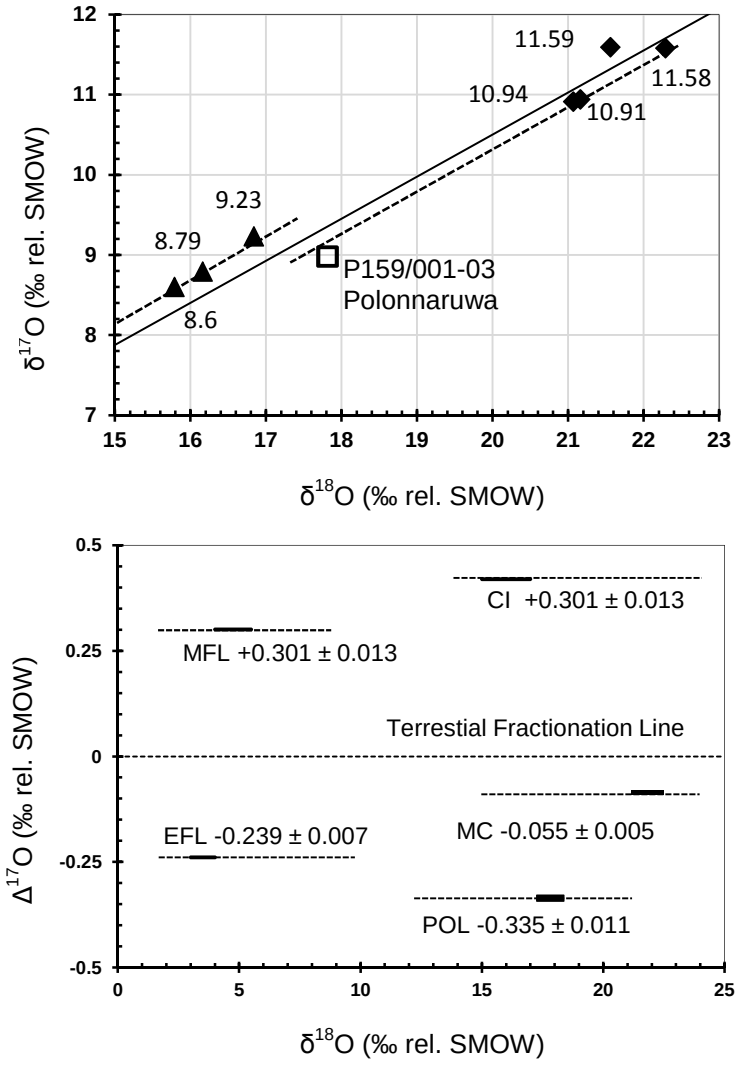

Figure 6.9. (Upper) Oxygen isotope compositions of sample P159/001-04 and of CI chondrites: Alais (8.6), Ivuna (9.23) and Orgueil (8.79) together with CI-like chondrites (Meta-C) B7904 (10.91), Y82162 (11.59), Y86720 (11.58) and Y86789 (10.94). Data from Clayton and Mayeda (1998). (right) Oxygen isotope $\Delta^{17}O$ (‰ rel. SMOW) values of sample P159/001-04 (POL). Data for MFL: martian fractionation from Franchi *et al.* (1999). EFL: eucrite fractionation from Greenwood *et al.*, (2005). CI: chondrites fractionation and MC: Meta-C (B9704 and Y86789) from Clayton *et al.*, (1998).

6.10 CHN ANALYSIS

Results of CHN analysis returned values of C = 4.64 wt%, N = 0 wt %, H = 0 wt% for sample P159 and C = 4.69 wt%, N = 0 wt %, H = 0 wt% for sample M224. The manufacturers of the apparatus quote LOD of 100 ppm and uncertainty of 0.3 wt%. These results were regarded as unsatisfactory

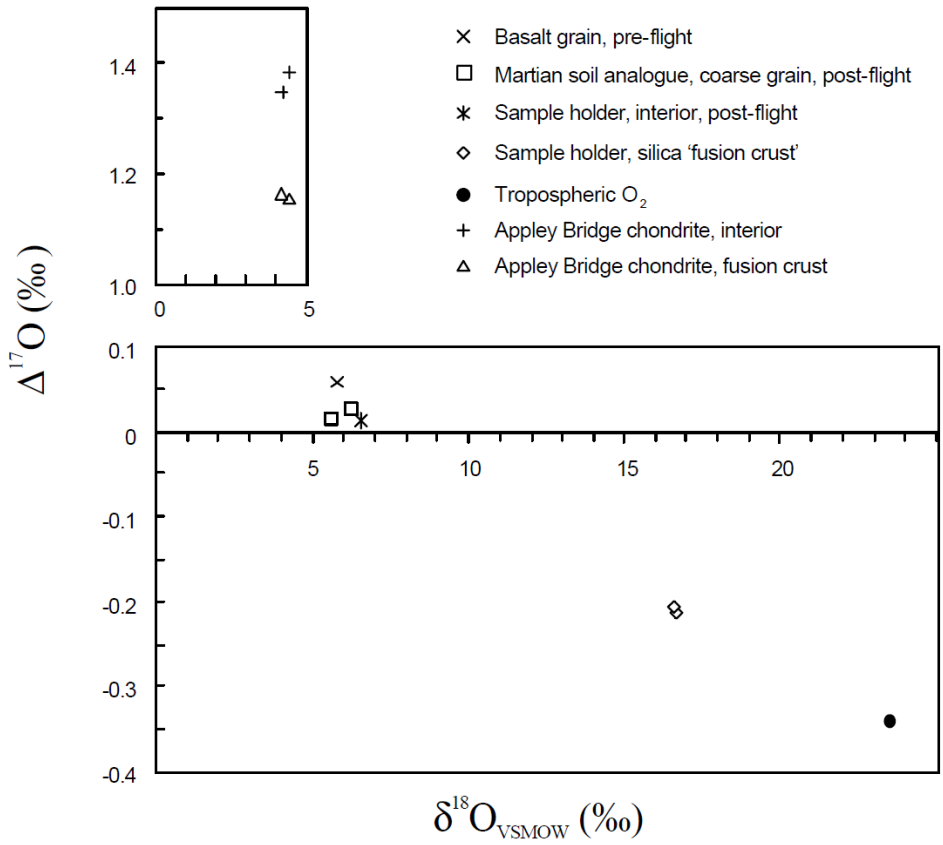

Figure 6.10 Shows oxygen isotope $\Delta^{17}O$ (‰ rel. SMOW) values for 'STONE' samples together with corresponding values for tropospheric O_2 and the fusion crust and interior of the Appley Bridge L6 chondrite. Note that the material lies on a mixing line defined by tropospheric O_2 and the carbonaceous interior of the sample holder. Figure and data taken from Brack et al., (2002).

for the purpose of this study and the analysis was outsourced to a commercial laboratory in the United States using a Perkin Elmer 2400 CHN Elemental Analyser.

Results returned were C = 4.65 wt%, N = 0.01 wt % for sample P159 and C = 4.69 wt%, N = 0.01 wt % for sample M224. Uncertainty was determined at 0.1 wt% (C and N) with LOD 100 ppm. These tolerances were verified by reference to publications by the Universität Wien Mikroanalytisches Laboratorium (Vienna University) for the same Perkin Elmer 2400 CHN Elemental Analyser.

Assuming all the carbon in the samples was of reduced organic form, results indicate a N/C atomic ratio for P159 and M224 < 0.003.

6.11 TRACE ELEMENTS

The increased abundance of Iridium in meteorites when compared to the Earth's crust has been extensively reported in the literature. This is thought to result from the tendency of iridium to bond with iron causing most iridium to have descended below the crust when the planet was young and still molten. Trace element abundances of iridium were determined by ICP-OES in sample P159/001, together with a sample of terrestrial fulgurite. The sample exhibited a high level of Iridium of between 0.7-0.8 ppm or approximately 10^3 times average levels reported in oceanic crust. Values for the control fulgurite were below the detectable limits of the apparatus.

6.12 DISCUSSION

Analysis of bulk chemical compositions, mineral phases and compositions, petrographic features, water content, CHN and triple oxygen isotope analysis allow the following conclusions to be reached about the Polonnaruwa and Ratkina stones:

a) The stones exhibit a highly porous (~80-90% porosity) Si and K-rich, Al-depleted, amorphous melt matrix enclosing a number of mineral grains (1-10µm, commonly <1µm) with elongate to equant shapes. Minerals included anorthoclase, albite, anorthite, quartz and Si-Al-rich melt inclusions. Inclusions are less common in the Ratkinda stones that also exhibit greater levels of shock/thermal deformation.

b) The bound H_2O content of the stones is very low <0.03wt% H_2O. This value is interpreted (in line with the findings of Beran and Koeberl, 1996) as evidence of origination from hypervelocity impact.

c) The carbon content of the stones show N/C atomic ratios < 0.003. This parameter assumes that all the carbon sampled was of organic origin.

d) Results of analysis show $\Delta^{17}O$ = - 0.335 with $\delta^{17}O$ = 8.978 ± 0.050 and $\delta^{18}O$ = 17.816 ± 0.100 . Computed $\delta^{17}O$/ $\delta^{18}O$ accord well with those of known CI chondrites with high $\delta^{18}O$ values within the range of CI and CI-like chondrites (Meta-C). Exchange with atmospheric oxygen was considered but is not regarded as a plausible explanation for observed fractionation parameters.

Chapter 7

Biological Morphologies in the Polonnaruwa Stones

7.1 INTRODUCTION

It has been over half a century since the first evidence of microbial fossils in carbonaceous chondrites was discovered and reported by Claus and Nagy (1961). Independent studies soon confirmed, or partially confirmed, the findings (Reimer, 1961; Staplin, 1962; Palik, 1962, 1963 and Cholnoky, 1962) though these were later challenged on the grounds of contamination by terrestrial organics and pollen (Anders and Fitch, 1962a, 1962b, 1964; Fitch and Andres, 1963a, 1963b; Fitch *et al.,* 1962). The Cronin *et al.,* (1988) review later resolved the matter in favour of an abiogenic origin of the structures though they found no particular mechanism adequate to explain their formation. Two decades later the problem of microbial fossils in carbonaceous meteorites was re-examined by Hans D. Pflug who used a process of *in situ* demineralisation to isolate carbonaceous structures (Pflug, 1984). Forms similar to the well-known bacterium *pedomicrobium* were identified while laser mass spectroscopy, Raman spectroscopy, UV and IR spot spectroscopy were used to establish the indigenous nature of the biological-type forms. While this work was never discredited, the debate over non-biotic artefacts resembling microbial microfossils has succeeded in preventing widespread acceptance of the results.

A decade later and the issue of microfossils again resurfaced, but this time in the form of the possible detection of bacteria-like fossils in the Allen Hills Martian meteorite ALH 84001 (McKay *et al.,* 1996). These results were challenged (Brearley, 1988; Brearly, 2003; Treiman, 2003; Golden et al., 2006) after it was demonstrated that both the abiotic thermal decomposition of Fe-rich carbonates and the formation of nanophase magnetite and pyrrhotite crystals may also have resulted in morphologies similar to those observed in ALH84001. This led to the currently accepted paradigm that morphology alone cannot be used unambiguously as a tool for primitive life detection. This belief ultimately defeated the independent studies of Hoover (2005) a decade later when he reported SEM observations of large complex filaments embedded in freshly fractured internal surfaces of a variety of carbonaceous meteorites the stones.

The subject of microfossils in meteorites remains highly controversial. Morphological characteristics consistent with microbial organisms that are cited as evidence of biology are particularly subject to criticism. The problem of contamination adds to the already difficult problem

of establishing non-terrestrial origin and to date no one study has managed to convince the scientific community of the presence of unambiguously biological structures that were indigenous to an accepted non-terrestrial source.

In this section, results of SEM and EDAX studies on freshly cleaved internal surfaces of the Polonnaruwa stones are reported. Preliminary inspection of a few of the SEM images revealed the presence of a number of highly carbonaceous biological structures and fossil diatoms. Some of these were deeply integrated in the surrounding mineral matrix indicating they could not have been recent biological contaminants. The visual nature of the structures places them beyond question as biological in origin.

7.2 EXPERIMENTAL METHODS AND SAMPLES

Scanning Electron Microscopy (SEM) was conducted using the FEI (Phillips) XL30 FEG ESEM (Environmental Scanning Electron Microscope) FEG (Field Emission Gun) at the School of Earth and Ocean Sciences at Cardiff University. The unit incorporates a secondary electron detector (SE), a back scatter electron detector (BSE) and a gaseous secondary electron detector (GSE). It also has an Oxford Instruments INCA ENERGY (EDX) x-ray analysis system. Image recording is via a SONY video graphics printer or digital by processing image frames in a 16 bit framestore computer for output to hard drive.

Further SEM studies were conducted at the NASA Marshall Space Flight Centre and the Paleontological Institute of the Russian Academy of Sciences in Moscow, Russia using a Hitachi S-3700N Field Emission Scanning Electron Microscope with images gathered using both the Back-Scatter Electron (BSE) and the Secondary Electron (SE) detectors (NASA MSFC), and a Camscan SEM (accelerating voltage of 20 kV) in Moscow.

Sample preparation involved the use of a flame sterilised wide-bore hypodermic needle to fracture the fragments before mounting on aluminium stubs. The samples utilised in this study comprise of four bulk samples prepared for interior section scanning at the School of Earth and Ocean Sciences at Cardiff University. Two of these samples were derived from sample P166/001, and two from sample M224/001 as detailed in a previous section (section 6.4). Studies at NASA MSFC and the Paleontological Institute in Moscow used uncoated freshly fractured surfaces only. Some samples at Cardiff University were coated with a gold/palladium surface to facilitate high resolution image capture.

7.3 SEM AND EDX RESULTS

Examination of the SEM images revealed the presence of fossils of filamentous (uniseriate and multiseriate) cyanobacteria as well as polarized filaments and heterocystous nitrogen fixing cyanobacteria. The stones also contained kerogenous morphotypes similar to extinct terrestrial life (acritarchs and hystrichospheres) and well-preserved and fossilized remains of many different genera and species of both freshwater and marine diatoms. Almost all of the diatoms found are raphid pennates, but the stones also contain rare examples of marine centrics and araphid pennates. Diatom frustules were embedded in the rock matrix and exhibited varying degrees of degradation, though a few examples of well preserved and even pristine diatom frustules and hystrichospheres were also present.

Figure 7.1 (a and b) shows a lattice type structure of inter-connecting organized 'pores' that range in size from <0.5 µm to ~5µm and span a diameter of ~ 50µm giving rise to a 'scaffold' effect that appears to have become imprinted on the matrix. Visual inspection reveals the presence of a fracture along the leading edge highlighting that this structure had been directly attached to the rock matrix and remained connected at the south end. EDX elemental abundances are shown in figure 7.2 along with a table of quantities for three spectra acquired from the structure (S1), attached matrix (S2) and nearby but unrelated matrix (S3). These spectra show the structure to be highly carbonaceous (S1 – C; 59.81%) but depleted in nitrogen (S1 – Nitrogen not detected). It is noted that the elemental abundances in the neighboring rock matrix indicate some level of elemental exchange taking place between the structure and the attached substrate. In particular, the carbon content of the attached substrate shows levels approximately half way between those of the unrelated substrate and the structure itself indicating a movement of carbon from the structure to the substrate. Similarly, oxygen, aluminum, silicone, potassium and iron abundances of the attached substrate show levels approximately half way between those of the unrelated rock and the structure. This again indicates a movement of these elements, but this time from the rock substrate to the biological structure.

A similar structure, almost entirely integrated into the surrounding matrix is shown embedded in the substrate of figure 7.1 (c). In this example, the lattice type like structure is observed as being imprinted on the matrix. The constituent shapes vary from rounded to angular and exist as a network of connected shapes giving rise to a 'honeycomb' effect. The size of the lattice appears as a ~ 25 x 30 µm spherical segment loosely connected to a smaller 15 x 20 µm segment at the south west end. These could possibly represent two separate spherical fossils that have become embedded into the rock in close proximity or could represent the remains of a partially degraded larger and

more complex arrangement that was imprinted on the substrate itself. Figure 7.1 (d) shows a morphologically dissimilar structure with similar levels of degradation that is barely visible on the substrate surface. The white arrows point to the structures in (c) and (d). Images in 7.1 (a) and (b) were taken at Cardiff University while (c) and (d) were taken at the SEM facilities in Moscow, Russia.

EDX data indicates they are severely depleted in nitrogen (N < 0.5%). Hoover (2007) explored the use of Nitrogen levels and biogenic element ratios for distinguishing between modern and fossil microorganisms as a mechanism for recognizing recent biological contaminants in terrestrial rocks and meteorites. Detectable (2-18%) levels of Nitrogen were encountered in the hair and tissues from mummies from Peru (2 Kya) and Egypt (5 Kya) and the hair/tissues of Pleistocene Woolly Mammoths (40-32 Kya).

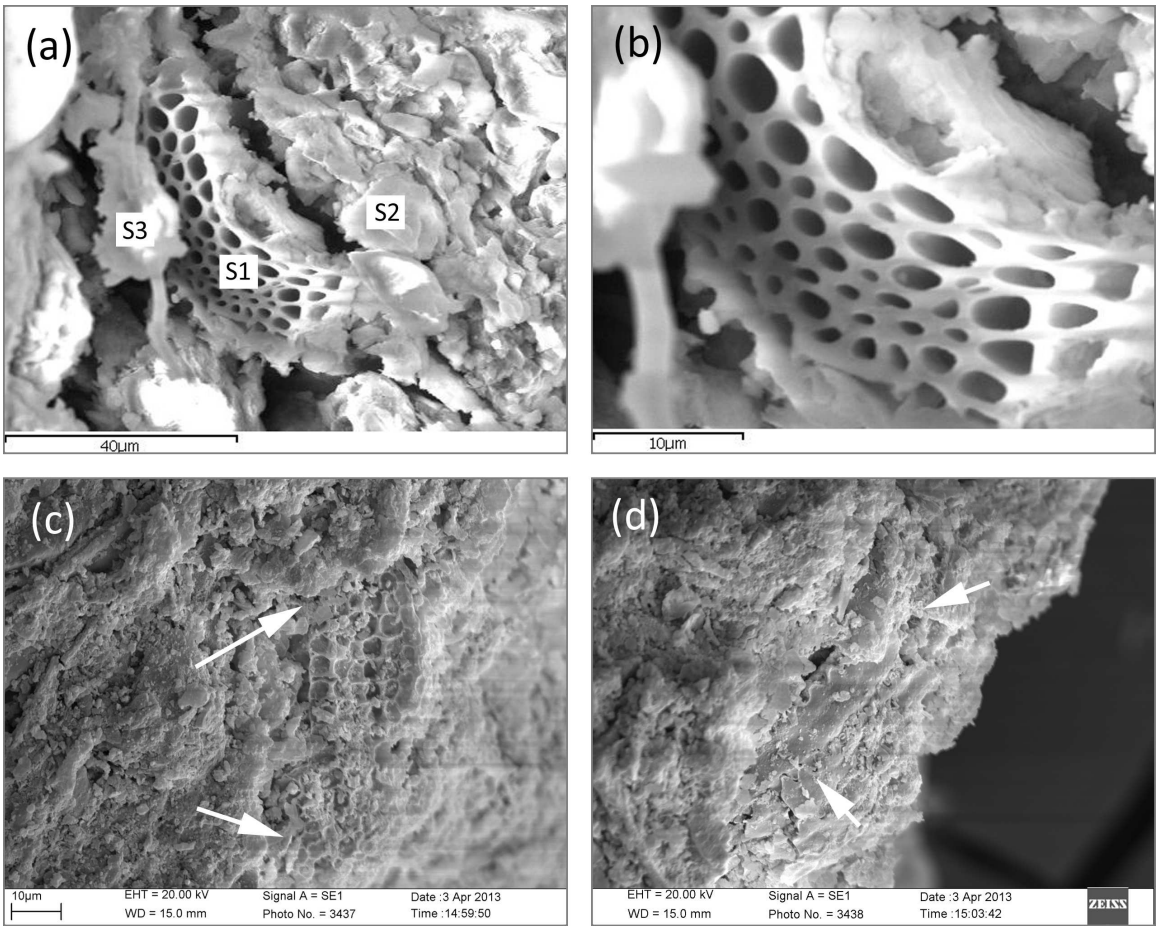

Figure 7.1 Shows a highly carbonaceous partially degraded biological structure. Note the apparent fracture from the surrounding mineral matrix along the leading edge. Points S1, S2 and S3 correspond to elemental abundances determined by EDX as detailed in Figure 7.2. Images a) and b) taken in Cardiff, (c) and (d) taken at the facilities in Moscow, Russia.

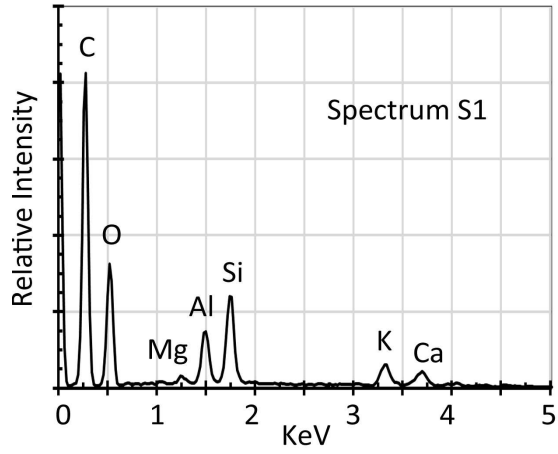

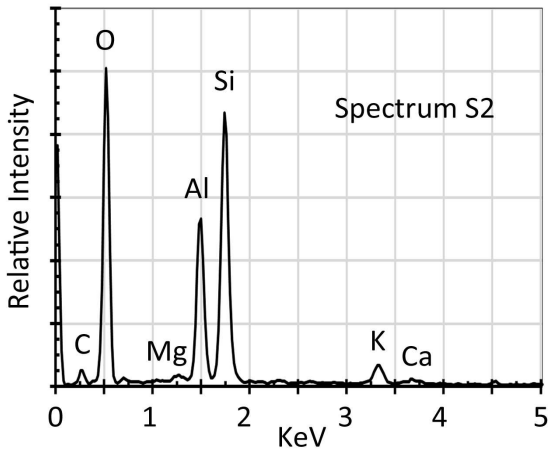

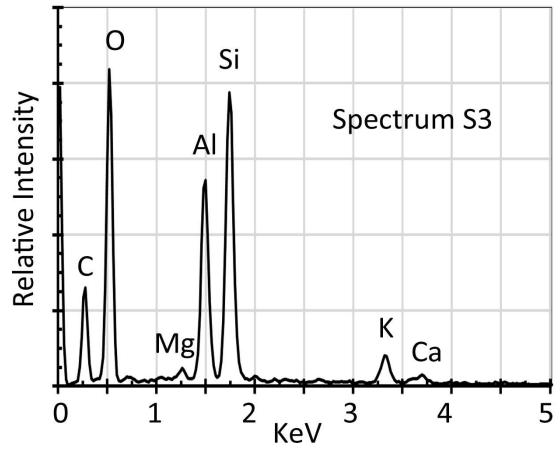

Spec	S1	S2	S3	Max	Min
C	59.81	29.26	0.00	59.81	0.00
N	0.00	5.11	0.00	5.11	0.00
O	31.3	44.98	60.53	60.53	31.3
Mg	0.34	0.42	0.00	0.42	0.34
Al	2.11	6.68	12.15	12.15	2.11
Si	3.55	9.98	20.91	20.91	3.55
P	0.00	0.23	0.00	0.23	0.23
S	0.00	0.00	0.33	0.33	0.33
K	1.38	1.47	2.14	2.14	1.38
Ca	1.04	0.42	0.53	1.04	0.42
Ti	0.00	0.00	0.57	0.57	0.57
Fe	0.47	1.45	2.84	2.84	0.47

Figure 7.2 Shows elemental abundances in the biological structure (S1), attached matrix (S2) and nearby but unrelated matrix (S3) of the biological structure shown in figure 7.1. Note that the carbon content of the attached substrate shows levels approximately half way between those of the unrelated substrate and the structure itself indicating a movement of carbon from the structure to the substrate. Similarly, oxygen, aluminum, silicone, potassium and iron abundances of the attached substrate show levels approximately half way between those of the unrelated rock and the structure. This again indicates a movement of these elements, but this time from the rock substrate to the biological structure.

Comparative studies on fossilized insects in Miocene (8.4 Ma) Amber, Cretaceous Ammonites (100 Ma), Cambrian trilobites of Wheeler Shale of Utah (505 Ma) and filamentous cyanobacteria from Karelia (2.7 Ga) showed nitrogen levels below the limit of detection with the FESEM EDS detector (N < 0.5%). This provides some evidence that these clearly biological artefacts, found embedded in the Polonnaruwa stones, are indigenous to the stones and not the result of post-arrival microbial contaminants.

Figure 7.3 (a-d) shows a thick walled carbon-rich (kerogenous) spherical strutcure ~110µm in diameter lodged between two angular edges of the matrix. The surface of the sphere is rough with strands of membronous material anchoring it from joints that originate from the surface and

comprise of a smooth, thick membrane containg flaps and waves of membrane that terminate at the neighbouring matrix. Morphologlogical fearures indictate that the observed strcucture is a 'hystrichosphere' thought to be associated with the resting stages of a group of partly extinct dinoflagellate. The dinophyte cysts usually contain spinal processes and are typically 120 µm in diameter (although they are known at sizes between 5-250µm).

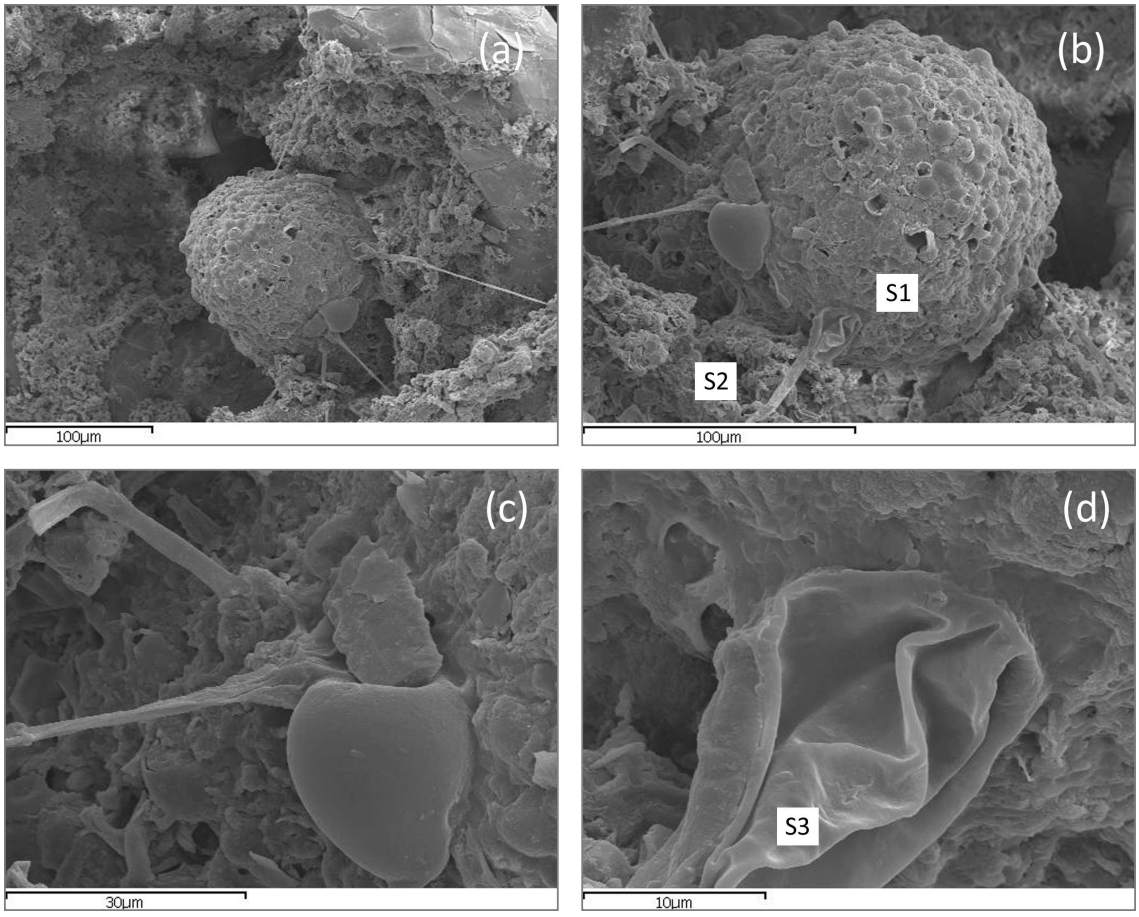

Figures 7.3 (a-d) shows images of a large (100 µm diameter) and very complex, thick-walled, carbon-rich (kerogenous) microfossil that we have tentatively identified as a hystrichosphere. Hystrichospheres are thought to be associated with the resting stages of a group of largely extinct marine dinoflagellate algae. The EDX data reveals a lack of detectable nitrogen and an anomalous C/O ratio (similar to bitumen) clearly establishes that this obviously biological form could not possibly represent a modern biological contaminant. The extremely well-preserved and very thin (2 µm diameter x 100 µm long) flagella are interpreted as indicating a low-gravity, low-pressure environment and rapid freeze-drying. In the vicinity of this form are highly carbonaceous embedded filaments of cyanobacteria ("blue-green algae"). Low nitrogen shows they are ancient fossils. Points S1, S2 and S3 relate to target corordinates of energy X-ray readings detailed in Figure 7.4. The sample was coated with a gold/palladium surface to facilitate high resolution image capture after first observing uncoated.

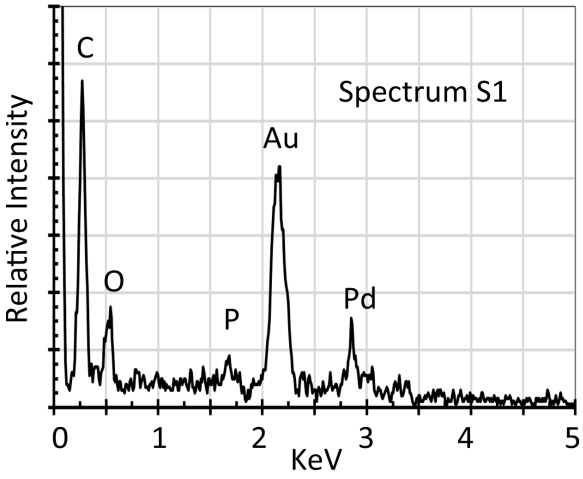

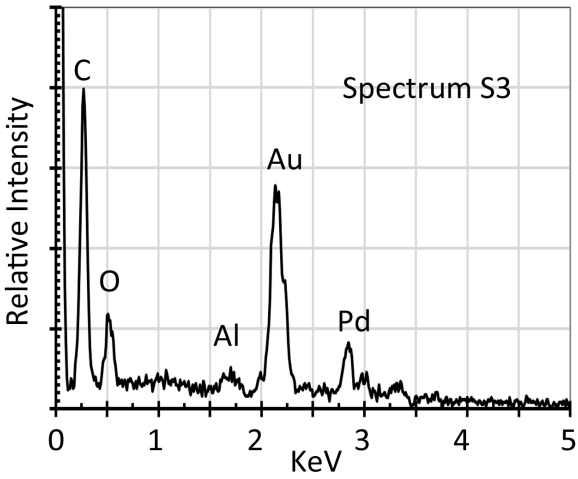

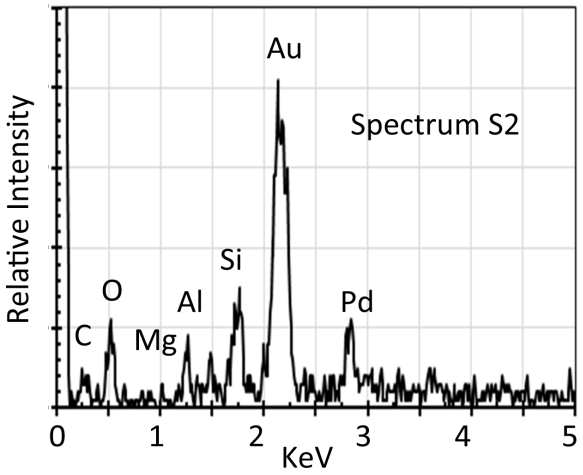

Spec	S1	S2	S3	Mean	SD	Max.
C	67.94	0.00	65.73	44.56	38.60	67.94
N	0.00	0.00	0.00	0.00	0.00	0.00
O	26.21	39.82	24.80	30.28	8.29	39.82
Na	0.00	0.00	0.00	0.00	0.00	0.00
Mg	0.00	13.02	0.00	4.34	7.52	13.02
Al	0.00	10.35	0.00	3.45	5.98	10.35
Si	0.00	36.81	2.17	12.99	20.66	36.81
P	0.00	0.00	0.00	0.00	0.00	0.00
S	0.00	0.00	0.00	0.00	0.00	0.00
K	5.85	0.00	7.29	4.38	3.86	7.29
Ca	0.00	0.00	0.00	0.00	0.00	0.00
Fe	0.00	0.00	0.00	0.00	0.00	0.00

Figure 7.4 Shows elemental abundances in the main biological structure (S1), neighboring substrate (S2) and attached flagella (S3) of the biological structure illustrated in figure 7.3 (a-d). Note that the carbon content of the neighboring substrate shows an absence of carbon with high O, Mg, Si and Al contents. Au and Pd values reflect the gold/palladium coating applied to facilitate high resolution image capture.

The outer layer of dinoflagellate cysts are usually made of a cellulose type material that decomposes or degrades when the organism dies leaving a tougher and more resistant organic inner layer which readily fossilizes. Dinoflagellates are predominantly marine plankton though some freshwater varieties are also known. EDX elemental abundances are presented in figure 7.4. These show both a depletion of nitrogen and also of elements normally associated with kerogens such as phosphorous, fluorine, sulphur and chlorine, no doubt a consequence of advanced fossilisation.

Further examples of embedded *bacillariophyta* (diatom) frustules were also observed. These comprise of hydrated silicon dioxide ($SiO_2.xH_2O$ - biogenic silica) with morphologies that

genetically determine the characteristic of the taxonomy of the diatom. The frustule usually comprises of two overlapping *thecae*, or shells, distinctive and identical in shape, except that one is slightly smaller (hypotheca) than the other (epitheca), facilitating an overlap that encases the eukaryote inside. The synthesis of the biogenic silica occurs inside the cell via polymerization of silicic acid monomers and is constructed according to a protein template leading to precise and complex patterned thecae consisting of a *valve*, or flat section, and *girdle bands* which appear as connecting or segmented rings or hoops. The patterns exhibited by the frustules are often elaborate giving rise to various ornamental shapes and morphologies making them amongst the most easily recognizable eukaryotes on Earth.

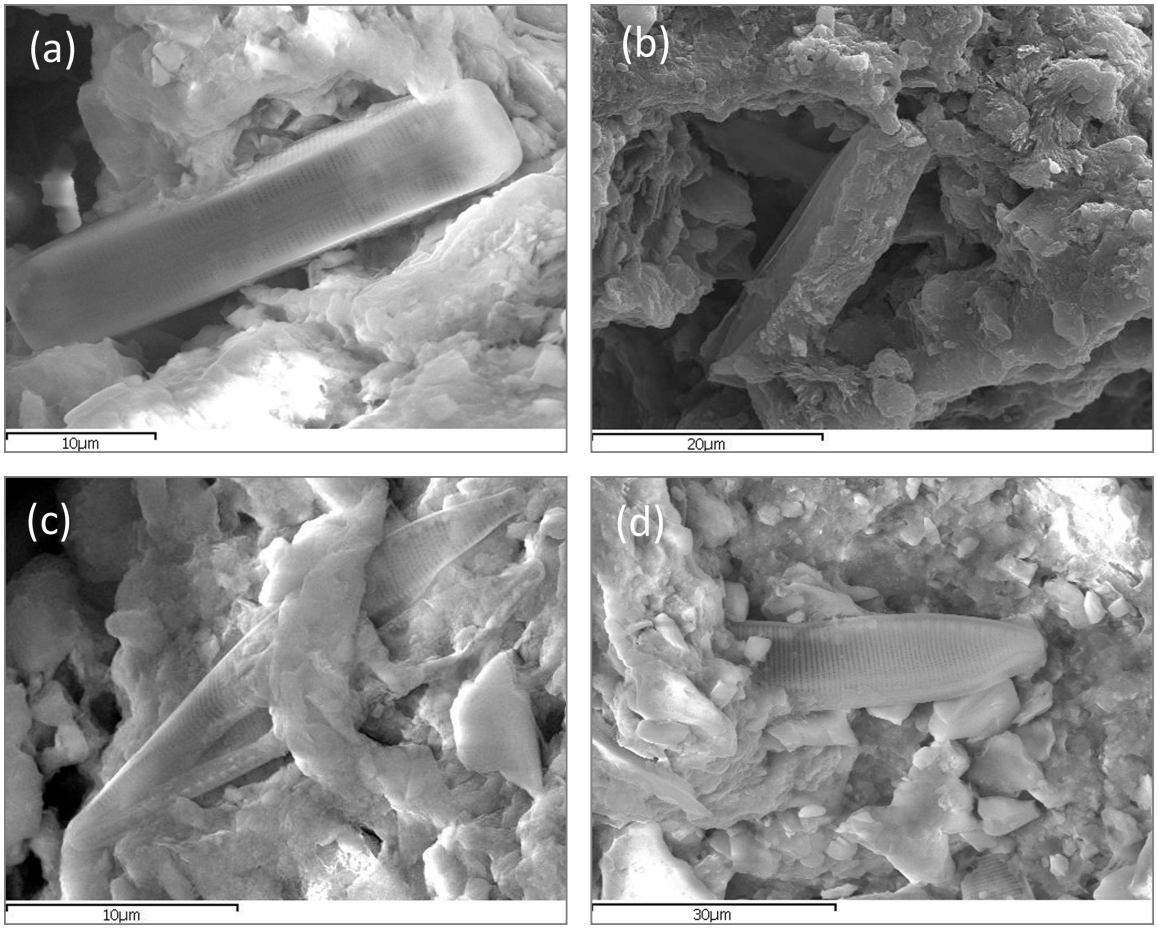

Figure 7.5 (a) shows various examples of embedded *bacillariophyta* (diatom) frustules in sample P166. (a) shows the girdle view of a 50 µm by 10 µm *fragilariophyceae* (pennate) diatom lodged between two sections of the rock matrix (b, c) similar diatoms exhibiting significant fusion and integration into the surrounding matrix, (d) shows a further example of a pennate diatom, the visible part of the frustule (approximately 35 µm in length) resting on loose substrate grains.

Figure 7.5 (a) shows the girdle view of a 50 µm by 10 µm *Fragilariophyceae* (pennate) diatom lodged between two sections of the rock matrix. The centre of the upper valve appears to show some fusing with the substrate indicating that this diatom has been present in the matrix for some time. Pennate diatoms exhibit motility by the gliding interaction between the substrate and the pennate's 'raphe' - observed as a fissure, or two slits running end-to-end along the mid-line of both valves (although some do exist as *monoraphids*). The diatom in figure 7.5 (a) appears to exhibit a bilaterally symmetrical pattern consisting of *striae,* or transverse lines, often observed optically as small holes or dots along the valve.

These diatoms are commonly found in freshwater, attached to plants and rocks, but are known to exist in marine environments and can thrive in saltwater. Figure 7.5 (b, c) show similar diatoms exhibiting significant fusion and integration into the surrounding matrix. Figure 7.5 (d) shows a further example of a pennate diatom, the visible part of the frustule (approximately 35 µm in length) resting on loose substrate grains. The opposite end of the frustule is completely fused into the matrix such that the biogenic silica is now indistinguishable from the siliceous substrate.

Figures 7.6 (a, b) show images of a colonial centric diatom embedded in the rock matrix. These diatoms primarily exist as unicellular organisms but are known to form colonies of *Fragilaria* (filaments or ribbons), *Meridion* (fans), *Tabellaria* (zig-zag shapes) and *Asterionella* (stars). Figure 7.6 (a) shows several cells of a linear colonial filament, approximately 50 µm in length, with the right end of the filament embedded in the rock matrix. At the left end several broken separation or interlinking spines are visible (white). Near the centre of the filament it is possible to see two diagonal slits on adjacent cells, which are interpreted and labelled as *rimoportule*.

Figure 7.6 (b) reveals further morphological detail such as separation lines (visible lines formed at the juncture between two cells), ringleiste (an internal silica ledge that projects into the cell from the column), areolae (small circular areas on the surface) and cribra (small domes of silica that make up the areolae. Many of these features are diagnostically useful in identifying the type of diatom presented.

Coscinodiscophyceae, or centric diatoms (which include most large marine planktonic diatoms) are typically radially symmetric and exhibit various shapes (multi-angular, square or elliptical) when seen in valve view. Additionally, the presence of the connecting spines, separation lines and ringleiste allow for an unambiguous classification of the genera as *Aulacoseira*. The short tri-angular connecting spines, presence of a ringleiste and mantle height to cell width ratio > 1 allows for a classification of the species as *Aulacoseira ambigua*. This species is found within both

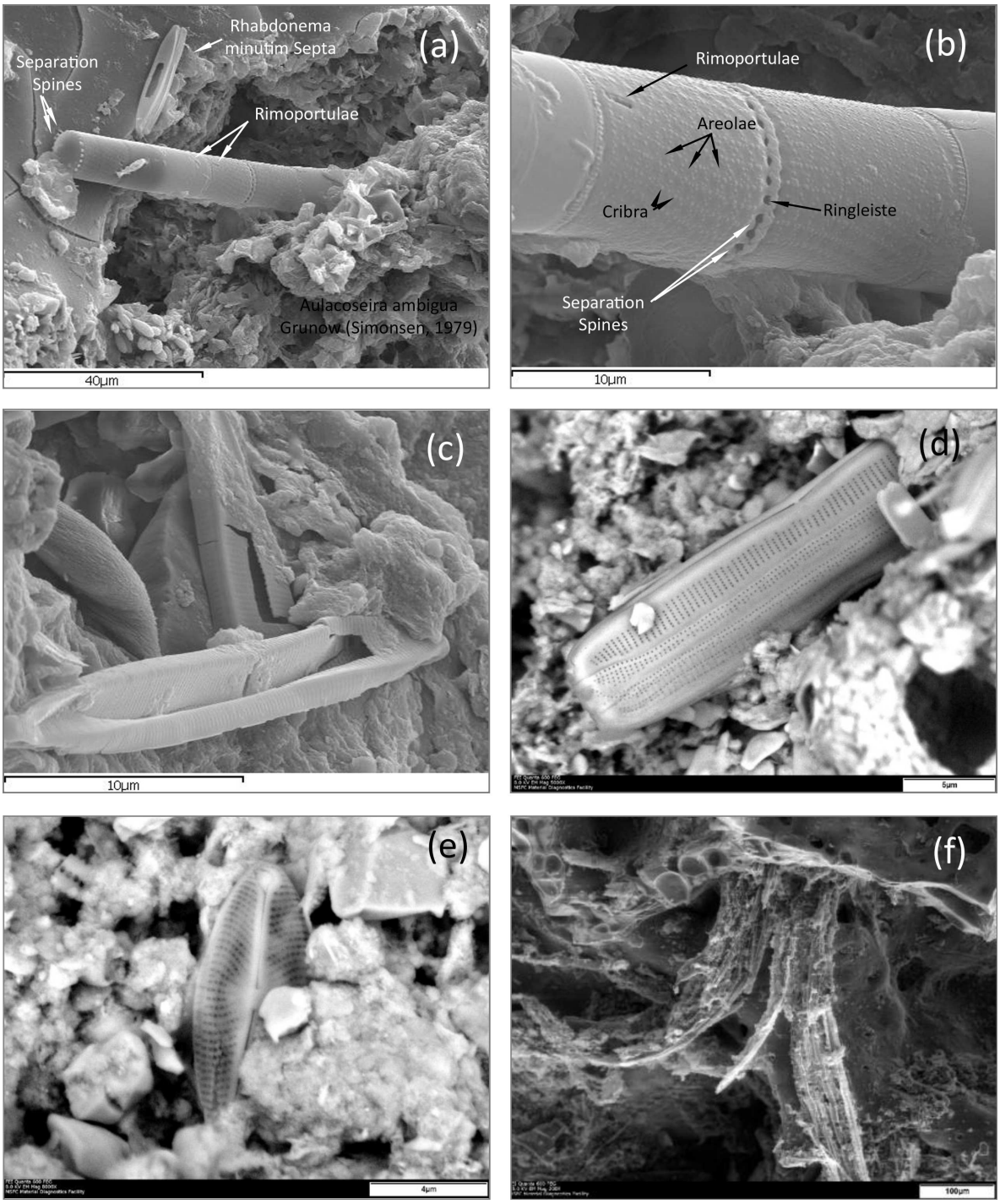

Figure 7.6 Shows planktonic diatoms in sample P166 (a) embedded colonial filament of *Aulacoseira ambigua* and septa of the marine araphid pennate *Rhabdonema minutum* (b) detail of portion of filament of *Aulacoseira ambigua* showing characteristic diagnostic features (Ringleiste, Rimoportulae, Areolae, Cribra, & Separation spines) of the species (c) two damaged frustules exhibiting typical lacerations, fractures and slices to the structure while partially fused into the substrate (d) complete frustule in girdle view of unidentified pennate (e) species Navicula reinhardti) and (f) Fossilized (kerogenous) remains of filamentous cyanobacteria interpreted *Rivularia sp.*

freshwater and saltwater environments. However, also present in figure 7.6 (a) is the septa of a diatom identified as being from the species *Rhabdonema Minutum* which is a polar marine diatom exclusively found within saltwater environments.

In addition to fossilized diatom frustules that were embedded or fused into the substrate, a number of damaged and degraded frustules were also observed. These included examples of raphid pennate diatoms with clear fractures to the thecae such that the previously attached segment of the shell had become detached and unavailable for observation. Figure 7.6 (c) shows examples of two damaged frustules exhibiting typical lacerations, fractures and slices to the structure while partially fused into the substrate.

Figure 7.6 (d) shows an image of embedded diatom pictured during the EM studies conducted at NASA/MFSC. This example contains a complete frustule in girdle view making identification of a raphe or classification to genus or species impossible. The study was able to identify an example of the species *Navicula reinhardti* as described by Grunow in Cleve and Moller (1877) which is pictured in figure 7.6 (e). This raphid pennate diatom of dimensions 11 µm by 4.2 µm has lanceolate elliptical valves. The raphe is filiform and its branches are straight. The striae strongly radiate and become alternately longer and shorter towards the centre. This species of diatom is found within freshwater and brackish waters and is observed in this sample completely embedded at the lower end such that the bottom right quadrant of the frustule is not visible in the field of view.

Figure 7.6 (f) shows an image of the fossilized (kerogenous) remains of filamentous cyanobacteria found in the sample and obtained on freshly fractured uncoated samples at NASA/Marshall Space Flight Centre using the Quanta 600 FEG Scanning Electron Microscope. Tapered embedded cyanobacteria filaments of the Family *Rivulariaceae* are clearly visible. The Rivularian cyanobacteria are very important as they are in the order Nostocales and have heterocysts and are capable of nitrogen fixation.

The presence of these structures may have further implications since diatoms are known to be unable to break the strong triple bond of the inorganic di-nitrogen (N_2) molecule and convert it into the organic nitrogen. Nitrogen in molecules such as NO_2 or NH_3 can be readily used for the construction of amino acids, proteins, DNA, RNA and other life-critical biomolecules. The function of nitrogen-fixation is carried out by the nitrogenous enzyme that is housed in structures known as heterocysts of several species of several genera (Nostoc Tolypothrix, etc.) of heterocystous cyanobacteria. Consequently, cyanobacteria are considered a crucial component of a self-reliant ecosystem.

7.4 GAS CHROMATOGRAPHY–MASS SPECTROMETRY (GC-MS) RESULTS

The problem of contamination in meteorites poses particular problems in the study of biomarkers, with previous work routinely compromised by the suggestion of terrestrial contamination (Claus and Nagy, 1961; Nagy *et al.*, 1962; Pflug, 1984; McKay, 1996; Hoover, 2005). In order to elucidate the nature of the organic component of the Polonnaruwa stones, gas chromatograph-mass spectrometry was utilised to establish the range of biologically relevant molecules present in the samples.

GC-MS studies were undertaken using a Perkin Elmer Turbomass, gas chromatograph-mass spectrometer, utilising a chloroform solvent. The machine was fitted with Phenomenex, Zebron, ZB-5MS column with 30m x 0.25mm x 0.25 um film thickness. The carrier gas was helium at 1ml/min. The temperature profile was 60 ^{o}C to 260 ^{o}C at 10 ^{o}C /min and held at 260 ^{o}C for 10 mins. Scanning of the mass spectrometer was from 50 to 450 Da at 2 scans per second.

Results indicated retention times of 2.789, 2.849 and 3.569 minutes, with corresponding relative intensities displayed in figure 7.7. These results indicate the presence of a variety of 50-450 Da molecular weight molecules within the sample. Detections in the 63, 65 and 67 Da range were interpreted as detection of the chloroform solvent utilised in the experiment that arose from column bleeding.

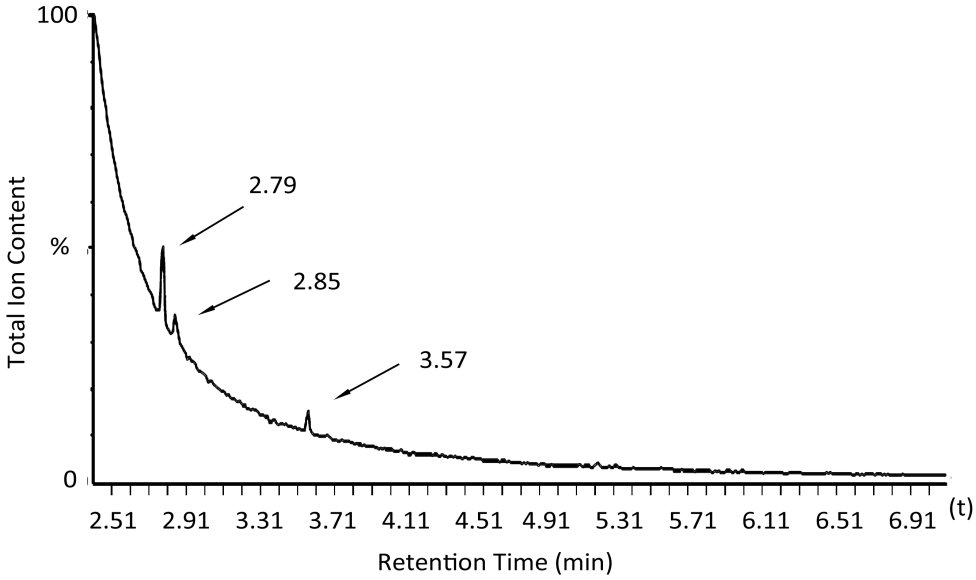

Figure 7.7 Gas chromatogram of Polonnaruwa sample P166. No amino acids were detected.

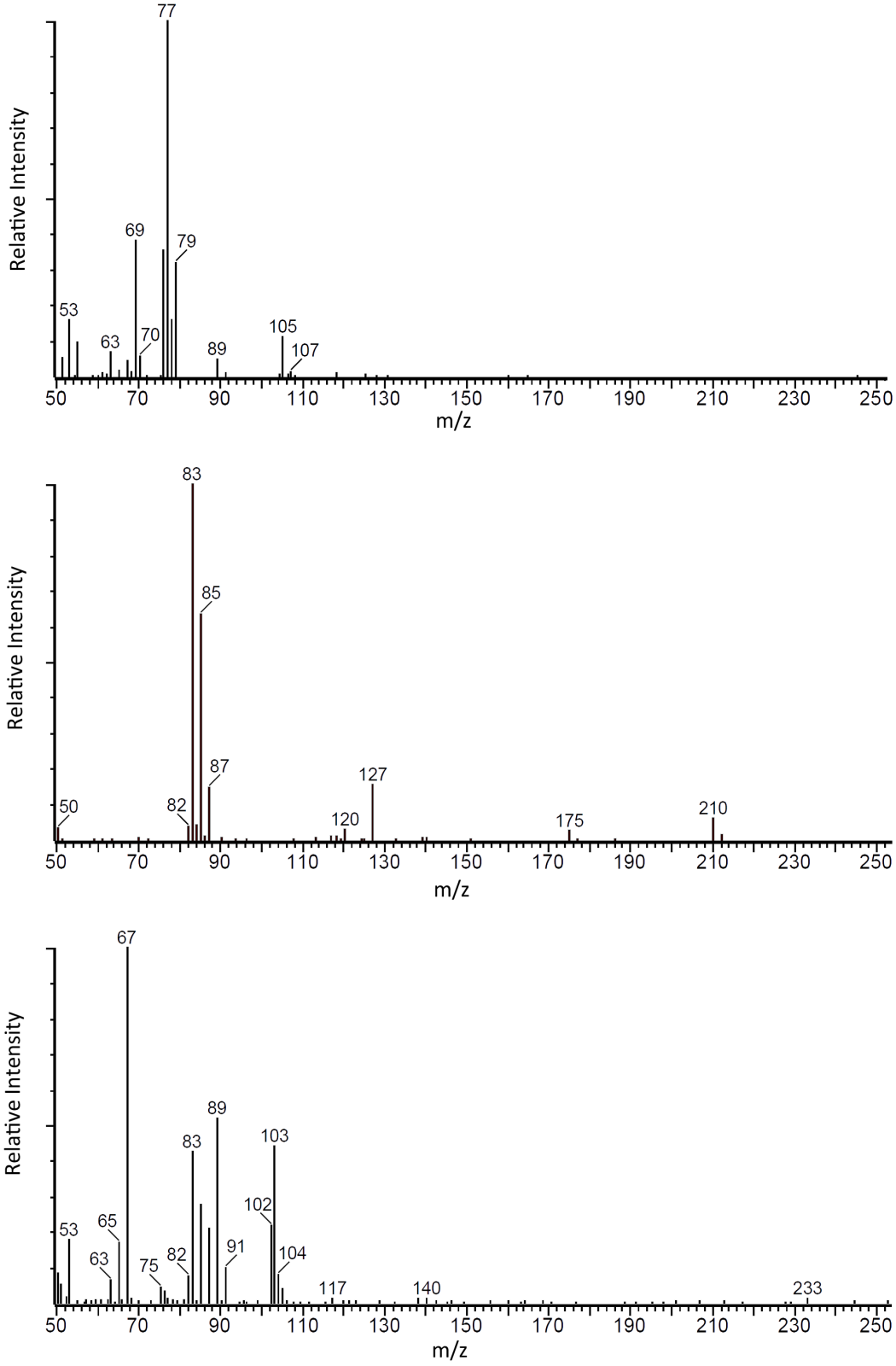

Figure 7.8 Shows the mass spectrum of three detections as shown in the gas chromatogram at 2.789, 2.849 and 3.569 minutes respectively.

Of note was the absence of biologically relevant organic compounds (amino acids) composed of amine (-NH_2) and carboxylic acid (-COOH) functional groups that would be expected from the presence of recently living organisms. For example, the amino acids Glycine (m/z = 246, 218), Glutamic acid (m/z = 432, 330, 272), Alanine (m/z = 260, 232, 158), Valine (m/z = 288, 260, 186), Proline (m/z = 286, 258, 184) and Aspartic acid (m/z = 418, 390, 316) that are ubiquitous to all life on Earth were not present in the sample.

This adds substantial weight to the evidence previously derived from SEM observations of frustules fully embed and fused into the substrate indicating fossilisation and not contamination by terrestrial organisms present in the Sri Lankan soil.

7.5 NITROGEN CONTENT: ATOMIC N/C DECREASE

The starting point for the N/C ratio of biological material depends on the amino acid content of the source organism (Pelet *et al.*, 1983). Planktonic organisms have an N/C ratio > 0.08 (H/C ratio from 1.3-1.5) while terrestrial plants generally have an N/C ratio <0.05 (H/C ratio ~1.0) (Vandenbroucke and Largeau, 2007). The main loss of Nitrogen occurs during diagenesis, with biomass degradation arising mainly from hydrolysis reactions, resulting in nitrogen depletion taking place chiefly in the form of amino acids and NH_4^+ (Schnitzer, 1985). It is difficult to assign strict timetables to this degradation process since liable nitrogen moieties may be protected by steric encapsulation into a resistant organic matrix. However, in very immature terrestrial organic sediments such as algal sapropel (a few thousand years old), nitrogen is mainly present in the form of amide groups while in immature sedimentary organic matter derived from *B. braunii* of a few million years, the nitrogen is mainly present in the form of pyrrole units (Knicker *et al.*, 1996; Derenne *et al.*, 1998).

The end of the diagenesis is defined as the stage when nitrogen in humin is no longer hydrolysable, and the N content of kerogen does not change much in terrestrial sediments until the end of the petroleum formation stage. At this stage nitrogen is released in the form of N_2 gas (Littke *et al.*, 1995; Gillaizeau *et al.*, 1997). During this period, Nitrogen speciation in kerogen and coal changes with increasing maturity (Patience *et al.*, 1992; Kelemen *et al.*, 1994).

N/C ratios in coal illustrate the above. In ~60Ma Lignite, C = ~68 wt%, N = ~1.23 wt% and N/C = ~0.015 (atomic ratio). In corresponding 100-150 Ma sub-bituminous coals, C = ~88 wt%, N = ~1.1 wt% and N/C = ~0.01 (atomic ratio) while in 300-350 Ma anthracite, C = ~95 wt%, N = ~0.7 wt% and N/C = ~0.007 (atomic ratio) (ASTM D3178-73, 1979; Bustin, Mastalerzb and Raudseppa,

1996). By the time we get to Precambrian microfossils (540 Ma to 4.6 By), N/C atomic ratios are reported in the range of 0.0015-0.03 (Beaumont and Robert, 1999).

The detection limit of nitrogen by EDAX is not as accurate as with heavier elements and is determined to be 0.5 wt% (Fisher, 2014). This corresponds to an N/C atomic ratio of 0.0064 and is slightly less than N/C atomic ratios reported on 300-350 Ma anthracite as well as being within the reported range of kerogen analysed within Precambrian microfossils > 540 Ma (Beaumont and Robert, 1999). These results are interpreted as indicating that the carbonaceous, clearly biological structures in the Polonnaruwa stones are older than ~300 Ma, this marking the approximate lower detection limits of the EDAX apparatus.

7.6 K-RICH SIO_2 INTERFACES

Two distinct phases were commonly observed in SEM studies. These were characterised by a smooth K-rich SiO_2 amorphous glass phase in which no biological structures were observed and a second, rough phase in which all observed biological structures were found. Substantial evidence was identified to illustrate that the rough, more processed phase represented a later stage alteration of the SiO_2 glass.

Figure 7.9 shows SEM images of the interface between amorphous glass and the rougher substrate phases characteristic of biological colonisation. Numerous examples of clean, sharp and clearly defined interfaces between the two phases were idenitified indicating a later precipitation of the rougher phases (figure 7.9 arrows C, D (lower) and F). Further evidence of precipitation could be found in examples of rough deposits separating from the smoother glass phase (figure 7.9 arrow F) and located in smooth cavities (figure 7.9, arrow B and 7.9 (f)). Finally, some evidence of the surface degradation of the smoother phases were detected (figure 7.9, arrow A and upper arrow D) as well as in areas of clean dissolution cavities (figure 7.9, arrow E). These observations are interpreted as evidence of the later stage colonisation of aqueous biological bodies within a substrate of amorphous SiO_2. The surface pitting and apparent degradation of the glass phase is interpreted as arising from the dissolution of the SiO_2 substrate by the activity of the diatoms and cyanobacteria.

Figure 7.10 shows the leaching effect of diatoms on glass. Here, diatoms and their accompanying bacteria were embedded in polysaccharides and coated on the surface of glass . After removal of the microorganisms the glass surfaces exhibited depressions and pitting zones (Brehm *et al.*, 2005) consistent with observations of the SiO_2 glass present in the Polonnaruwa stones.

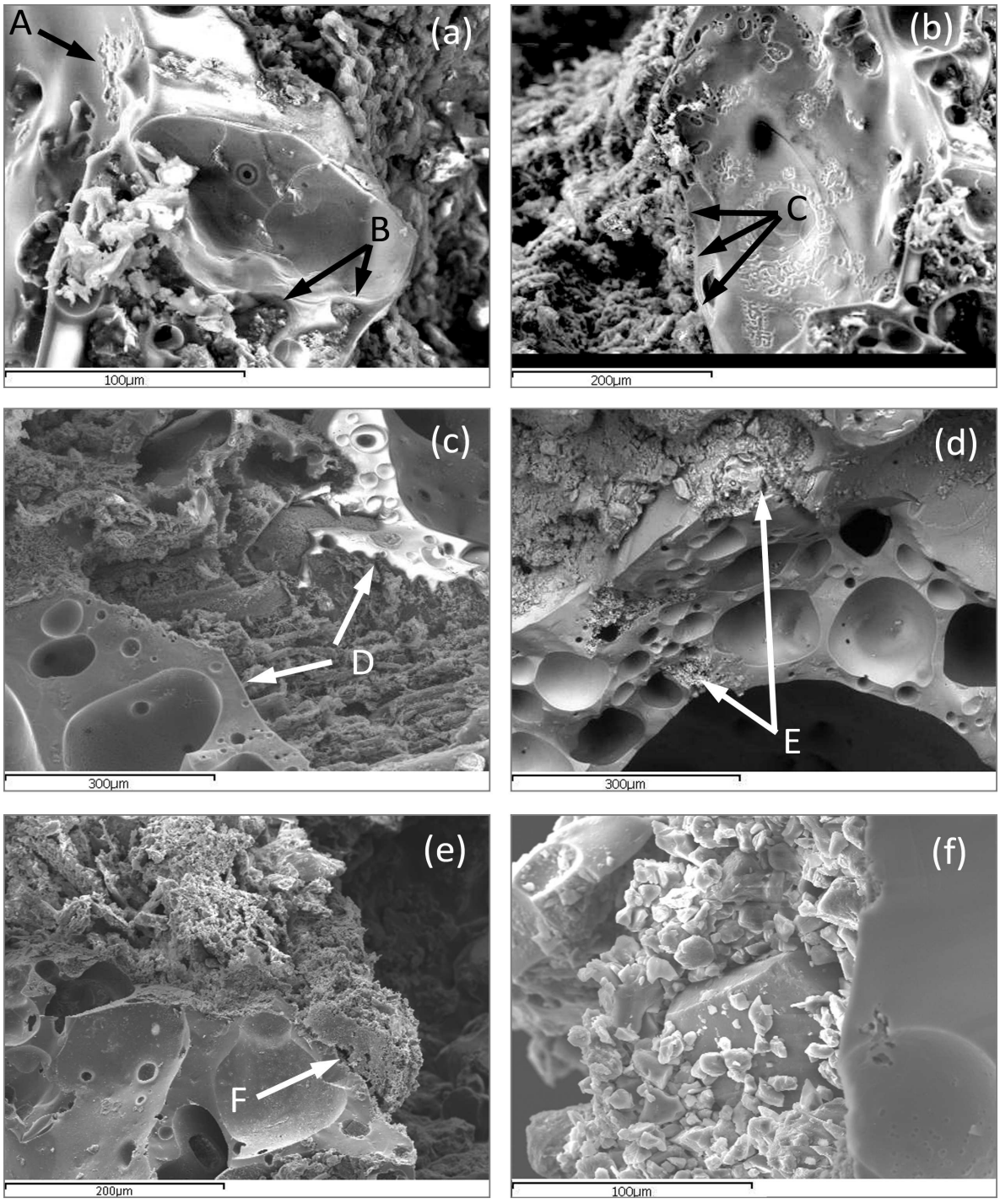

Figure 7.9 Shows SEM images of the interface between amorphous glass and the rougher substrate phases characteristic of biological colonisation. (a) shows degradation of precipitation of the two phases. Arrow A shows evidence of the surface degradation of the K-rich SiO_2 phase while B shows evidence of precipitation of the rought substrate, (b) shows the interface between the two distinct phases as marked by arrow C. (c) shows both clean (lower arrow D) and partly degraded interfaces (upper arrow D) while (e) shows evidence of the separation of the rough precipitate with the main amorphous substrate. (f) shows precipitation of larger more angular fragments.

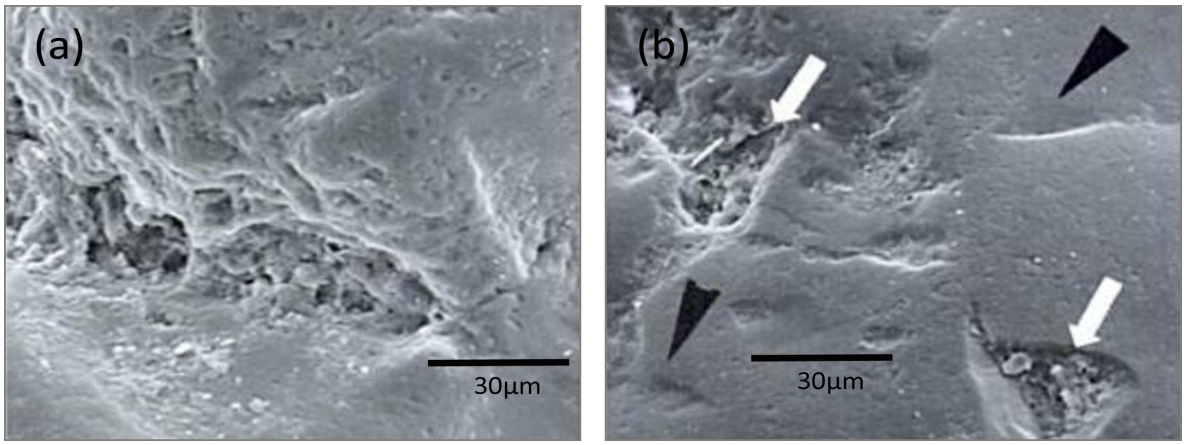

Figure 7.10 (a) shows a close up of a biogenetic pit with traces of two colonies of cyanobacteria (b) comparative micrograph of biogenetic (white arrows) and typical mechanical/chemical pits (black arrows) on quartz surface (Brehm *et al.*, 2005).

7.7 CONCLUSIONS

SEM studies to date have established the following:

a) The highly carbonaceous structures observed in sample P166 are both biological and indigenous to the Polonnaruwa stones. Visual inspection of the SEM images confirmed the presences of multiple examples of clearly biological structures embedded or fused into the sample substrate. Further images showed structures biologically anchored to their surroundings, with numerous further examples of partially degraded and damaged diatom frustules.

b) The biological structures observed comprised entirely of fossil remains. GC-MS analysis confirmed the absence of biologically relevant organic compounds (amino acids) composed of amine (-NH2) and carboxylic acid (-COOH) functional groups that would be expected from the presence of recently living organisms. In particular, Glycine, Glutamic acid, Alanine, Valine, Proline and Aspartic acid that are ubiquitous to all life on Earth were not detected in the sample. Furthermore, EDX elemental comparisons of one biological structure and its attached rock matrix confirmed that elemental exchange had taken place between the structure and the substrate. Finally, N/C atomic ratios indicated that diagenesis had taken place with N/C atomic ratios comparable to coals and kerogen in ancient microfossils.

c) Fossil remains date back at least ~300 Ma. Atomic N/C ratio decrease showed N/C ratios of 0.0064 as an upper limit determined by the 0.5 % detection limit of nitrogen by the EDAX apparatus. This is consistent with 300-350 Ma anthracite (atomic N/C = ~0.007) but also falls within the range of Precambrian microfossils (540 Ma to 4.6 By) where N/C atomic ratios are reported in the range of 0.0015-0.03.

d) The biological microorganisms represent the late stage colonisation of an existing substrate. Examination of the interface between the amorphous glass and the rougher substrate phases characteristic of biological colonisation revealed evidence of microbial pitting consistent with diatom and cyanobacteria dissolution of glass. This demonstrates occupancy and biological activity within the substrate over an extended period of time.

Chapter 8

On the Authenticity and Origin of the Polonnaruwa Stones

8.1 INTRODUCTION

The results of the previous chapter were reported in a series of short bulletins during the early part of 2013 (Wickramasinghe *et al.,* 2013a; Wickramasinghe *et al*., 2013b; Wickramasinghe *et al.*, 2013c; Wickramasinghe *et al*., 2013d). Repudiation of these results – albeit of a perfunctory, ritualistic kind – inevitably followed, and it came as no surprise when it emanated from the ranks of online scientific commentators rather than scientists engaged in active research. Phil Platt (2013) expressed this repudiation in the form of an argument supported by a series of cursory observations borrowed from scientists active in associated areas of research. These observations led Phil Platt to the conclusion that terrestrial contamination by freshwater was the most obvious explanation. In addition to these criticisms, a number of more considered observations were made regarding the possible origin and authenticity of the stone artefacts and their biological cargo.

Early examination of the Polonnaruwa stones at the Department of Geology, University of Peradeniya, and the Arthur C. Clarke Institute for Modern Technologies in Sri Lanka, resulted in initial dismissal of the fragments as possible meteorites (Hiru FM News, 2013; The Sunday Times, 2013). XRD and optical microscope analysis determined that the stones comprised predominantly of amorphous silica together with small quantities of quartz, results that were consistent with similar studies at Cardiff University. This led the Sri Lankan geologists to reject the suggestion of the stone's meteoritic origin on the grounds that any silica should only be present in trace amounts and quartz is rarely observed in meteorites (Korotev, 2005). An alternative explanation that the stones comprised of terrestrial fulgurite, the glassy product of tubes formed when quartzose sand, silica, or soil is heated by lightning strikes was offered (The Sunday Times, 2013).

Subsequent optical and SEM microscopic studies at the Planetary Exploration Research Center in Japan confirmed both bulk chemical composition abundances and petrological observations of the Cardiff study (Arai, 2013). Porosity of between 80-90 % was determined and it was concluded that these values made the artefacts too fragile to be able to survive atmospheric re-entry based on current canonical models. These models show fragile meteorites suffering catastrophic fragmentation at high altitude unless the bolide speed was unusually low or is protected against

thermal shock by vigorous ablation. An alternative terrestrial origin for the stones has consequently been suggested with volcanic glasses being the most likely candidate.

A further attempt to reconcile the triple oxygen isotope results with a terrestrial origin was offered by Pack (2013). Here, it was suggested that the stones may comprise of an industrial by-product that had been thermally processed by high pressure O_2 giving rise to high $\delta^{18}O$ values (17.816 ± 0.100) and possibly explaining the $\Delta^{17}O$ = - 0.335 fractionation phenomenon. The known tropospheric fractionation of O_2 also gave rise to the suggestion that the Polonnaruwa stones may represent the return of previously ejected terrestrial material already embedded with the biological structures (MIT Technoloogy Review, 2013).

One final critiscism of note came in the form of the general observation that the Polonnaruwa stones, comprising principally of amorphous silica, were unlike comparable stones generally recovered from non-terrestrial environments. In effect, the Polonnaruwa stones were unlike any other meteorite, and by implicaton, unlikely to be one.

In the section that follows, each of the above observations is considered in the light of subsequent analysis and experimental results (Wallis *et al.*, 2013a; Wallis *et al.*, 2013b, Wallis, 2014 - this study). A final hypothesis regarding the origin and authenticity of the stones is then presented that incorporates all experimental and observational data acquired to date.

8.2 ATMOSPHERIC ENTRY OF THE POLONNARUWA BOLIDE

In order to examine the likely effects of atmospheric entry on the Polonnaruwa stones it is necessary to consider the motion of a body as it encounters the frictional effects of atmospheric resistence. An object entering the atmosphere from space faces the problem of re-entry and the consequential transformation of its potential energy into kinetic energy. This kinetic energy is lost through deceleration and ablation (Baldwin, 1971; Bronshten, 1983; Melosh, 1989). The motion of the bolide can be described by the equation (Chyba *et. al.*, 1993),

$$m\frac{dv}{dt} = -\frac{1}{2}C_D\rho_a A v^2 + mg\ \cos\theta \qquad eq.8.1$$

where A is the cross sectional area, ρ_a is atmospheric density, g is the gravitational acceleration (a function of height), m mass, v velocity, C_D the drag coefficient and θ the zenith angle of trajectory (Chyba *et. al.*, 1993). Since the bolide is hypersonic its motion compresses the air it encounters into a dense layer that is discontinuous from the surrounding atmosphere. This discontinuity, and the

resulting ionised plasma is called a shock front. Radiation from the shock front heats the bolide causing evapouration or ablation. For the purposes of this calculation, we are going to ignore the term $mg\cos\theta$ as the term is small and contributes little in most cases involvng cometary progenitors. The resulting rate of loss of kinetic energy of the solid meteor, *Q* corresponding to equation 8.1 is then given by,

$$\frac{dQ}{dt} = -\frac{1}{2}C_D\rho_a A v^3 \qquad eq.8.2$$

Some of this energy goes into the processes of ablation such as the latent heat of vaporization of the ablating surface material, absorption of energy (transpiration), convective blockage, viscosity changes and others (Hamm, 1990) and some tranfers to the air. If a fraction f_Q of the energy goes into ablation of the meteor, and if the heat of ablation is ζ then the rate of loss of the meteor mass by ablation is given by,

$$\frac{dm}{dt} = -\frac{1}{2}\left[\frac{f_Q}{\zeta}\right][AC_D\rho_a v^3] \qquad eq.8.3$$

Walker (1986) and Zahnle (1992) determined that the the temperature at the shock front was heavily dependent on thermal ionisation with a very weak dependence on velocity size and composition of the bolide and was consequentially regulated to ~25,000 – 30,000K. The maximum ablation rate is then given by,

$$\frac{dm}{dt} = -\left[\frac{f_Q}{\zeta}\right]A\sigma\, T_{max}^4 \qquad eq.8.4$$

where σ is Stefan's constant and $T_{max} = 25{,}000\,K$ (Biberman *et al.*, 1980). Zahnle (1992) thus suggested rewriting eq. 8.2, which in our notation is

$$\frac{dm}{dt} = -A\left[\frac{f_Q}{\zeta}\right]\min\left(\frac{1}{2}\,C_D\rho_a v^3, \sigma\, T_{max}^4\right) \qquad eq.8.5$$

It is immediatley obvious from eq. 8.5 that the rate of loss of the meteor mass by ablation is heavily dependent on the term $A[f_Q/\zeta]$ i..e the cross sectional area of the incoming bolide (A) and the heat of ablation (ζ). Now the values of the parameters f_Q and ζ are not actually known for most bolides. However, if we consider a cometary progenitor (Leonid meteor) of mass 526 g, and bulk density ~1g cm^{-3}, then the most likely value of the drag coefficient C_D would be about 0.6 (Liepman & Roshko, 1957). By determining the value A (Zinn *et al.*, 2010) we obtain a value of,

$$\left[\frac{f_Q}{\zeta}\right] = 2.1 \text{ x } 10^{-10}\ \text{s}^2\ \text{cm}^{-2}$$

and since f_Q must be less than 1 then this implies ζ must be less than 4.8 x10^9 erg g^{-1}. Zinn *et al.*, (2010) note that this is about five times smaller than the heat of vaporization of ice, and a meteor entering the atmosphere is subject to very large surface shear forces. The energy required to disassociate solid particles from the surface may be much less than the heat of vaporization.

The probability survival dependence on the $\left[\frac{f_Q}{\zeta}\right]$ parameter can also be illustrated by obtaining an expression for the velocity *v* by dividing equation 8.1 with equation 8.3 and rearranging terms to get

$$\left[\frac{f_Q}{\zeta}\right] vdv = \frac{dm}{m} \qquad eq\ 8.6$$

If $\left[\frac{f_Q}{\zeta}\right]$ is taken to be constant we can integrate eq 8.6 to give

$$\left[\frac{f_Q}{\zeta}\right]\left[v^2 - v_i^2\right] = \ln\frac{m}{m_i} \qquad eq.\ 8.7$$

where m_i and v_i are the initial mass and velocity of the bolide prior to encountering the atmosphere. It can be seen that in the case of fast moving objects like the Leonids for which v_i is quite large (about 70 km/s, or 7 x 106 cm/s), unless $\left[\frac{f_Q}{\zeta}\right]$ is smaller than about 1 x 10^{-12} s^2 cm^{-2} the velocity remains essentially constant until the meteor is almost completely ablated away Zinn *et al.*, (2010).

It would be fortunate if we could derive the value of $\left[\frac{f_Q}{\zeta}\right]$ for the Polonnaruwa stones theoretically, but this parameter is a function of both the material and the environment to which it is subjected and requires the characteristics of the flow of a liquid layer under the influence of a hypersonic gaseous boundary layer (with mass transfer) to be determined. These equations are highly complex due primarily to the variation of viscosity with temperature, but also because of the need to match parameters at the interface with the dissociated gaseous hypersonic boundary layer (Steg and Lew, 1972). Fanucci and Lew (1959) modelled the flow of a liquid layer with vaporization under the influence of a gaseous hypersonic boundary layer, taking account of variation between laminar and turbulent flow. These were made a funtion of the region of the body concerned and a proper account of the history of the flow from the stagnation point was considered. Their results were confirmed by the analysis of Scala (1960) under reduced considered conditions.

For commonly encountered meteors the $\left[\frac{f_Q}{\zeta}\right]$ parameter is normally deduced by applying observed ablation coefficients to the known heat of vapourisation appropriate to iron, stoney and cometary progenitors. Baldwin and Sheaffer (1971) determined the heat of vapourisation for iron and stoney

meteorites to be 8 x 10^{10} erg g^{-1}. However, while this process benefits from the application of observational parameters in commonly encountered meteoroids, it does not apply well in situations such as the Polonnaruwa stones, where the composition of the material differs from the normal stone, iron or carbonaceous component. The heat of ablation of fused silica (such as in the Polonnaruwa stones) is likely to differ significantly from that of the carbonaceous or stoney meteorites since its melt is highly viscous so that the liquid can be heated to near boiling temperature before aerodynamic forces remove it. Amorphous SiO_2 by its very nature may be super-cooled without the molecules falling into the ordered array of a crystal. Gruntfest (1959) and Sutton (1960) showed that data on glasses indicate that amorphous SiO_2 has the highest viscosity and under certain conditions gives evidence of superior ablation characteristics.

Furthermore, high silica glasses are known to be resistent to thermal shock (Steg and Lew, 1962) and when vapourised form both the gaseous dioxide and monoxide in the following highly endothermic reactions:

$$SiO_2\ (s) \rightleftharpoons SiO_2\ (1) \rightleftharpoons SiO\ (g) + \frac{1}{2} O_2\ (g) \qquad \text{eq. 8.8}$$

$$SiO_2\ (s) \rightleftharpoons SiO_2\ (1) \rightleftharpoons SiO_2\ (1) \qquad \text{eq. 8.9}$$

These reactions indicate that the heated solid dioxide softens and forms a liquid layer which vapourises and injects the gaseous dioxide, the monoxide, and the oxygen into the gaseous boundary layer, thickening the layer (Steg and Lew, 1962). The effect of the above is to distance the dissociated gaseous hypersonic boundary layer from the bolide surface decreasing the heat flux to the surface.

This has long been recognised as a crtical feature in minimising ablation and was first suggested during the 1950s when the thermal problems of atmospheric re-entry were encountered with missiles of ever increasing range. A model flow diagram is presented in figure 8.1 showing the movement of the liquid layer vapourising and injecting gaseous dioxide, monoxide and oxygen into the boundary layer effectively forcing the shock front from the bolide surface.

The heat of ablation properties of amorphous silica has been investigated in several studies that have demonstrated its substantial qualities for thermal protection. Steg and Lew (1962) examined ablation rates for satellite re-entry trajectories, and compared ablation rates of amorphous SiO_2 with those of highly protective materials such as teflon and graphite.

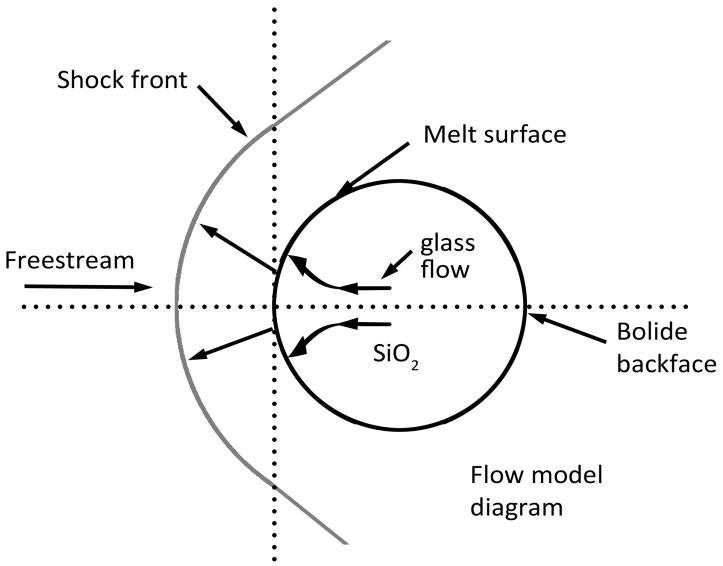

Figure 8.1 Model flow diagram showing the movement of the liquid layer vapourising and injecting gaseous dioxide, monoxide and oxygen into the boundary layer

The results, are shown in figure 8.2 and demonstrate that amorphous SiO_2 offers substantial thermal protection with consequentially low backface temperatures.

Early experiments by Centolanzi and Chapman, (1966) on the mass loss of fused silica during aerodynamic ablation provide an indication of the SiO_2 heat of ablation parameter. In their experiment an enthalpy equivalent to a flight velocity of 9.6 km sec^{-1} was computed using the properties of silica as listed by Hidalgo (1960) and from peak heating and ablation results suggest a likely heat of ablation of 11,000 cal g^{-1} or 4.6 x 10^{11} erg g^{-1}.

This compares with equivalent values of 0.8 x 10^{11} erg g^{-1} for iron and stone pregenitors and 0.25 x 10^{11} erg g^{-1} for carbonaceous chondrites (Chyber, 1993). The maximum ablation rate given by eq. 8.4 is also dependent on cross sectional area. A simple calculation of mass ratios shows stone meteroites would be subject to a cross sectional area scaling factor of ~1.7, carbonaceous meteorites ~2.3 and the Polonnaruwa stones about ~6.3, given equal mass projenitors to those of iron meteorites. This implies that the maximum rate of ablation would increase by a factor of ~6.3 for the Polonnaruwa stones over an iron or stone meteorite, but improved heat of ablation parameters would then reduce this such that the Polonnaruwa stones would suffer a rate of maximum ablation close to that of iron meteorites but less than that of mass equivalent stone meteroites.

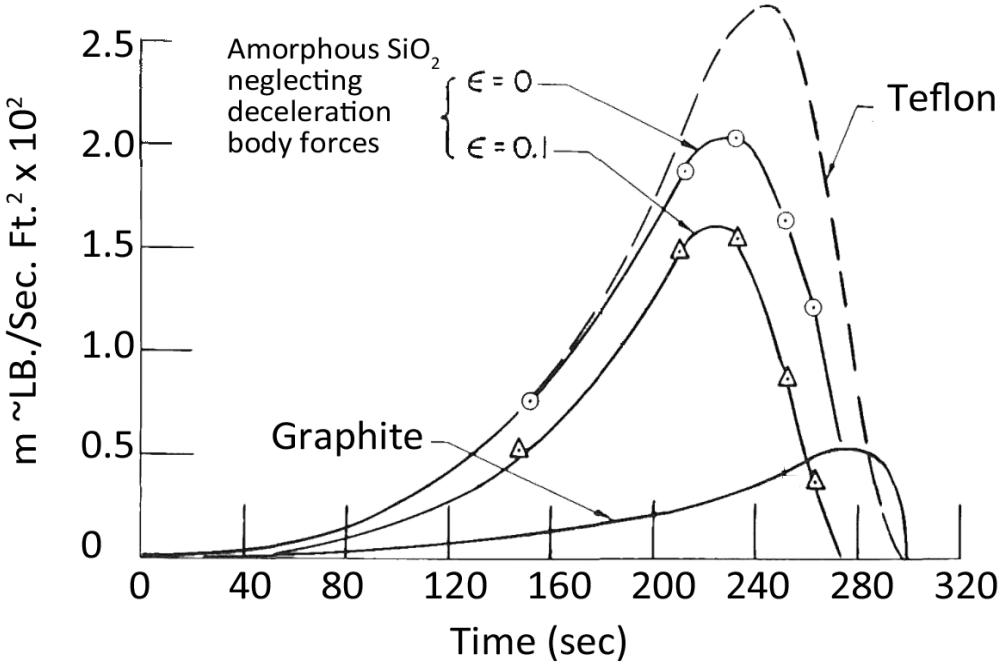

Figure 8.2 Material ablation rates for satellite re-entry trajectories. Figure adapted from Steg and Lew (1962)

The strength of a meteoroid is commonly considered through the application of a one-dimensional index that gauges the relative strength of a meteoroid (bulk density, fragmentation propensity and ablation rate) based on the luminous fireball end height. This PE value is defined by Cepla and McCrosky (1976) as

$$PE = \log(\rho_E) - 0.42\ \log(m_\infty) + 1.49 \log(V_\infty) - 1.29\ \log(\cos Z_R) \qquad eq.8.10$$

where ρ_E is the atmospheric mass density at the height of the fireball endpoint; m_∞ is the entry mass; V_∞ is the entry speed and Z_R is the entry angle from the Zenith. Larger PE values correspond to stronger material showing less ablation. Because tensile strength is inversely proportional to density, it is commonly assumed that less dense meteoroids face lower prospects of survival. This is certainly true for carbonaceous meteroites but would not apply to the Polonnaruwa stones. Furthermore, traditional modelling implies some common characteristics for possible meteorite producing fireballs including relatively low end heights (<35km) and low terminal velocities (< 10 km s^{-1}). Again, this would not apply in the case of a porous silica glassy ablator of the Polonnaruwa type due to its viscosity characteristics during ablation.

These popular modelling parameters present a further problem and have led to a strong bias towards only searching for meteorites from the very brightest fireballs (Halliday *et al.*, 1989). This may be the reason that prior to the last decade only three meteroites had been recovered among the >1000 fireballs recorded by the major photographic fireball networks. More recently, the more intensive spirit of meteorite search and recovery coming from amateur meteorite collectors (which led to the Maribo meteorite being recovered) could assist in recovering meteorites from far more modest fireballs. Of note, Brown *et al.*, (2013) consider that that current perceptions of likely meteorite producing fireballs has seriously biased the type of material currently being recovered.

Consideration of the atmospheric entry characteristics of the Polonnaruwa stones clearly indicates that these stones would certainly survive atmospheric re-entry. These arguments are intuitively correct. The Polonnaruwa stones comprise of an amorphous silica matrix with ~90 % porosity. Early thermal protection systems developed for the space shuttle program comprised of a matrix of silica glass of ~ 94% porosity while a 10 cm cube of the material could readily be crushed in one hand.

8.3 TERRESTRIAL ORIGIN HYPOTHESIS

The suggestion that the Polonnaruwa stones comprised of terrestrial fulgurites was discussed in Wallis *et al.*, (2013) where the hypothesis was challenged on a number of grounds. Firstly, fulgurites have an average density of ~2.50 g cm^{-3}, which is inconsistent with the density of the Polonnaruwa stones at <1 g cm^{-3} suggesting a different formation process. Secondly, none of the stones examined were in the form of hollow tubes or required excavation from the ground which are characteristic features of fulgurites. Thirdly, the temperature required to melt quartose sand and form a fulgurite (1,770 °C) would certainly have vaporized and burned all carbon-rich biological (cyanobacterial filaments, hystrichospheres, etc.) structures. Fourthly, representative oxide compositions for SiO_2 (73-76 wt%) were low in Polonnaruwa stones compared to terrstrial fulgarites that showed values of between 90.2 wt% (Holland) to 99.0 wt% (Illinois) (Saikia *et al*., 2008) while K_2O values (9-14 wt%) were too high compared to typical values for fulgurites of between 0.5-0.75 wt%. Finally, the results of triple oxygen isotope analysis give a $\Delta^{17}O$ value of -0.335 which is incosistent with previous studies on the oxygen isotope composition of fulgurites (Robert and Javoy, 1992) that showed no marked isotope exchange with atmospheric molecular oxygen during the formation process.

One further hypothesis is that the Polonnaruwa stones comprise of pumice, a volcanic material created when super-heated, highly pressurized rock is violently ejected from a volcano. Pumice is

composed of highly microvesicular glass with a porsity of ~90 %, similar to that of the Polonnaruwa stones. Under light microscope petrological features between pumice and the Polonnaruwa stones are not that dissimilar while variations in bulk chemical compositions can be readily explained in terms of heteorgeneity or origin. Other volcanic glasses have also been suggested and are included in the analysis for the purpose of this discussion.

Abundant data is available on terrestrial glasses of volcanic or mid-ocean ridge basalt (MORB) origin (e.g. Dixon *et al.*, 1988; Sisson and Layne, 1993 and references therein). Much of this data relates to the structurally bound H_2O content of the glasses and provides a useful yardstick for comparison. Similarly, the H_2O content of tecktites and impactites has long been recognised as a distinguishing quantity between glassess of impact origin and those of volcanic origin. Impactites are glasses that are formed by hypervelocity impacts on Earth and represent melts of surficial, predominantly sedimentary, precursor rocks of upper crustal composition (Koeberl, 1994). Tektites are a sub-group of impactites thought to arise from the vapourisation and subsequent rapid atmospheric cooling of melt components.

The possibility that the Polonnaruwa stones could represent the residue of a hypervelocity impact melt on Earth should also be considered. However, this hypothesis is inconsistent with the triple oxygen isotope analysis. The $\delta^{18}O$ values of terrestrial impactites are typially between + 9‰ and +11.5‰. The Polonnaruwa $\delta^{18}O$ values are high at 17.816‰ ± 0.100‰. More significantly, terrestrial impactites exhibit no oxygen fractionation with $\Delta^{17}O \sim 0$, whereas the Polonnaruwa stones exhibit significant variation from the terrestrial fractionation trend with a $\Delta^{17}O$ value of -0.335 ± 0.011.

The $\delta^{18}O$ values of the Polonnaruwa stones poses further difficulties when considering precursor rock compositions. The observation that terrestrial impactites typically have $\delta^{18}O$ values ~4 to 4.5‰ lower than their host materials (Blum and Chamberlain, 1992; Taylor and Epstein, 1966; Blum JD *et al.* 1992; Jones, 1985) would imply a $\delta^{18}O$ value for the parent mix of the Polonnaruwa stones of ~22.5‰. This would suggest a likely carbonate or pelagic clay parent rock ($\delta^{18}O$ from ~19 to 28‰ for carbonates and ~17 to 24.5‰ for pelagic clays). The ultramafic, basaltic, andersite and rhyolite rocks are too low ($\delta^{18}O$ values < 11‰) though the upper limit for siliciclastic metamorphic rocks is closer at ~ 21‰ (all data $\delta^{18}O$ values from Bindman, 2008). However, the chemical compositions of the Polonnaruwa stones do not favour a carbonate or pelagic clay precursor, both of which contain notable quantities of Al_2O_3 which is absent in the Polonnaruwa stones. The abundance of Al_2O_3 in terrestrial impactites is approximately comparable to their precursor parent and its absence in the Polonnaruwa stones strongly implies absence as a notable component in the parent body. In

summary, the evidence detailed above amounts to an insuperable obstacle for the terrestrial origin model of the Polonnaruwa stones by any natural process.

8.4 ANTHROPOGENIC ORIGIN HYPOTHESIS

An attempt to reconcile the triple oxygen isotope results with a terrestrial origin was offered by Pack (2013). Here, it was speculated that the stones may comprise of a steel slag produced using high purity O_2 as part of the steel smelting process. Such O_2 would have high $\delta^{18}O$ values and is known to exhibit fractionation values similar to those of the Polonnaruwa stones ($\Delta^{17}O$ = - 0.335). Steel slag is a by product of the steelmaking and steel refining processes that may include basic-oxygen-furnace (BOF) steelmaking, electric-arc-furnace (EAF) steelmaking, and ladle-furnace steel refining processes. In particulr, the slag from the tundish was suggested as a possible area for further investigation since rice husk ash (RHA), a high SiO_2 by product of rice production, is often utilised as a tundish slag to protect the steel melt from contact with atmospheric oxygen.

However the chemical composition of iron smelting slag bears no resemblance to the composition of the Polonnaruwa stones. Table 8.1 shows representative oxide compositions from all three steel making processes. Items 1 to 9 relate to the basic-oxygen-furnace process, items 10 to 15 to the electric-arc-furnace process and 16 to 20 to the ladle-furnance process. Data is taken from Das *et al.* (2007), Juckes (2003), Mahieux *et al.* (2009), Poh *et al.* (2006); Shen *et al.* (2009), Shi (2004), Tossavainen *et al*. (2007), Waligora *et al*. 2010), Xuequan *et al.* (1999), Barra *et al.* (2001), Luxán *et al*. (2000), Manso *et al.* (2006), Shi (2004), Tossavainen *et al.* (2007), Tsakiridis *et al.* (2008), Nicolae *et al*. (2007), Shi (2004), Qian *et al.* (2002), Setién *et al*. (2009), Tossavainen *et al.* (2007) respectively. In particular, tundish slag is known to undergo major changes during the casting process with consequential enrichment of TiO_2, Al_2O_3, MnO, CaO, MgO, and Na_2O. It is noted that Al_2O_3 is absent as a major component of the Polonnaruwa stones, with bulk elemental Al in both XRF and ICP-OES independent studies showing abundances <500 ppm.

Furthermore, the oxygen isotope composition of the Polonnaruwa stones is found to be inconsistent with that of tundish slag that originates from reduced rice husks. The $\Delta^{17}O$ value of rice husk has not been analysed but can be deduced from the triple oxygen isotope fractionation exponent for cellulose water. This can be assumed to fall within the range of published low-*T* oxygen isotope equilibrium exponents as provided by Barken and Luz (2005). This method was recently used by Horvath *et al.* (2012) in the $\Delta^{17}O$ calculation for wood based on equilibrium fractionation between cellulose and leaf water. A resulting $\Delta^{17}O \approx$ -0.06‰ (using a reference line with slope 0.522 and zero intercept) was deduced and accorded well with triple oxygen isotope analysis of combusted

CO_2 that showed $\Delta^{17}O$ values sitting on a mixing line of $\Delta^{17}O$ parameters comprising of wood ($\Delta^{17}O$ = -0.06‰) and atmospheric oxygen ($\Delta^{17}O$ = -0.34‰).

The SiO_2 content of roots, stem and leaf (SL) and husks of rice plants has been analysed by Ding *et al.* (2005). These authors confirmed the earlier conclusions of Barber and Shone (1966) that the silica in the rice husks originate from water soluble $Si(OH)_4$ in the soils. Thus the $\delta^{18}O$ values for rice husks would certainly accord with those of woods. Spruce wood has $\delta^{18}O$ ~25‰ (Jaggi *et al.*, 2003) and this high value arises from the equilibrium fractionation between leaf water and cellulose which is ~27‰ (Horvath *et al.,* 2012). The computed $\Delta^{17}O$ = -0.06‰ of Horvath *et al.* (2012) for wood can thus be taken as an applicable parameter for rice husks. However, this value is further diluted in the rice husk reduction process that involves relatively low temperature combustion well below the melting point of silica. Comparable open air combustion experiments reported by Horvath *et al.,* (2012) indicate that ~1/3 of the oxygen in combustion CO_2 sources from oxygen intrinsic to the wood, implying that $\Delta^{17}O$ parameters for rice husk ash would be further reduced. Given that the combustion reduction process for rice husk reduces the dried husk mass by ~80% a resulting $\Delta^{17}O$ ~.01‰ follows.

The reduced rice husk ash is then added in the tundish to protect the molten steel melt from atmospheric O_2. It is immediately obvious that the oxygen fractionation composition of the Polonnaruwa stones would require near 100% isotope exchange with the atmosphere to account for reported $\Delta^{17}O$ of -0.335. No mechanism for the provision of such an istope exchange is known and any isotopic exchange that did take place would result in $\Delta^{17}O$ parameters sitting on a mixing line of $\Delta^{17}O$ parameters comprising of rice husk ash ($\Delta^{17}O$ = -0.01‰) and atmospheric oxygen ($\Delta^{17}O$ = -0.34‰).

This problem becomes worse since isotope exchange with the atmosphere does not occur in the tundish (Pack, 2000) due to the steep temperature gradient in the tundish slag. The top side of the tundish slag is relatively cool and is not molten. Only at the interface between the slag and steel melt a film of silica melt forms (Pack, 2000). Consequently it can be seen that both the triple oxygen isotope composition and the chemical composition of the Polonnaruwa stones is entirely inconsistent with a steel processing slag.

Finally, it is appropriate to consider the possibility that the Polonnaruwa stones may comprise of a by-product of some other industrial process. An immediate observation arsisng from this hypothesis is that such a formation process for the Polonnaruwa stones would be entirely inconsistent with the results of SEM and EDAX analysis presented in the previous chapter.

Table 8.1 – Compositions of Steel Slag

	CaO	SiO_2	Al_2O_3	MgO	FeO	Fe_2O_3	Fe total	SO_3	MnO	TiO_2	P_2O_5	Free CaO
1	47.9	12.2	1.2	0.8	26.3	—	—	0.3	0.3	—	3.3	—
2	36–45	10–15	1–3.4	4–7	—	—	~24	.1–.2	2–4	—	1–1.5	~12
3	47.5	11.8	2	6.3	—	22.6	—	—	1.9	0.5	2.7	—
4	52.2	10.8	1.3	5.04	17.2	10.1	—	—	2.5	0.6	1.3	10.2
5	39.3	7.8	0.98	8.56	—	38.06	—	0	4.2	0.9	—	—
6	30–55	8–20	1–6	5–15	10–35	—	—	.1–0.2	2–8	.4–2	0.2–2	—
7	45	11.1	1.9	9.6	10.7	10.9	—	—	3.1	—	—	—
8	47.7	13.3	3	6.4	—	24.4			2.6	0.7	1.5	9.2
9	45–60	10–15	1–5	3–13	7–20	3–9	—	—	—	—	1–4	—
10	29.5	16.1	7.6	5	—	32.56	—	0.6	4.5	0.78	0.6	—
11	24.4	15.4	12.2	2.9	34.4	—	—	—	5.6	0.56	1.2	—
12	23.9	15.3	7.4	5.1	—	—	42.5	0.1	4.5	—	—	0.5
13	35–60	9–20	2–9	5–15	15–30	—	—	.1–0.2	3–8	—	0–0.3	—
14	38.8	14.1	6.7	3.9	5.6	20.3	—	—	5	—	—	—
15	35.7	17.5	6.3	6.5	—	26.4	—	—	2.5	0.8	—	—
16	49.6	14.7	25.6	7.9	0.44	0.22	0.17	0.8	0.4	—	0.2	—
17	30–60	2–35	5–35	1–10	0–15	—	—	0.1–1	0–5	—	.1–.4	—
18	49.5	19.59	12.3	7.4	—	0.9	—	—	1.4	—	0.4	2.5
19	~55	~16	~12	~9	—	~2.5	—		.4–.5	.3–.9	0.01	~19
20	42.5	14.2	22.9	12.6	0.5	1.1	0.4	—	0.2	—	—	—

Table 8.1 shows chemical compositions of steel making slag. Items 1 to 9 relate to the basic-oxygen-furnace process, items 10 to 15 to the electric-arc-furnace process and 16 to 20 to the ladle-furnance process. Data taken from Das *et al.* (2007), Juckes (2003), Mahieux *et al.* (2009), Poh *et al.* (2006); Shen *et al.* (2009), Shi (2004), Tossavainen *et al.* (2007), Waligora *et al.* 2010), Xuequan et al. (1999), Barra *et al.* (2001), Luxán *et al.* (2000), Manso *et al.* (2006), Shi (2004), Tossavainen *et al.* (2007), Tsakiridis *et al.* (2008), Nicolae *et al.* (2007), Shi (2004), Qian *et al.* (2002), Setién *et al.* (2009), Tossavainen *et al.* (2007) – items 1 to 20 respectively

Here fossil remains of biological structures were found to date back at least ~300 Ma on the basis of atomic N/C decrease trends that showed N/C ratios of 0.0064 as an upper limit. These were comparable to 300-350 Ma anthracite (atomic N/C = ~0.007) and also within the range of 540 Ma to 4.6 Ba Precambrian microfossils.

The further observation of the interface between the amorphous glass and the rougher substrate phases (characteristic of biological colonisation) and of microbial pitting consistent with diatom and cyanobacteria dissolution of glass strongly infer a later stage colonisation of the existing substrate.

This immediately suggests the Polonnaruwa glass matrix is older than its biological cargo, and falls well outside any estimate for the onset of anthropogenic activity.

8.5 COMPARISON OF POLONNARUWA WITH INTERSTELLAR GRAINS

The nature of both the organic and inorganic inventory of comets and interplanetary dust particles (IDPs) is often inferred through the analysis and interpretation of features in the infrared spectra (IR). These features are particularly dominant in the mid-IR (2.5 to 15µm) where both organics and minerals exhibit strong diagnostic bands. A large library of IR spectra has now been amassed that indicates that amorphous silicates are ubiquitous in the interstellar medium and crystalline silicates such as olivine and pyroxene contribute < 2% by mass (Kemper *et al.*, 2004; 2005). These initial results were confirmed by the Stardust mission that returned samples of dust fragments from comet 81P/Wild 2 thus providing an opportunity to obtain FTIR spectra directly from materials of known origin and compare them with both astronomical measurements and laboratory spectra of IDPs.

The mid-IR spectra of cometary material and IDPs is dominated by a broad Si-O stretching absorption feature that occurs between 1050 cm^{-1} and 850 cm^{-1}. The majority of amorphous phases in IDPs occur as glass with embedded metal and sulphide grains (GEMS) typically < 1µm in diameter containing variable amounts of nanophase FeNi metal and Fe sulphide grains (Flynn *et al.*, 2006). Other mineral inclusions range from anorthite to Al, Ti diopside (Joswiak and Brownlee, 2014) and give rise to small inflective features in the 1200 cm^{-1} to 1000 cm^{-1} wavelength range.

Figure 8.3 shows the IR spectra of two dust fragments from comet 81P/Wild 2 recovered during the Stardust mission (C2054,0,35,20 and FC3,0,2,2) compared with similar spectra obtained from the Polonnaruwa and Ratkinda stones (P166/100 and M224/100). Spectra are shown for the range 1300-700 cm^{-1}. The broad similarity in the main absorption feature for amorphous Si-O phases is clear, but some finer features, particularly at ~1150 cm^{-1} and 1080 cm^{-1} wavelengths in the spectra for the cometary particle C2054,0,35,20 and Polonnaruwa sample are also present. This indicates that both bulk and polymineralic inclusions in both samples exhibit some level of similarity.

Furthermore, the widespread occurrence of amorphous silica in non-terrestrial evironments is well documented. Quartz grains embedded in amorphous silica substrates have been reported in the lunar meteorite Asuka-881757 (Ohtani *et al.*, 2011) while impact glasses in general are common in both meteorites (Aoudjehane, *et al.*, 2012) and at meteorite impact sites. Similarly, amorphous silica recovered from non-terrestrial sources is remarkably similar to amorphous silica and silicate phases recovered from non-terrestrial sources. Figure 8.4 (a) shows a scanning electron microscope image

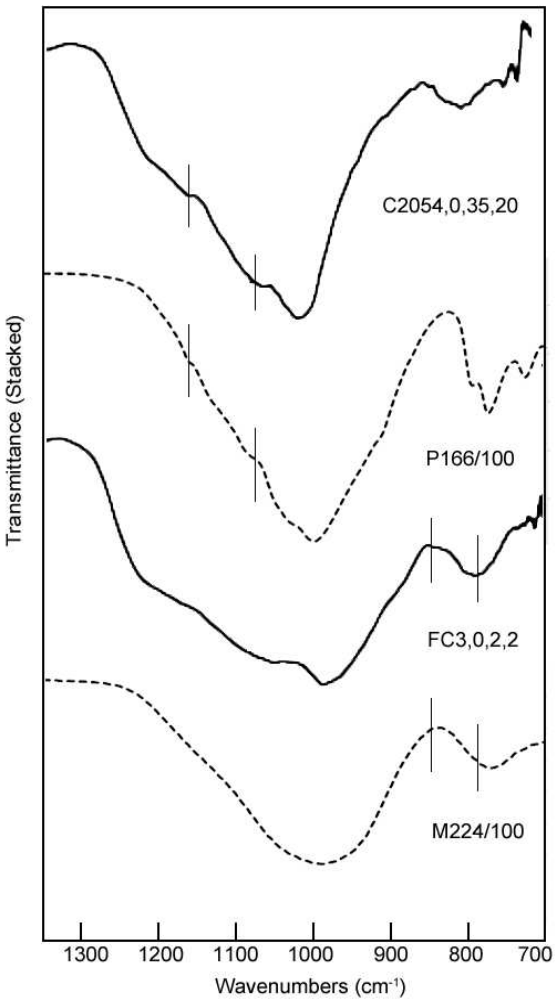

Figure 8.3 FTIR spectra for two dust fragments from comet 81P/Wild 2 recovered during the Stardust mission (labelled C2054,0,35,20 and FC3,0,2,2) compared to similar spectra for Polonnaruwa (P166/100) and Ratkinda stone (M224/100). Note the broad similarity in the main absorption feature for amorphous Si-O phases together with finer features, particularly at ~1150 cm^{-1} and 1080 cm^{-1} wavelengths in the spectra for the cometary particle C2054,0,35,20 and Polonnaruwa sample P166/100.

of a chondritic porous interplanetary dust particle comprising of amorphous silicate and SiO_2 phases while image (b) shows for comparison an amorphous silicate/silica fragment extracted from oil shale residue. Consquently, the suggestion that the composition of the Polonnaruwa stones is at variance with the composition of previously recovered meteorite fragments is inconsistent with the literature.

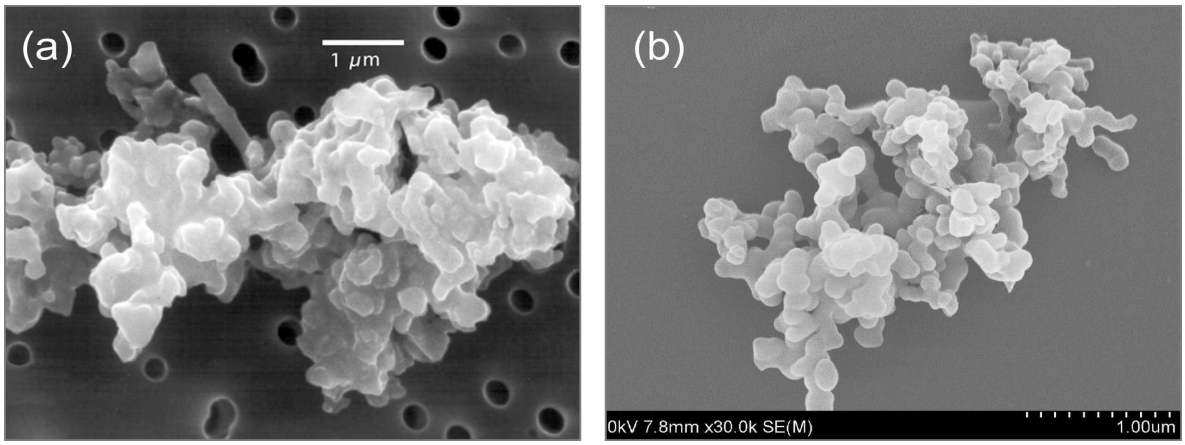

Figure 8.4 Scanning electron microscope image of (a) a chondritic porous interplanetary dust particle and (b) an amorphous silicate/silica fragment extracted from oil shale residue.

8.6 DISCUSSION

The chemical compositions of the Polonnaruwa stones provide a useful indicator of possible source, but these alone are not sufficient to establish their precise origin. Similarities in chemical composition can readily be made with artefacts from non-terrestrial sources, but proceeding on the basis of bulk chemistry alone is likely to lead the argument astray. This has happened with meteorites on more than one occasion and especially with impact glasses where characteristics may represent a refractory residue following severe heating of the source material. Some of the compositions may also represent material condensed from vapour phase in which case few elemental signatures characteristic of the source rock survive. This led to the controversial and stimulating theory on the lunar origin of tektite glasses than lasted over 75 years. Towards the end of the debate, the major advocates, including NASA scientists John A. O'Keefe and aerodynamicist Dean R. Chapman, argued for the lunar origin hypothesis based on REE, isotopic, and bulk compositions (O'Keef, 1978; Provenmire, 2000). Results of complex orbital computer models and wind tunnel tests provided further support for the argument that tektites originated from the Rosse ejecta ray of the large crater Tycho on the Moon's nearside (Chapman, 1971).

The argument was eventually resolved, at least to the satisfaction of most scientists engaged in the debate, in 1969 following the Apollo 11 mission. In the final analysis the issue was decided on three key points. Firstly, the CRE and isotope data established that tektites could only have originated from the Earth or Moon. They could not have arrived from outside the solar system, or indeed from anywhere else within it. Secondly, $\delta^{18}O$ values for tektites ranged between +9‰ and +11.5‰.

Lunar $\delta^{18}O$ values established after the Apollo missions showed that comparable values for Lunar rocks were low. These ranged from +4‰ for ilmenite and +7‰ for cristobalite. In effect, the $\delta^{18}O$ values for tektites fell within terrestrial rock ranges, and outside sampled Lunar rock ranges. Finally, the chemical composition of tektites fell within ranges observed on Earth, with elemental losses during fusion being restricted to elements and compounds more volatile than cesium. In contrast, Lunar basalts exhibited Cr abundances two orders of magnitude higher than tektites, distinctive REE patterns, large Eu anomolies, high Fe and low SiO_2 and others not found in tektites. In effect, the chemical compositions of Tektites fell with the range of observed values on Earth but were discordant with those observed in Lunar rocks.

The same observations can be applied to the terrestrial origin hypothesis of the Polonnaruwa stones. Triple oxygen isotope fractionation parameters ($\Delta^{17}O$ = -0.335‰) are consistent with non-terrestrial sources (e.g. Meta-C chondrites such as B9704 and Y86789 – Clayton and Mayeda, 1999) but fall outside comparable values for terrestrial rocks.

Corresponding $\delta^{18}O$ values for the Polonnaruwa stones ($\delta^{18}O$ = 17.816‰ ± 0.100‰) that match terrestrial rocks (allowing for melt fractionation) imply a precursor carbonate or pelagic clay, yet these would appear incompatable with Polonnaruwa bulk elemental abundances. Finally, N/C atomic ratios of kerogen imply an age (>300My) for the biological cargo that is inconsistent with the geological record. The earliest known diatoms on the Earth are marine centrics (*Pyxidicula* is the oldest dating back 190 million years and described by C.G Ehrenberg in 1833) which places their origin during the Jurassic. However, it remains unclear whether or not diatoms pre-date our observations of the siliceous frustules in the fossil record. It may be that this record represents a bio-mineralisation event and denotes the stage at which these unicellular algae began silicification of their cell walls and may not be evidence of an abrupt appearance or even an evolutionary event. However, molecular clock calculations, which analysed the rate of mutation observed in rRNA indicate it is highly unlikely that diatoms pre-dated 266 Ma ago.

These calculations therefore show that if diatoms did exist and evolve in a ‘non-siliceous’ form then they did so for a maximum period of ~70 Ma (meaning they could not predate the Permian) making their appearance in the record abrupt and sudden whether their earliest existence was in siliceous form or not. Moreover, the remaining classes appear at discrete points over a geologically long period of time. The early species were exclusive to marine environments and lived only in the Earth’s oceans and seas. The araphid pennates are not observed in the record until the Campanian of the Upper Cretaceous ~75 Ma ago and these were also exclusive to wet habitats of high salinity. It

isn't until the middle Eocene ~45 Ma ago, a 145 Ma after their first appearance in terrestrial ecosystems do we observe freshwater (pennate and centric forms) diatoms for the very first time.

The long time period that lapsed between the first appearance of marine diatoms and the first appearance of freshwater diatoms is difficult to reconcile with the relatively fast rate of evolution exhibited by centric diatoms, the conditions on the Earth throughout this period and the fact that terrestrial elements would have delivered an abundance of marine diatom species into freshwater.

Hoover *et al* (1986) explain this time anomaly and the abrupt appearance of the different diatom groups within the fossil record by suggesting that diatoms did not evolve on the Earth. Instead, the theory of Panspermia could explain these observations as the different groups being introduced to the terrestrial ecosystem by different impact events occurring from outside the Earth.

An alternative hypothesis, and the one favoured here, is that the Polonnaruwa and Ratkinda stones represent the non-volatile mass fraction of a comet that suffered a localised impact event (but not catastrophic destruction) resulting in the formation of K-Si-rich impact melts. These melt areas were then recolonized by diatom and cyanobacteria colonies present in sub-surface liquid water pockets during the remaining life of the comet. As such, the Polonnaruwa stones represent the first well documented example of a meteorite carrying undeniably non-terrestrial biological morphologies providing substantial support for the Hoyle-Wickramasinghe Panspermia hypothesis.

REFERENCES

Abel, D. L. (2009) 'The Universal Plausibility Metric (UPM) & Principle (UPP), Theor Biol Med Model', *Academia.edu,* 6(1), pp. 27. [Online]. Available at: http://www.academia.edu/1203732/Abel_D.L._2009_The_Universal_Plausibility_Metric_UPM_and_Principle_UPP_Theor_Biol_Med_Model_6_1_27 (Accessed: 19 January 2014).

Abel, D. L. and Trevors, J. T. (2006) 'Self-organization vs. self-ordering events in life-origin models', *Physics of Life Reviews*, 3(4), pp. 211.

Ahrenkiel, R. K. (1971), 'Modified Kramers-Kronig Analysis of Optical Spectra', *Journal of the Optical Society of America*, 61(12), pp. 1651.

Aiken, G. R., McKnight, D. M., Wershaw, R. L., and MacCarthy, P. (1985) *Humic Substances in Soil, Sediment and Water: Geochemistry, Isolation and Characterization*. Hoboken: Wiley-Interscience Publications.

Aitken, D. K., Roche, P. F., Spenser, P. M. and Jones, B. (1979) '8-13 micron spectrophotometry of planetary nebulae', *ApJ*, 233, pp. 925.

Akashi, K. I., Miyata, H., Itoh, H. & Kinosita, K. Jr. (1996) 'Preparation of giant liposomes in physiological conditions and their characterization under an optical microscope', *Biophysical Journal*, 71(6), pp. 3242–3250.

Alexander, C.M.O'D., Fogel, M., Yabuta, H. and Cody, G. D. (2007) 'The origin and evolution of chondrites recorded in the elemental and isotopic compositions of their macromolecular organic matter', *Geochimica Cosmochimica Acta*, 71, pp. 4380-4403.

Allen, D. A. and Wickramasinghe, D. T. (1981) 'Diffuse interstellar absorption bands between 2.9 and 4.0 μm', *Nature*, 294, pp. 239–240.

Allwood, A. C., Walter, M. R. and Marshall, C. P. (2006) 'Raman spectroscopy reveals thermal palaeoenvironments of c. 3.5 billion-year-old organic matter', *Vibrational Spectroscopy*, 41(2), pp. 190–197.

Altermann, W. (2000) 'The oldest fossils of Africa—a brief reappraisal of reports from the Archean', *Journal of African Earth Sciences*, 33(3), pp. 427–436.

Anders, E. (1962) 'Meteoritic Hydrocarbons and Extraterrestrial life', *Annals of the New York Academy of Sciences*, 93, pp. 651-657.

Anders, E. and Fitch, F. (1962) 'Search for organized elements in carbonaceous chondrites', *Science*, 138, pp. 1392-1399.

Anders, E. and Grevesse, N. (1989) 'Abundances of the elements: Meteoritic and solar', *Geochimica Cosmochimica Acta*, 53, pp. 197–214.

Anders, E., Dufresne, E. R., Hayatsu, R., Cavaille, A., Dufresne, A. and Fitch, F. W. (1964) 'Contaminated meteorite', *Science*, 146, pp. 1157-1161.

Aoudjehane, H. C., Jambon, A., Boudouma, O., Barrat, J. A., Greenwood, R. C. and Franchi, I. A. (2012) *'Tissint: The First Martian Meteorite Falll of the Century in Morocco': 75th Annual Meteoritical Society Meeting.* Cairns, 12 – 17 August 2012.

Arai, T. (2013) [*email communication*].

Arrhenius, S. (1903) 'The Propagation of Life in Space', *Die Umschau*, 7, pp. 481.

Arrhenius, S. (1908) *Worlds in the Making; the evolution of the universe.* Harper: London.

Asta, M. P., Cama, J., Soler, J. M., Arvidson, R. S. and Luttge, A. (2008) 'Interferometric study of pyrite surface reactivity in acidic conditions', *Am. Mineral.*, 93, pp. 508–519.

ASTM, (1996) 'Preparing coal samples for microscopical analysis by reflected light', *In Annual book of ASTM Standards, Part 26, D2979, Gaseous Fuels: Coal and Coke*, ASTM: West Conshohocken, PA.

Baas, F., Geballe, T. R., Walther, D. M. (1986) 'Spectroscopy of the 3.4 micron emission feature in comet Halley: Part 2 - Letters to the Editor (ISSN 0004-637X)', *Astrophysical Journal*, 311, pp. 97-101.

Bada, J. L., Glavin, D. P., McDonald, G. D. and Becker, L. (1998) 'A Search for Endogenous Amino Acids in Martian Meteorite AL84001', *Science* 279, pp. 362-365.

Baker, V. R. and Milton, D. J. (1974) 'Erosion by catastrophic floods on Mars and Earth', *Icarus*, 23, pp. 27–41.

Baldwin, B. and Shaeffer, Y. (1971) 'Ablation and breakup of large meteoroids during atmospheric entry', *J. Geophys. Res.* 76, pp. 4653-4668.

Barber, D. A., and Shone, M. G. T. (1966) 'The absorption of silica from aqueous solutions by plants', *J. Exp. Bot.*, 17, pp. 569–578.

Barkan, E. and Luz, B. (2005) 'High precision measurements of 17O 16O and 18O 16O ratios in H2O,' *Rapid Commun. Mass Spectrom.* 19, pp. 3737–3742.

Barra, M., Ramonich, E. V. and Munoz, M. A. (2001) 'Stabilization of soils with steel slag and cement for application in rural and low traffic roads', in *Proceedings of the Beneficial Use of Recycled Materials in Transportation Application*, pp. 423–432. Arlington: RMCR University of Durham.

Barrat, J. A., Zanda, B., Maynier, F., Bollinger, C., Liorzou, C. and Bayon, G. (2012) 'Geochemistry of CI chondrites: Major and trace elements, and Cu and Zn Isotopes', *Geochimica Cosmochimica Acta*, 83, pp. 79-92.

Bass, M. N. (1971) 'Montmorillonite and serpentine in Orgueil meteorite', *Geochimica Cosmochimica Acta*, 35, pp. 139-147.

Bauer, M., (2008) *Influence of Natural Organic Matter on the Mobility of Arsenic in Aquatic Systems, Soils and Sediments*. PhD Thesis. Universität Bayreuth.

Beaumont, V. and Robert, F. (1999) 'Nitrogen isotope ratios of kerogens in Precambriancherts: a record of the evolution of atmosphere chemistry?' *Precambr. Res.*, 96, pp. 63–82.

Bebie, J. A. and Schoonen, M. A. A. (2000) 'Pyrite surface interaction with selected organic aqueous species under anoxic conditions', *Geochemical Transactions*, 1(47).

Becker, L., Popp, B., Rust, T. and Bada, J. L. (1999) 'The origin of organic matter in the martian meteorite ALH84001', *Earth and Planetary Science Letters*, 167, pp. 71-79.

Becquerel, P. (1924) 'La Vie Terrestre provient-elle d'un Autre Monde?: Bulletin', *Astronomical Society*, 38, pp. 393-417.

Bennett, J. C. and Tributsch, H. (1978) 'Bacterial leaching on pyrite crystal surfaces', *J.Bacteriol*, 134, pp. 310–317.

Beny-Bassez, C. and Rouzaud, J. M. (1985) 'Characterization of carbonaceous materials by correlated electron and optical microscopy and Raman microspectroscopy', *Scanning Electron Microscopy*, 1, pp. 119–132.

Beran, A. and Koeberl, C. (1997) 'Water in tektites and impact glasses by FTIR spectrometry', *Meteoritics and Planetary Science*, 32, pp. 211-216.

Bernal, J. D. (1951) *The Physical Basis of Life*, London: Routledge and Kegan Paul.

Bernard, S., Benzerara, K., Beyssac, O., Menguy, N., Guyot, F., Brown, G. E. and Goffe, B. (2007) 'Exceptional preservation of fossil plant spores in high-pressure metamorphic rocks', *Earth and Planetary Science Letters*, 262, pp. 257–272.

Bertie, J. E., Labbe, H. J. and Whalley, E. (1969) *Journal of Physical Chemistry*, 50, pp. 4501.

Biberman, L. M., Bronin, S. Y. and Brykin, M. V. (1980) 'Moving of a blunt body through the dense atmosphere under conditions of severe aerodynamic heating and ablation', *Acta Astronautica*, 7(1), pp. 53.

Bigg, E. K. (1984) *Fundamental Studies and the Future of Science*, [ed. Wickramasinghe, N.C.], Cardiff: University College Cardiff Press.

Biggs, M. H. and Kitto, G. B. (1962) 'Complex organic micro-structures in the Mokoia meteorite', *Nature*, 193(4821), pp. 1126-1127.

Bindeman, I. (2008) 'Oxygen Isotopes in Mantle and Crustal Magmas as Revealed by Single Crystal Analysis', *Reviews in Mineralogy & Geochemistry*, 69, pp. 445-478.

Bischoff, A. and Stoffler, D. (1993) 'Shock metamorphism as a fundamental process in the evolution of planetary bodies: Information from Meteorites', *European Jounrnal of Minerology*, 4, pp. 707-755.

Blum, J. D. and Chamberlain, C. P. (1992) 'Oxygen isotope constraints on the origin of impact glasses from the Cretaceous-Tertiary Boundary', *Science*, 257(1) pp. 1104-1107.

Blum, J. D., Papanastassiou, D. A. and Koeberl, C. and Wasserburg, G.J. (1992) 'Nd and Sr isotopic study of Australasian tektites: New constraints on the provenance and age of target material', *Geochim Cosmochim Acta*, 56, pp. 483-492.

Blum, S. J., Burns Bindi, A., Buzzelli, J., Stolz, J. G. and Oremland, R. S. (1998) 'Bacillus arsenicoselenatis, sp. nov., and Bacillus selenitireducens, sp. nov.: two haloalkaliphiles from Mono Lake, California that respire oxyanions of selenium and arsenic', *Arch. Microbiol*., 171, pp. 19.

Böhler, C., Nielsen, P. E. and Orgel, L. E. (1995) 'Template switching between PNA and RNA oligonucleotides', *Nature*, 376(6541), pp. 578-81.

Bower, D. M., Steele, A., Fries, M. D. and Kater, L. (2013) 'Micro Raman spectroscopy of carbonaceous material in microfossils and meteorites: improving a method for life detection', *Astrobiology*, 13, pp. 103-113.

Brack, A., Baglioni, P., Borruat, G., Brandstatter, F., Demets, R., Edwards, H. G. M., Genge, M. J., Kurat, G., Miller, M. F., Newton, E. M., Pillinger, C. T., Roten, C. A. and Wasch, A. (2002) 'Do meteoroids of sedimentary origin survive terrestrial atmospheric entry? The ESA artificial meteorite experiment STONE', *Planetary and Space Science*, 50, pp. 763 – 772.

Bradley, J. P. (2003) 'Interplanetary Dust Particles', *Treatise on Geochemistry*, 1, [Editor: Andrew M. Davis. Executive Editors: Heinrich D. Holland and Karl K. Turekian], pp. 689-711. ISBN 0-08-043751-6. Elsevier.

Bradley, J. P., Brownlee D. E. and Fraundorf, P. (1984) 'Carbon compounds in interplanetary dust: Evidence for heterogeneous catalyses', *Science*, 223, pp. 56-58.

Brasier, M. D., McLoughin, N., Green, O. and Wacey, D. A. (2006) 'Fresh look at the fossil evidence for early Archaean cellular life', *Philosophical Transactions of the Royal Society Biological Sciences*, 361, pp. 887–902.

Brearley, A. J. (1998) 'Magnetite in ALH84001: Product of decomposition of ferroan carbonate', *Lunar and Planetary Science XXIX*, Abstract no. 1451, CD-ROM.

Brearley, A. J. (2003) 'Magnetite in ALH 84001: An origin by thermal decomposition of Fe-bearing carbonate', *Meteoritics & Planetary Science*, 38, pp. 849-870.

Brehm, U., Gorbushina, A. A. and Mottershead, D. (2005) 'The role of microorganisms and biofilms in the breakdown and dissolution of quartz and glass', *Palaeogeography, Palaeoclimatology and Palaeoecology*, 219, pp. 117–129.

Brewster, M. Q. and Kunitomo, T. (1984) 'The Optial Constants of Coal, Char, and Limestone' *Transactions of the ASME*, 106, pp. 678-683.

Briggs, M. H. and Kitto, G. B. (1962) 'Complex organic micro-structures in the Mokoia meteorite', *Nature*, 193, pp. 1123.

Britt, D. T. and Consolmagno, G. J. (2003) 'The Density and Porosity of Meteorites: A review of the data through 2001', *Meteoritics and Planetary Science*, 38, pp. 1161-1180.

Bronshten, V. A. (1983) *Physics of Meteoritic Phenomena*, Dordrecht: Reidel Publishing Company.

Brooke, T. Y., Tokunaga, A. T. and Knacke, R. F. (1991) 'Detection of the 3.4 micron emission feature in Comets P/Brorsen-Metcalf and Okazaki-Levy-Rudenko (1989r) and an observational summary', *Astronomical Journal*, 101, pp. 268–278.

Brown, P., Marchenko, V., Moser, D. E., Weryk, R. and Cooke, W. (2013) 'Meteorites from meteor showers: A case study of the Taurids', *Meteorit. Planet. Sci.*, 48, pp. 270–288.

Brownlee, D. E. (1978) 'Microparticle studies by sampling techniques, in Cosmic Dust', *Cosmic Dust*, ed. McDonnell, J. A. M., New York: J. Wiley Interscience Publications.

Brownlee, D., Tsou, P., Aleon, J., Alexander, C. and Araki, T. et al. (2006) 'Comet 81P/Wild 2 Under a Microscope', *Science*, 314, pp. 1711–1716.

Brucato, J. R., Rotundi, A. and Epifani, E. M. (2009) 'Sample return missions from minor bodies: Achievements, future plan and observational support', *Earth, Moon, and Planets*, 105, pp. 273–282.

Buckley, A. N. and Walker, W. (1988) 'The surface composition of arsenopyrite exposed to oxidizing environments', *Applied Surface Science*, 35, pp. 227 –240.

Buick, R. (2001) *Paleobiology II*, eds. Briggs, D. E. G. and Crowther, P. R., Malden: Blackwell Science Limited.

Bukovský, A. (1915) 'The Poisonous Earth from Kutná Hora (in Czech)' *prebiotic environment. Phil. Trans. R. Soc. B*361, pp. 1809–1818.

Bunch, T. E., Cohen, J. and Dence, M. R., (1967) 'Natural Terrestrial Maskelynite', *The American Minerologist*, 52, pp. 244-253.

Busemann, H., Alexander, C. M. O'D. and Nittler, L. R. (2011) 'Carbon Raman Spectroscopy Results on Stardust, Interplanetary Dust Particles And Meteorites', *Corals II* . Abstract #4086.

Busemann, H., Alexander, C. M.O'D. and Nittler, L. R. (2007) 'Characterization of insoluble organic matter in primitive meteorites by microRaman spectroscopy', *Meteorit and Planetary Science*, 42, pp. 1387–1416.

Bustin, R. M., Mastalerz, M. and Wilks, K. R. (1993) 'Direct determination of carbon, oxygen, and nitrogen content in coal using the electron microprobe', *Fuel*, 72, pp. 181-185.

Cairns-Smith, A. G. (1966) 'The origin of life and the nature of the primitive gene', *Journal of Theoretical Biology*, 10, pp. 53.

Capps, R. W., Gillett, F. C. and Knacke, R. F. (1978) 'Infrared observations of the OH source W33A', *Astrophys. J.*, 226, pp. 863.

Carr, M. H. (1978) 'Formation of martian flood features by release of water from confined aquifers', *Journal of Geophysical Research*, 84, pp. 2995–3007.

Carr, M. H. and Head, J. W. (2010) 'Geologic History of Mars', *Earth and Planetary Science Letters*, 294, pp. 185–203.

Cassan, A., Kubas, D., Beaulieu, J.P., Dominik, M., Horne, K., Greenhill, J., Wambsganss, J., Menzies, J., Williams, A., Jorgensen, U. G., Udalski, A., Bennett, D. P., Albrow, M. D., Batista, V. , Brillant, S., Caldwell, J. A. R., Cole, A., Coutures, Ch., Cook, K. H., Dieters, S., Dominis D., Donatowicz, J., Fouqué, P., Hill, K., Kains, N., Kane, S., Marquette, J.-B., Martin, R., Pollard, K. R., Sahu, K. C., Vinter, C., Warren, D., Watson, B., Zub, M., Sumi, T., Szymański, M. K., Kubiak, M., Poleski, R., Soszynski, I., Ulaczyk, K., Pietrzyński, G. and WyrzykowskiL (2012) 'One or more bound planets per Milky Way star from microlensing observations', *Nature*, 431, pp. 167-169.

Cataldo, F., Keheyan, Y. and Heymann, D. (2002) ‘A new model for the interpretation of the unidentified infrared bands (UIB's) of the diffuse interstellar medium and of the protoplanetary nebulae’, *International Journal of Astrobiology*, 1, pp. 79-86.

Centolanzi, F. J. and Chapman, D. R. (1966) ‘Vapor Pressure of Tektite Glass and Its Bearing on Tektite Trajectories Determined from Aerodynamic Analysis’, *Journal Of Geophysicarle Search,* 71(6) pp. 15.

Ceplecha, Z. and McCroskey, R. E. (1976) ‘Fireball end heights: A diagnostic for the structure of meteoric material’, *J. Geophys. Res*., 81(35), pp. 6257-6275.

Ceplecha, Z., Borovička, J., Elford, W. G., Revelle, D. O., Hawkes, R. L., Porubčan, V. and Simek, M. (1998) ‘Meteor phenomena and bodies’, *Space Science Reviews*, 84, pp. 327–471.

Cerling, T. E. and Quade, J. (1993) ‘Stable Carbon and Oxygen Isotopes in Soil Carbonates’, In P.K. Swart, K.C. Lohmann, J.A.McKenzie, and S.M.Savin, eds., *Climate Change in Continental Isotope Records*, Amer Washington: Geophysical Union, pp. 217-231.

Chapman, D. R. (1971) ‘Australasian tektite geographic pattern, crater and ray of origin, and theory of tektite events’, *Journal of Geophysical Research,* 76(26), pp. 6309–6338.

Chen, J. H., Papanastassiou, D. A. and Wasserburg, G. J. (1999) ‘Re-Os and Pd-Ag systematics in Metal rich chondrite Portales Valley (abstract #1472)’, *30th Lunar and planetary Science Conference.*

Chen, M., Sharp, T. G., El Goresy, A., Wopenka, B. and Xie, X. (1996) ‘The Majorite-Pyrope + Magnesiowüstite Assemblage: Constraints on the History of Shock Veins in Chondrites’, *Science*, 271, pp. 1570.

Chen, M., Wopenka, B., El Goresy, A. and Sharp, T. G. (1996) ‘The Peace River (L6) chondrite: compositions and pressure temperature history’, *Annual Meteoritical Society Meeting*, 31, A27.

Cholnoky, B. J. (1962) ‘Beitrage zur Kenntnis der Okologie der Diatomeen in Ost’, *Transvaal Hydrobiologia*, 19, pp. 57-119.

Christensen, P. R., Bandfield, J. L., Clark, R. N., Edgett, K. S. and Hamilton, V. E., Hoefen,, T., Kieffer, H.H., Kuzmin, R.O., Lane, M.D., Malin, M.C., Morris, R.V., Pearl, J.C., Pearson, R., Roush, T.L., Ruff, S.W. and Smith, M.D. (2000) ‘Detection of crystalline hematite mineralization on Mars by the Thermal Emission Spectrometer: Evidence for near-surface water’, *Journal Geophysical Research,* 105(E4), pp. 9623–9642.

Christophe Michel-Levy, M. and Lautié, A. (1981) ‘Microanalysis by Raman spectroscopy of carbon in the Tieschitz chondrite’, *Nature*, 292, pp. 321-322.

Chyba, C. F., Thomas, P. J. and Zahnle, K. J. (1993) ‘The 1908 Tunguska explosion: atmospheric disruption of a stony asteroid’, *Nature*, 361, pp. 40-44.

Claus, G. and Nagy, B. (1961) ‘A microbiological examination of some carbonaceous chondrites’, *Nature*, 192(4803), pp. 594-596.

Claus, G., Nagy, B. and Europa, D. L. (1963) ‘Further observations on the properties of the “organized elements’ *Annals of the New York Academy of Sciences*, 108, pp. 580.

Clayton, R. N. and Mayeda, T. K. (1999) ‘Oxygen Isotope Studies of carbonaceous chondrites’ *Geochimica et Cosmochimica Acta*, 63(13/14), pp. 2089-2104.

Clemett, S. J., Maechling, C. R., Zare, R. N., Swan, P. D. and Walker, R. M. (1993) ‘Identification of complex aromatic molecules in individual interplanetary dust particles’, *Science*, 262, pp. 721-725.

Cleve, P. T. and Möller, J. D. (1877) ‘Diatoms. Part I’, *Upsala: Esatas Edquists Boktryckeri.*, 1-48.

Cody, G. D., Alexander, C. M. O., and Tera, F. (2002) 'Solid-state (1H and 13C) nuclear magnetic resonance spectroscopy of insoluble organic residue in the Murchison meteorite: A self-consistent quantitative analysis', *Geochimica Cosmochimica Acta*, 66, pp. 1851–1865.

Cody, G. D., Boctor, N. Z., Filley, T. R., Hazen, R. M., Scott, J. H., Sharma, A. and Yoder, H. S. Jr. (2000) 'Primordial carbonylated iron-sulfur compounds and the synthesis of pyruvate', *Science*, 289, pp. 1337-1340.

Cohen, H. M. and Rov, R. (1965) 'Densification of glass at very high presswe', *Physics and Chemistry of Glasses*', 6, pp. 149-161.

Cohen, M. (1980) 'Infrared observations of young stars VIII - Spectra in the ten-micron region' *Monthly Notices of the Royal Astronomical Society*, 191, pp. 499-509.

Cohn, C. A., Hansson, T. K., Larsson, H. S., Sowerby, S. J. and Holm, N. G. (2001) 'Fate of prebiotic adenine', *Astrobiology*, 1, pp. 477-480.

Coulson, S. G. (2009) 'On the deceleration of cometary fragments in aerogel', *International Journal of Astrobiology*, 8, pp. 9–17.

Coulson, S. G. and Wickramasinghe, N. C. (2003) 'Frictional heating of micron-sized meteoroids in the Earth's upper atmosphere', *Monthly Notices of the Royal Astronomical Society*, 343, pp. 1123-1130.

Coulson, S., Wallis, M., Miyake, N., Wallis, J. and Wickramasinghe, N. C. (2013) 'Dynamics of the Polonnaruwa Meteorite', *European Planetary Science Congress*.

Crick, F. H. C. (1968) 'Origin of genetic code', *J. Mol.Biol*, 38, pp. 367.

Cronin, J. R., Pizzarello, S. and Cruikshank, D. P. (1988) 'Organic matter in carbonaceous chondrites, planetary satellites, asteroids, and comets', pp. 819–857 [of JF Kerridge and MS Matthews, Editors, *Meteorites and the Early Solar System*, Univ. Arizona Press].

Crovisier, J., Leech, K., Bockelée-Morvan, D., Brooke, T. Y. and Hanner, M. S. Altieri, B., Keller, H.U. and Lellouch, E. (1997) 'The spectrum of comet Hale-Bopp (C/1995 O1) observed with the Infrared Space Observatory at 2.9 astronomical units from the Sun', *Science*, 275, pp. 1904.

Dai, Z. R. and Bradley, J. (2001) 'Iron-nickel sulfides in anhydrous interplanetary dust particles' *Geochim. Cosmochim. Acta*, 65, pp. 3601–3612.

Danks, A., Encrenaz, T., Bouchet, P., Le Bertre, T., Chalabaev, A. and Epchtein, N. (1986) 'Observation of an emission feature at 3.4|im in the spectrum of comet Halley', Proc. 20th ESLAB Symposium on the Exploration of Halley's Comet III', *European Space Agency*, S-250, pp. 103-106.

Darbon, S., Perrin, J. M. and Sivan, J. P. (1998) 'Extended Red Emission (ERE) detected in the 30 Doradus nebula', *Astronomy and Astrophysics*, 333, pp. 264.

Das, B., Prakash, S., Reddy, P. S. R. and Misra, V. N. (2007) 'An overview of utilization of slag and sludge from steel industries', *Resources, Conservation and Recycling*, 50(1), pp. 40–57.

Day, A. L. and Allen, E. T. (1925) 'The volcanic activity and hot springs of Lassen Peak', Carnegie Institution for Science, 360, pp. 1901.

Deamer, D., Singaram, S., Rajamani, S., Kompanichenko, V. and Guggenheim, S. (2006) 'Selfassembly processes in the prebiotic environment', *Philosophical Transactions of the Royal Society of Biological Sciences*, 361, pp. 1809–1818.

Debye, P. (1909) *Ann Physik*, 30, pp. 59.

Delano, J. W. (1986) 'Pristine Lunar Glasses: criteria, data and implications' *Proceedings of the 16th Lunar and Planetary Science Conference*, D201-D213.

Derenne, S., Knicker, H., Largeau, C. and Hatcher, P.G. (1998) 'Timing and mechanisms of changes in nitrogen functionality during biomass fossilization', In: Stankiewicz, B.A., van

Bergen, P.F. (Eds.), *Nitrogen-Containing Macromolecules in the Bio- and Geosphere*, American Chemical Society Symposium Series, 707, Washington, DC: American Chemical Society, pp. 243-253.

Di Muro, A.,Villemant, B., Montagnac, G., Scaillet, B. and Reynard, B. (2006) 'Quantification of water content and speciation in natural silicic glasses (phonolite, dacite, rhyolite) by confocal Micro-Raman spectroscopy', *Geochimica et Cosmochimica Acta*, 70, pp. 2868-2884.

Dickinson, T., Taylor, G. J., Keil, K., Schmitt, R. A., Hughes, S. S. and Smith, M. R. (1985) 'Apollo 14 aluminous mare basalts and their possible relationship to KREEP, Proceedings of the 15th Lunar Science Conference', *Journal of Geophysical Research*, 90, C365–C375.

Ding, T. P., Ma, G. R., Shui, M. X., Wan, D. F. and Li, R. H. (2005) 'Silicon isotope study on rice plants from the Zhejiang province, China' *Chem Geol*, 218, pp. 41–50.

Dixon, J. E., Stolper, E. M. and Delaney, J. R. (1988) 'Infrared spectroscopic measurements of CO2 and H2O glasses in the Juan de Fuca Ridge basaltic glasses', *Earth Planet. Sci. Lett.*, 90, pp. 87-104.

Dombrowski, H. J. (1963) 'Bacteria from Paleozoic Salt Deposits' *Annals of the New York Academy of Science*, 108, pp. 453-460.

Dove, M. T., Craig, M. S., Keen, D. A., Marshall, W. G., Redfern, S. A. T., Trachenko, K. O. and Tucker, M. G. (2000) 'Crystal structure of the high-pressure monoclinic phase-II of cristobalite, SiO2 Locality: synthetic Note: P = 3.5 GPa, refinement by constrained Rietveld analysis', *Mineralogical Magazine*, 64, pp. 569-576.

Dove, P. M. and Rimstidt, J. D. (1985) 'The solubility and stability of scorodite, FeAsO Ø2H O.Am Mineral', *American Mineralogist*, 70, pp. 828 –844.

Downs, R. T. (2006) 'The RRUFF Project: an integrated study of the chemistry, crystallography, Raman and infrared spectroscopy of minerals', *Program and Abstracts of the 19th General Meeting of the International Mineralogical Association*, Kobe: Japan, O03-13.

Duley, W. W. and Williams, D. A. (1981) 'The infrared spectrum of interstellar dust-Surface functional groups on carbon', *Monthly Notices Royal Astronomical Society*, 196, pp. 269.

Edwards, K. J., Goebel, B. M., Rodgers, T. M., Schrenk, M. O., Gihring, T. M., Cardona, M. M., McGuire, M. M., Hamers, R. J., Pace, N. R. and Banfield, J. F. (1999) 'Geomicrobiology of Pyrite(FeS2) dissolution: case study at Iron Mountain, California', *Geomicrobiol*, J.16, pp. 155-179.

Edwards, K. J., Schrenk, M. O., Hamers, R. J. and Banfield, J. F. (1998) 'Microbial oxidation of pyrite: experiments using microorganisms from an extreme acidic environment', *Am. Miner*, 83, pp. 1444-1453.

El Goresy, A., Wopenka, B., Chen, M., Weinbruch, S. and Sharp, T. G. (1997) 'Evidence for two different shock induced high-pressure events and alkali-vapor metasomatism in Peace River and Tenham (L6) chondrites', *28th Annual Lunar and Planetary Science Conference*, pp. 329.

Elwood Madden, M. E., Bodnar, R. J. and Rimstidt, J. D. (2004) 'Jarosite as an indicator of water-limited chemical weathering on Mars', Nature, 431, pp. 821-823.

Engelhardt, W., Arndt, J., Muller, W. F. and Stoffler, D. (1970) 'Shock metamorphism of lunar rocks and origin of the regolith at the Apollo landing site', *Geochim. Cosmochim. Acta*, 1, pp. 363-384.

Etzel, K., Huber, H., Rachel, R., Schmalz, G., Thomm, M. and Depmeier, W. (2007) 'Ptritesurface alteration of synthetic single crystals as effect of microbial activity and crystallographic orientation', *Adv. Mat. Res*. 20–21, pp. 350-353.

Fanucci, J. and Lew, H. (1959) ‘Effect of Mass Transfer and Body Forces on Two Phase Boundary Layer’, *General Electric Report*, TIS 59SD380.

Festou, M. C., Rickman, H. and West, R. M. (1993) ‘Comets. I - Concepts and observations’, *Astronomy and Astrophysics*, 4, 4, pp. 363.

Fisher, P. (2014) [*Email communication*].

Fitch, F. and Anders, E, (1963) ‘Organized element: possible identification in Orgueil meteorite’, *Science*, 140, pp. 1097-1099.

Fitch, F. and Anders, E. (1963) ‘Observations of the nature of "organized elements" in carbonaceous chondrites’, *Annals of the New York Academy of Sciences*, 108, pp. 495-513.

Fitch, F., Schwarz, H. P. and Anders, E. (1962) ‘Organized elements in carbonaceous chondrites’, *Nature*, 193, pp. 1123-125.

Flynn G. J., Bleuet, P., Borg, J., Bradley, J. P., Brenker, F. E., Brennan, S., Bridges, J., Brownlee, D. E., Bullock, E. S., Burghammer, M., Clark, B, C., Dai, Z, R., Daghlian C, P., Djouadi, Z., Fakra, S., Ferroir, T., Floss, C., Franchi, I. A., Gainsforth, Z., Gallien, J, P. and Gillet, P. et al. (2006) ‘Elemental compositions of comet 81P/Wild 2 samples collected by Stardust’, *Science*, 314, pp. 1731-173.

Foit, F. F. and Peacor, D. R. (1973) ‘The anorthite crystal structure at 410 and 830 C T = 830 C’, *American Mineralogist*, 58, pp. 665-675.

Folco, L., Franchi, I. A., D'Orazio, M., Rocchi, S. and Shultz, L. (2000) ‘A new martian meteorite from the Sahara: The shergottite Dar al Gani 489’, *Meteoritics and Planetary Science*, 35, pp. 827–839.

Forrest, W. J., Gillett, F. C. and Stein, W. A. (1975) ‘Circumstellar grains and the intrinsic polarization of starlight’, *Journal of Astrophysics*, 192, pp. 351.

Forrest, W. J., Gillett, F. C. and Stein, W. A. (1975) *Astrophys J.*, 192, pp. 351.

Forrest, W.J., Gillett, F. C. and Stein, W.A. (1975) ‘Circumstellar grains and the intrinsic polarization of starlight’, *Journal of Astrophysics*, 195, 423.

Foster, P. J. and Howarth, C. R. (1968) ‘Optical Constants of Carbons and Coals in the Infrared’ *Carbon*, 6, pp. 719-729.

Franchi, I. A., Wright, I. P., Sexton, A. S. and Pillinger, C. T. (1999) ‘The oxygen isotope composition of Earth and Mars’, *Meteoritics & Planetary Science*, 34, pp. 657-661.

Furton, D. G. and Witt, A. N. (1992) *Journal of Astrophysics*, 386, pp. 587.

Garcia-Ruiz, J. M. (1999) ‘Morphological behavior of inorganic precipitation systems’, Proc. SPIE 3755, *Instruments, Methods, and Missions for Astrobiology II*, 74.

Gehler, A., Tütken, T. and Pack, A. (2011) ‘Triple oxygen isotope analysis of bioapatite as tracer for diagenetic alteration of bones and teeth’, *Palaeogeography, Palaeoclimatology, Palaeoecology*, 310, 1-2, pp. 84-91.

Gehlhausen, J. M. and Camahan, J. W. (1991) ‘Simultaneous Determination of Elemental Ratios in Coal by Direct Powder Injection into a Helium Microwave Induced Plasma’, *Anal. Chem*, 63, pp. 2430-2434.

Gibson, C. H. (1996) ‘Turbulence in the ocean, atmosphere, galaxy and universe’, *Appl. Mech. Rev.49*, 5, pp. 299–315.

Gibson, C. H. (2000) ‘Turbulent mixing, viscosity, diffusion and gravity in the formation of cosmological structures: the fluid mechanics of dark matter’, *Journal of Fluids Engineering*, 122, pp. 830-835.

Gibson, C. H. (2004) ‘The first turbulence and the first fossil turbulence’, *Flow, Turbulence and Combustion*, 72, pp. 161–179.

Gibson, C. H. (2005) ‘The first turbulent combustion’, *Combust. Sci. and Tech*, 177, pp. 1049–1071.

Gibson, C. H. and Schild, R. E. (2002) ‘Interpretation of the Tadpole VV29 Merging Galaxy System using Hydro-Gravitational Theory’, *Cornell University Library*. [Online]. Available at: http://arxiv.org/pdf/astro-ph/0210583.pdf (Accessed: 24 January 2014).

Gibson, C. H. and Schild, R. E. (2007) ‘Interpretation of the Helix Planetary Nebula using Hydro-Gravitational-Dynamics: Planets and Dark Energy’, *Cornell University Library*. [Online]. Available at: http://arxiv.org/abs/astro-ph/0701474 (Accessed: 24 January 2014).

Gibson, C. H. and Schild, R. E. (2007) ‘Interpretation of the Stephan Quintet Galaxy Cluster using Hydro-Gravitational-Dynamics: Viscosity and Fragmentation’, *Journal of Cosmology*. [Online]. Available at: http://journalofcosmology.com/JoC16pdfs/*126GibsonSchildStephanQuintet.pdf. (Accessed: 24 January 2014).

Gibson, C. H. and Schild, R. E. (2009) ‘Hydro-Gravitational-Dynamics of Planets and Dark Energy, J. Appl. Fluid Mech’, 2(2), pp. 35-41, Cornell University Library. [Online]. Available at: http://arxiv.org/abs/0808.3228 (Accessed: 24 January 2014).

Gibson, C. H., Schild, R. E. and Wickramasinghe, N. C. (2010) ‘The Origin of Life from Primordial Planets’, *Int. J. Astrobiology* (accepted, in press).

Gihring, T. M. and Banfield, J. F. (2001) ‘Arsenite oxidation and arsenate respiration by a new Thermus isolate’, *FEMS Microbiol. Lett*, 204, pp. 335.

Gilbert, L. A., (1962) ‘Refractive Indices and Absorption Coefficients of Coal in Bulk Measured in the Range 6000 to 2400 Å by a Polarized Light Technique’, *Fuel*, 41, pp. 351-358.

Gilbert, W. (1986) ‘The RNA World’, *Nature*, 319, pp. 6055.

Gilchrist J., Thorpe A. N. and Senftle F. E. (1969) ‘Infrared analysis of water in tektites and other glasses’, *J. Geophys. Res*., 74, pp. 1475-1483.

Gillaizeau, B., Behar, F., Derenne, S. and Largeau, C. (1997) ‘Nitrogen fate during laboratory maturation of a type I kerogen (Oligocene, Turkey) and related algaenan: nitrogen mass balances and timing of N2 production versus other gases’, *Energy & Fuels*, 11, pp. 1237–1249.

Gillet, P. J., Barrat, E., Deloule, M., Wadhwa, A., Jambon, V., Sautter, B., Devouard, D., Neuville, K., Benzerara and Lesourd, M. (2002) ‘Aqueous alteration in the northwest Africa 817 (NWA 817) Martian meteorite’, *Earth Planet. Sci. Lett*. 203, pp. 431–444.

Gillett, F. C., Forrest, W. J. and Merrill, K. M. (1973) ‘8 - 13-micron spectra of NGC 7027, BD +30 3639, and NGC 6572’, *Journal of Astrophysics*, 183, pp. 87.

Gilmour, I. (2003) in *Treatise on Geochemistry - Vol. 1*, (A. M. Davis, Ed.), Elsevier: Oxford, pp. 269–280.

Golden, D. C., Lauer, H. V., Ming, D. W. and Morris, R. V. (2006) ‘Nanophase magnetite and pyrrhotite in ALH84001 Martian meteorite: Evidence for an abiotic origin’, *National Aeronautics and Space Administration.*

Gómez-Serrano, V., Fernández-González, M. C., Rojas-Cervantes, M. L., Alexandre-Franco, M. F. and Macías-García, A. (2003) ‘Carbonization and Demineralization Of Coals - A Study By Means Of Ft–Ir Spectroscopy Bull. Mater’. *Sci*., 26(7), pp. 721–732.

Greenwood, R. C., Franchi, I. A., Jambon, A. and Buchanan, P. C. (2005) ‘Widespread magma oceans on asteroidal bodies in the early solar system’, *Nature*, 435, pp. 916-918.

Gruntfest, I. J. (1959) ‘Behavior of Reinforced Plastics at Very High Temperatures - Part 2’ *Modern Plastics*, 36(8), pp. 137-148, 204.

Gualtieri, A. F. (2000) ‘Accuracy of XRPD QPA using the combined Rietveld-RIR method Locality: Baveno, Novara, Italy’, *Journal of Applied Crystallography*, 33, pp. 267-278.

Guillois, O., Ledoux, G. and Nenner, I. et al. (1999) ‘Solid Interstellar Matter: The ISO Revolution. Les Houches, No.11’, *EDP Sciences*, Les Ulis.

Guttler, A. (1952) *Ann. Phys*, 6, Bd. 11, pp. 65.

Haack, H., Grau, T., Bischoff, A., Horstmann, M., Wasson, J., Sørensen, A., Laubenstein, M., Ott, U., Palme, H., Gellissen, M., Greenwood, R. C., Pearson, V. K., Franchi, I. A., Gabelica, Z. and Schmitt-Kopplin, P. (2012) ‘A new CM fall from Denmark’, *Meteoritics & Planetary Science*, 47, 30, pp. 50-66.

Haffert, L., Craw, D. and Pope, J. (2010) ‘Climatic and compositional controls on secondary arsenic mineral formation in high-arsenic mine wastes, South Island, New Zealand’, *New Zealand Journal of Geology and Geophysics*, 53, pp. 91-101.

Hahn, B., Herkenhoff, K. E., Hurowitz, J. A., Johnson, J. R., Johnson, S. S., Jolliff, B., Klingelhöfer, G., Knoll, A. H., Learner, Z., Malin, M. C., McSween, H. Y. Jnr., Pocock, J., Ruff, S. W., Soderblom, L. A., Squyres, S. W., Tosca, N. J., Watters, W. A., Wyatt, M. B. and Yen, A. (2005) ‘Provenance and diagenesis of the evaporite-bearing Burns formation, Meridiani Planum’, *Mars Earth Planet. Sci. Lett*, 240, pp. 95–121.

Haldane, J. B. S. (1929) *The Origin of Life*, Chatto and Windys: London.

Halliday, I., Blackwell, A. T. and Griffin, A. A. (1989) ‘The flux of meteorites on the Earth’s surface’ *Meteoritics*, 24, pp. 173–178.

Haloda J., Tycova, P., Korotev, R. L., Fernandes, V. A., Burgess, R., Thoni, M., Jelenc, M., Jakes, P., Gabzdyl, P. and Kosler, J. (2009) ‘Petrology, geochemistry, and age of low-Ti mare-basalt meteorite Northeast Africa 003-A: A possible member of the Apollo 15 mare basaltic suite’, *Geochimica et Cosmochimica Acta*, 73, pp. 3450–3470.

Hamm, M. K. (1990) ‘Ablative heat shield studies for NASA Mars/Earth Return Entry Vehicles’, *PhD Thesis.* Monterey, California: Naval Postgraduate School.

Hannington, M. D., Jonasson, I. R., Herzig, P. M. and Petersen, S. (1995) in ‘*Seafloor hydrothermal systems*’, ed. Humphris, S. E., Zierenberg, R. A., Mullineaux, L. S. and Thomson, R. E. *Geophysical Monograph Series*, 91, pp. 115-117.

Harlow, G. E. (1982) ‘The anorthoclase structures: The effects of temperature and composition Grande Caldeira, Or = 32.5, T = 400 deg C feldspar’, *American Mineralogist*, 67, pp. 975-996.

Harris, M.J., Wickramasinghe, N.C., Lloyd, D., Narlikar, J.V., Rajaratnam, P., Turner, M.P., Al-Mufti, S., Wallis, M.K., Ramadurai, S. and Hoyle, F. (2002) ‘Detection of living cells in stratospheric samples’, *Proc. SPIE*, 4495, pp. 192-198.

Harvey, C. F., Swartz C. H., Badruzzaman A. B. M., Keon-Blute, N., Yu, W., Ali, M. A., Jay, J., Beckie, R., Niedan, V., Brabander, D., Oates, P. M., Ashfaque, K. N., Islam, S., Hemond, H. F. and Ahmed M. F. (2002) ‘Arsenic mobility and groundwater extraction in Bangladesh’, *Science*, 298(5598), pp. 1602-1606.

Hatton, B. and Rickard, D. (2008) ‘Nucleic acids bind to nanoparticulate iron (II) monosulphide in aqueous solution’, *Origins of Life and Evolution of Biospheres*, 38, pp. 257-270.

Hazen, R. M. (1977) ‘Effects of temperature and pressure on the crystal structure of ferromagnesian olivine T = 600 deg C, P = 1 atm’, *American Mineralogist*, 62, pp. 286-295.

Head, J. W. and Marchant, D. R. (2003) ‘Cold-based mountain glaciers on Mars, western arsia mons’, *Geology*, 31(7), pp. 641-644.

Head, J. W. and Pratt, S. (2001) 'Extensive Hesperian-aged south polar ice sheet on Mars: evidence for massive melting and retreat, and lateral flow and ponding of meltwater', *J. Geophys*, Res. 106, (E6), pp. 12275–12299.

Henke, K. (2009) *Arsenic: Environmental Chemistry, Health Threats and Waste* Treatment, Sussex: John Wiley and Sons Ltd.

Hidalgo, H. (1960) 'Ablation of glassy material around blunt bodies of revolution', *ARS Journal*, 30 (9), pp. 806-814.

Hiru FM News (2013) *'Aralaganwila stones are not meteors; says Peradeniya University'*

Holl, C. M., Smyth, J. R., Jacobsen, S. D. and Frost D. J. (2008) 'Effects of hydration on the structure and compressibility of wadsleyite, beta-(Mg2SiO4) Locality: synthetic Sample: SS0403, 0.38 wt% H2O', *American Mineralogist*, 93, pp. 598-607.

Hoover, R. B. (2005) In: Hoover, R. B., Rozanov, A.Y. and Paepe, R.R. eds. *Perspectives in Astrobiology*. Amsterdam: IOS Press, 366, pp. 43.

Hoover, R. B. (2007) 'Ratios of Biogenic Elements for Distinguishing Recent from Fossil Microorganisms', *Instruments, Methods, and Missions for Astrobiology X, 6694*.

Hoover, R. B. (2011) 'Fossils of Cyanobacteria in CI1 Carbonaceous Meteorites: Implications to Life on Comets, Europa, and Enceladus', *Journal of Cosmology*, 13.

Hoover, R. B. and Pikuta, E. V. (2009) 'Life in Ice: Implications to Astrobiology', *SPIE*, 7441, pp. 1-14.

Hoover, R. B. and Pikuta, E. V. (2012) 'Microscopic and Microbiological Investigations of Mississippian Sylvite', *SPIE*, 8521, pp. 1-9.

Hoover, R. B., Hoyle, F., Wickramasinghe, N. C., Hoover, M. J. and Al-Mufti, S. (1986) 'Diatoms on Earth comets, Europa and in interstellar space', *Earth Moon Planets*, 35, pp. 19-45.

Horvath, B., Hofmann, M. E. G. and Pack, A. (2012) 'On the triple oxygen isotope composition of carbon dioxide from some combustion processes', *Geochimica et Cosmochimca Acta*, 95, pp. 160-168.

Hossain, M. K., Strezov, V., Chan, K. Y., Ziolkowski, A. and Nelson, P. F. (2011) 'Influence of pyrolysis temperature on production and nutrient properties of wastewater sludge biochar', *Journal of Environmental Management*, 92(1), pp. 223-228.

Hoyle, F. & Wickramasinghe, N. C. (1962) 'On graphite particles as interstellar grains', *MNRAS*, 124, pp. 417.

Hoyle, F. and Wickramasinghe, N. C. (1969) 'Interstellar Grains', *Nature*, 223, pp. 459.

Hoyle, F. and Wickramasinghe, N. C. (1977) 'Identification of the λ2, 200Å interstellar absorption feature', *Nature*, 270, pp. 323–324.

Hoyle, F. and Wickramasinghe, N. C. (1981) *Comets and the Origin of Life*, ed. Ponnamperuma, C. Dordrecht: D. Reidel.

Hoyle, F. and Wickramasinghe, N. C. (1982) 'Proofs that Life is Cosmic', *Mem. Inst. Fund. Studies Sri Lanka*, No. 1 (www.panspermia.org/proofslifeiscosmic.pdf).

Hoyle, F. and Wickramasinghe, N. C. (1984) *Fundamental Studies and the Future of Science*, ed. Wickramasinghe, N. C., Cardiff: Univ. College Cardiff Press.

Hoyle, F. and Wickramasinghe, N. C. (1985) *Living Comets*, Cardiff: Univ. College Cardiff Press.

Hoyle, F. and Wickramasinghe, N. C. (1991) *The Theory of Cosmic Grains*, Dordrecht: Kluwer Academic Press.

Hoyle, F. and Wickramasinghe, N. C. (1993) *Our Place in the Cosmos*, London: J.M. Dent.

Hoyle, F. and Wickramasinghe, N. C. (1996) 'Biofluorescence and the extended red emission in astrophysical sources', *Astrophys.Sp.Sci.*, 235, pp. 343.

Hoyle, F. and Wickramasinghe, N. C. (1999) 'The Universe and Life: Deductions from the Weak Anthropic Principle', *Astroph. Space Sci*., 268, pp. 89-102.

Hoyle, F. and Wickramasinghe, N. C. (1999) *Astronomical Origins of Life: Steps towards Panspermia*, Dordrecht: Kluwer Academic Publ.

Hoyle, F. and Wickramasinghe, N. C. (2000) *Astronomical Origins of Life: Steps towards Panspermia*, Doredrecht: Kluwer Academic Press.

Hoyle, F., Wickramasinghe, N. C. and Al-Mufti, S. (1982) 'Organo-siliceous biomolecules and the infrared spectrum of the Trapezium nebula', *Astrophys. Space. Sci*. 86, pp. 63.

Hoyle, F., Wickramasinghe, N. C. and Al-Mufti, S. (1982) 'The infrared spectrum of interstellar dust', *Astrophys. Space. Sci.* 86, pp. 341.

Huber, R. M., Sacher, M., Vollmann, A., Huber, H. and Rose, D. (2000) 'Respiration of arsenate and selenate by hyperthermophilic archaea', *Appl. Microbiol*. 23, pp. 305.

Huntjens, F. J. and van Krevelen, D. W. (1954) 'Chemical and Physical Properties of Coal II', *Fuel*, 33, pp. 88.

Huss, G. R., Rubin, A.E., and Grossman, J.N. (2006) 'Thermal metamorphism in chondrites', in *Meteorites & the Early Solar System II*, pp. 567–586.

Ibhi, A., Nachit, H. and Abia, El H. (2013) 'Tissint Meteorite: New Mars Meteorite fall in Morocco', *J. Mater. Environ. Sci*, 4(2), pp. 293-298.

Irving, A. J., Kuehner, S. M., Tanaka, R., Herd, C. D. K., Chen, G. and Lapan, T. J. (2012) 'The Tissint depleted permafic olivine-phyric Shergottite: Petrologic, elemental and isotopic characterization of a recent Martian Fall in Morocco', *Lunar Planet. Sci.XLIII*, Lunar Planetary Institute @ the Woodlands.

Jäggi, M., Saurer, M., Fuhrer, J. and Siegwolf, R. (2003) 'Seasonality of d18O in needles and wood of Picea abies', *New Phytologist*, 158, pp. 51–59.

Jan, L., Čejka, J., Sejkora, J., Plasil, J., Novak, M., Frost, R. L., Palmer, S. and Keeffe, E. C. (2011) 'A Raman spectroscopic study of bukovskýite Fe2(AsO4)(SO4)(OH).7H2O, a mineral phase with significant role in arsenic migration', *Journal of Raman Spectroscopy*, 42(7), pp. 1596-1600.

Javaux, E., Marshall, C. and Bekker, A. (2010) 'Organic-walled microfossils in 3.2-billion-year-old shallow-marine siliciclastic deposits', *Nature*, 463(7283), pp. 934–938.

Jeans, J. H. (1902) 'The Stability of a Spherical Nebula', *Philosophical Transactions of the Royal Society of London*, Series A, 199, pp. 1–53.

Jessen, S, Larsen, F, Koch, C. B. and Arvin, E. (2005) 'Sorption and desorption of arsenic to ferrihydrite in a sand filter', *Environ Sci Technol*, 39(8045), pp. 51.

Johan, Z. (1986) 'Crystal Symmetry and unit cell of bukovskyite $Fe_2^{3+}(AsO_4)(SO_4)(OH)\cdot 7H_2O$', *Neues Jahrbuch für Mineralogie*, Monatshefte, pp. 445-451.

Jones, W. B. (1985) 'Chemical analyses of Bosumtwi crater target rocks compared with the Ivory Coast tektites', *Geochimica et Cosmochimica Acta*, 49(12), pp. 2569–2576.

Joswiak, D. J. and Brownlee, D. E. (2014) 'Refractory-rich Materials in Comets: CAIs, Al-rich Chondrules and AOAs from Comet Wild 2 and a Giant Cluster Interplanetary Dust Particle (IDP) of Probable Cometary Origin and Comparison to Refractory-rich Objects in Chondrites', *45th Lunar and Planetary Science Conference.*

Joy, K. H., Anand, M., Crawford, I. A. and Russell S. S. (2007) 'Petrography and bulk composition of Miller Range 05035: A new lunar VLT gabbro (abstract #1867)', *38th Lunar and Planetary Science Conference*. CD-ROM.

Juckes, L. M. (2003) 'The volume stability of modern steelmaking slags', *Mineral Processing and Extractive Metallurgy*, 112(3), pp. 177–197.

Jull, A. J. T., Courtney, C., Jeffrey, D. A. and Beck, J. W. (1998) 'Isotopic Evidence for a Terrestrial Source of Organic Compounds Found in Martian Meteorites Allan Hills 84001 and Elephant Moraine 79001', *Science*, 279, pp. 366-369.

Kelemen, S. R., Gorbaty, M. L. and Kwiatek, P. J. (1994) 'Quantification of nitrogen forms in Argonne Premium coals' *Energy & Fuels*, 8(4), pp. 896–906.

Keller, L. P., Hony, S., Bradley, J. P., Molster, F. J., Waters, L.B., Bouwman, J., De Koter, A., Brownlee, D. E., Flynn, G. J., Henning, T. and Mutschke, H. (2002) 'Identification of iron sulphide grains in protoplanetary disks', *Nature*, 417, pp.148–150.

Kemper, F., Vriend, W. J. and Tielens A. G. G. M. (2005) 'Erratum: the absence of crystalline silicates in the diffuse interstellar medium', *ApJ*, 633, pp. 534.

Kemper, F., Vriend, W. J. and Tielens, A. G. G. M. (2004) 'The Absence of Crystalline Silicates in the Diffuse Interstellar Medium', *ApJ*, 609(2), pp. 826.

Khare, B. N., Thompson, W. R., Sagan, C., Arakawa, E. T., Meisse, C. and Gilmour, I. (1990) 'Optical Constants of Kerogen from 0.15 to 40 micron: Comparison with Meteoritic Organics' In *NASA, Goddard Space Flight Center, First International Conference on Laboratory Research for Planetary Atmospheres*, pp. 340-356.

Kimata, M. (1997) *LPSC*, XXVIII, pp. 329-330.

King, P. L., Dalby, K. D., Russell, S. D. J., Ireland, T., McSween, H. Y. Jr. and Bischoff, A. (2005) 'Meteorite impact! The danger from space and South Africa's mega-impact, the Vredefort structure', *Meteorit. Planet. Sci*., 40, A82.

Kissel, J. and Krueger, F. R. (1987) 'The organic component in dust from comet Halley as measured by the PUMA mass spectrometer on board Vega 1', *Nature*, 326(6115), pp. 755-760.

Kitamura, R., Pilon, L. and Jonasz, M. (2007) 'Optical constants of silica glass from extreme ultraviolet to far infrared at near room temperature', *Applied Optics*, 46(33), pp. 8118-8133.

Knacke, R. F. (1977) 'Carbonaceous compounds in interstellar dust', *Nature*, 269, pp. 132-134.

Knacke, R. F., Brooke, T. Y. and Joyce, R. R. (1986) 'Observations of 3.2-3.6 micron emission features in comet Halley', *Astrophysical Journal*, Part 2 - Letters to the Editor (ISSN 0004-637X), 310, pp. L49-L53.

Knacke, R. F., Gaustad, J. E., Gillett, F. C. and Stein, W. A. (1969) 'A Possible Identification of Interstellar Silicate Absorption in the Infrared Spectrum of 119 Tauri', *Astrophysical Journal*, 155, pp. 189.

Knicker, H., Scaroni, A. W. and Hatcher, P. G. (1996) '13C and 15N spectroscopic investigation on the formation of fossil algal residues', *Organic Geochemistry*, 24(6-7), pp. 661–669.

Koeberl, C. (1994) 'Tektite origin by hypervelocity asteroidal or cometary impact: Target rocks, source craters, and mechanisms, Large Meteorite Impacts and planetary Evolution', *Geological Society of America*, Special Paper 293, pp. 133-151.

Korotev, R. L. (2005) 'Lunar geochemistry as told by lunar meteorites', *Chemie der Erde*, 65, pp. 297–346.

Korotev, R. L. (2013) 'Meteorite or meteowrong?' [Quote: "If you can see quartz with the naked eye, then the rock is not a meteorite."] *Department of Earth and Planetary Sciences, Washington University in St. Louis*'.

Krause, E. and Ettel, V. A. (1988) 'Solubility and stability of scorodite, FeAsO4Ø2H2O new data and further discussion', *Am Mineral*, 73, pp. 850 –854.

Krevelen, V. (1961) 'Coal', *Elsevier Publishing Comp*, pp. 182-189.

Kroto, H. (1983) Speaking at the 145th meeting of the British Association for the advancement of science: Brighton, reported in: *New Scientist*, (25 August 1983), pp. 556.

Kumar, A. and Srivastava, S. K. (2013) 'Disposition Pattern of Sulphur Functional Groups in High Sulphur Ledo Coals of Assam', *IOSR Journal of Applied Chemistry*, 4(3), pp. 01-08.

Kwok, S. (2009) 'Organic matter in space: from star dust to the solar system', *Astrophys Space Sci*., 319, pp. 5–21.

Lal, S., Archarya, Y. B., Patra, P. K., Rajaratnam, P., Subbarya, B. H. and Venkataramani, S. (1996) 'Balloon-borne cryogenic air sampler experiment for the study of atmospheric trace gases', *Indian J. Radio Space Phys*, 25, pp. 1-7.

Landais, P. and Gize, A. P. (1997) 'Organic matter in hydrothermal ore deposits', In *Geochemistry of hydrothermal ore deposits*, Edited by: Barnes, H. L. Hoboken: John Wiley, pp. 613-656.

Landau, L. D. and Lifshitz, E. M. (1987) 'Course of Theoretical Physics, Vol. 6: Fluid Mechanics 2 Ed.', *Pergamon Press*, pp. 336-343.

Larsen, F. and Postma, D. (1997) 'Nickel mobilization in a groundwater well field: Release by pyrite', *Environ. Sci. Technol*., 31, pp. 2589.

Lauretta, D. S. and the OSIRIS-Rex Team (2012) 'An overview of the OSIRIS-Rex asteroid sample return mission (abstract #1659)', *43rd Lunar and Planetary Science Conference*, CD-ROM.

Lavina, B., Princivalle, F. and Della Giusta, A. (2005) 'Controlled time-temperature oxidation reaction in a synthetic Mg-hercynite Spinel structure Sample: Annealing temperature and time T = 600 C, t = 236 h', *Physics and Chemistry of Minerals*, 32, pp. 83-88.

Leblanc, M., Achard, B., Othman, D. B. and Luck, J. M. (1996) 'Accumulation of arsenic from acidic mine waters by ferruginous bacterial accretions (stromatolites)', *Applied Geochemistry*, 11, pp. 541-554.

Lefticariu, L., Pratt, L. A., LaVerne, J. A. and Schimmelmann, A. (2010) 'Anoxic pyrite oxidationby water adiolysis products –a potential source of biosustaining energy', *Earth and Planetay Science Letters*, 292(1-2), pp. 57-67.

Lefticariu, L., Pratt, L. M. and Ripley, E. M. (2006) 'Mineralogic and sulfur isotopic effects accompanying oxidation of pyrite in millimolar solutions of hydrogen peroxide attemperatures from 4 to 150 °C', *Geochimica et Cosmochimica Acta*, 70(19), pp. 4889-4905.

Leroux, H. and Cordier, P. (2006) 'Magmatic cristobalite and quartz in the NWA856 Martian meteorite', *Meteorit. & Planet. Sci*., 41, pp. 913.

Lespade, P., Al-Jishi, R. and Dresselhaus, M. S. (1982) 'Model for Raman scattering from incompletely graphitized carbons', *Carbon*, 20, pp. 427-43t.

Leventhal, J. S., Grauch, R. I., Threlkeld, C. N., Lichte, F. E. and Harper, C. T. (1987) 'Unusual organic matter associated with uranium from the Claude deposit, Cluff Lake, Canada', *Economic Geology*, 82, pp. 1169-1176.

Levine, R. and Evers, C. (1999) *The Slow Death of Spontaneous Generation (1668-1859)*, Washington, D.C.: National Health Museum.

Levy, J., Head, J. W. and Marchant, D. R. (2009) 'Thermal contraction crack polygons on Mars: classification, distribution and climate implications from global HiRISE observations', *J. Geophys. Res*., 114(31), pp. 641–644.

Liepmann, H. W. and Roshko, A. (1957) *Elements of gasdynamics*, New York: John Wiley & Sons.

Lin, Y., El Goresy, A., Hu, S., Zhang, J., Gillet, P., Xu, Y., Hao, J., Miyahara, M., Ouyang, Z., Ohtani, E., Xu, L., Yang, W., Feng, L., Zhao, X., Yang, J. and Ozawa, S. (2013) 'Nanosims Analysis of Organic Carbon from Mars: Evidence for a Biogenetic Origin', *44th Lunar and Planetary Science Conference*.

Lin, Y., Guan, Y., Wang, D., Kimura, M. and Leshin, L. A. (2005) 'Petrogenesis of the New Lherzolitic Shergottite Grove Mountains 99027: Constraints of Petrography, Mineral Chemistry, and Rare Earth Elements', *Meteoritics & Planetary Science*, 40, pp. 1599-1619.

Lindgren, P., Parnell, J., Holm, N. G. and Broman, C. (2011) 'A demonstration of an affinity between pyrite and organic matter in a hydrothermal setting', *Geochemical Transactions*, 12(3), pp. 1467-4866.

Littke, R., Krooss, B., Idiz, E. and Frielingsdorf, J. (1995) 'Molecular nitrogen in natural gas accumulations: generation from sedimentary matter at high temperatures', *American Association of Petroleum Geologists Bulletin*, 79(3), pp. 410–430.

Liu, Y., Floss, C., Day, J. M. D., Hill, E. and Taylor, L. A. (2009) 'Forthcoming. Petrogenesis of lunar mare basalt meteorite Miller Range 05035', *Meteoritics & Planetary Science*, 44, pp. 261–284.

Loun, J., Plasil, J. C. J. S. J., Novak, M., Frost, R. F., Palmer, S. and Keeffe, E. C. (2011) 'A Raman spectroscopic study of bukovskýite $Fe_2(AsO_4)(SO_4)(OH).7H_2O$, a mineral phase with significant role in arsenic migration', *Journal of Raman Spectroscopy*, 42(7), pp. 1596-1600.

Lucchitta, B. K. (1984) 'Ice and debris in the fretted terrain', *J. Geophys. Res.*, 80, pp. B409–B418.

Luxán, M. P., Sotolongo, R., Dorrego, F., and Herrero, E., (2000) 'Characteristics of the slags produced in the fusion of scrap steel by electric arc furnace', *Cement and Concrete Research*, Vol. 30 (No. 4), pp. 517–519.

Luz, B., Barkan, E., Bender, M. L., Thiemens, M. H. and Boering, K. A. (1999) 'Triple-isotope composition of atmospheric oxygen as a tracer of biosphere productivity', *Nature*, 400(547), pp. 5062.

Machatschki, F. (1936) 'Kristallstruktur von Tiefquarz', *Fortschritte der Mineralogie*, 20, pp. 45-47.

Mahieux, P. Y., Aubert, J. E. and Escadeillas, G. (2009) 'Utilization of weathered basic oxygen furnace slag in the production of hydraulic road binders', *Construction and Building Materials*, 23(2), pp. 742–747.

Majzlan, J., Lazic, B., Armbruster, T. M., Johnson, M. B., White, M. A., Fisher, R. A., Plasil, J., Loun, J., Skodan, R. and Novak, M. (2012) 'Crystal structure, thermodynamic properties, and paragenesis of bukovskyite, Fe2(AsO4)(SO4)(OH)*9H2O', *Journal of Mineralogical and Petrological Sciences*, 107(3), pp. 133-148.

Malhotra, R. (2012) *Fossil Energy: Selected Entries from the Encyclopedia of Sustainability Science and Technology*. New York: Springer.

Manga, M. (2004) 'Martian floods at Cerberus Fossae can be produced by groundwater discharge', *Geophys. Res. Lett.* 31, L02702.

Manso, J. M., Polanco J. A., Losañez, M. and González, J. J. (2006) 'Durability of concrete made with EAF slag as aggregate', *Cement and Concrete Composites*, 28(6), pp. 528–534.

Mareels, J. (2004) 'ICP-MS analysis, geochemistry, and petrogenesis of granites from the Variscan Northern Vosges (France)', *Unpublished PhD thesis*, Katholieke Universiteit: Leuven, pp. 360.

Márquez, M., Gaspar, J., Bessler, K. E. and Magela, G. (2006) 'Process mineralogy of bacterial oxidized gold ore in São Bento Mine (Brasil)', *Hydrometallurgy*, 83, pp. 114.

Marshall, C. P., Edwards, H. G. M., and Jehlicka, J. (2010) 'Understanding the application of Raman spectroscopy to the detection of traces of life', *Astrobiology*, 10, 229–243.

Martins, Z., Botta, O., Fogel, M. L., Sephton, M. A., Glavin, D. P., Watson, J. S, Dworkin, J. P., Schwartz, A. W. and Ehrenfreund, P. (2008) 'Extraterrestrial nucleobases in the Murchison meteorite', *Earth and Planetary Science Letters*, 270(1-2), pp. 130-136.

Masursky, H. (1973), 'An overview of geological results from Mariner 9', *J. Geophys. Res.* 78, pp. 4037.

Matson, J. (2010) ‘Meteorite That Fell in 1969 Still Revealing Secrets of the Early Solar System’, *Scientific American*, Retrieved 2010-02-15.

Matsui, T. and Kimata, M. (1997) ‘Crystal chemistry of synthetic Mn-bearing anorthite: Incorporation of MnAl2Si2O8 end-member into feldspar Note: U(1,1) for Obo altered to reproduce Uiso", *European Journal of Mineralogy*, 9, pp. 333-344.

Matsuoka, K., Nagao, T., Marconi, A., Maiolino, R. and Taniguchi, Y. (2011) ‘The mass-metallicity relation of SDSS quasars’, *Astronomy and Astrophysics*, 527, pp. A100.

Mattila, K. (1979) ‘Optical extinction and surface brightness observations of the dark nebulae LYNDS 134 and LYNDS 1778/1780’, *Astronomy and Astrophysics*, 78, pp. 253.

McArthur, J. M., Banerjee, D. M., Hudson-Edwards, K. A., Mishra, R., Purohit, R., Ravenscroft, P., Cronin, A., Howarth, R. J., Chatterjee, A., Talukder, T., Lowry, D., Houghton, S. and Chadha, D. K. (2004) ‘Natural organic matter in sedimentary basins and its relation to arsenic in anoxic groundwater: the example of West Bengal and its worldwide implications’, *Appl. Geochem.*, 19, pp. 1255-1293.

McCartney, T. J. and Ergun, S. (1959) ‘Optical Properties of Graphite and Coal’, *Proceeding of Third Carbon Conference*, Pergamon Press, pp. 223-231.

McKay, D. S., Gibson, E. K. Jr., Thomas-Keprta, K. L., Vali, H., Romanek, C. S., Clemett, S. J., Chillier, X. D. F., Maechling, C. R. and Zare, R. N. (1996) ‘Search for Past Life on Mars: Possible Relic Biogenic Activity in Martian Meteorite ALH84001’, *Science*, 273, pp. 924–930.

McKay, D. S., Thomas-Keprta, K. L., Clemett, S. J., Gibson, E. K. Jr., Spencer, L., and Wentworth S.J. (2009) ‘Life on Mars: new evidence from martian meteorites, instruments and methods for astrobiology and planetary missions XII’, *Proc. SPIE*, pp. 7441.

McLaughlin, H., Anderson, P. S., Shields, F. E. and Reed, T. B. (2009) ‘All biochars are not created equal, and how to tell them apart’ *Proceedings North American Biochar Conference*, Colorado: Boulder.

McLennan, S. M., Bell III, J. F., Calvin, W. M., Christensen, P. R., Clark, B. C., de Souza Jr., P. A., Farmer, J., Farrand, W. H., Fike, D. A., Gellert, R., Ghosh, A., Glotch, T. D., Grotzinger, J. P., Hahn, B., Herkenhoff, K. E., Hurowitz, J. A., Johnson, J. R., Johnson, S. S., Jolliff, M. B., Klingelhöfer, G., Knoll, A. H., Learner, Z., Malin, M. C., McSween, H. Y. Jr., Pocock, J., Ruff, S. W., Soderblom, L. A., Squyres, S. W., Tosca, N. J., Watters, W. A., Wyatt, M. B. and Yen, A. (2005) ‘Provenance and diagenesis of the evaporite-bearing Burns formation, Meridiani Planum, Mars’, *Earth & Planet. Sci. Letters*, 240(1), pp. 95-121.

McSween, H. and Harvey, R. (1998) ‘An evaporative model for formation of carbonates in the ALH84001 martian meteorite’, *Intl. Geol. Rev.*, 40, pp. 774-783.

Melosh, H. J. (1989) *Impact cratering: a geologic process*, Oxford: Oxford University Press.

Merrill, K. M. and Soifer, B. T. (1974) *Astrophys.J,*. (Letters), 189, pp. L27.

Merrill, K. M., Russell, R. W. and Soifer, B. T. (1976) *Astrophys J*., 207, pp. 763.

Messenger, S. (2002) *M&PS*, 37, pp. 1491–1505.

Meyer, C. (1998) *Mars Meteorite Compendium—1998*. NASA, Lyndon B. Johnson Space Center, Houston, Texas, USA, pp. 237.

Mie, G. (1908) ‘Beiträge zur Optik trüber Medien, speziell kolloidaler Metallösungen’, *Ann. Physik*, 330(3), pp. 377.

Miller, S. L. and Urey, H. C. (1959) ‘Organic Compound Synthesis on the Primitive Earth’, *Science*, 130, pp. 245.

Milliken, R. E., Mustard, J. F. and Goldsby, D. L. (2003) 'Viscous flow features on the surface of Mars: observations from high-resolution Mars Orbiter Camera (MOC) images', *J. Geophys. Res*., 108, pp. 5057.

MIT Technoloogy Review, (2013) Available at: http://www.technologyreview.com/view/512381/astrobiologists-find-ancient-fossils-in-fireball-fragments/ (Accessed: 13 April 2014).

Mittlefehldt, D. W., McCoy, T. J., Goodrich, C. A. and Kracher, A. (1998) 'Non-chondritic meteorites from asteroidal bodies', in *Planetary materials*, edited by Papike, J. J. Washington, D.C.: Mineralogical Society of America, 4(1), pp. 195.

Miyake, N. (2009) 'Laboratory Studies of Stratospheric Dust – Relevance to the theory of Cometary Panspermia', *PhD thesis*, Cardiff University: UK.

Moore, M. H. and Donn, B. (1982) 'The infrared spectrum of a laboratory-synthesised residue: implications for the 3.4um interstellar absorption feature', *Astrophys J*., 257, pp. L47.

Motta, V., Mediavilla, E., Mufioz, J. A., Falco, E., Kochanek, C. S., Arribas, S., Garcia-Lorenzo, B., Oscoz, A. and Serra-Ricart, M. (2002) 'Detection of the 2175A Extinction Feature at z = 0.83', *Astrophys. J*., 574, pp. 719–725.

Mustard, J. F., Cooper, C. D. and Rifkin, M. K. (2001), 'Evidence for recent climate change on Mars from the identification of youthful near-surface ground ice', *Nature*, 412, pp. 411–414.

Nagy, B. and Bitz, M. C. (1963) 'Long-chain fatty acids in the Orgueil meteorite', *Arch. Biochem Biophys.*, 101, pp. 240-248.

Nakamura, K., Zolensky, M. E., Tomita, S., Nakashima, S. and Kazushige, T. (2002) 'Hollow organic globules in the Tagish Lake meteorite as possible products of primitive organic reactions'. *International Journal of Astrobiology*, 1, pp. 179-189.

Nakashima, S. (1992) 'Complexation and reduction of uranium by lignite', *Science of the Total Environment*, 117-118, pp. 425-437.

Nakashima, S. and Shiota, D. (2001) 'Organic–inorganic interactions and the origin and evolution of life', *Geochemistry and the Origin of Life*, Tokyo: Universal Academy Press, pp. 135–178.

Nandy, K. (1964) *Publ. Roy. Obs. Edin*., 3(6).

Nandy, K. and Wickramasinghe, N. C. (1965) *Publ. Roy. Obs. Edin*., 5(3).

Nardi, S., Binda, P. L., Baccelle, L. S. and Concheri, G. (1994) 'Amino acids of Proterozoic and Ordovician sulphide-coated grains from western Canada: Record of biologically-mediated pyrite precipitation', *Chemical Geology*, pp. 111:1-15.

Narlikar, J. V., Wickramasinghe, N. C., Wainwright, M. and Rajaratnam, P. (2003) 'Detection of microorganisms at high altitudes', *Current Science*, 85(1), pp. 29.

Neal, C. R. and Kramer, G. Y. (2006) 'Apollo 14 High-Al Basalt Petrogenesis', 1535 Proceedings of the 15th Lunar Science Conference, in *Journal of Geophysical Research*, 90, C375.C395.

Neal, C. R., Taylor, L. A. and Lindstrom, M. M. (1988) 'Apollo 14 mare basalt petrogenesis: Assimilation of KREEP-like components by a fractionating magma', *Proceedings of the 18th Lunar Science Conference*, pp. 139–153.

Nemanich, R. J., and Solin, S. A. (1979) 'First and second-order Raman scattering from finite-size crystals of graphite', *Physical Review B*, 20, pp. 392-401.

Nesbitt, H. W, and Muir, I. J. (1998) 'Oxidation states and speciation of secondary products on pyrite and arsenopyrite reacted with mine waters and air', *Mineral Petrol*., 62, pp. 123 –144.

Nesbitt, H. W., Muir, I. J. and Pratt, A. R. (1995) 'Oxidation of arsenopyrite by air, air-saturated, distilled water, implications for mechanism of oxidation' *Geochim Cosmochim Acta*, 59(9), pp. 1773 – 1786.

Newman, D. K., Beveridge, T. J. and Morel, F. M. M. (1997) 'Precipitation of As2S3 by Desulfotomaculum auripigmentum', *Appl Environ Microbiol*, 63, pp. 2022–2028.

Ney, E. P. and Allen, D. A (1969) 'The Infrared Sources in the Trapezium Region of M42', *Astrophysics Journal*, 155, pp.193.

Nicolae, M., Vîlciu, I. and Zăman, F. (2007) 'X-ray diffraction analysis of steel slag and blast furnace slag viewing their use for road construction', *UPB Scientific Bulletin Series B*, 69(2), pp. 99–108.

Nordstrom, D. K. and Parks, G. A. (1987) 'Solubility and stability of scorodite, (FeAsO4Ø2H2O)', *Dis Am Mineral*, 72, pp. 849 –851.

Novák, F., Povondra, P. and Vtělenský, J. (1967) 'Bukovskýite, Fe3+ from Kaňk, near Kutná Hora - a new mineral', *Acta Univ. Carol., Geol.*, 4, pp. 297-325.

Ohtani, E., Ozawa, S., Miyahara, M., Ito, Y., Mikouchi, T., Kimura, M., Arai, T., Sato, K. and Hiraga, K. (2011) 'Coesite and stishovite in a shocked lunar meteorite, Asuka-881757, and impact events in lunar surface', *Proceedings of the National Academy of Sciences of the United States of America*, 108(2), pp. 463-466.

Ojima, J. (2003) 'Determining of crystalline silica in respirable dust samples by infrared spectrophotometry in the presence of interferences', *J. Occup. Health*, 45, pp. 94.

O'Keefe, J. A. (1976) 'Tektites and Their Origin', *Developments in Petrology*, 4, pp. 266.

Okuda, H., Shibai, H., Nakagawa, T., Matsuhara, H., Kobayashi, Y., Kaiful, N., Nagata, T., Gatley, I. and Geballe, T. (1990) 'An Infared Quintuplet Near the Galatic Center', *Astrophysics Journal*, 351, pp. 89-97.

Oparin, A. I. (1953) *The Origin of Life* (trans. S. Margulis). New York: Dover Publications.

Oremland, R. S. and Stolz, J. F. (2003) 'The ecology of arsenic', *Science*, 300, pp. 939–944.

Orgel, L. E. (1968) 'Evolution of genetic apparatus', *J. Mol.Biol*, 38, pp. 381.

Pack, A. (2000) 'Tracing the Origin of Oxide Inclusions in Continuously Casted Steel Using Stable Oxygen Isotopes-An Interdisciplinary Approach', *PhD Thesis*, Georg-August-Universität Göttingen.

Pack, A. (2008) 'Fractionation of refractory lithophile elements in bulk chondrites and chondrite components', *Lunar and Planetary Science Conference*, Houston.

Pack, A. (2013) [*Email communication*].

Palik, P. (1962), 'Further life-forms in the Orgueil meteorite', *Nature*, 194, pp. 1065.

Palik, P. (1963), *Micropaleontology*, cited by Claus, G.

Papike, J. J. (1998) 'Comparative planetary mineralogy: Chemistry of melt-derived pyroxene, feldspar, and olivine', In *Planetary materials*. Edited by Papike, J. J., in *Reviews in mineralogy*, 36, Washington, D.C.: Mineralogical Society of America. pp. 7–1-7-11.

Papike, J. J., Ryder, G. and Shearer, C. K. (1998) 'Chapter 5. Lunar Samples', In *Reviews in Mineralogy*, 36, Planetary Materials (ed. J. J. Papike), pp. 5-1-5-234, Mineralogical Society of America: Washington.

Parnell, J., Carey, P. F. and Bottrell, S. (1994) 'The occurrence of authigenic minerals in solid bitumens', *Journal of Sedimentary Research*, A64, pp. 95-100.

Parthasarathy, G., Kunwar, A. C. and Srinivasan, R. (2001) 'Occurrences of moganite-rich chalcedony in Deccan flood basalts, Killari, Maharahastra.,India', *Eur. J. Mineral.*, 13, pp. 127.

Pasteris, J. D. and Wopenka, B. (2003) 'Necessary, but not sufficient: Raman identification of disordered carbon as a signature of ancient life', *Astrobiology*, 3, pp. 727–738.

Pasteur, L. C. R. (1857) 'Mémoire sur la fermentation appelée lactique', *Acad. Sci.*, 45, pp. 913.

Patience, R. L., Baxby, M., Bartle, K. D., Perry, D. L., Rees, A. G. W. and Rowland, S. J. (1992) 'The functionality of organic nitrogen in some recent sediments from the Peru upwelling region', *Organic Geochemistry*, 18(2), pp. 161-169.

Peace River and Tenham (L6) chondrites', *Lunar and Planetary Science*, 28, pp. 329-330.

Peacor, D. R. (1973) 'High-temperature single-crystal study of the cristobalite inversion Note: Cell has been corrected Sample: T = 65 C Locality: Ellora Caves, Hyderabad State, India', *Zeitschrift fur Kristallographie*, 138, pp. 274-298.

Pedersen, H. D., Postma, D. and Jakobsen, R. (2006) 'Release of arsenic associated with the reduction and transformation of iron oxides', *Geochim. Cosmochim. Acta*, 70(16), pp. 4116-4129.

Pelet, R. (1983) 'Preservation of sedimentary organic matter' [In: Bjøroy et al. (Eds.)], *Advances in Organic Geochemistry 1981*, Chichester: Wiley Heiden Ltd., pp. 241–250.

Perrin, J. M., Darbon, S. and Sivan, J. P. (1995) 'Observation of extended red emission (ERE) in the halo of M82', *Astron. and Astrophys.*, 304, pp. L21.

Pflug, H. D. (1967) 'Structured organic remains from the Fig Tree Series (Precambrian) of the Barberton mountain land (South Africa)', *Rev. Palaeobot. Palynol.*, 5, pp. 9–29.

Pflug, H. D. (1984a) 'Microvesicles in meteorites, a model of pre-biotic evolution', *Naturwissenschaften*, 71, pp. 531-533.

Pflug, H. D. (1984b) In: [N.C. Wickramasinghe, ed.] *Fundamental Studies and the Future of Science*, Cardiff: Univ. College Cardiff Press.

Platt, P. (2013) 'No, Diatoms Have Not Been Found in a Meteorite', Available at: www.slate.com – Astronomy, (Accessed: 13 April 2014).

Platts, S. N. (2014) *The PAH World - Discotic polynuclear aromatic compounds as a mesophase scaffolding at the origin of life*, Available at: http://www.pahworld.com/ (Accessed: 7 February 2014).

Poh, H. Y., Ghataora, G. S. and Ghazireh, N. (2006) 'Soil stabilization using basic oxygen steel slag fines', *Journal of Materials in Civil Engineering*, 18(2), pp. 229–240.

Pontes-Buarques, M., Tessis, A. C., Bonapace, J. A. P., Monte, M. B. M., Cortés-Lopez, G., de Souza-Barros, F. and Vieyra, A. (2001) 'Modulation of adenosine 5'-monophosphate adsorption onto aqueous resident pyrite: Potential mechanisms for prebiotic reactions', *Origins of Life and Evolution of the Biosphere*, 31(343), pp. 362.

Povenmire, H. (2000) *Tektites: A Cosmic Enigma*, Indian Harbour Beach, Florida: Florida Fireball Network, pp. 209.

Qayyum, M. F., Diedrich, S., Hans, P. R. and Sven, S. (2012) 'Kinetics of Carbon Mineralization of Biochars Compared with Wheat Straw in Three Soils', *Journal of Environmental Quality* 41(4) pp. 1210-1220.

Qian, G. R., Sun, D. D., Tay, J. H. and Lai, Z. Y. (2002) 'Hydrothermal reaction and autoclave stability of Mg bearing RO phase in steel slag ', *British Ceramic Transactions*, 101(4), pp. 159–164.

Rath, R. K., Subramanian, S. and Pradeepy, T. (2000) 'Surface Chemical Studies on Pyrite in the Presence of Polysaccharide-Based Flotation Depressants', *Journal of Colloid and Interface Science*, 229, pp. 82–91.

Rauf, K. and Wickramasinghe, C. (2010) 'Evidence for biodegradation products in the interstellar medium', *Int. J. of Astrobiology*, 9(1), pp. 29–34.

Rauf, K., Hann, A. and Wickramasinghe, N. C. (2010a) 'Microstructure and elemental composition of the Tagish Lake meteorite and its astrobiological implications', *Int. J. Astrobiology*, 9, pp. 35–43.

Rauf, K., Hann, A., Wallis, M. K. and Wickramasinghe, N. C. (2010b) 'Evidence for putative microfossils in space dust from the stratosphere', *Int. J. Astrobiology*, (in press).

Reimer, C. W. (1961), cited by Claus, G. 1963.

ReVelle, D. O. (1979) 'A quasi-simple ablation model for large meteorite entry: Theory vs. observations', *Journal of Atmospheric and Terrestrial Physics*, 41, pp. 453–473.

Richardson, S. and Vaughan, D. J. (1989) 'Arsenopyrite: a spectroscopic investigation of altered surfaces', *Mineral Mag*., 53, pp. 223 –229.

Rietmeijer, F. J. M. and Mackinnon, J. D. R. (1985) 'Poorly graphitized carbon as a new cosmothermometer for primitive extraterrestrial materials', *Nature*, 316, pp. 733-736.

Rietmeijer, F. J. M. and Mackinnon, J. D. R. (1987) 'Metastable carbon in two chondritic porous interplanetary dust particles', *Nature*, 326, pp. 162-165.

Robert, F. and Javoy, M. (1992) 'Oxygen Isotope Compositions of Fulgarites', *Meteoritics*, 27, pp. 281.

Roberts, L. C., Hug, S. J., Ruettimann, T., Billah, M., Khan, A. W. and Rahman, M. T. (2004) 'Arsenic removal with iron(II) and iron(III) waters with high silicate and phosphate concentrations', *Environ. Sci. Technol*., 38(1), pp. 307-315.

Rosen, J. M. (1969) 'Stratospheric dust and its relation - ship to the meteoric influx', *Space Sci. Rev*., 9, pp. 58–89.

Ross, R. (1962) 'Extraterrestrial taxa', *Taxon*, 11, pp. 178.

Rossignol-Strick, M. and Barghoom, E. S. (1971) 'Extraterrestrial abiogenic organization of organic matter: The hollow spheres of the Orgueil meteorite', *Space Life Sci*., 3, pp. 89-107.

Russell, R. W., Soifer, B. T. and Forrest, W. J. (1975) *Astrophys, J*. 198, pp. 41.

Ruzicka, A. and Hutson, M. (2010) 'Comparative petrology of silicates in the Udei Station (IAB) and Miles (IIE) iron meteorites: Implications for the origin of silicate-bearing irons', *Geochim. Cosmochim. Acta*, 74, pp. 394-433.

Ruzicka, A., Hutson, M. and Floss, C. (2006) 'Implications for the origins of IIE-type silicate-bearing irons', *Meteoritics & Planetary Science*, 41, Nr 11, pp. 1797–1831.

Ruzicka, A., Hutson, M. and Floss, C. (2006) 'Petrology of silicate inclusions in the Sombrerete ungrouped iron meteorite: Implications for the origins of IIE-type silicate-bearing irons' *Meteoritics & Planetary Science'*, 41(11), pp. 1797–1831.

Ruzicka, A., Hutson, M. and Floss, C. (2006) 'Petrology of silicate inclusions in the Sombrerete ungrouped iron meteorite: Implications for the origins of IIE-type silicate-bearing irons', *Meteoritics & Planetary Science*, 41(11), pp. 1797-1831.

Saikia, B. J., Parthasarathy, G., Sarmah, N. C. and Baruah, G. D. (2008) 'Fourier-transform infrared spectroscopic characterisation of naturally occurring glassy fulgurites', *Bull Mater. Sci*., 31(2), pp. 155-158.

Saikia, B. K., Boruah, R. K. and Gogoi, P. K. (2007) 'FT-IR and XRD analysis of coal from Makum coalfield of Assam', *J. Earth Syst. Sci*., 116(6), pp. 575–579.

Sato, K. (1984) 'Reflectivity Spectra and Optical Constants of Pyrites (FeS2, CoS2 and NiS2) between 0.2 and 4.4eV', *Journal of Physical Society of Japan*, 53(5) pp.1617-1620.

Scala, S. M. (1960) 'Sublimation in a Hypersonic Environment', *Journal Aerospace Sciences*, 27(1), pp. 620-621.

Schieber, J. (2002) 'Sedimentary pyrite: A window into the microbial past', *Geology*, 30, pp. 531-534.

Schild, R. (1996) 'Microlensing variability of the gravitationally lensed quasar Q0957+561AB', *Astrophys J*., 464, pp. 125-130.

Schild, R. E. and Gibson, C. H. (2008) 'Lessons from the Axis of Evil', *arXiv[astro-ph]*, 0802.3229v2.

Schmitt-Kopplin, P., Gabelica, Z., Gougeon, R. D., Fekete, A., Kanawati, B., Harir, M., Gebefuegi, I., Eckel, G. and Hertkorn, N. (Published online before print February 16, 2010) 'High molecular diversity of extraterrestrial organic matter in Murchison meteorite revealed 40 years after its fall', (PDF), *PNAS*, 107(7), pp. 2763–2768.

Schneider, H. (1974) 'Shock-induced thermal transformations of Ries-biotites', *Contrib. Miner. Petr*., 43, pp. 233.

Schnitzer, M. (1985) 'Nature of nitrogen in humic substances' [McKnight, D.M., Aiken, G.R., Wershaw, R.L. MacCarthy, P. (Eds.)] *Humic Substances in Soil, Sediment and Water: Geochemistry, Isolation and Characterization.* New York & Chichester: Wiley & Sons, pp. 303–325.

Schoonen, M. A. A., Xu, Y. and Strongin, D. R. (1998) 'An introduction to geocatalysis', *J. Geochem. Explor*., 62, pp. 201.

Schoonen, M., Smirnov, A. and Cohn, C. (2004) 'A perspective on the role of minerals in prebiotic synthesis', *Ambio*., 33, pp. 539-551.

Schopf, J. W., Kudryavstev, A. B., Agresti, D. G., Czaja, A. D. and Wdowiak, T. J. (2005) 'Raman imagery: a new approach to assess the geochemical maturity and biogenicity of permineralized Precambrian fossils', *Astrobiology*, 5 (3), 333–371.

Scott, E. R. D. (1999) 'Origin of carbonate-magnetite-sulfide assemblages in Martian meteorite ALH84001' *Journal of Geophysical Research: Planets*, 104(2), pp. 3803-3813.

Setién, J., Hernández, D. and González, J. J. (2009) 'Characterization of ladle furnace basic slag for use as a construction material' *Construction and Building Materials*, 23(5), pp. 1788–1794.

Sharp, R. P. (1973) 'Mars: troughed terrain', *J. Geophys. Res*., 78, pp. 4063–4072.

Shearer, C. K. and Papike, J. J. (1993) 'Basaltic magmatism on the Moon: A Perspective from volcanic picritic glass beads', *Geochimica et Cosmochimica Acta*, 57, pp. 4785-4812.

Shen, D. H., Wu, C. M. and Du, J. C. (2009) 'Laboratory investigation of basic oxygen furnace slag for substitution of aggregate in porous asphalt mixture,' *Journal of Construction and Building Materials*, 23(1), pp. 453–461.

Shervais, J. W., Taylor, L. A. and Lindstrom, M. M. (1985) 'Apollo 14 mare basalts: Petrology and geochemistry of clasts from consortium breccia 14321', Journal of Geophysical Research: Solid Earth, 90(S02), pp. C375–C395.

Shi, C. (2004) 'Steel slag—its production, processing, characteristics, and cementitious properties,' *Journal of Materials in Civil Engineering*, 16(3), pp. 230–236.

Sisson, T. W. and Layne, G. D. (1993) 'H2O in basaltic and andersite glass inclusions from four subduction-related volcanoes', *Earth Planet, Sci.Lett.*, 117, pp. 619-635.

Sivan, J. P. and Perrin, J. M. (1993) 'Scattering and luminescence in the Bubble Nebula', *Astrophys. Journal*, 404, pp. 258.

Slavík, F. (1925) 'Nerosty Kutnohorska, jejich výskyt a vznik. — Sborník vlastivědných statí o politickém okrese kutnohorském. Knihovna příruček z vlastivědy kutnohorská a Uhlířskojanovicka', *Kutná Hora*, 1, pp. 67-90.

Smith, J.D.T., Draine, B.T., Dale, D.A., Moustakas, J., Kennicutt, R.C. Jr., Helou, G., Armus, L., Roussel, H., Sheth, K., Bendo, G.J., Buckalew, B.A., Calzetti, D.A., Engelbracht, C.W., Gordon, K.D., Hollenbach, D.J., Li, A., Malhotra, S., Murphy, E.J., & Walter, F. (2007) 'The Mid-Infrared Spectrum of Star-forming Galaxies: Global Properties of Polycyclic Aromatic Hydrocarbon Emission', *Astrophys. J.*, 656, pp. 770.

Soifer, B. T., Russell, R. W. and Merrill, K. M. (1976) *ApJ*, 207, pp. 83.

Sokol, A. K., Bischoff, A., Marhas, K. K., Mezger, K. and Zinner, E. (2007a) 'Late accretion and lithification of chondritic parent bodies: Mg isotope studies on fragments from primitive chondrites and chondritic breccias', *Meteorit. Planet. Sci*., 42, pp. 1291.

Staplin, F. L. (1962) Microfossils from the Orgueil meteorite', *Micropaleontology*, 8(3), pp. 343.

Stecher, T. P. (1965) 'The spectral energy distribution of the Earth's ultraviolet night airglow', *Journal of Geophysical Research*, 70(9), pp. 2209–2211.

Steel, A. (2006) 37th Lunar and Planetary Science Conference XXXVII, March 13–17, 2006.

Steele, A. (1996) *PhD*. University of Portsmouth, UK.

Steele A., McCubbin, F. M., Benning L.G., SiljestrÖem S, Cody G., Goreva, Y., Hauri, E. H., Wang, J, Kilcoyne, A.L.D, Grady M., Smith C., Freissinet C., Glavin, D. P, Burton, A., Fries, M. D, Blanco J.D.R., Glamoclija M., Rogers, K.L., Mikhail, S, Dworkin J. (2013) 'Organic Carbon Inventory of the Tissint meteorite'. *44th Lunar and Planetary Science Conference*.

Steele, A., Fries, M. D., Amundsen, H. E. F., Mysen, B. O., Fogel, M. L. and Schweizer, M. and Boctor N.Z. (2007) 'Comprehensive imaging and Raman spectroscopy of carbonate globules from Martian meteorite ALH 84001 and a terrestrial analogue from Svalbard', *Meteoritics and Planetary Science*, 42(9), 1549–1566.

Steele, A., McCubbin, F. M., Fries, M., Kater, L., Boctor, N. Z., Fogel, M. L., Conrad, P. G., Glamoclija, M., Spencer, M., Morrow, A. L., Hammond, M. R., Zare, R. N., Vicenzi, E. P., Siljeström, S., Bowden, R., Herd, C. D., Mysen, B. O., Shirey, S. B., Amundsen, H. E., Treiman, A. H., Bullock, E. S. and Jull, A. J. (2012) 'A Reduced Organic Carbon Component in Martian Basalts', *Science*, 337, pp. 212.

Steele, A., Westall, F., Goddard, D. T., Stapleton, D., Toporski, J. K. W. and McKay, D. S. (1999) 'Imaging of the biological contamination of meteorites: A practical assessment', paper presented at *Lunar and Planetary Science Conference XXX, Abstract #1321*.

Steg, L. and Lew, H. (1962) 'Hypersonic Ablation', *AGARD Hypersonic Conference TCEA*, Rhode-St., Geneva, Belgium.

Stein, W. A. and Gillett, F. C. (1969) 'Spectral Distribution of Infrared Radiation from the Trapezium Region of the Orion Nebula', *ApJ*, 155, pp. 197.

Stephan, T., Jessberger, E. K., Heiss, C. H. and Rost, D. (2003) 'TOF-SIMS analysis of polycyclic aromatic hydrocarbons in Allan Hills 84001', *Meteor and Planet Sci*., 38, pp. 109.

Sugitani, K., Grey, K., Allwood, A., Nagaoka, T., Mimura, K., Minami, M., Marshall, C. P., Van Kranendonk, M., Marshall, C. and Walter, M. (2007) 'Diverse microstructures from Archaean chert from the Mount Goldsworthy–Mount Grant area, Pilbara Craton, Western Australia: microfossils, dubiofossils, or pseudofossils?', *Precambr. Res.*, 158, pp. 228–262.

Sumi, T., Kamiya, K., Bennett, D. P., Bond, I. A., Abe, F., Botzler, C. S., Fukui, A., Furusawa, K., Hearnshaw, J. B., Itow, Y., Kilmartin, P. M., Korpela, A., Lin, W., Ling, C. H., Masuda, K., Matsubara, Y., Miyake, N., Motomura, M., Muraki, Y., Nagaya, M., Nakamura, S., Ohnishi, K., Okumura, T., Perrott, Y. C., Rattenbury, N., Saito, To., Sako, T., Sullivan, D. J., Sweatman, W. L., Tristram, P. J., Udalski, A., Szymański, M. K., Kubiak, M., Pietrzyński, G., Poleski, R., Soszyński, I., Wyrzykowski, Ł. and Ulaczyk, K. (2011) 'Unbound or distant planetary mass population detected by gravitational microlensing', *Nature*, 473, pp. 349.

Sun, X. H. and Doner, H. E. (1998) 'Adsorption and oxidation of arsenite on goethite', *Soil Sci.*, 163(4), pp. 278-287.

Sutton, G. W. (1960) 'The Ablation of Reinforced Plastics in Supersonic Flow', *Journal of the Aero/Space Sciences*, 27(5), pp. 377-385.

Szomouru, A. and Guhathakurta, P. (1998) 'Optical Spectroscopy of Galactic Cirrus Clouds: Extended Red Emission in the Diffuse Interstellar Medium', *Astrophys.J*., 494, L93.

Taylor, H. P. and Epstein, S. (1966) 'Science', 153, pp.173-175.

Taylor, L. A., Nazarov, M. A., Shearer, C. K., McSween, H. Y. Jr., Neal, C. R., Badjukov, D. D., Ivanova, M. A., Barsukova, L. D., Clayton, R. N. and Mayeda, T. K. (2002) 'Martian meteortie Dhofar 019: A new Shergottite', *Meteor. Planet. Sci*., 37, pp. 1107-1128.

Tessis, A. C., Penteado-Fava, A., Pontes-Buarques, M., de Amorim, H. S., Bonapace, J. A. P., de Souza-Barros, F., Monte, M. B. M. and Vieyra, A. (1999) 'Pyrite suspended in artificial sea water catalyzes hydrolysis of adsorbed ATP: Enhancing effect of acetate', *Origins of Life and Evolution of the Biosphere*, 29, pp. 361-374.

The Sunday Times (2013) 'Jigsaw puzzle from outer space divides scientists', *The Sunday Times of Sri Lanka.* (Retrieved 2013-01-20).

Timofeev, N. (1962) *Micropaleontology*, cited by Claus, G, (1963).

Tokunaga, A. T., Smith, R. G., Nagata, T., Depoy, D. L. and Sellgren, K. (1982) '3 micron spectroscopy of comet Halley', *Astrophysical Journal*, Part 2 - Letters to the Editor (ISSN 0004-637X), 310, pp. L45-L48.

Tossavainen, M., Engstrom, F., Yang, Q., Menad, N., Larsson, M. L. and Bjorkman, B. (2007) 'Characteristics of steel slag under different cooling conditions', *Waste Management*, 27(10), pp. 1335–1344.

Treiman, A. H. (2003) 'Submicron magnetite grains and carbon compounds in Martian meteorite ALH84001: inorganic, abiotic formation by shock and thermal metamorphism', *Astrobiology*, 3(2), pp. 369-392.

Treiman, A. H. (2003) 'Submicron magnetite grains and carbon compounds in martian meteorite ALH84001: Inorganic, abiotic formation by shock and thermal metamorphism', *Astrobiology*, 3, pp. 369.

Tsakiridis, P. E., Papadimitriou, G. D., Tsivilis, S. and Koroneos, C., (2008) 'Utilization of steel slag for Portland cement clinker production,' *Journal of Hazardous Materials*, 152(2), pp. 805–811.

Ulrich, F. (1930) 'Contributions to the topographic mineralogy of Bohemia II', *Vestnik Statniho geologickeho ustavu CSR*, 7, pp. 98-110. (in Czech).

Van de Hurst, H. C. (1957) *Light Scattering by Small Particles*, New York: Dover.

Vandenbroucke, M. and Largeau, C. (2007) 'Kerogen origin, evolution and structure', *Organic Geochemistry*, 38, pp.719–833.

Wacey, D., Saunders, M., Brasier, M. D. and Kilburn, M. R. (2011) 'Earliest microbially mediated pyrite oxidation in ~3.4 billion-year-old sediments', *Earth Planet Science Letters*, 301(1-2), pp. 393-402.

Wachtershauser, G. (1988) 'Pyrite Formation, the First Energy Source for Life: a Hypothesis', *Syst. Appl. Microbiol*., 10, pp. 207.

Wachtershauser, G. (1990) 'Evolution of the first metabolic cycles', *Proc. Natl. Acad. Sci.* USA, 87, pp. 200.

Wachtershauser, G. (1990) 'Origins of life and evolution of the biosphere', *Biochem.*, 20, pp. 173.

Wachtershauser, G. (1991) Royal Swedish Academy of Sciences Nobel Symposium, London: Oxford University Press, pp. 239.

Wachtershauser, G. (1992) 'Groundworks for an evolutionary biochemistry: The iron-sulphur world', *Prog. Biophys. Mol. Biol.,* 58, pp. 85.

Wachtershauser, G. (1993) 'The cradle chemistry of life—on the origin of natural-products in a pyrite-pulled chemo-autotrophic origin of life', *J. Pure Appl. Chem*., 65, pp. 1343.

Wainwright, J., Parsons, A. J., Müller, E. N., Brazier, R. E., Powell, D. M. and Fenti, B. (2008) 'A transport-distance approach to scaling erosion rates: 1. background and model development', *Earth Surface Processes and Landforms*, 33, pp. 813–826.

Wainwright, M., Rose, C., Baker, A. and Wickramasinghe, N. (2013) 'Isolation of Biological Entities from The Stratosphere (22–27km)', *Journal of Cosmology*, 22, pp. 10189-10193.

Wainwright, M., Rose, C., Baker, A. and Wickramasinghe, N. (2013) 'Filamentous Biological Entities Obtained from the Stratosphere', *Journal of Cosmology*, 22, pp. 10206-10209.

Wainwright, M., Rose, C., Baker, A., Briston, K. and Wickramasinghe, N. (2013) 'Isolation of A Diatom Frustule Fragment from The Lower Stratosphere (22-27km)-Evidence For A Cosmic Origin', *Journal of Cosmology*, 22, pp. 10183- 10186.

Wainwright, M., Wickramasinghe, N. C., Narlikar, J. V. and Rajaratnam, P. (2008) 'Are these stratospheric nanoparticles bacteria?', *Microbiology Comment*.

Wainwright, M., Wickramasinghe, N. C., Narlikar, J. V., Rajaratnam, P. and Perkins. J. (2004) 'Confirmation of the presence of viable but non-culturable bacteria in the stratosphere', *Int. J. Astrobiology*, 3(1), pp. 13-15.

Waligora, J., Bulteel, D., Degrugilliers, P., Damidot, D., Potdevin, J. L. and Measson, M. (2010) 'Chemical and mineralogical characterizations of LD converter steel slags: a multi-analytical techniques approach', *Materials Characterization*, 61(1), pp. 39–48.

Walker, J. C. G. (1986) 'Impact erosion of planetary atmospheres.' *Icarus*, 68, pp. 87–98.

Wallis, D. H. (1998) *Phd Thesis*, University of Wales.

Wallis, D. H. and Wickramasinghe N. C. (1999) 'Determination of Optical Spectra by a Modified Kramers Kronig', *Integral Astrophysics and Space Science*, 262, pp. 193–213.

Wallis, J., Miyake, N., Hoover, R. B., Oldroyd, A., Wallis, D. H., Samaranayake, A. and Wickramasinghe, N. C. (2013a). 'The Polonnaruwa meteorite: oxygen isotope, crystalline and biological composition', *arXiv preprint arXiv*, pp. 1303-1845.

Wallis, J., Wickramasinghe, N. C., Wallis, D. H., Miyake, N., Wallis, M. K., Hoover, R. B and Oldroyd, A. (2013) 'Physical, chemical, and mineral properties of the Polonnaruwa stones', In *SPIE Optical Engineering+ Applications*, International Society for Optics and Photonics.

Wallis, J., Wickramasinghe, N. C., Wallis, D. H., Miyake, N., Wallis, M. K., Di Gregorio, B. and Hoover, R. (2012) 'Possible biological structures in the Tissint Mars Meteorite', *Proc. SPIE 8521, Instruments, Methods, and Missions for Astrobiology XV*, pp. 85210R.

Wallis, J., Wickramasinghe, N. C., Wallis, D. H., Miyake, N., Wallis, M. K. and Hoover, R. B. (2014) 'Carbonaceous structures in the Tissint Martian Meteorite', *In review.*

Wallis, M. K., Al-Mufti, S., Wickramasinghe, N. C., Rajaratnam, P. and Narlikar, J. V. (2002) 'SEM Imaging of Stratospheric Particles of Non-terrestrial Origin, Conf. Microscopy and Chemistry of Airborne Particles', *Current Research*, Univ. West of England, Bristol, UK.

Wallis, M. K., Miyake, N. and Wickramasinghe, N. C. (2006) 'Space Dust recovered from the Stratosphere', presentation at *Aerosol Society*, UCL London, 28 March 2006 http://www.astrobiology.cf.ac.uk/ Stratosphere.ppt 8.

Walsh, M. M. (1992) 'Microfossils and possible microfossils from the early Archean Onverwacht Group, Barberton Mountain Land, South Africa', *Precambr. Res.*, 54, pp. 271–292.

Wang, S. L. and Mulligan, C. N. (2006) 'Effect of natural organic matter on arsenic release from soils and sediments into groundwater', *Environ. Geochem. Health*, 28(3), pp. 197-214.

Wang, Y., Alsmeyer, D. C. and McCreery, R. L. (1990) 'Raman spectroscopy of carbon materials: structural basis of observed spectra', *Chem Mater*, 2, pp. 557–563.

Warren, P. H., Greenwood, J. P., Richardson, J. W., Rubin, A. E. and Verisha, R. S. (2000) 'Geochemistry of Los Angeles, a ferroan, La- and Th-rich basalt from Mars (abstract)', *Lunar Planet. Sci.*, 31, Lunar and Planetary Institute, Houston, Texas, USA.

Waychunas, G. A., Rea, B. A., Fuller, C. C. and Davis, J. A. (1993) 'Surface-Chemistry of Ferrihydrite .1. Exafs Studies of the Geometry of Coprecipitated and Adsorbed Arsenate', *Geochim. Cosmochim. Acta*, 57(10), pp. 2251-2269.

Weisberg, M. K., McCoy, T. J. and Krot, A. N. (2006) 'Systematics and Evaluation of Meteorite Classification', *Meteorites & the Early Solar System II*, pp. 19–52.

Wetherill, G. W. and ReVelle, D. O. (1981) 'Which fireballs are meteorites? A study of the Prairie Network photographic meteor data' *Icarus*, 48, pp. 308–328.

Wickramasinghe, C., Wallis, J., Gibson, C. H. and Schild, R. E. (2010) 'Evolution of Primordial planets in relation to the cosmological origin of life', *Proc. SPIE*, 7819, arXiv: 1008.4955.

Wickramasinghe, D. T. and Allen, D. A. (1980) 'The 3.4-μm interstellar absorption feature', *Nature*, 287, pp. 518−519.

Wickramasinghe, D. T. and Allen, D. A. (1986) 'Discovery of organic grains in comet Halley', *Nature*, 323, 6083, pp. 44-46.

Wickramasinghe, D. T., Hoyle, F., Wickramasinghe, N. C. and Al-Mufti, S. (1986) 'A model of the 2-4 micron spectrum of Comet Halley', *Earth, Moon, and Planets*, 36, pp. 295-299.

Wickramasinghe, J. T., Wickramasinghe, N. C. and Napier, W. M. (2010) *Comets and the Origin of Life*, Singapore: World Scientific Publ.

Wickramasinghe, N. C. (1967) *Interstellar Grains*, London: Chapman & Hall.

Wickramasinghe, N. C. (1993) In: [Mampaso, A., Prieto, M. and Sanchez, F. eds.] *Infrared Astronomy*, Cambridge University Press, pp. 303.

Wickramasinghe, N. C., Hoyle, F. and Lloyd, D. (1996) 'Eruptions from comet Hale-Bopp at 6.5AU', *Astrophys. Sp. Sci*., 240, pp. 161.

Wickramasinghe, N. C., Harris, M. J., Lloyd, D., Narlikar, J. V., Rajaratnam, P., Turner, M. P., Al-Mufti, S., Wallis, M. K., Ramadurai, S. and Hoyle, F. (2002) 'Detection of living cells in stratospheric samples', *Proc. SPIE*, 4495, pp. 192.

Wickramasinghe, N. C., Samaranayake, A., Wickramarathne, K., Wallis, D. H., Wallis, M. K., Miyake, N., Coulson, S. J., Hoover, R. B., Gibson, C. H. & Wallis, J. (2013). 'Living Diatoms in The Polonnaruwa Meteorite – Possible Link to Red and Yellow Rain', *Journal of Cosmology*, 21, pp. 40.

Wickramasinghe, N. C., Wallis, J., Miyake, N., Wallis, D. H., Samaranayake, A., Wickramarathne, K. and Wallis, M. K. (2013) 'Authenticity of the life-bearing Polonnaruwa meteorite', *Journal of Cosmology*, 21, pp. 39.

Wickramasinghe, N. C., Wallis, J., Wallis, D. H. and Samaranayake, A. (2013) 'Fossil diatoms in a new carbonaceous meteorite', *arXiv preprint arXiv*, pp. 1303.2398.

Wickramasinghe, N. C., Wallis, J., Wallis, D. H., Schild, R. E. and Gibson, C. H. (2012) 'Life-bearing primordial planets in the solar vicinity', *Astrophysics and Space Science*, DOI: 10.1007/s10509-012-1092-8.

Wickramasinghe, N. C., Wallis, J., Wallis, D. H., Wallis, M. K., Al-Mufti, S., Wickramasinghe, J. T. and Wickramarathne, K. (2013) 'On the cometary origin of the Polonnaruwa meteorite.' *Journal of Cosmology*, 21, pp.38.

Wickramasinghe, N. C. (1974) 'Formaldehyde polymers in interstellar space', *Nature*, 252, pp. 462–463.

Willner, S. P., Russell, R. W., Puetter, R. C., Soifer, B. T. and Harvey, P. M. (1979) 'The 4 to 8 micron spectrum of the galactic center', *Astrophysics J.*, 229, pp. L65.

Woese, C. (1967) *The Genetic Code*. New York: Harper and Row.

Woolf, N. J. (1973) in *Interstellar Dust and Related Topics*, [eds Greenberg, J. M. & van de Hulst, H. C.] Reidel: Dordrecht.

Woolf, N. J. and Ney, E. P. (1969) 'Circumstellar Infrared Emission from Cool Stars', *ApJ*, 155, pp. 181.

Wyckoff, R. W. G. (1963) *Crystal Structures 1,* 'New York rocksalt structure', 2nd Edn, New York: Interscience Publishers, pp. 85-237.

Xu, Y. and Schoonen, M. A. A. (1995) 'The stability of thiosulfate in the presence of pyrite in low-temperature aqueous solutions', *Geochim. Cosmochim. Acta*, 59, pp. 4605.

Xu, Y., Schoonen, M. A. A. and. Strongin, D. R. (1996*)* 'Thiosulfate oxidation: Catalysis of synthetic sphalerite doped with transition metals', *Geochim. Cosmochim.* Acta, 60, pp. 4701.

Xuequan, W., Hong Z., Xinkai, H. and Husen, L. (1999) 'Study on steel slag and fly ash composite Portland cement', *Cement and Concrete Research*, 29(7), pp. 1103–1106.

Yamanaka, T., Fukuda, T. and Tsuchiya, J. (2002) 'Bonding character of SiO2 stishovite under high pressures up to 30 GPa Sample: P = 5.23 GPa', *Physics and Chemistry of Minerals*, 29, pp. 633-641.

Yano, H., Kubota, T., Miyamoto, H., Okada, T., Scheeres, D., Takagi, Y., Yoshida, K., Abe, M., Abe, S., Barnouin-Jha, O., Fujiwara, A., Hasegawa, S., Hashimoto, T., Ishiguro, M., Kato, M., Kawaguchi, J., Mukai, T., Saito, J., Sasaki, S. and Yoshikawa, M. (2006) 'Touchdown of the Hayabusa spacecraft at the Muses Sea on Itokawa', *Science*, 312, pp. 1350–1353.

Ying-Mei, X., Ji, Q., De-Min, H., Dong-Mei, W., Hui-Ying, C. H., Jun, G. and Qiu-Min, Z. (2010) 'Preparation of Amorphous Silica from Oil Shale Residue and Surface Modification By Silane Coupling Agent' *Oil Shale*, 27(1), pp. 37–46.

Yoshikawa, M., Yano, H. and Kawaguchi, J. (2008) 'Japan's future plans for missions to primitive bodies: Hayabusa-2, Hayabusa-MK2, and Marco Polo', (abstract #1747), *39th Lunar and Planetary Science Conference*, CDROM.

Zahnle, K. J. (1992) 'Airburst origin of dark shadows on Venus', *J. Geophys. Res*., 97(E6), pp. 10243–10255.

Zeigler, R. A., Korotev, R. L., Jolliff, B. L., Haskin, L. A. and Floss, C. (2006) 'The geochemistry and provenance of Apollo 16 mafic glasses', *Geochimica et Cosmochimica Acta*, 70, pp. 6050-6067.

Zhang, L., Dawes, W. R. and Walker, G. R. (2001) 'Response of mean annual evapotranspiration to vegetation changes at catchment scale', *Water Resour. Res*. 37, pp. 701.

Zhmur, S. I., Rozanov, A. Y. and Gorlenko, V. M. (1997) 'Lithified Remnants of Microorganisms in Carbonaceous Chondrites', *Geochemistry International*, 35 pp. 58-60.

Zinn, J., Close, S., Colestock, P. L., MacDonell, A. and Loveland, R. (2011) 'Analysis of ALTAIR 1998 meteor radar data', *J. Geophys. Res*., 116.

Zipfel, J., Scherer, P., Spettel, B., Dreibus, G. and Schultz, L. (2000) 'Petrology and chemistry of the new shergottite Dar al Gani 476', *Meteorit. Planet. Sci*., 35, pp. 95–106.

Zita, M., Botta, O., Fogel, M. L., Sephton, M. A., Glavin, D. P., Watson, J. S., Dworkin, J. P., Schwartz, A. W. and Ehrenfreund, P. (2008) 'Extraterrestrial nucleobases in the Murchison meteorite', *Earth and Planetary Science Letters.*

Zolensky, M. E. and Thomas, K. (1995) 'Iron- and iron-nickel sulfides in chondritic interplanetary dust particles', *Geochim. Cosmochim. Acta*, 59, pp. 4707– 4712.

Zolotov, M. Y. and Shock, E. L. (2000) 'An abiotic origin for hydrocarbons in the Allan Hills 84001 martian meteorite through cooling of magmatic and impact generated gases', *Meteorit. Planet. Sci*. 35, pp. 629.